Consistent Modeling and Parameter Estimation of Voltage Regulating Transformers for Power System Studies

Md Rejwanur Rashid Mojumdar

Department of Electrical Engineering
University of Oviedo
PhD Programme in Energy and Process Control

This dissertation is submitted as a requirement for the degree of
Doctor of Philosophy

Campus de Gijón June 2022

Modelado Consistente y Estimación de Parámetros en Transformadores Reguladores de Tensión para Estudios de Sistemas de Potencia

Md Rejwanur Rashid Mojumdar

Departamento de Ingeniería Eléctrica, Electrónica, Comunicaciones y Sistemas
Universidad de Oviedo
Programa de Doctorado en Energía y Control de Procesos

Esta tesis se presenta como requisito para obtener el grado de
Doctor

Campus de Gijón Junio 2022

Universidad de Oviedo

RESUMEN DEL CONTENIDO DE TESIS DOCTORAL

1.- Título de la Tesis	
Español: Modelado Consistente y Estimación de Parámetros en Transformadores Reguladores de Tensión para Estudios de Sistemas de Potencia	Inglés: Consistent Modeling and Parameter Estimation of Voltage Regulating Transformers for Power System Studies

2.- Autor	
Nombre: Md Rejwanur Rashid Mojumdar	Pasaporte:
Programa de Doctorado: Energía y Control de Procesos	
Órgano responsable: Centro Internacional de Postgrado	

RESUMEN (en español)

La regulación de tensión es una de las preocupaciones más importantes a tener en cuenta en el diseño y operación de redes eléctricas. Por esta razón, los transformadores con cambiador de tomas son un activo clave en la adecuada regulación tanto de la magnitud como de la fase de la tensión en los sistemas de potencia. Este trabajo de doctorado surge del hallazgo y la demostración de que dos de los modelos de transformador de cambio de toma más ampliamente utilizados son inconsistentes entre sí, ya que generan resultados discrepantes dependiendo de la toma seleccionada y del punto de operación. Así, esta investigación ha propuesto un nuevo modelo de transformador con cambiador de tomas que abarca tanto a los transformadores reguladores de tensión como a los transformadores desfasadores. Este modelo, conocido como modelo consistente, tiene en cuenta, de forma explícita, la contribución diferenciada de ambos devanados del transformador a la impedancia de cortocircuito. El nuevo modelo ha demostrado su capacidad para reconciliar el debate existente al respecto. Además, de cara a clarificar cualquier ambigüedad en el modelado del transformador con tomas, este trabajo desarrolla y presenta diferentes variaciones de los modelos convencionales y del nuevo modelo propuesto, abordando todo tipo de situaciones operativas, cualquier tipo de elección de bases de referencia y sentando los fundamentos de los modelos multifásicos.

El modelo consistente propuesto en este trabajo introduce un nuevo parámetro, la ratio de impedancia de cortocircuito, que representa la relación entre la impedancia de cortocircuito en p.u. del devanado nominal y la del devanado con tomas. Sin embargo, este parámetro no es, en general, proporcionado por el fabricante, y no puede obtenerse mediante cálculo directo a partir de las hojas de características de la máquina. Para superar este problema, en este trabajo se ha desarrollado un método de estimación de parámetros fuera de línea con vectores de estado aumentados capaz de proporcionar una estimación precisa de su valor. Se ha demostrado, además, que la precisa estimación de este parámetro da lugar a que los estimadores de estado que operan en línea conduzcan a mejores estimaciones de los estados del sistema.

A continuación, esta tesis doctoral se extiende hacia el modelado de reguladores de tensión con tomas en redes desequilibradas. Significativamente, de cara a facilitar la aplicación de algoritmos de flujo de cargas trifásicos, este trabajo presenta modelos precisos basados en ecuaciones matriciales de tipo general capaces de representar de forma adecuada este tipo de dispositivos, independientemente de su tipo y configuración. A continuación, estos modelos son adaptados para su utilización en redes desequilibradas mediante el empleo de un sistema de referencia estacionaria, αβ0. Todos los modelos son validados mediante un estudio de flujo de cargas desequilibrado en una red de prueba de 4 nudos derivada de un estándar existente propuesto por Kersting. A continuación, para varios escenarios y distintas configuraciones de los reguladores de tensión, se realizan estudios de flujo de cargas trifásicos en los que se pueden observar los efectos de la optimización de tomas en entornos desequilibrados. La publicidad dada a estos resultados y el hecho que éstos incluyan todas las posibles configuraciones de los reguladores, permiten convertir a este sistema de 4 nudos modificado

en un nuevo estándar para la evaluación y verificación de este tipo de modelos en aplicaciones de software y futuros desarrollos científicos.

Por último, este trabajo aporta un método original para integrar los transformadores desfasadores en el algoritmo de cálculo de flujo de cargas de aproximación directa (DA). El método DA es un algoritmo de cálculo de flujo de cargas extremadamente eficiente utilizado en redes radiales o débilmente malladas. Sin embargo, el uso de transformadores desfasadores no era, hasta la fecha, soportado por este método, debido al hecho de que su matriz de admitancia es inherentemente asimétrica. Para resolver este problema, en esta tesis se han extendido, tanto los modelos convencionales de transformador desfasador como el nuevo modelo consistente propuesto, de tal forma que el método DA puede ser ahora aplicado a redes que incluyen este tipo de dispositivos.

Para ilustrar todos estos desarrollos y garantizar la validez de las propuestas, el trabajo incluye un completo conjunto de casos prácticos basados en redes estandarizadas. En conjunto, este trabajo doctoral contribuye de forma significativa a la modelización consistente de los transformadores con cambiadores de tomas y, con ello, a la mejora de los métodos de análisis de los sistemas eléctricos.

RESUMEN (en inglés)

Voltage regulation is a most important concern for the design and operation of power grids. Therefore, voltage-regulating transformers are a key asset in regulating voltage magnitude and phase in power systems. This doctoral work has burgeoned with the finding and demonstration that the two widely used formulations of the tap-changing transformer model are inconsistent with each other, as they generate different results depending on the selected tap and operating point. Thereby, this research has proposed a novel class of single-phase and multi-phase transformer models that can consider a share of short-circuit impedance on both sides of their winding and demonstrated the consistency of this way of modeling to reconcile this debate for tap-changing and phase-shifting transformer modeling. Furthermore, shedding light on the ambiguity in tap-changing transformer's modeling, different variations of the conventional and consistent models are derived and presented for different cases of off-nominal or nominal operations, chosen bases, and number of phases.

The aforementioned consistent models introduce a parameter, per-unit (p.u.) impedance ratio, which stands for the ratio between the p.u. impedance of the nominal and tapped winding of the transformer. However, this impedance ratio parameter is not provided and cannot be obtained by straightforward calculation from standard datasheets. To overcome this problem, this work has established an offline state-vector-augmented parameter estimation method capable of providing an accurate estimate of this novel parameter. It has been demonstrated that this estimation can effectively lead power system state estimators to better estimates of system states.

Then this doctoral thesis extends toward the modeling of step-voltage regulators (SVRs) in unbalanced grids. Significantly, for a suitable three-phase power flow method, exact and general matrix-based equation models for three-phase step-voltage regulators (SVR) with all possible configurations are developed. After that, those models are incorporated in the complex vector-based model of the unbalanced distribution system in αβ0 stationary reference frame. After incorporation, all the models are validated by an unbalanced power flow study in a proposed 4-node test feeder with regulators in terms of Kersting's models. Then, importantly, for various scenarios and SVR configuration cases, three-phase power flow studies are conducted where effects of tap optimization can be observed in balanced and unbalanced loading with respect to their operation at central tap positions. Consequently, an extensive 4-node test system for testing and evaluation of three-phase SVR connections is established through this work.

Finally, a method for integrating phase-shifting transformers in the Direct Approach (DA) power flow method has been developed. DA is an extremely efficient power flow algorithm used in radial and weakly meshed grids. However, the use of phase-shifting transformers in a network to be solved by the DA method was unresolved before due to their inherent non-symmetrical admittance matrix. Thus, both the conventional and the proposed consistent model for phase-shifting transformers have been extended in this dissertation, which allows the use of the DA method in grids that include such devices.

Universidad de Oviedo

For all the developments, a set of case studies has been conducted in the context of standard test-beds to demonstrate the validity of the proposals. Altogether, this doctoral work contributes highly to the consistent modeling of voltage regulating transformers and consequent improvement in power system studies.

SR. PRESIDENTE DE LA COMISIÓN ACADÉMICA DEL PROGRAMA DE DOCTORADO EN ENERGÍA Y CONTROL DE PROCESOS

Thanks and Acknowledgements

So many thanks to my supervisor, Prof. José Manuel Cano Rodríguez, for his endless support and motivation. Thanks a lot to my wife, parents, and well-wishers for being supportive, patient, and motivating. Especially, I want to mention my M.Sc. supervisor and mentor, Prof. Pablo Arboleya, Prof. Cristina González-Morán, and the team thereby - for bringing me on this path. I am thankful to all fellow researchers, colleagues, and thereby the working and research opportunities at the University of Oviedo, the INESC TEC, the University of Stavanger, and the ABB AS. In essence, I am thankful to the Almighty for all the blessings.

Abstract

Voltage regulation is a most important concern for the design and operation of power grids. Therefore, voltage-regulating transformers are a key asset in regulating voltage magnitude and phase in power systems. This doctoral work has burgeoned with the finding and demonstration that the two widely used formulations of the tap-changing transformer model are inconsistent with each other, as they generate different results depending on the selected tap and operating point. Thereby, this research has proposed a novel class of single-phase and multi-phase transformer models that can consider a share of short-circuit impedance on both sides of their winding and demonstrated the consistency of this way of modeling to reconcile this debate for tap-changing and phase-shifting transformer modeling. Furthermore, shedding light on the ambiguity in tap-changing transformer's modeling, different variations of the conventional and consistent models are derived and presented for different cases of off-nominal or nominal operation, chosen bases, and number of phases.

The aforementioned consistent models introduce a parameter, per-unit (p.u.) impedance ratio, which stands for the ratio between the p.u. impedance of the nominal and tapped winding of the transformer. However, this impedance ratio parameter is not provided and cannot be obtained by straightforward calculation from standard datasheets. To overcome this problem, this work has established an offline state-vector-augmented parameter estimation method capable of providing an accurate estimate of this novel parameter. It has been demonstrated that this estimation can effectively lead power system state estimators to better estimates of system states.

Then this doctoral thesis extends toward the modeling of step-voltage regulators (SVRs) in unbalanced grids. Significantly, for a suitable three-phase power flow method, exact and general matrix-based equation models for three-phase step-voltage regulators (SVR) with all possible configurations are developed. After that, those models are incorporated in the complex vector-based model of the unbalanced distribution system in $\alpha\beta 0$ stationary reference frame. After incorporation, all the models are validated by an unbalanced power flow study in a proposed 4-node test feeder with regulators in terms of Kersting's models. Then, importantly, for various scenarios and SVR configuration cases, three-phase power flow studies are conducted where effects of tap optimization can be observed in balanced and unbalanced loading with respect to their operation at central tap positions. Consequently, an extensive 4-node test system for testing and evaluation of three-phase SVR connections is established through this work.

Finally, a method for integrating phase-shifting transformers in the Direct Approach (DA) power flow method has been developed. DA is an extremely efficient power flow algorithm used in radial and weakly meshed grids. However, the use of phase-shifting transformers in a network to be solved by the DA method was unresolved before due to their inherent non-symmetrical admittance matrix. Thus, both the conventional and the proposed consistent model for phase-shifting transformers have been extended in this dissertation, which allows the use of the DA method in grids that include such devices.

For all the developments, a set of case studies has been conducted in the contexts of standard test-beds to demonstrate the validity of the proposals. Altogether, this doctoral work contributes highly to the consistent modeling of voltage regulating transformers and consequent improvement in power system studies.

Resumen

La regulación de tensión es una de las preocupaciones más importantes en el diseño y operación de redes eléctricas. Por esta razón, los transformadores con tomas son un activo clave en los sistemas de potencia. Este trabajo surge del hallazgo de que dos de los modelos de transformador de cambio de toma más utilizados son inconsistentes entre sí, generando resultados discrepantes según la toma seleccionada y el punto de operación. Esta investigación propone un nuevo modelo que abarca tanto a los transformadores reguladores de tensión como a los transformadores desfasadores. Este modelo, conocido como modelo consistente, tiene en cuenta la contribución diferenciada de ambos devanados del transformador a la impedancia de cortocircuito. El nuevo modelo ha demostrado su capacidad para reconciliar el debate existente al respecto. De cara a clarificar cualquier ambigüedad en el modelado del transformador con tomas, este trabajo desarrolla diferentes variaciones de los modelos convencionales y del nuevo modelo propuesto, abordando distintas situaciones operativas, cualquier tipo de elección de bases de referencia y sentando los fundamentos de los modelos multifásicos.

El modelo propuesto en este trabajo introduce un nuevo parámetro, que representa la relación entre la impedancia de cortocircuito del devanado nominal y del devanado con tomas. Sin embargo, este parámetro no es proporcionado por el fabricante y no puede obtenerse mediante cálculo directo a partir de las hojas de características. Para superar este problema, este trabajo desarrolla un método de estimación de parámetros off-line con vectores de estado aumentados capaz de proporcionar una estimación precisa de su valor. La estimación de este parámetro da lugar a una mejora de los resultados de los estimadores de estado que operan en línea.

Este trabajo aborda también el modelado de reguladores de tensión con tomas en redes desequilibradas. De cara a facilitar la aplicación de algoritmos de flujo de cargas trifásicos, este trabajo presenta modelos precisos basados en ecuaciones matriciales de tipo general que resultan ser independientes de su configuración. Además, estos modelos son adaptados para su utilización en redes desequilibradas mediante el empleo de un sistema de referencia estacionario, $\alpha\beta 0$. Todos los modelos son validados mediante un estudio de flujo de cargas desequilibrado en una red de prueba de 4 nudos derivada de un estándar existente propuesto por Kersting. A continuación, se realizan estudios de flujo de cargas trifásicos en los que se pueden observar los efectos de la optimización de tomas en entornos desequilibrados. La publicidad dada a estos resultados y el hecho que éstos incluyan todas las posibles configuraciones de los reguladores, permite convertir a este sistema de 4 nudos

modificado en un nuevo estándar para la evaluación y verificación de este tipo de modelos en aplicaciones de software.

Por último, este trabajo aporta un método original para integrar transformadores desfasadores en el algoritmo de cálculo de flujo de cargas de aproximación directa (DA). El método DA es extremadamente eficiente, siendo utilizado en redes radiales o débilmente malladas. Sin embargo, el uso de transformadores desfasadores no era, hasta la fecha, soportado por este método, debido al hecho de que su matriz de admitancia es inherentemente asimétrica. Para resolver este problema, en esta tesis se han extendido los modelos de transformador desfasador, de tal forma que el método DA puede ser ahora aplicado a redes que incluyen este tipo de dispositivos.

Para ilustrar todos estos desarrollos y garantizar la validez de las propuestas, el trabajo incluye un completo conjunto de casos prácticos basados en redes estandarizadas. En conjunto, este trabajo doctoral contribuye de forma significativa a la modelización consistente de los transformadores reguladores de tensión, y con ello, a la mejora de los métodos de análisis de los sistemas eléctricos.

Thesis Contributions

Altogether, this doctoral work contributes to the consistent modeling of various voltage regulating transformers, i.e. tap-changing transformers, phase-shifting transformers, and step-voltage regulators. Major contributions can be listed as follows:

- This work demonstrates the inconsistency in voltage magnitude, phase angle, and voltage stability studies caused by the use of two alternative models of tap-changing and asymmetrical phase-shifting transformers operating in off-nominal tap positions.
- This work reconciles this inconsistency by establishing the consistent models of tap-changing and phase-shifting transformers for both single-phase and multi-phase studies. These models are consistent in both nominal and off-nominal tap positions.
- This work proposes a novel parameter called transformer p.u. impedance ratio, k, which enables assigning definite shares of transformer short-circuit impedance on both windings. With elaborate studies, this dissertation demonstrates that, even with a fair assumption of providing an equal share of short-circuit impedance on each winding, the new transformer models deliver reconciled results between two extreme alternatives of conventional transformer models.
- This work presents different variations of tap-changing transformer models for the cases of off-nominal or nominal operation, chosen bases, and number of phases.
- This work proposes a multi-snapshot-based parameter estimation method to determine the novel parameter, transformer p.u. impedance ratio, k. Through this determination, highly accurate transformer models can be reached.
- This work demonstrates that with the estimation of k, the online state estimators can provide better estimates of the system.
- This work delivers the derivatives of the different measurement functions in terms of the impedance ratios, which would be essential for any linearized state estimator while using the proposed consistent models of transformers.
- This work develops and validates the unbalanced SVR models considering all possible configurations. Furthermore, for various scenarios and SVR configuration cases, three-phase power flow studies are conducted where effects of tap optimization can

be observed in balanced and unbalanced loading with respect to their operation at central tap positions. Consequently, an extensive 4-node test system for testing and evaluation of three-phase SVR connections is established through this work.

- This work extends both the conventional and consistent models for phase-shifting transformers into pseudo π-equivalent forms to be embedded into the DA power flow method.

Document Structure

In the first chapter, the foundation, background literature, and reasoning for new contributions of this dissertation have been introduced. In chapter 2, the consistent tap-changing transformer model, and thereby, the emergence of the impedance ratio parameter is presented. Also, further case studies have been presented illustrating the advantages of the proposed consistent model over the conventional tap-changing transformer models. Chapter 3 derives variations of transformer models, both conventional and consistent, according to operational setup, chosen bases, and the number of phases. Then, chapter 4 similarly establishes the consistent models for phase-shifting transformers. Thereafter, chapter 5 presents a multi-snapshot-based equality-constrained state estimation method to accurately estimate p.u. transformer impedance ratios. Models for all configurations of three-phase SVRs are presented in chapter 6 with a 4-node test feeder to validate SVR models. Then, chapter 7 presents the modification of conventional and consistent phase-shifting transformer models for integration into the DA power flow method. Thereafter, chapter 8 summarizes this doctoral work, its contribution, findings, and the plan for future extension. Appendix A presents all the resulted tables for the case studies of chapter 6. Finally, a list of related works published through this doctoral work is included in appendix B.

Table of contents

List of figures

List of tables

Chapter 1

Foundation of the Dissertation

In this chapter, the foundation of this dissertation is laid by presenting the necessary review, theory, background, reasoning, and outline of this work. Necessarily, the conventional modeling of the tap-changing transformer, phase-shifting transformer, and auto-transformers are discussed. Consequently, the problems with the existing models are pointed out, and thereafter the contributions of this doctoral work are outlined.

1.1 Background and Context

The voltage regulating transformers, the tap-changing, and phase-shifting transformers as well as step-voltage regulators (SVRs) play a vital role in the power systems by regulating voltage magnitude and phasor angle as contributions towards controlling power quality and power transfer in the system. In this context, voltage-regulating transformers serve as the vanguard for voltage regulation in power systems. Moreover, the majority of the power systems consist of them, therefore, models of these devices are intensively used in the different fields of electric energy systems analysis and operation. Evidently, accurate and consistent modeling of these voltage regulating transformers for steady-state power system studies is a crucial issue.

Nonetheless, the limited amount of information generally available about voltage regulating transformers leads to the fact that a quite simplified model of these devices is used in such usual tasks as load flow analysis or state estimation (SE). The data is obtained from the nameplate of the device and comprises the rated power and voltage values, short-circuit impedance, and tap positions. Only transformers with a tapping range exceeding $\pm 5\%$ are obliged by standards to provide further information about the short-circuit impedance (at least, values for the extreme tappings are required in that case) [3].

Consequently, the models of the voltage regulating transformers conventionally used in steady-state balanced studies, such as the ones conducted during power flow calculations or voltage stability analyses, have been burdened with a long-standing controversy [4]. Indeed,

two alternative tap-changing transformer models can be found in the description of these devices in different books and simulation software packages [5–8]. Similarly, phase-shifting transformers also have two alternative models and they follow similar principles as the two alternative models of tap-changing transformers. The differences in these models arise from the fact that they consider the short-circuit impedance either provided exclusively by the nominal or off-nominal turns side winding of the device. Under specific operating conditions, using one of these models or another can lead to results with significant differences, which produces a serious lack of consistency in reporting the outcome of the analysis of electric grids with embedded regulating transformers.

Thereby, to reconcile this dispute, this doctoral work introduces the consistent model for tap-changing transformer through [9, 10] and for phase-shifting transformer in [11] which reflect that the short-circuit impedance is in fact shared by both sides of a voltage regulating transformer. In this dissertation, it is also shown that the models of the tap-changing transformers, both the conventional and consistent ones, vary due to the operational setup, chosen references for base quantities and number of phases to be considered. These model variations, for both the conventional and consistent alternatives are derived and presented in this work.

It is noteworthy that, particularly the new consistent models introduce a parameter, k, which stands for the per-unit (p.u.) impedance ratio between the nominal winding and tapped winding of the tap-changing transformer. By the introduction of this parameter, assigned shares of the short-circuit impedance can be attributed to both sides of the transformers. However, admittedly, during the initial proposals, the user could not obtain the value of this parameter k, from standard transformer datasheets or even through straightforward calculations. In response to that, this work argued and demonstrated that if this parameter is not available, assuming $k = 1$, i.e. considering an equal share of the impedance at both sides of the transformer produces results that minimize the maximum expected errors. Nonetheless, it was pointed out that, to achieve accurate results, the p.u. impedance ratio could be obtained in real scenarios from the application of state estimation (SE) techniques.

To overcome this problem of estimation of k for particular power systems, this doctoral work later proposed and established through [12] - an offline state-vector-augmented parameter estimation method capable of providing accurate estimates of transformer impedance ratios. It is demonstrated that their use can effectively lead state estimators to better estimates of system states. That work also contributes with the derivatives of the different measurement functions in terms of the impedance ratios, which are essential for this or any other linearized state estimator.

Then this doctoral thesis plunge into three-phase step voltage regulator (SVR) modeling. SVRs are key assets and have been employed in power feeders for many decades [13–16]. Their modeling possesses particular importance in power flow studies of unbalanced distribution networks [17–19] and is gaining even more importance in distribution feeders

with the proliferation of Distributed Generation (DG) [20]. Type A or Type B - there are two types of single-phase SVRs, both of which can be configured to raise position or lower position. Then six configurations of three-phase SVRs are implemented in practice - Wye Type A, Wye Type B, Close Delta Type A, Close Delta Type B, Open Delta Type A, Open Delta Type B, all of which are built from single phase SVRs and can operate in either raise position or lower position. Models of these three-phase SVRs for all these configurations were not available in the literature but they are essential for any unbalanced power flow calculations which have SVRs embedded in their network. Therefore this doctoral work comes up with two major contributions: First, the development of three-phase SVR models considering all possible configurations and second, the proposal of a 4-node test system for testing and evaluation of three-phase SVR connections.

Finally, this work extends the consistent models for phase-shifting transformers into a suitable form to be embedded into the Direct Approach (DA) power flow method. The DA method is a very efficient formulation that was proposed in [21]. The DA method avoids the time-consuming tasks of LU factorization and forward and backward substitution of the Jacobian or admittance matrices, which are commonplace in conventional formulations. The characteristics of the DA method make it ideal for real-time applications in the smart grid context. Then, modeling of phase-shifting transformers in any power flow studies is a non-trivial problem, as they cannot be represented by a π-equivalent component due to their inherent asymmetric admittance matrix [22]. A set of different phase-shifting transformer models is available for application in various fields of study, to both steady-state [23–27] and transient simulation [28]. In [29], a survey on phase-shifting transformer models for steady-state analysis is presented; however, none of them are expressed in a suitable form to be embedded in the DA solver. Therefore, in this work, importantly, the earlier established consistent models for phase-shifting transformers are extended into a suitable form to overcome this limitation.

Altogether this doctoral work contributes highly to the consistent modeling of various voltage regulating transformers, i.e. tap-changing transformers, phase-shifting transformers, and step-voltage regulators. The reasoning, theories, background, and outline of this work are discussed in the following sections.

1.2 Tap-changing Transformer Defining Equations

In this section, the tap-changing transformer equivalent circuit and equations explaining the relationship between the voltage, current, and impedance of both winding are discussed.

1.2.1 In Physical Quantities

The equivalent circuit of an ideal transformer, as shown in Fig. 1.1, is well known. Here, primary and secondary side of the transformer are denoted with subscript i and j,

respectively, and thereby, R_i, X_{li}, v_i, i_i, e_i and N_i are the primary-side resistance, leakage reactance, terminal voltage, current, induced electromotive force and turns ratio, whereas R_j, X_{lj}, v_j, i_j, e_j and N_j are the similar entities at the secondary-side. Moreover, R_c, X_m and i_φ denote the magnetizing resistance, reactance and current accordingly. Definitions, description, relationships between these components are described in detail at [1]. However, for the background of this dissertation, two key points from transformer literature are necessary to recall: (a) the very basic relationships of voltage, current, and impedance between primary and secondary sides of the transformer, and (b) method of deriving short-circuit impedance of a transformer.

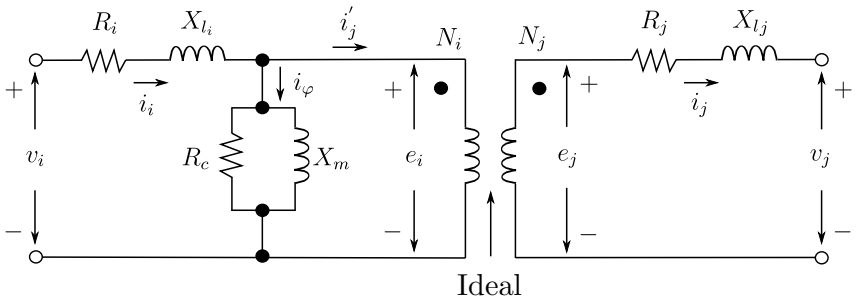

Fig. 1.1 Equivalent circuit of an ideal transformer [1]

The basic relationship for tap-changing transformer voltage, current, and turns ratio is

$$\frac{v_i}{v_j} = \frac{N_i}{N_j} = \frac{i_j}{i_i} \tag{1.1}$$

Therefore, the secondary side transformer impedance $Z_j = R_j + jX_{lj}$ transferred to the primary side is

$$Z_j' = \left(\frac{N_i}{N_j}\right)^2 Z_j. \tag{1.2}$$

Similarly, the primary side impedance Z_i transferred to the secondary side is

$$Z_i' = \left(\frac{N_j}{N_i}\right)^2 Z_i. \tag{1.3}$$

1.2.2 In the Per-Unit System

In general, a large number of transformers are embedded in any typical power system, and therefore, power systems are represented in the per-unit system so that quantities expressed as per-unit would not change when they are referred from one side of a transformer to the other side. Therefore, the use of per-unit (p.u.) system for the development of power system studies is universal. In fact, it is so widespread that a detailed explanation would be out of context in this work. However, just to mention, in p.u. system, every electrical quantity such as voltage, current, power, impedance, admittance, turns ratio, etc. are

calculated in their p.u. quantities where

$$\text{At p.u. Quantity} = \frac{\text{Physical Quantity}}{\text{Base Quantity}}. \tag{1.4}$$

As most of the power flow studies are conducted in p.u. system, it is also important to note how the transformer relationship equations work thereby. In p.u. system, transformer turns ratio is also taken into p.u. in terms of the nominal turns ratios. So, if a transformer is operating at nominal turns ratio, the transformer ratio at p.u. system will be $1:1$. However, in practical cases for voltage regulation, one side of the transformer, generally the primary side, is operated at taps other than the nominal to obtain the desired voltage magnitude at the secondary side. There, the off-nominal to nominal side transformer turns ratio is denoted as $a:1$, where practically $|a|$ is operated within the limits of $0.9 \leq |a| \leq 1.1$. So, in mathematical terms, the p.u. turns ratio is

$$\left.\frac{\frac{N_i}{N_i^{nom}}}{\frac{N_j}{N_j^{nom}}}\right|_{\text{where } N_j = N_j^{nom}} = \frac{a}{1}. \tag{1.5}$$

If, voltage and current quantities are also expressed in p.u. quantities, we can state

$$a = \frac{v_i}{v_j} = \frac{i_j}{i_i}. \tag{1.6}$$

Therefore, in p.u. system, considering impedance, admittance and turns ratio are expressed in p.u., the equations(1.1) to (1.3) can be transferred as

$$Z_j^{'} = a^2 Z_j \tag{1.7}$$

$$Z_i^{'} = \frac{1}{a^2} Z_i \tag{1.8}$$

As admittance is reciprocal to transformer impedance, we can state for tap-changing transformer

$$Y_j^{'} = \frac{1}{a^2} Y_j \tag{1.9}$$

$$Y_i^{'} = a^2 Y_i. \tag{1.10}$$

1.3 Phase-shifting Transformer Defining Equations

Phase-shifting transformers can regulate phase angle between off-nominal and nominal sides whereas, depending on their type, they may or may not regulate p.u. voltages between their sides. There are various types of phase-shifting transformers such as symmetric, asymmetric, direct, or indirect, which will be discussed in the relevant chapter. However, in general, at p.u. entities, the basic relationships for phase-shifting transformer voltage,

current, and turns ratio are

$$\frac{v_i}{v_j} = a = |a|\, e^{j\theta} \tag{1.11}$$

$$\frac{i_i}{i_j} = \frac{1}{a^*} = \frac{1}{|a|} e^{j\theta}. \tag{1.12}$$

Therefore, the secondary side phase-shifting transformer impedance $Z_j = R_j + jX_{lj}$ transferred to the primary side is

$$Z_j^{'} = |a|^2 Z_j. \tag{1.13}$$

Similarly, the primary side impedance Z_i transferred to the secondary side is

$$Z_i^{'} = \frac{1}{|a|^2} Z_i. \tag{1.14}$$

Again, as admittance is reciprocal to transformer impedance, we can state for phase-shifting transformer

$$Y_j^{'} = \frac{1}{|a|^2} Y_j \tag{1.15}$$

$$Y_i^{'} = |a|^2 Y_i. \tag{1.16}$$

1.4 Transformer Short-circuit Impedance

In this section, approximation for the derivation of transformer short-circuit impedance is discussed. For the sake of discussion, let us continue to focus on the tap-changing transformers. However, similar takeaways will also be applicable for phase-shifting transformers.

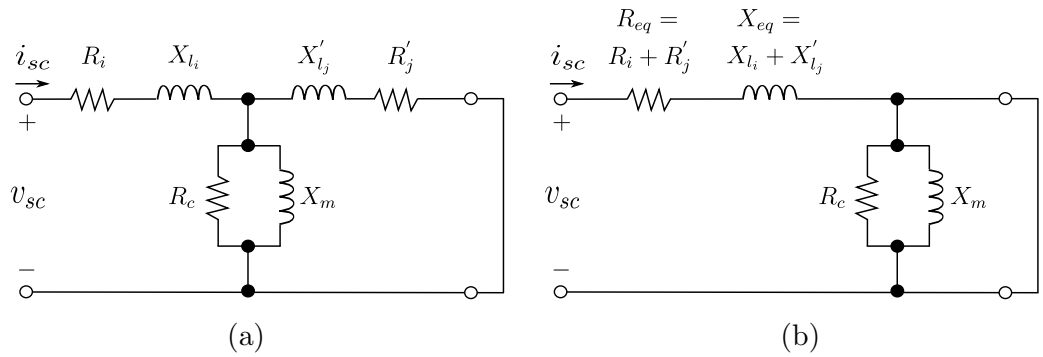

Fig. 1.2 Equivalent circuit with short-circuited secondary. (a) Complete equivalent circuit. (b) Cantilever equivalent circuit with the exciting branch at the transformer secondary [1]

The transformer model illustrated in Fig. 1.1 is extensive, a detail-oriented model. However, static power flow studies need to use a much simpler transformer model to be able to include it in their equation system. To do so, simply the short-circuit impedance of transformer obtained from short-circuit test [1] is used as total transformer impedance.

For short-circuit test, any arbitrary side of the transformer is shorted and a rated current is applied to the other side. For the sake of discussion, let's consider that the secondary side is shorted and voltage is applied to the primary. Then Fig. 1.2 (a) illustrates this set-up of transformer short-circuit test. Here, the short circuit impedance of the transformer by looking into the primary side is

$$Z_{sc} = R_i + jX_{li} + \frac{Z_\varphi(R_j^{'} + jX_{li}^{'})}{Z_\varphi + R_j^{'} + jX_{li}^{'}}. \tag{1.17}$$

At this point, short-circuit test follows an approximation. Due to the fact that the impedance Z_φ of the excitation branch is much larger than that of the secondary leakage impedance transferred to the primary side (considering excessive voltage is not applied during short-circuit test, i.e. the transformer core is not heavily saturated), the short-circuit impedance is approximated as

$$Z_{sc} \approx R_i + jX_{li} + R_j^{'} + jX_{lj}^{'} = R_{eq} + jX_{eq}. \tag{1.18}$$

This approximation can be further perceived by relating it to the approximation made in reducing towards the cantilever equivalent [1], as shown in Fig. 1.2 (b) where the excitation branch is directly shorted out by the short-circuit on the secondary side.

1.5 Transformers as Passive Two-Port Networks

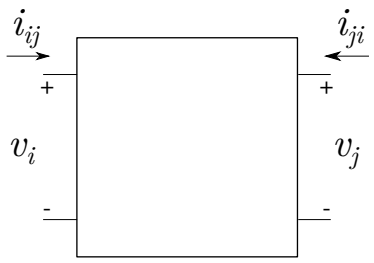

Fig. 1.3 Two-port electrical network

Voltage regulating transformers fall in the class of linear electrical network that has two terminal pairs. Moreover, they are passive elements so that there is no output without some input and there are no dependent sources involved. Fig. 1.3 illustrates such a two-port network. A good description of how to define two-port networks are given in [30]. Accordingly, this network can be defined in two ways - a) admittance parameter point of view or, conversely, b) impedance parameter point of view. The admittance parameter point of view defines the network by the currents at its terminals in terms of the voltages.

For the Fig. 1.3, this would describe the network as [30]:

$$\begin{bmatrix} i_{ij} \\ i_{ji} \end{bmatrix} = \begin{bmatrix} Y_{ii} & Y_{ij} \\ Y_{ji} & Y_{jj} \end{bmatrix} \begin{bmatrix} v_i \\ v_j \end{bmatrix}, \tag{1.19}$$

where v, i, and Y, stands for voltage, current, and elements of admittance matrix respectively in p.u. quantities and subscript i or j stands for the numbering of the corresponding port or node of the network. Here the elements of the admittance matrix are defined as:

$$Y_{ii} = \frac{i_{ij}}{v_i}\Big|_{\text{while } v_j=0} \tag{1.20}$$

$$Y_{ij} = \frac{i_{ij}}{v_j}\Big|_{\text{while } v_i=0} \tag{1.21}$$

$$Y_{ji} = \frac{i_{ji}}{v_i}\Big|_{\text{while } v_j=0} \tag{1.22}$$

$$Y_{jj} = \frac{i_{ji}}{v_j}\Big|_{\text{while } v_i=0} \tag{1.23}$$

On the other hand, the impedance parameter point of view defines the network by the voltages in terms of the currents at the terminals, such as [30]:

$$\begin{bmatrix} v_i \\ v_j \end{bmatrix} = \begin{bmatrix} Z_{ii} & Z_{ij} \\ Z_{ji} & Z_{jj} \end{bmatrix} \begin{bmatrix} i_{ij} \\ i_{ji} \end{bmatrix}, \tag{1.24}$$

where Z, stands for elements of impedance matrix at p.u. quantities. Here the elements of the impedance matrix are defined as:

$$Z_{ii} = \frac{v_i}{i_{ij}}\Big|_{\text{while } i_{ji}=0} \tag{1.25}$$

$$Z_{ij} = \frac{v_i}{i_{ji}}\Big|_{\text{while } i_{ij}=0} \tag{1.26}$$

$$Z_{ji} = \frac{v_j}{i_{ij}}\Big|_{\text{while } i_{ji}=0} \tag{1.27}$$

$$Z_{jj} = \frac{v_j}{i_{ji}}\Big|_{\text{while } i_{ij}=0} \tag{1.28}$$

These two points of view and their relationships are, of course, the inverse of each other, that is:

$$\begin{bmatrix} Y_{ii} & Y_{ij} \\ Y_{ji} & Y_{jj} \end{bmatrix} = \begin{bmatrix} Z_{ii} & Z_{ij} \\ Z_{ji} & Z_{jj} \end{bmatrix}^{-1} \tag{1.29}$$

Then, out of these two points of view, admittance-based representation is most frequently used in the power flow and state estimation methods of power systems. Naturally, this representation is used in the derivations and development of this work. It is often useful to express this admittance-based two-port network representation in terms of π-equivalent circuits as in Fig. 1.4 and develop voltage regulating transformer models accordingly. The relationships between the elements of the admittance matrix in (1.19) and π-equivalent circuits in Fig. 1.4 can be straightforwardly found using Kirchhoff's current law (KCL)

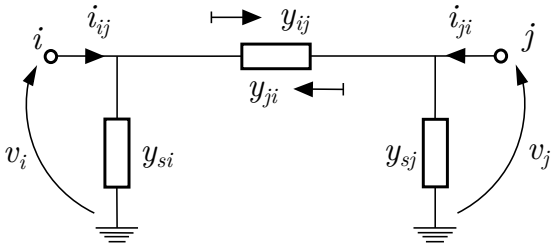

Fig. 1.4 The π-equivalent circuit of admittance based two-port representation

and Ohm's law. Using KCL we have

$$i_{ij} = v_i y_{si} + (v_i - v_j) y_{ij} = v_i (y_{si} + y_{ij}) - v_j y_{ij}, \tag{1.30}$$

$$i_{ji} = v_j y_{sj} + (v_j - v_i) y_{ji} = -v_i y_{ji} + v_j (y_{sj} + y_{ji}). \tag{1.31}$$

Comparing (1.30) and (1.31) to (1.19), it can be seen that

$$\begin{bmatrix} i_{ij} \\ i_{ji} \end{bmatrix} = \begin{bmatrix} Y_{ii} & Y_{ij} \\ Y_{ji} & Y_{jj} \end{bmatrix} \begin{bmatrix} v_i \\ v_j \end{bmatrix} = \begin{bmatrix} y_{si} + y_{ij} & -y_{ij} \\ -y_{ji} & y_{sj} + y_{sj} \end{bmatrix} \begin{bmatrix} v_i \\ v_j \end{bmatrix}. \tag{1.32}$$

So, the relationships between the elements of admittance matrix in (1.19) and π-equivalent circuits in Fig. 1.4 are

$$y_{ij} = -Y_{ij}, \tag{1.33}$$

$$y_{ji} = -Y_{ji}, \tag{1.34}$$

$$y_{si} = Y_{ii} + Y_{ij}, \tag{1.35}$$

$$y_{sj} = Y_{jj} + Y_{ji}. \tag{1.36}$$

These relationships will be used while presenting conventional models and deriving rather consistent voltage regulating transformer models in the later sections and chapters.

1.6 Conventional Models of Transformers

The two-port conventional models of voltage regulating transformer are developed with the focus of integrating them into the conventional power flow methods which are mostly admittance matrix based. However, the elements of the two-port admittance bus matrix of transformer models need to be formulated from the transformer short-circuit impedance found from short-circuit test. In this section, the conventional models for voltage-regulating transformers, i.e. both tap-changing transformers and phase-shifting transformers are discussed where elements of admittance matrix are formed in terms of the transformer short-circuit admittance, y_{sc} from the short-circuit test.

1.6.1 Models of Tap-changing Transformers

Two different tap-changing transformer models can be found today in both the literature and practical software implementations [31, 7, 8]. At the first alternative among two models, as shown in Fig. 1.5, the total of the transformer short-circuit admittance, y_{sc} is considered on the off-nominal side of the transformer.

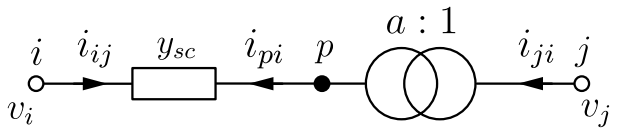

Fig. 1.5 Tap-changing transformer with short-circuit impedance at the off-nominal side

Then, let's consider a point p on the off-nominal side of the transformer. We can express, according to Ohm's law

$$\begin{bmatrix} i_{ij} \\ i_{pi} \end{bmatrix} = \begin{bmatrix} y_{sc} & -y_{sc} \\ -y_{sc} & y_{sc} \end{bmatrix} \begin{bmatrix} v_i \\ v_p \end{bmatrix}. \tag{1.37}$$

However, according to tap-changing transformer relationships in (1.6)

$$\begin{bmatrix} i_{ij} \\ \frac{i_{ji}}{a} \end{bmatrix} = \begin{bmatrix} y_{sc} & -y_{sc} \\ -y_{sc} & y_{sc} \end{bmatrix} \begin{bmatrix} v_i \\ av_j \end{bmatrix}. \tag{1.38}$$

Therefore:

$$\begin{bmatrix} i_{ij} \\ i_{ji} \end{bmatrix} = \begin{bmatrix} y_{sc} & -ay_{sc} \\ -ay_{sc} & a^2 y_{sc} \end{bmatrix} \begin{bmatrix} v_i \\ v_j \end{bmatrix}. \tag{1.39}$$

Hence, according to (1.33) - (1.36), this first alternative among conventional π-equivalent models of tap-changing transformer is shown in Fig. 1.7 (a).

At the second alternative among two models, all of the transformer short-circuit admittance, y_{sc} is considered on the nominal side of the transformer. From (1.9) it can be seen how this nominal side admittance can be referred to the off-nominal side. Accordingly, in Fig. 1.6, $y_{sc}^{off} = \frac{1}{a^2} y_{sc}$ is shown in the off-nominal side. Now, the same derivation as through (1.37)-(1.39) can be carried for this model, and ultimately the elements of admittance matrix will be multiplied by $\frac{1}{a^2}$ and it will be

$$\begin{bmatrix} i_{ij} \\ i_{ji} \end{bmatrix} = \begin{bmatrix} \frac{y_{sc}}{a^2} & -\frac{y_{sc}}{a} \\ -\frac{y_{sc}}{a} & y_{sc} \end{bmatrix} \begin{bmatrix} v_i \\ v_j \end{bmatrix}. \tag{1.40}$$

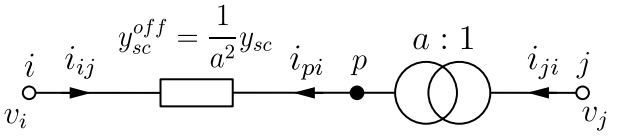

Fig. 1.6 Tap-changing transformer with short-circuit impedance at the nominal side

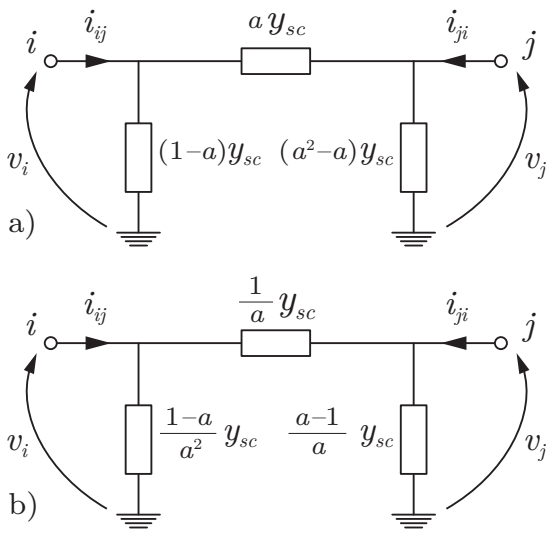

Fig. 1.7 The π equivalent conventional models of tap-changing transformers. (a) y_{sc} considered on off-nominal side, and (b) y_{sc} considered on nominal side

Again, according to (1.33) - (1.36), this second alternative among conventional π-equivalent models of tap-changing transformer is shown in Fig. 1.7 (b).

1.6.2 Models of Phase-shifting Transformers

Similar to tap-changing transformers, two alternative models of the phase-shifting transformer are found in literature [32, 6, 33, 8]. For one alternative among two models, as shown in Fig. 1.8, all of the short-circuit admittance, y_{sc} is considered on the off-nominal side of the transformer.

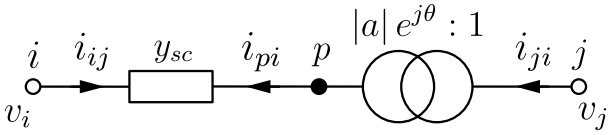

Fig. 1.8 Phase-shifting transformer with short-circuit impedance at the off-nominal side

Then again, let us consider a point p on the off-nominal side of the transformer. So, we can express, according to Ohm's law

$$\begin{bmatrix} i_{ij} \\ i_{pi} \end{bmatrix} = \begin{bmatrix} y_{sc} & -y_{sc} \\ -y_{sc} & y_{sc} \end{bmatrix} \begin{bmatrix} v_i \\ v_p \end{bmatrix}. \tag{1.41}$$

However, according to phase-shifting transformer relationships in (1.11) - (1.12)

$$\begin{bmatrix} i_{ij} \\ \frac{i_{ji}}{a^*} \end{bmatrix} = \begin{bmatrix} y_{sc} & -y_{sc} \\ -y_{sc} & y_{sc} \end{bmatrix} \begin{bmatrix} v_i \\ a v_j \end{bmatrix}. \tag{1.42}$$

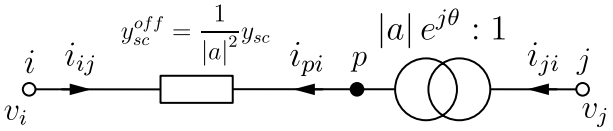

Fig. 1.9 Phase-shifting transformer with short-circuit impedance at the nominal side

Therefore:

$$\begin{bmatrix} i_{ij} \\ i_{ji} \end{bmatrix} = \begin{bmatrix} y_{sc} & -a y_{sc} \\ -a^* y_{sc} & |a|^2 y_{sc} \end{bmatrix} \begin{bmatrix} v_i \\ v_j \end{bmatrix}. \tag{1.43}$$

Hence, according to (1.33) - (1.36), this first alternative among conventional π-equivalent models of phase-shifting transformer is shown in Fig. 1.10 (a). Here an important observation emerges that for phase-shifting transformer's two-port network, $Y_{ij} \neq Y_{ji}$ so that the series branch of its π-equivalent model has two different admittance depending on the flow of current, which is shown in the 1.10 with the help of two opposite direction of arrows in the series branch. This is further discussed in subsection 1.8.3. In fact, this asymmetry of the phase-shifting transformer's two-port network makes it very challenging to be integrated into power flow methods like Direct Approach (DA) method. In chapter 7, the solution to this problem has been presented in detail.

Similarly, at the second alternative among two models, all of the transformer short-circuit admittance, y_{sc} is considered on the nominal side of the transformer. From (1.15) it can be seen how this nominal side admittance can be referred to the off-nominal side. Accordingly, in Fig. 1.9, $y_{sc}^{off} = \frac{1}{|a|^2} y_{sc}$ is shown in the off-nominal side. Once again, the same derivation as through (1.41)-(1.43) can be carried for this model, and ultimately the elements of admittance matrix will be multiplied by $\frac{1}{|a|^2}$ and it will be

$$\begin{bmatrix} i_{ij} \\ i_{ji} \end{bmatrix} = \begin{bmatrix} \frac{y_{sc}}{|a|^2} & -\frac{y_{sc}}{a^*} \\ -\frac{y_{sc}}{a} & y_{sc} \end{bmatrix} \begin{bmatrix} v_i \\ v_j \end{bmatrix}. \tag{1.44}$$

Again, according to (1.33) - (1.36), this second alternative among conventional π-equivalent models of phase-shifting transformer is shown in Fig. 1.10 (b). It is noteworthy that, for this alternate model's two-port network also, $Y_{ij} \neq Y_{ji}$.

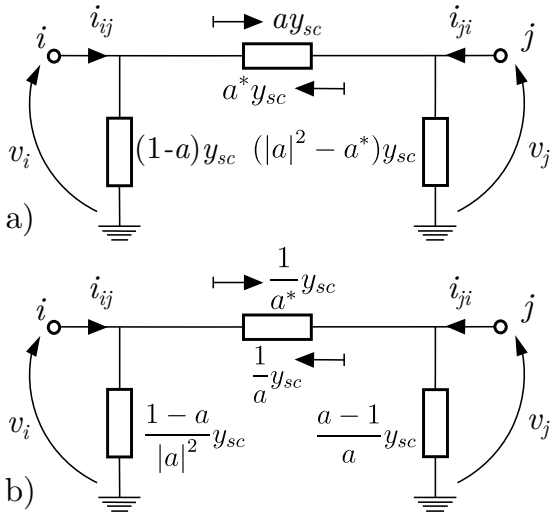

Fig. 1.10 The π equivalent conventional models of phase-shifting transformers. (a) y_{sc} considered on off-nominal side, and (b) y_{sc} considered on nominal side

1.7 Power Flow Methods

Any power flow method is basically a method of solving a set of nonlinear equations which describe the quasi-static relationship of a power network in terms of the bus voltages (phasor), complex power injection, and admittances (or impedance) between buses. There are many power flow methods discussed in the literature with their merits and demerits and that is an extensive area of study. Detailed discussion about power flow methods is, however, out of the scope of this dissertation. This dissertation does not propose any new power flow method; however, it uses such methods for case studies and also, significantly, proposes a phase-shifting transformer model which can be integrated into a very useful power flow method for distribution system study - the direct approach (DA). In this section, just the very basics of two power flow methods are presented for the sake of highlighting the need for a new phase-shifting transformer model to be integrated into the DA power flow method.

1.7.1 Admittance Matrix Based Power Flow Methods

Admittance-based power flow method is the most conventional method which is widely used for power flow studies of the balanced transmission grids. In principal, as detailed in [22], this method is similar to the two-port networks discussed in section 1.5, however, for a power system, there will be many ports instead of two. Fundamentally, this method

holds all the network equations in a matrix formation like

$$\begin{bmatrix} I_{i=1} \\ I_{i=2} \\ I_{i=3} \\ \vdots \\ I_{i=N} \end{bmatrix} = \begin{bmatrix} Y_{ij=11} & Y_{ij=12} & Y_{ij=13} & \cdots & Y_{ij=1N} \\ Y_{ij=21} & Y_{ij=22} & Y_{ij=23} & \cdots & Y_{ij=2N} \\ Y_{ij=31} & Y_{ij=32} & Y_{ij=33} & \cdots & Y_{ij=3N} \\ \vdots & \vdots & \vdots & \ddots & \vdots \\ Y_{ij=N1} & Y_{ij=N2} & Y_{ij=N3} & \cdots & Y_{ij=NN} \end{bmatrix} \begin{bmatrix} V_{j=1} \\ V_{j=2} \\ V_{j=3} \\ \vdots \\ V_{j=N} \end{bmatrix}, \tag{1.45}$$

or in short form

$$I = YV, \tag{1.46}$$

where N is the number of buses in the network, I is the vector of bus phasor current injections, V is the vector of bus phasor voltages and Y is the bus admittance matrix. Similar to the two-port network, the elements of the bus admittance matrix are obtained as

$$Y_{ij} = \frac{i_{ij}}{v_j}\Big|_{\text{while other bus voltages} = 0}. \tag{1.47}$$

From (1.45), any bus current injection can be calculated as

$$I_i = \sum_{j=1}^{N} Y_{ij} V_j. \tag{1.48}$$

And any bus complex power injection can be obtained as

$$S_i = V_i \sum_{j=1}^{N} {Y_{ij}}^* V_j^*. \tag{1.49}$$

When this equation is set for a given network with the necessary amount of data available to have a solvable system (i.e. number of unknowns becomes less or equal to the number to node equations), it can be solved iteratively by methods such as Newton-Raphson.

From (1.32), it is easy to notice that the two-port models of the transformer are developed in the manner so that they can be integrated into this bus admittance matrix. Even for the two-port models of phase-shifting transformers where $y_{ij} \neq y_{ji}$, the bus impedance matrix can easily integrate them. However, this is not the case for other important power flow methods such as DA.

1.7.2 The Direct Approach Method for Power Flow

The Direct Approach (DA) method, as detailed in [21], is a very robust and time-efficient method for radial power networks which is very popular in distribution system applications. DA method does not use admittance matrix-based formulation to avoid the time-consuming LU decomposition and forward/backward substitution of the Jacobian matrix required in the conventional admittance matrix-based power flow methods. Rather, it uses two

developed matrices, namely, the bus-injection to branch-current matrix and the branch-current to bus-voltage matrix to obtain load flow solutions directly. For example, let us consider a simple radial distribution grid as shown in Fig. 1.11.

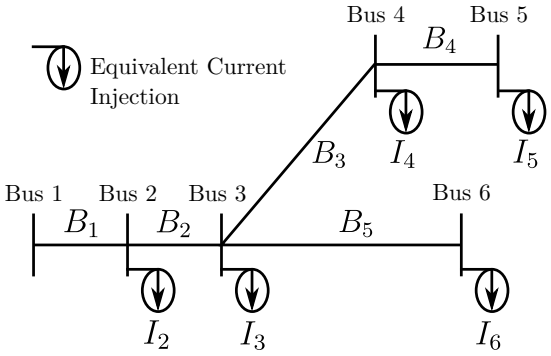

Fig. 1.11 A radial distribution system

Steps to solve power flow through the DA method are described below with respect to this simple grid.

- At each iteration k, current injection at each bus is calculated by

$$I_i^k = \left(\frac{P_i + jQ_i}{V_i^k} \right)^* , \tag{1.50}$$

  where P_i, Q_i, I_i^k, V_i^k are measured active power injection at bus i of current solution (for all iterations), measured reactive power injection at bus i of current solution (for all iterations), calculated current injection at bus i and iteration k and calculated bus voltage of bus i and iteration k, respectively.

- Then, at each iteration k, the output vector for voltage differences between each bus and the slack bus in the network, ΔV^{k+1}, are calculated from the vector of injection currents of the network buses, $\left[I^k\right]$, as below

$$\left[\Delta V^{k+1}\right] = [DLF] \left[I^k\right] . \tag{1.51}$$

  Here, the development of $[DLF]$, the load flow matrix is the most interesting contribution of this power flow method which enables it to avoid time-consuming LU factorization operation. $[DLF]$ matrix is indeed obtained as the product of two other matrices, $[BCBV]$ and $[BIBC]$, as below

$$[DLF] = [BCBV] [BIBC] . \tag{1.52}$$

  Here, the bus injection to branch current (BIBC) matrix is a network-specific matrix that follows Kirchhoff's Current Law (KCL) to derive the branch current vector of the network from the bus injection vector of the network. From the example grid of

Fig. 1.11, formation of $[BIBC]$ can be seen as below,

$$\begin{bmatrix} B_1 \\ B_2 \\ B_3 \\ B_4 \\ B_5 \end{bmatrix} = \begin{bmatrix} 1 & 1 & 1 & 1 & 1 \\ 0 & 1 & 1 & 1 & 1 \\ 0 & 0 & 1 & 1 & 0 \\ 0 & 0 & 0 & 1 & 0 \\ 0 & 0 & 0 & 0 & 1 \end{bmatrix} \begin{bmatrix} I_2 \\ I_3 \\ I_4 \\ I_5 \\ I_6 \end{bmatrix}. \tag{1.53}$$

In general form, it can be stated that

$$[B] = [BIBC]\,[I]\,. \tag{1.54}$$

Similarly, the branch-current to bus-voltage (BCBV) matrix is also a network-specific matrix that follows Kirchhoff's Voltage Law (KVL) to derive the output vector for voltage differences between each bus and the slack bus in the network from the bus injection vector of the network. From the example grid of Fig. 1.11, formation of $[BCBV]$ can be seen as below,

$$\begin{bmatrix} V_1 \\ V_1 \\ V_1 \\ V_1 \\ V_1 \end{bmatrix} - \begin{bmatrix} V_2 \\ V_3 \\ V_4 \\ V_5 \\ V_6 \end{bmatrix} = \begin{bmatrix} Z_{12} & 0 & 0 & 0 & 0 \\ Z_{12} & Z_{23} & 0 & 0 & 0 \\ Z_{12} & Z_{23} & Z_{34} & 0 & 0 \\ Z_{12} & Z_{23} & Z_{34} & Z_{45} & 0 \\ Z_{12} & Z_{23} & 0 & 0 & Z_{36} \end{bmatrix} \begin{bmatrix} B_1 \\ B_2 \\ B_3 \\ B_4 \\ B_5 \end{bmatrix}. \tag{1.55}$$

Or, in general form

$$[\Delta V] = [BCBV]\,[B]\,. \tag{1.56}$$

- At final step of each iteration k, the vector of bus voltages for the network, $\left[V^{k+1}\right]$ is calculated simply by

$$\left[V^{k+1}\right] = \left[V^{0}\right] + \left[\Delta V^{k+1}\right]. \tag{1.57}$$

Subsequently, changes in the bus voltages are monitored and if the highest change (compared to the previous iteration) in any bus voltage is lower than a preselected threshold, it is assumed that the power flow has converged. Otherwise, the power flow proceeds to the same steps described here for the next iteration.

1.8 Inconsistencies and Deficiencies in Transformer Modeling

After laying out the foundation in transformer modeling and significant power flow methods, importantly, some inconsistencies and deficiencies in transformer modeling are outlined in

this section. Based on these key findings, this dissertation becomes a requisite for power system modeling.

1.8.1 Transformers Operating at Off-nominal Turn-ratios

The conventional models for both tap-changing and phase shifting transformers work perfectly for transformers operating at nominal turn-ratios. In fact, it is a remarkable that at nominal operation the two alternative π-equivalent models of transformers (phase-shifting or voltage regulating) becomes equal. According to Fig. 1.7, if $a = 1$ at both π-equivalent models both model (a) and (b) become exactly the same. Similarly, both π-equivalent models of phase-shifting transformer becomes exactly the same if $|a| = 1$ at the Fig.1.10 (a) and (b).

However, for voltage regulation purposes, tap-changing and phase-shifting transformers most often operate at off-nominal turn-ratios and the conventional system for transformer modeling is inaccurate for such off-nominal operations. In fact, the problem for transformer modeling operating at off-nominal turn-ratios is two-fold. The first problem is of practical nature: in the majority of cases, the transformer short-circuit impedance at different off-nominal ratios cannot be obtained from the datasheet of the machine. Theoretically, the derivation and approximations for the short-circuit impedance calculation, as discussed in 1.4, are acceptable. However, in most of the cases, the datasheet of the transformer provides short-circuit impedance only at the nominal tap position, i.e $a = 1$. Therefore, from (1.18) we can see that, for most of the cases, the short-circuit impedance provided in the manufacturer data sheet is indeed

$$Z_{sc-test} = Z_i + Z_j, \tag{1.58}$$

as, at the nominal tap position, the a^2 term has no effect as $a = 1$ (or $|a| = 1$, for phase-shifting transformers), and $Z_{sc-test}$ needs no consideration of referring transformer impedance from one winding to another. However, for the modeling of transformers operating at off-nominal turn-ratios, the user would require the short-circuit impedance measured at particular off-nominal tap positions and that would be

$$Z_{sc-test} = Z_i + |a|^2 Z_j, \tag{1.59}$$

when referred to primary/off-nominal winding. Most frequently, this data of short-circuit impedance depending on different taps is unavailable.

The second and critical problem is that the conventional transformer models themselves are inaccurate for transformers operating at off-nominal turns ratios. Even if a user is provided with detailed transformer-short circuit data at different tap positions, by means of conventional transformer models, it is not possible to model such transformers operating at different off-nominal taps. As shown in section 1.6, for both tap-changing and phase-shifting

transformers, there are two alternative transformer modeling approaches available in the literature. One of the modeling approaches considers all of the short-circuit impedance at the off-nominal side of the transformer and the other approach considers it on the nominal side. However, a model of a transformer operating at off-nominal taps should have its short-circuit impedance shared among its winding as discussed in 1.4 and expressed by (1.18).

Therefore, we can conclude, new models of voltage-regulating transformers, both tap-changing and phase-shifting, are required to accurately model transformers that operate at both nominal and off-nominal turns ratios and share their short-circuit impedance between both of their winding. Also if any novel parameter arises to develop such novel models of voltage-regulating transformers, methods to derive all practical data from the currently available transformer data sheets have to be developed. After laying all the foundation throughout the chapter, it can be ascertained that these necessities of modeling regarding very fundamental equipment of power system, voltage-regulating transformers, is the key point to resolve throughout this dissertation.

1.8.2 Model variations Due to Chosen Bases and Number of Phases

Beyond the ambiguity appearing at off-nominal operation, transformer models, whether conventional or consistent, can vary depending on the chosen bases and number of phases to be considered. Firstly, models can be derived in physical quantities instead of being represented in the per-unit (p.u.) system; which is the approach considered by important tools such as [34]. While deriving in the per-unit system as well, the transformer's short-circuit impedance can be referred to different bases, i.e. the transformer's own base quantities, or a different set of system quantities. This fact leads to more complex versions of the models that should be taken into account.

Most power systems analyses are conducted in balanced conditions. In that case, single-phase models of transformers are sufficient for steady-state studies. However, these single-phase models are not applicable to the appropriate analysis of unbalanced power systems. For such systems, three-phase models of transformers are required for steady-state studies. Thus, the different variations of conventional and consistent transformer models require three-phase counterparts to allow the analysis of unbalanced systems. Thereby, transformer models can have a large number of variations, and there lies a considerable amount of ambiguity that needs to be addressed.

1.8.3 Integration of Phase-Shifting Transformers into the DA Method

Conventionally, the two-port network models of transformers were developed to be integrated into admittance matrix-based power flow methods. However, the formulation of

the DA method is not admittance matrix-based, so the conventional voltage-regulating transformer models require adaptations to be integrated into the DA method. In fact, the required adaptation for the case of the tap-changing transformer was already available in the literature and that will be explained in detail in the relevant chapter of this dissertation. However, other than the work of this dissertation, there was no resolution on how to adapt the conventional phase-shifting transformer model (or any two-port model that is not reciprocal) into the DA method of power flow.

For the tap-changing transformers, as can be seen from (1.39) - (1.40), two-port network models are reciprocal so that the transfer impedance or transfer admittances of them are the same in both directions, that is:

$$Z_{ij} = Z_{ji} \quad : \text{for tap-changing transformers} \tag{1.60}$$

$$Y_{ij} = Y_{ji}. \tag{1.61}$$

However, it is an important distinction, as can be seen from (1.43) - (1.44), for the phase-shifting transformers two-port network models, are not reciprocal so that the series impedance in both of their π-equivalent models are not the same in both directions, that is:

$$Z_{ij} \neq Z_{ji} \quad : \text{for phase-shifting transformers} \tag{1.62}$$

$$Y_{ij} \neq Y_{ji}. \tag{1.63}$$

From (1.55), it can be easily seen that the DA method needs a defined series impedance for its branches which are used in its branch-current to bus-voltage (BCBV) matrix. As the series impedance changes are not fixed for phase-shifting transformer models, there was no straightforward method to use the DA method for any network having a phase-shifting transformer. This dissertation contributes with a resolve for that.

1.9 Single Phase SVRs

Basically, a SVR is an auto-transformer with a load tap-changing mechanism (line drop compensator) on its series winding [2]. Detailed theories, control mechanism with line drop compensator and generalized constant matrix models for SVRs are available in [2]. With the basic understanding of how auto-transformer works, for modeling, the next requirement is to clearly understand the working topology of two available connections of SVRs denoted as Type A or Type B.

For these Type A or Type B regulators, the function of the reversing switch is to reverse the direction of the currents in the series and shunt windings so that the regulator is reversing between raising or lowering the voltage to the secondary side. According to the dot convention, a dot indicates positive voltage polarity of the coil and the current

direction to or from a dot is opposite in primary and secondary coil. Due to the reversing switch, the raising or lowering of voltage in the regulated circuit towards secondary side can be understood by the application of KVL, or, it is rather easier to understand observing the current directions and applying KCL in the node.

Below, four topologies of single-phase regulators are presented together with their corresponding equations.

1.9.1 Type B SVR

Type B regulator connection is the more common in SVRs. As opposed to Type A, the shunt winding (N_1) of the Type B regulator is directly connected to the secondary regulated circuit of the system whereas one end of the series winding (N_2) is connected to the shunt winding (N_1) and other end is connected via taps to the primary circuit of the system.

1.9.1.1 Defining Equations: Type B in Raise

The detailed and abbreviated equivalent circuit of a Type B SVR in the raise position is shown in Figure 1.12.

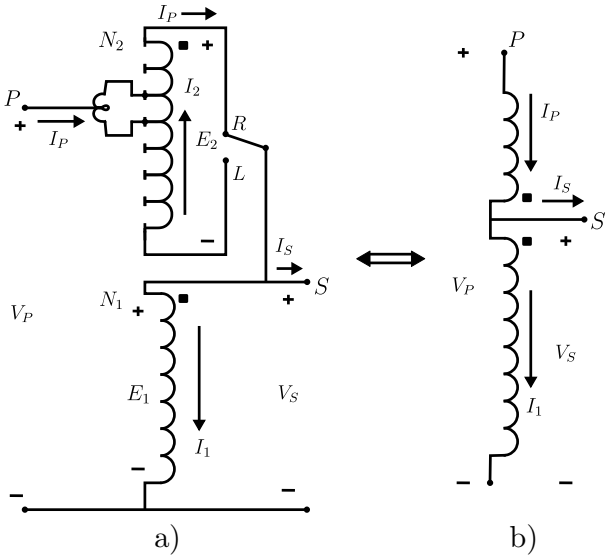

Fig. 1.12 Type B SVR in the raise position: a) Detailed b) Concise [2]

Observing Fig. 1.12, the defining voltage and current equations for the Type B voltage regulator in raise position are explained in Table 1.1:

Table 1.1 Defining Equations of Type B Raise Position[2]

Voltage Equations		**Current Equations**	
Voltage Ratio:	$\frac{E_1}{N_1} = \frac{E_2}{N_2}$	Current Ratio:	$N_1 I_1 = N_2 I_2$
Primary Voltage:	$V_P = E_1 - E_2$	Primary Current:	$I_P = I_2$
Secondary Voltage:	$V_S = E_1$	Secondary Current:	$I_S = I_P - I_1$
As:	$E_2 = \frac{N_2}{N_1} E_1 = \frac{N_2}{N_1} V_S$	As:	$I_1 = \frac{N_2}{N_1} I_2 = \frac{N_2}{N_1} I_P$
So:	$V_P = (1 - \frac{N_2}{N_1}) V_S$	So:	$I_S = (1 - \frac{N_2}{N_1}) I_P$
Denote:	$a_R = (1 - \frac{N_2}{N_1})$	Denote:	$a_R = (1 - \frac{N_2}{N_1})$
Finally:	$V_P = a_R V_S$	Finally:	$I_S = a_R I_P$

1.9.1.2 Defining Equations: Type B in Lower

Fig. 1.13 shows Type B regulator in lower position. Here, a reversing switch changes the direction of the currents through the series and shunt windings.

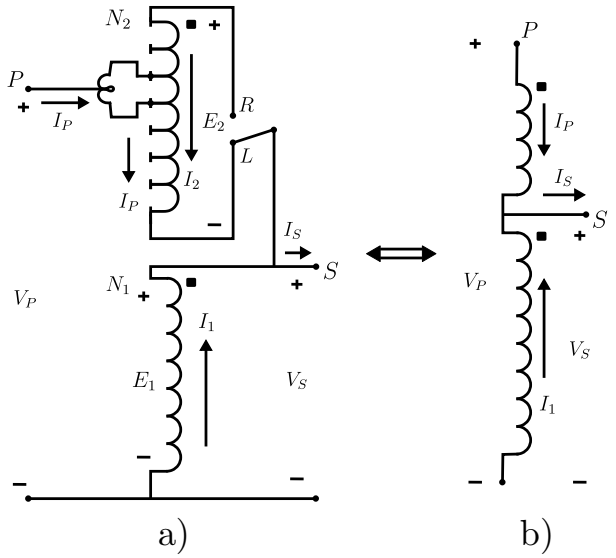

Fig. 1.13 Type B SVR in the lower position: a) Detailed b) Concise [2]

Observing Fig. 1.13, the defining voltage and current equations for the Type B voltage regulator in lower position are explained in Table 1.2:

Table 1.2 Defining Equations of Type B Lower position [2]

Voltage Equations		**Current Equations**	
Voltage Ratio:	$\frac{E_1}{N_1} = \frac{E_2}{N_2}$	Current Ratio:	$N_1 I_1 = N_2 I_2$
Primary Voltage:	$V_P = E_1 + E_2$	Primary Current:	$I_P = I_2$
Secondary Voltage:	$V_S = E_1$	Secondary Current:	$I_S = I_P + I_1$
As:	$E_2 = \frac{N_2}{N_1} E_1 = \frac{N_2}{N_1} V_S$	As:	$I_1 = \frac{N_2}{N_1} I_2 = \frac{N_2}{N_1} I_P$
So:	$V_P = (1 + \frac{N_2}{N_1}) V_S$	So:	$I_S = (1 + \frac{N_2}{N_1}) I_P$
Denote:	$a_R = (1 + \frac{N_2}{N_1})$	Denote:	$a_R = (1 + \frac{N_2}{N_1})$
Finally:	$V_P = a_R V_S$	Finally:	$I_S = a_R I_P$

1.9.2 Type A SVR

The shunt winding (N_1) of the Type A regulator is directly connected to the primary circuit of the system whereas one end of the series winding (N_2) is connected to the shunt winding (N_1) and other end is connected via taps to the regulated secondary circuit.

1.9.2.1 Defining Equations: Type A in Raise

The detailed and abbreviated equivalent circuit of a Type A SVR in the raise position is shown in Fig. 1.14.

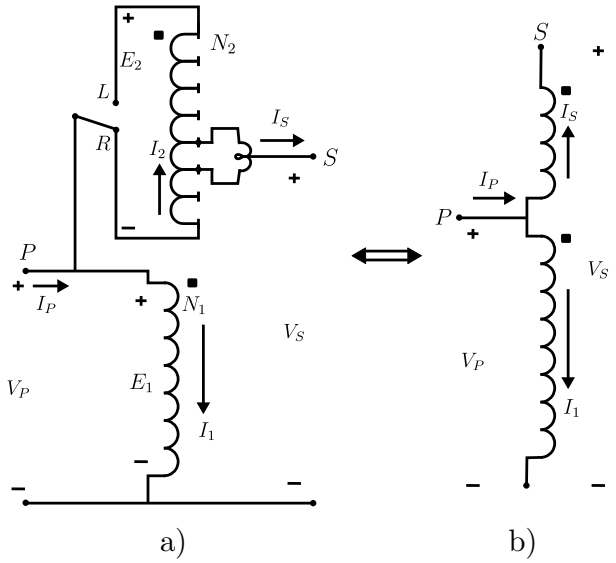

Fig. 1.14 Type A SVR in the raise: a) Detailed b) Concise [2]

Observing Fig. 1.14, the defining voltage and current equations for the Type A voltage regulator in raise position are explained in Table 1.3:

Table 1.3 Defining Equations of Type A Raise Position

Voltage Equations		**Current Equations**	
Voltage Ratio:	$\frac{E_1}{N_1} = \frac{E_2}{N_2}$	Current Ratio:	$N_1 I_1 = N_2 I_2$
Primary Voltage:	$V_P = E_1$	Primary Current:	$I_P = I_1 + I_2$
Secondary Voltage:	$V_S = E_1 + E_2$	Secondary Current:	$I_S = I_2$
As:	$E_2 = \frac{N_2}{N_1} E_1 = \frac{N_2}{N_1} V_P$	As:	$I_1 = \frac{N_2}{N_1} I_2 = \frac{N_2}{N_1} I_S$
So:	$V_S = (1 + \frac{N_2}{N_1}) V_P$	So:	$I_P = (1 + \frac{N_2}{N_1}) I_S$
Denote:	$a_R = (1 + \frac{N_2}{N_1})$	Denote:	$a_R = (1 + \frac{N_2}{N_1})$
Finally:	$V_S = a_R V_P$	Finally:	$I_P = a_R I_S$

1.9.2.2 Defining Equations: Type A in Lower

The detailed and abbreviated equivalent circuit of a Type A SVR in the lower position is shown in Fig. 1.15.

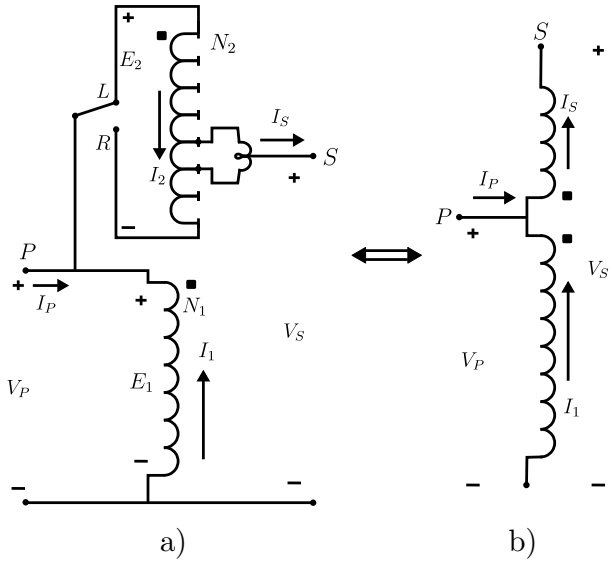

Fig. 1.15 Type A SVR in the lower: a) Detailed b) Concise [2]

Observing Fig. 1.15, the defining voltage and current equations for the Type A voltage regulator in lower are explained in Table 1.4:

Table 1.4 Defining Equations of Type A Lower Position

Voltage Equations		**Current Equations**	
Voltage Ratio:	$\frac{E_1}{N_1} = \frac{E_2}{N_2}$	Current Ratio:	$N_1 I_1 = N_2 I_2$
Primary Voltage:	$V_P = E_1$	Primary Current:	$I_P = I_2 - I_1$
Secondary Voltage:	$V_S = E_1 - E_2$	Secondary Current:	$I_S = I_2$
As:	$E_2 = \frac{N_2}{N_1} E_1 = \frac{N_2}{N_1} V_P$	As:	$I_1 = \frac{N_2}{N_1} I_2 = \frac{N_2}{N_1} I_S$
So:	$V_S = (1 - \frac{N_2}{N_1}) V_P$	So:	$I_P = (1 - \frac{N_2}{N_1}) I_S$
Denote:	$a_R = (1 - \frac{N_2}{N_1})$	Denote:	$a_R = (1 - \frac{N_2}{N_1})$
Finally:	$V_S = a_R V_P$	Finally:	$I_P = a_R I_S$

1.9.3 Generalized Equations for Single-Phase Regulators

In the Tables 1.1, 1.2, 1.3, 1.4 and 1.5, the effective regulator ratio is denoted as a_R which is either the ratio or the inverse ratio of the number of effective turns on the secondary side to the number of effective turns on the primary side of the single phase regulator for any connection. In all the derivations presented here:

$$a_R = 1 \pm \frac{N_2}{N_1} \tag{1.64}$$

In practice, the particular turns of the regulators will be unknown but the tap positions of each single-phase regulators will be known. Due to the fact that standard step regulators contain a reversing switch enabling a ±10% regulation range, usually in 32 steps, per step amounts to a 20/32% = 5/8% or 0.00625 per-unit change [2]. Hence, effective regulator

ratio can be expressed as a function of the tap position given by:

$$a_R = 1 \pm 0.00625 \text{ Tap} \tag{1.65}$$

Finally, Table 1.5 summarizes the relationships the relationships between the primary voltage and current to the secondary voltage and current, for both the Type A and Type B regulators whether in raise position or lower:

Table 1.5 Generalized Equations for Single-Phase Regulators [2]

Type	**Voltage Eq**	**Current Eq**	a_R **for Raise**	a_R **for Lower**
A	$V_P = \frac{1}{a_R} V_S$	$I_P = a_R I_S$	$a_R = 1 + \frac{N_2}{N_1}$	$a_R = 1 - \frac{N_2}{N_1}$
B	$V_P = a_R V_S$	$I_P = \frac{1}{a_R} I_S$	$a_R = 1 - \frac{N_2}{N_1}$	$a_R = 1 + \frac{N_2}{N_1}$

1.10 Three-Phase SVRs

Three-phase SVRs can be built by external connection of single-phase regulators with their own compensation circuits. For externally connected regulators, the taps on each single-phase regulator are changed separately [2]. Typical connections for externally connected three-phase regulators are:

- Three regulators connected in grounded wye
- Three regulators connected in closed delta
- Two regulators connected in open delta

Three-phase SVRs are also built through connection between the single-phase windings internal to the regulator housing. Here, a single phase current and voltage are sampled by only one compensator circuit and the taps on all windings are gang-operated to the same change [2].

Possible connections are taken such that each configurations of grounded wye and closed delta to be built with Type A raise position, Type A lower position, Type B raise position and Type B lower position regulators so that there are eight configurations. And for open delta, four possible cases each can have three different phasings between primary side phases A, B, C with Type A regulators and secondary side phases A, B, C so that there are total of 12 models. Hence, there are total twenty possible connections of SVRs that are needed to be considered in this development.

The three-phase SVR models developed here will be same for external or internal connection of single-phase regulators. But, depending on individual or gang operation of taps, there will be different control scheme for the regulator models while accommodating in the power flow model.

While describing the three-phase SVR models developed in this chapter, the phases on the primary side of the regulator are denoted by uppercase letters A, B, C and the secondary side phases are denoted by lowercase letters A, B, C.

For derivation of the voltage equations, phase-to-ground voltages are used for grounded wye configuration whereas phase-to-phase voltages are used in closed delta and open delta configurations due to the fact that there is no neutral conductor available in these configurations.

For all the configurations, Z_A, Z_B and Z_C are the corresponding regulator winding impedances referenced to the primary side to consider the effect of the regulator winding impedances. However, the regulator winding impedances can be considered as equal in each phase so that, in a matrix form, they can be denoted as:

$$\mathbf{Z}_{reg} = \begin{pmatrix} Z_A & 0 & 0 \\ 0 & Z_B & 0 \\ 0 & 0 & Z_C \end{pmatrix} = Z \begin{pmatrix} 1 & 0 & 0 \\ 0 & 1 & 0 \\ 0 & 0 & 1 \end{pmatrix} \tag{1.66}$$

Chapter 2

Consistent Tap-changing Transformer Modeling and Impacts

The tap-changing transformer models used in steady-state power system studies have been recognized as controversial for a long period. Indeed, discrepant versions arise depending on different underlying assumptions. As a consequence, two alternative models are conventionally implemented in power system simulation software packages. In this chapter, several case studies are introduced in order to highlight the important inconsistencies which can be drawn from the use of the conventional versions. A new model is proposed here to reconcile those versions, leading the way in removing the ensuing ambiguity. Moreover, a consistent model that fully explains those differences is proposed. The new model allows to adopt a third alternative that, without requiring further data than those used by conventional formulations, leads to highly improved results. Altogether, this chapter demonstrates that the adoption of the new model solves the aforementioned ambiguity, thus being a valuable tool to provide consistent results in power system studies on grids with embedded tap-changing transformers.

2.1 Introduction

TAP-changing transformers are a key asset in the regulation of voltage in power systems. Thus, models of these devices are intensively used in the different fields of electric energy systems analysis and operation. Nonetheless, the models of the tap-changing transformer conventionally used in steady-state balanced studies, such as the ones conducted during power flow calculations or voltage stability analyses, have been burdened with a long-standing controversy [4]. As described in 1.6.1, two alternative tap-changing transformer models can be found in the description of these devices in different books and simulation software packages [5–8]. Under specific operating conditions, using one model

or the other can lead to results with significant differences, which produces a serious lack of consistency in reporting the outcome of the analysis of electric grids with embedded tap-changing transformers. This fact was previously observed by other authors in [4] but, they chose one of the alternatives and focused their efforts on the manipulation of the other model to reach the same results. On the contrary, this chapter explains the causes of those discrepancies and proposes a reconciled solution.

The limited amount of information generally available about transformers, and specifically about tap-changing transformers, leads to the practice of using highly simplified models of these devices in load flow analysis or state estimation. The data is obtained from the nameplate of the device and comprises the rated power and voltage values, short-circuit impedance and tap positions. Only transformers with a tapping range exceeding $\pm 5\%$ are obliged by standards to provide further information about the short-circuit impedance (at least, values for the extreme tappings are required in that case) [3].

In [9, 10] as well as in this chapter, a consistent model is proposed with the aim of solving the aforementioned controversy. Here, the theoretical background that explains the differences caused by conventional models is presented. Moreover, by introducing an additional parameter, the new model allows to produce consistent results free of any ambiguity. This chapter tries to highlight the importance of adopting the new model by state-of-the-art software packages. With this aim, the discrepancies between conventional models are theoretically assessed and the benefits of the consensus model are clearly displayed. Furthermore, a couple of case studies, based on a classical IEEE test bus system are introduced, in order to demonstrate that the differences in the outcomes offered by the conventional models cannot be neglected even in normal operating conditions.

In section 2.2, the two conventional models, previously pointed out in chapter 1, are presented with detail. Then in section 2.3, a new model for the tap-changing transformer is proposed, which opens the door to a much more accurate description of the device. Section 2.4 uses the new model to clearly explain the reasons for the aforementioned discrepancies. An assessment of the errors caused by conventional models is also presented therein. Section 2.5 describes three case studies to highlight the importance of the new proposal. Finally, the conclusions of this study are drawn in section 2.6.

2.2 Conventional Tap-Changing Transformer Models

As pointed out in subsection 1.6.1, the most widely used conventional tap-changing transformer models are derived from two different (and not easy to justify) alternatives: either considering that all the short-circuit impedance of the transformer, z_{sc}, is provided by the winding at the off-nominal side (Type 1) or by the one at the nominal side (Type 2). Both extreme assumptions are shown in Fig. 2.1 for a transformer with an off-nominal turns ratio $a : 1$, where y_{sc} is the short-circuit admittance of the transformer (typically provided by the manufacturer as the short-circuit impedance at the principal tap position

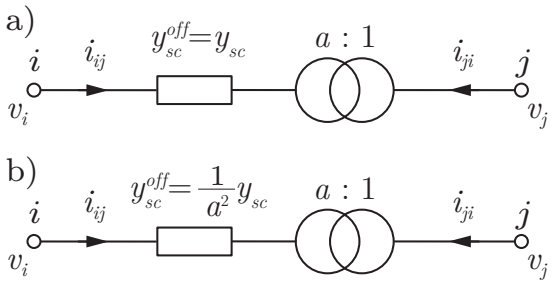

Fig. 2.1 Alternative assumptions made in conventional tap-changing transformer models. (a) Type 1, and (b) Type 2

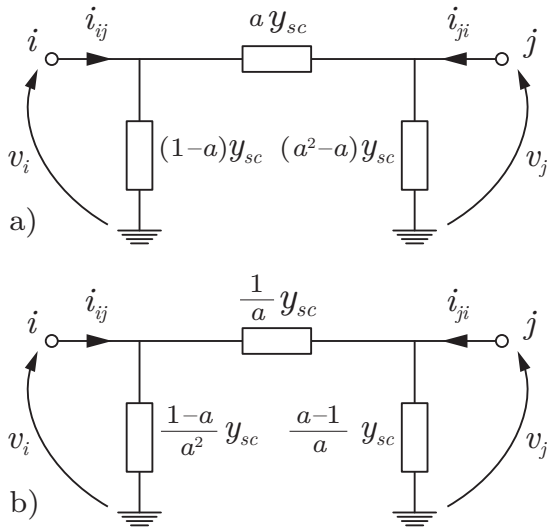

Fig. 2.2 The π-equivalent circuit of conventional tap-changing transformer models. (a) Type 1, and (b) Type 2

and shown in the nameplate of the device). In this figure, the short-circuit admittance has been referred in both cases to the off-nominal side, and thus designated as y_{sc}^{off}.

The well-known relations that apply to ideal transformers, together with Kirchhoff's Laws yield

$$v_i = \frac{i_{ij}}{y_{sc}^{off}} + a v_j, \tag{2.1}$$

$$i_{ij} = -\frac{i_{ji}}{a}, \tag{2.2}$$

and thus, the nodal equations of the device can be written in a compact form as

$$\begin{bmatrix} i_{ij} \\ i_{ji} \end{bmatrix} = \begin{bmatrix} Y_{ii} & Y_{ij} \\ Y_{ji} & Y_{jj} \end{bmatrix} \begin{bmatrix} v_i \\ v_j \end{bmatrix}. \tag{2.3}$$

The elements of the bus-admittance matrix, Y_{bus}, are discussed in chapter 1 and also shown in Table 2.1 for the Type 1 and Type 2 models, according to the value of y_{sc}^{off} used in each case. From those values, as discussed in chapter 1, the parameters of the π-equivalent circuit of both transformer models can be straightforwardly derived. They have been explicitly shown in Fig. 2.2.

2.3 Description of the Consistent Model

Power system studies do not normally require the shunt branch of the equivalent model of the transformer to be taken into account. Thus, when dealing with nominal turns ratios, the use of the detailed or simplified model of the transformer makes no difference, as in both cases the device is reduced to a series impedance. However, this is no longer true when the transformer is using an off-nominal turns ratio. As it is demonstrated in this chapter, the simplified model of the transformer can lead to important errors.

Thus a new model, presented in [9] and also in this chapter, was proposed in order to remove any ambiguity from the results of power system studies with embedded tap-changing transformers. This model, designated in the following as Type 3, includes a new parameter in order to account for the contribution of each of the transformer windings to the short-circuit impedance. This parameter, k, is defined as the ratio between the p.u. impedance of the winding at the nominal turns side, z_j and the p.u. impedance of the tapped winding (i.e. the one at the off-nominal turns side), z_i. Thus, from the off-nominal side, the series admittance can then be calculated as

$$y_{sc}^{off} = \frac{1}{z_i + a^2 z_j} = \frac{1}{z_i(1 + ka^2)} \tag{2.4}$$

As discussed in 1.4 and 1.8.1, y_{sc}, the short-circuit admittances obtained during the short-circuit test and shown at the nameplate are most commonly obtained at the principal tap ($a = 1$). So the short-circuit admittance is

$$y_{sc} = \frac{1}{z_i + z_j} = \frac{1}{z_i(1 + k)}. \tag{2.5}$$

Therefore:

$$z_i = \frac{1}{y_{sc}(1 + k)}. \tag{2.6}$$

From 2.4 and 2.6, we can deduce

$$y_{sc}^{off} = \frac{1}{z_i + a^2 z_j} = \frac{1}{z_i(1 + ka^2)} = \frac{1 + k}{1 + ka^2} y_{sc}. \tag{2.7}$$

By applying (2.1) and (2.2) to the new value of y_{sc}^{off}, the parameters of the Y_{bus} matrix in (2.3) can be immediately determined for the Type 3 model. They have also been shown in Table 2.1.

$$Y_{ii} = \frac{1 + k}{1 + ka^2} y_{sc}, \tag{2.8}$$

$$Y_{ij} = Y_{ji} = -\frac{a\,(1 + k)}{1 + ka^2} y_{sc}, \tag{2.9}$$

$$Y_{jj} = \frac{a^2\,(1 + k)}{1 + ka^2} y_{sc}. \tag{2.10}$$

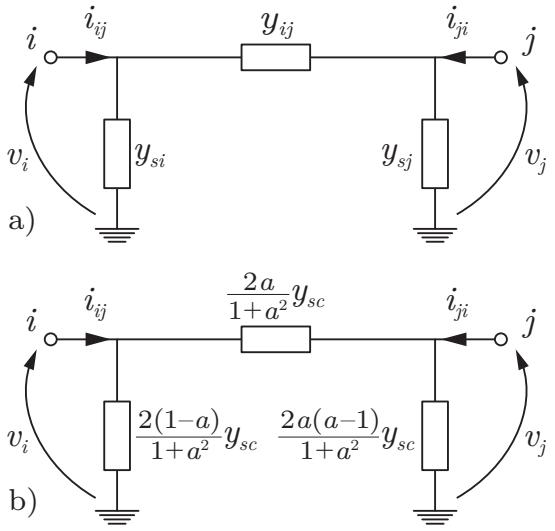

Fig. 2.3 Consensus model of the tap-changing transformer. (a) General model, and (b) Recommended set-up

Table 2.1 Y_{bus} Matrix for the Different Tap-changing Transformer Models

Y_{bus}	**Type 1**	**Type 2**	**Type 3**	**Type 3** ($k = 1$)
Y_{ii}	y_{sc}	$\frac{1}{a^2}y_{sc}$	$\frac{1+k}{1+ka^2}y_{sc}$	$\frac{2}{1+a^2}y_{sc}$
$Y_{ij} = Y_{ji}$	$-ay_{sc}$	$-\frac{1}{a}y_{sc}$	$-\frac{a(1+k)}{1+ka^2}y_{sc}$	$-\frac{2a}{1+a^2}y_{sc}$
Y_{jj}	a^2y_{sc}	y_{sc}	$\frac{a^2(1+k)}{1+ka^2}y_{sc}$	$\frac{2a^2}{1+a^2}y_{sc}$

From those values, the different admittances of the corresponding π-equivalent circuit, as depicted in Fig. 2.3(a), can be directly obtained as

$$y_{ij} = -Y_{ij} = \frac{a\,(1+k)}{1+ka^2}y_{sc}, \tag{2.11}$$

$$y_{si} = Y_{ii} + Y_{ij} = \frac{(1-a)\,(1+k)}{1+ka^2}y_{sc}, \tag{2.12}$$

$$y_{sj} = Y_{jj} + Y_{ij} = \frac{a\,(a-1)\,(1+k)}{1+ka^2}y_{sc}. \tag{2.13}$$

It is important to notice that the conventional models, Type 1 and Type 2, are just particular cases of the proposed general model, Type 3. Indeed, assigning the values 0 and ∞ to parameter k in (2.11)–(2.13) yields to the well-known values already presented in Fig. 2.2.

2.4 Error Assessment and Reconciliation of Conventional Models

The practical use of the new model should take into account that, usually, the data provided to the engineering practitioner in order to model the different components of the power system, and specifically, tap-changing transformers, is quite limited. The particular contribution of each transformer winding to the short-circuit impedance is not a nameplate value and, since this specification is not required by standards [35], it is seldom provided by the manufacturer. Thus, setting up the value of the new parameter, k, turns to be challenging.

The discrepancy of conventional models with respect to the consensus model, assessed using the differences that arise in the voltage of the nominal winding, v_j, when the off-nominal turns side is fed at a fixed voltage, v_i, and a fixed current, i_{ij}, can be obtained, as a function of k, according to

$$\Delta v_j^0 = v_j^0 - v_j^k = \frac{k\,(a^2-1)}{a\,(1+k)}\frac{i_{ij}}{y_{sc}}, \tag{2.14}$$

$$\Delta v_j^\infty = v_j^\infty - v_j^k = \frac{1-a^2}{a\,(1+k)}\frac{i_{ij}}{y_{sc}}, \tag{2.15}$$

where v_j^0, v_j^∞ and v_j^k stand for the values obtained with Type 1, Type 2 and Type 3 models, respectively.

From (2.14) and (2.15), it can be concluded that the discrepancies in v_j between the different models grow with the loading of the transformer as well as with the tap position (extreme tap positions, i.e. those further from the central tap, exacerbate the differences). Due to the mainly inductive behavior of transformer short-circuit impedances, the effect of those discrepancies mostly affects the magnitude of voltage when feeding reactive loads (e.g., in that case, Δv_j^0 is close to aligned with v_j^0 and v_j^k). Conversely, resistive loads tend to magnify the differences in voltage phase angle. A detailed analysis of these facts can be found in [9].

Another interesting conclusion that can be drawn from (2.14) and (2.15) is that the particular case $k = 1$ is the midpoint between the extreme assumptions implied by conventional models. Certainly, for $k = 1$, it can be followed that $\Delta v_j^0 = -\Delta v_j^\infty$. Thus, using $k = 1$ guarantees the minimization of the maximum error caused by the lack of precise knowledge of the contribution of each transformer winding to the short-circuit impedance. The Y_{bus} elements of this recommended set-up are shown in Table 2.1 and the corresponding π-equivalent circuit is depicted in Fig. 2.3(b). Specifically, using $k = 1$ assures that the error is limited to

$$\Delta v_j^{max} = \pm\frac{a^2-1}{2a}\frac{i_{ij}}{y_{sc}}. \tag{2.16}$$

The use of $k = 1$ implies the assumption of an equal contribution of both transformer windings (expressed in per-unit values) to the short-circuit impedance. In fact, this is a conventional engineering practice used in detailed transformer modeling [36–38], which reinforces the recommendation to use this set-up when no further data is available.

Undoubtedly, the use of parameter estimation techniques may allow to improve the quality of the set-up of tap-changing transformer models in real scenarios by obtaining accurate values of k for each specific device from the off-line analysis of field measurements. This issue is discussed in detail and a resolution is presented in chapter 5. However, it should be highlighted that, regardless of the accuracy of the model, which is dependent on the quality of the estimation of k, the consensus model puts an end to the lack of consistency in communicating the results of power system studies, provided that the set-up of this parameter is included in the data set.

2.5 Case Studies

The discrepancies in the results provided by the conventional tap-changing transformer models are not trivial. A set of case studies are provided in this section in order to highlight this fact, and thus, to urge the adoption of the new model by power system software packages. As it is demonstrated in this section, the use of the new model can guarantee the consistency of the results obtained in such common power system studies as power flow or voltage stability analysis.

2.5.1 Analysis of the Discrepancies in a Single Tap-changing Transformer

The first case study is performed on a very basic test-bed with just one tap-changing transformer in it, as the one represented in Fig. 2.1. Let us consider an 80 MVA, 50 Hz, 220/132 kV ±10% transformer with a nameplate short-circuit impedance, z_{sc}, of $0.01+0.12j$ and a tap changer, located on the highest voltage side, with 21 positions and a tapping step of 1%. If further data about the short-circuit impedance at extreme tap positions were available, as it should be according to [3], a different value of z_{sc} could be calculated by linear interpolation for any tap position. In any case, this straightforward task will not be used in this case study not to obscure the core of the proposal.

Fig. 2.4 shows the voltage of the transformer at the nominal turns side when fed by a constant voltage of 1 pu at the off-nominal turns side for each tap position available. In each case, the transformer is delivering the rated current at the off-nominal turns side. Two different power factors are considered by selecting the phase angle between v_i and i_{ij}, which is called θ in the following: (a) a unity power factor, $\theta = 0°$, and (b) a pure capacitive case, $\theta = 90°$. The voltage is calculated both for the conventional models ($k = 0$ and $k = \infty$) and for the proposed model, assuming a fair contribution of both windings

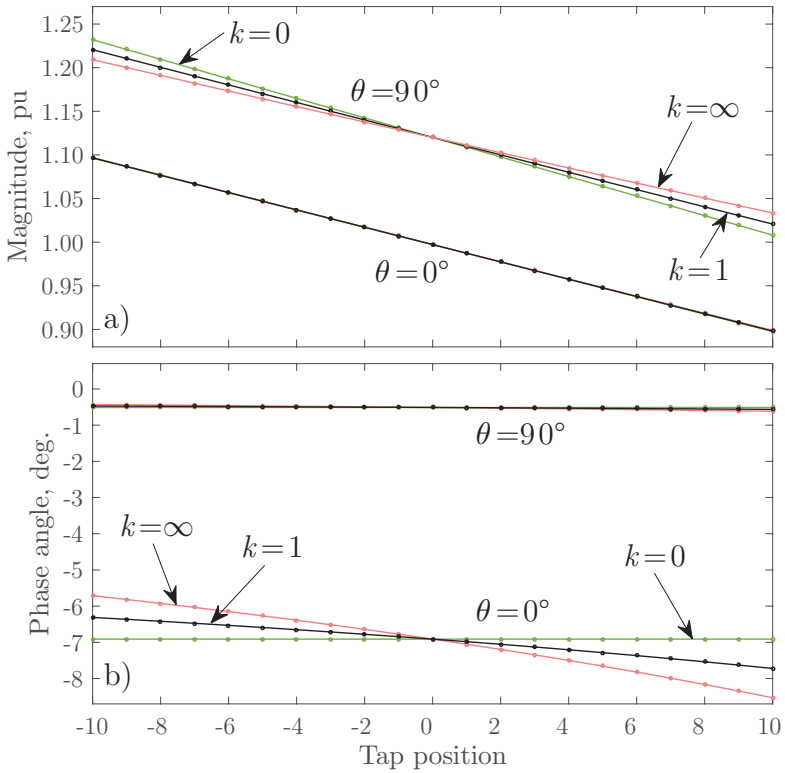

Fig. 2.4 Nominal-turns side voltage for the different tap positions. Transformer at rated current with two different power factors: unity ($\theta = 0°$) and pure capacitive ($\theta = 90°$). (a) Voltage magnitude, and (b) Voltage phase angle

to the short-circuit impedance, i.e. $k = 1$. Although this assumption is probably not exact (this data is seldom provided by the manufacturer), as discussed in 2.4, it is for sure a better estimate in line with accepted engineering practices. In Fig. 2.4.(a) the module of the voltage at the off-nominal turns side is shown. At high power factors, the differences between the alternative transformer models can be ignored. However, important discrepancies arise at poor power factors. On the other hand, Fig. 2.4.(b) shows the phase angle of the voltage at the off-nominal turns side. The differences between the different models result evident now at high power factors. The new model offers a consensus estimate even if k is not accurately known.

The errors arisen from the use of conventional models, calculated by taking the new model as a reference (with $k = 1$), were obtained at rated current for every tap position and power factor (including reverse power flow). In Fig. 2.5.(a) the maximum deviation of the voltage at the nominal turns side, $|v_j^0| - |v_j^1|$ and $|v_j^\infty| - |v_j^1|$, is depicted for each power factor. This graph proves that the error in the calculation of the voltage can rise to near 1.3% in extreme positions of the tap changer when dealing with poor power factors. Notice that the same result can be obtain from (2.14) and (2.15). Fig. 2.5.(b) shows the maximum deviation of the phase angle of the voltage at the nominal turns side. Noticeably, this error evolves in the opposite direction, being maximum for high power factors, when it reaches values as high as 0.8°, and negligible for reactive power flows. In a symmetrical tap changer, as the one considered in this chapter, the maximum errors are found at the

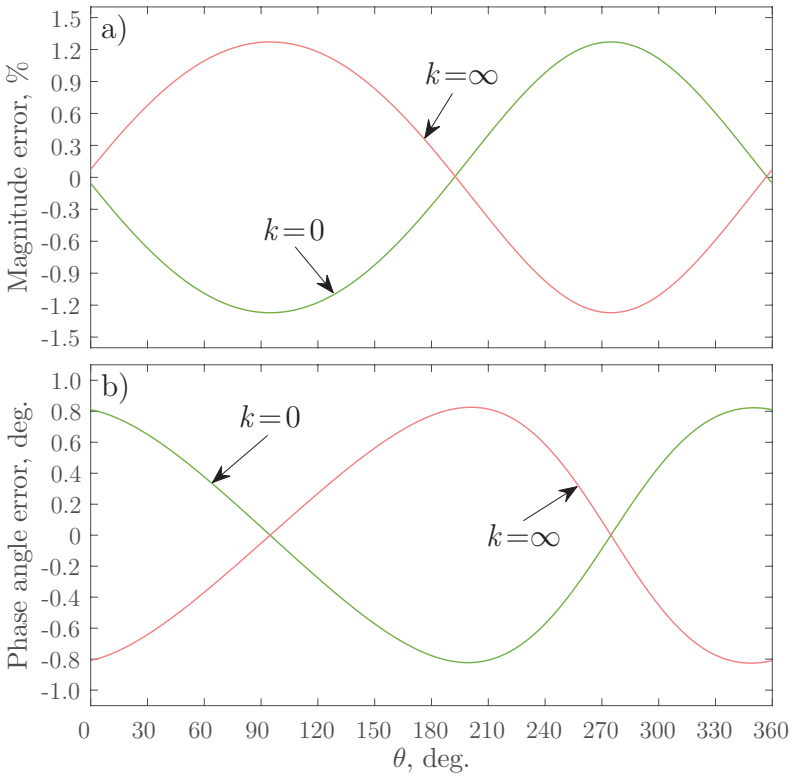

Fig. 2.5 Maximum deviation in the calculation of the nominal-turns side voltage at rated current. (a) Voltage magnitude, and (b) Voltage phase angle

highest position of the tap (and not at the lowest), as can be easily proved from (2.14) and (2.15).

2.5.2 Power Flow Analysis

For this case study, the IEEE 57-bus system, which is shown in Fig. 2.6, has been adopted as a test case [39]. It represents a simple approximation of the American Electric power system in the U.S. Midwest as it was in the early 1960s which has been extensively used as a test system by the power community. The IEEE 57-bus system comprises 57 buses, 7 generators, 42 loads and 17 transformers. It is important to note that 15 of these transformers are set out of the principal tap at the operating point defined by the test case. This fact makes the system especially suitable to test the new tap-changing transformer model. Table 2.2 shows the parameters and set-up of those transformers as described in the IEEE 57-bus system data files.

The state variables of the IEEE 57-bus system have been calculated by using a Newton-based power flow method for the different tap-changing transformer models under evaluation. MATPOWER [40] was used to conduct this implementation. It is important to note that this open-source electric power system simulation tool assumes one of the conventional tap-changing transformer models commented in this chapter. Specifically, MATPOWER considers all the short-circuit impedance of the tap-changing transformer as being provided by the winding at the nominal turns side (i.e. $k = \infty$) [41]. The

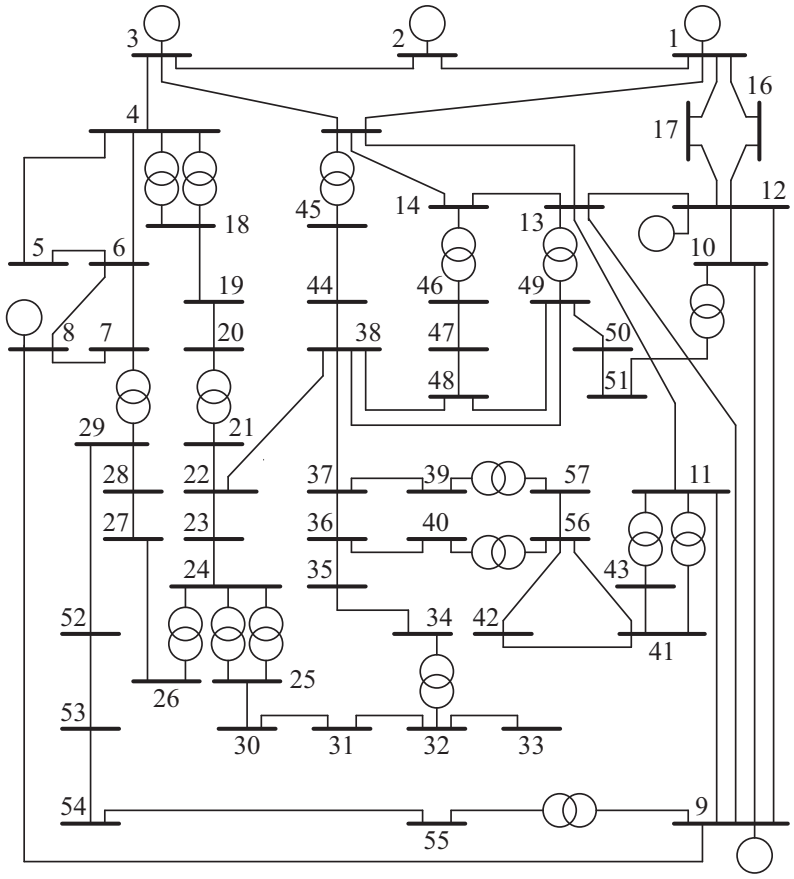

Fig. 2.6 IEEE 57-bus system.

Table 2.2 Transformers Set Out of the Principal Tap in the IEEE 57-bus System

From bus	**To bus**	R, **p.u**	X, **p.u**	**Tap,** a
4	18	0	0.5550	0.970
4	18	0	0.4300	0.978
21	20	0	0.7767	1.043
24	26	0	0.0473	1.043
7	29	0	0.0648	0.967
34	32	0	0.9530	0.975
11	41	0	0.7490	0.955
11	45	0	0.1042	0.955
14	46	0	0.0735	0.900
10	51	0	0.0712	0.930
13	49	0	0.1910	0.895
11	43	0	0.1530	0.958
40	56	0	1.1950	0.958
39	57	0	1.3550	0.980
9	55	0	0.1205	0.940

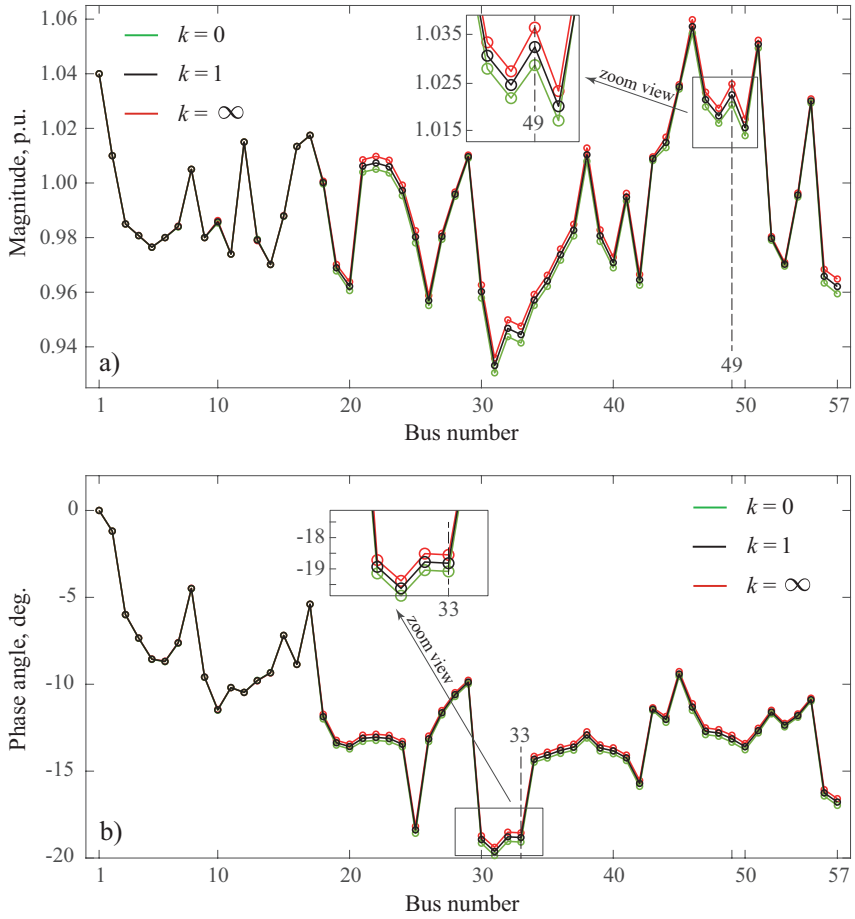

Fig. 2.7 Voltage profile of the IEEE 57-bus system using the conventional and new tap-changing transformer models. (a) Voltage magnitude and (b) Phase angle.

modification of those functions of the software devoted to the construction of the bus admittance matrix, has allowed to test also the other alternatives (i.e, the conventional model which considers all the short-circuit impedance as provided by the off-nominal turns side, $k = 0$, and the new proposal, in which a balanced contribution is considered, $k = 1$). Those alternative transformer models can be directly implemented in MATPOWER by considering equations (2.11)–(2.13). Fig. 2.7 shows the resulting voltage profile of the IEEE 57-bus system according to the different tap-changing transformer models. The detailed results, for those buses showing the highest inconsistencies, are reported in Table 2.3.

Table 2.3 Bus Voltages Showing the Highest Discrepancies

	Tap-changing transformer model					
	Type 1 ($k = 0$)		**Type 2** ($k = \infty$)		**Type 3** ($k = 1$)	
Bus	Magnitude (p.u.)	Phase angle (deg.)	Magnitude (p.u.)	Phase angle (deg.)	Magnitude (p.u.)	Phase angle (deg.)
33	0.941	−19.081	0.948	−18.552	0.944	−18.819
49	1.029	−13.336	1.036	−12.936	1.032	−13.141

As it is shown in Table 2.3 and is also highlighted in Fig. 2.7, the maximum discrepancy in the calculation of voltage magnitudes between the two conventional models (i.e. $k = \infty$ and $k = 0$) takes place at bus 49. This discrepancy reaches a value of 7.63×10^{-3} p.u. (i.e. 0.763%), which can be considered a significant amount even though the transformers of the IEEE 57-bus system are not set at particularly extreme tap positions. In the same vein, the maximum discrepancy in the calculation of voltage phase angle arises at bus 33 with a value of 0.529 deg. Obviously, those differences in the state variables spread to the post-calculation of other magnitudes with an important impact on active and reactive power flows, currents, etc.

This test clearly reinforces the conclusion of the present contribution. Indeed, it confirms that the use of different tap-changing transformer models, such as the widely adopted $k = 0$ (Type 1) and $k = \infty$ (Type 2) versions, leads to different and thus, inconsistent results. Conversely, the adoption of the new model by software packages for power system analysis can solve the problem, just by allowing the user to fix and report the specific value of k utilized in the study. If further information is not available to precisely determine this parameter, selecting it as $k = 1$ provides a sensible estimation that leads to results that lie between the two conventional solutions and, what is more, minimizes the maximum expected error.

2.5.3 Voltage Stability Analysis

Taking again the IEEE 57-bus system as a basis, voltage stability has been tested by gradually increasing the active power demand at bus 49. Notice that this bus was selected for the study in view of the results of the power flow analysis shown in subsection 2.5.2. Indeed, these results demonstrate that the voltage magnitude at bus 49 show the highest discrepancy when calculated using different conventional tap-changing transformer models.

According to [39], the active power demand at bus 49 in the IEEE 57-bus system is 18 MW. This active power was increased in steps of 1 MW and, in each case, the power flow analysis of the system was repeated for the conventional tap-changing transformer models and for the new proposed model with the recommended set-up of $k = 1$. The results, in the form of the power-voltage curve (also known as "nose" curve or P-V curve), are depicted in Fig. 2.8.

Notice that voltage collapse is reached at quite different values of the active power demand at bus 49. While stability is lost at 364 MW in the case of $k = 0$, collapse is not reached until 404 MW if the model with $k = \infty$ is considered. The first case may be a too conservative approach while the second is certainly underestimating the voltage drop. On the contrary, the use of the new model with $k = 1$ estimates that the voltage collapse would take place at 382 MW which is certainly a sensible compromise.

Once more, this voltage stability analysis comes to emphasize the important differences that may arise from the use of the different versions of conventional tap-changing transformers. Security constraints may be compromised by using simplified assumptions,

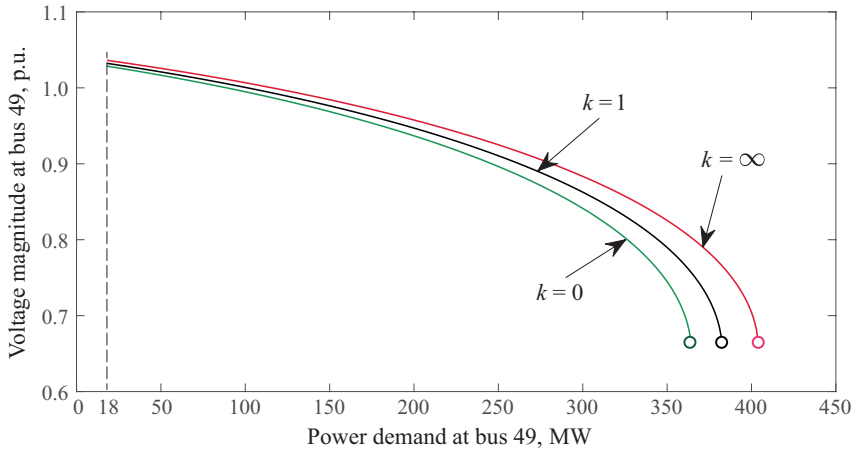

Fig. 2.8 Power-voltage curves at bus 49 for the conventional tap-changing transformer models ($k = \infty$ and $k = 0$) and for the new proposed model ($k = 1$).

such as the ones implied in conventional models. What is more, even if $k = 1$ is a sensible estimation in a context of scarce data, a precise knowledge of this parameter could add certainty to the results obtained in this type of power system studies.

2.6 Conclusion

The use of the simplified equivalent model of the transformer is universally admitted when conducting power system studies, due to the low impact of the magnetizing branch and the inherent benefit of removing a useless bus from the problem. However, neglecting the fact that the short-circuit impedance is the result of contributions from two different windings can lead to unacceptable discrepancies in the formulation of the tap-changing transformer model. This chapter proposes a new general model which includes the contribution of each winding to the short-circuit impedance. Although this data is not generally available, the new model allows to consider a fair contribution (50/50) of both windings to this parameter, which is an accepted practice in engineering. The new model can be tuned to match the results from conventional alternatives, which consider the short-circuit impedance as caused by only one of the transformer windings, either the off-nominal or nominal turns side. This fact makes the new model useful to understand the basis of each formulation, providing a clear perspective on the influence of the underlying assumptions. The chapter demonstrates that the discrepancies caused by conventional models can be unacceptable at extreme tap positions and are greatly influenced by the operating point of the transformer. The studies conducted here demonstrate that those discrepancies can be significant even in the case of a well-known standard grid, which is illustrated by a power flow analysis and a stability analysis. The inclusion of the proposed tap-changing transformer model in power system software packages, tuned with the recommended values shown in this chapter, can significantly help to improve the consistency of power system studies without the need to provide additional data.

Chapter 3

Tap-changing Transformer Modeling Variations

Models of the tap-changing transformers, both the conventional and consistent ones, vary due to the operational setup, chosen references for base quantities and number of phases to be considered. For instance, these models will differ depending on whether tap-changing transformers are operating at nominal or off-nominal turn-ratios. Models can be formed in physical quantities; however, most frequently they are expressed in the per-unit system. Even when the model is expressed in the per-unit system, it varies depending on chosen bases. Moreover, distribution systems are often unbalanced, so, they cannot be accurately modeled through single-phase equivalents. Therefore, to model unbalanced distribution systems for static power system studies, three-phase models of transformers are required. In this chapter, shedding light on the ambiguity in tap-changing transformer's modeling, different variations of the models are derived and presented for different cases of off-nominal or nominal operation, chosen bases, and number of phases.

3.1 Introduction

Modeling voltage-regulating transformers, i.e., tap-changing transformers is a complex task. There are various ambiguities in forming the π-equivalent models for such transformers. In chapter 1 and 2, it was shown that while two conventional models work properly at the central tap, they differ in results while operating in off-nominal turn-ratios. Hence, a consistent model is established in chapter 2.

In this chapter, it will be shown that tap-changing transformer models, operating at both nominal and off-nominal turn-ratios also varies depending on the chosen base for referring to the per-unit system. In this regard, the established consistent model is further extended in this chapter for the variation of chosen bases. For both nominal and

off-nominal operation, tap-changing transformer models expressed in physical quantities are also derived and presented here. Then, importantly, three-phase models of tap-changing transformers both in nominal and off-nominal operation are derived in this chapter. In this regard, the established consistent model in chapter 2 is also extended for three-phase steady-stated power system studies.

3.2 Single-phase Transformer Model at Nominal Turn-ratios

In this section, a π-equivalent model for the tap-changing transformer operating at the nominal (central) tap is derived. Although the model of the tap-changing transformer at the central tap is well-known (turns out to be the same as the model of a fixed turn-ratio transformer, it is included here to establish a methodology that is extended later in this chapter to the model at other taps and, subsequently, to the three-phase transformer.

3.2.1 In Physical Quantities

In this sub-section, three models of the single-phase transformer in physical quantities are derived, corresponding to the traditional ones and the consensus model. The results will confirm that the resulting models become identical when operating at nominal turn-ratios.

3.2.1.1 Short-circuit Impedance at the Nominal Side

As described in chapter 1, one of the traditional models of the tap-changing transformer considers that all the short-circuit impedance of the device is provided by the nominal side. See Fig. 3.1.

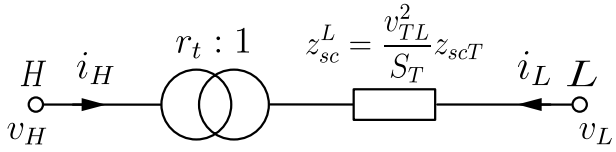

Fig. 3.1 Tap-changing transformer with short-circuit impedance at the nominal side

Let z_{scT} be the impedance of the transformer expressed in p.u. at its own bases (i.e. v_{TH}, the base voltage at the primary side, v_{TL}, the base voltage at the secondary side, and S_T, the base power of the transformer). So if it is assumed that the impedance is entirely provided by the nominal side, the impedance in ohms, z_{sc}^L, is calculated as

$$z_{sc}^L = \frac{v_{TL}^2}{S_T} z_{scT}. \tag{3.1}$$

Let r_t be the transformation ratio in physical quantities of the transformer. Therefore, as in (1.40), the nodal equations are

$$\begin{bmatrix} i_H \\ i_L \end{bmatrix} = \begin{bmatrix} \frac{1}{r_t^2 z_{sc}^L} & \frac{-1}{r_t z_{sc}^L} \\ \frac{-1}{r_t z_{sc}^L} & \frac{1}{z_{sc}^L} \end{bmatrix} \begin{bmatrix} v_H \\ v_L \end{bmatrix}. \tag{3.2}$$

The components of the π-equivalent model can then be expressed as

$$y_{ij} = \frac{1}{r_t z_{sc}^L}, \tag{3.3}$$

$$y_{si} = \frac{1}{r_t z_{sc}^L}\left(\frac{1}{r_t} - 1\right), \tag{3.4}$$

$$y_{sj} = \frac{1}{z_{sc}^L}\left(1 - \frac{1}{r_t}\right). \tag{3.5}$$

By definition of transformation ratio,

$$r_t v_{TL} = v_{TH}. \tag{3.6}$$

If the impedance value of the transformer in p.u., z_{scT}, is used with the bases of own transformer, from (3.1), (3.2), and (3.6), the nodal equations can be expressed as

$$\begin{bmatrix} i_H \\ i_L \end{bmatrix} = \begin{bmatrix} \frac{S_T}{v_{TH}^2 z_{scT}} & \frac{-S_T}{v_{TH} v_{TL} z_{scT}} \\ \frac{-S_T}{v_{TH} v_{TL} z_{scT}} & \frac{S_T}{v_{TL}^2 z_{scT}} \end{bmatrix} \begin{bmatrix} v_H \\ v_L \end{bmatrix}. \tag{3.7}$$

And the components of the π-equivalent model are

$$y_{ij} = \frac{S_T}{v_{TH} v_{TL} z_{scT}}, \tag{3.8}$$

$$y_{si} = \frac{S_T}{v_{TH} z_{scT}}\left(\frac{1}{v_{TH}} - \frac{1}{v_{TL}}\right), \tag{3.9}$$

$$y_{sj} = \frac{S_T}{v_{TL} z_{scT}}\left(\frac{1}{v_{TL}} - \frac{1}{v_{TH}}\right). \tag{3.10}$$

3.2.1.2 Short-circuit Impedance at the Off-nominal Side

The second type of the traditional models of the tap-changing transformer, as described in chapter 1, considers that all the short-circuit impedance of the device is provided by the off-nominal side. See Fig. 3.2. Thus, the impedance (expressed in ohms) at this side, z_{sc}^H, can be calculated as from the nameplate values of the transformer as:

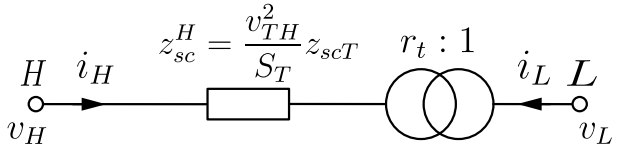

Fig. 3.2 Tap-changing transformer with short-circuit impedance at the off-nominal side

$$z_{sc}^{H} = \frac{v_{TH}^2}{S_T} z_{scT}. \tag{3.11}$$

Applying the nodal equations, as in (1.39), the following expression is obtained

$$\begin{bmatrix} i_H \\ i_L \end{bmatrix} = \begin{bmatrix} \frac{1}{z_{sc}^H} & \frac{-r_t}{z_{sc}^H} \\ \frac{-r_t}{z_{sc}^H} & \frac{r_t^2}{z_{sc}^H} \end{bmatrix} \begin{bmatrix} v_H \\ v_L \end{bmatrix}. \tag{3.12}$$

The π-equivalent model can then be expressed as

$$y_{ij} = \frac{r_t}{z_{sc}^H}, \tag{3.13}$$

$$y_{si} = \frac{1}{z_{sc}^H}(1 - r_t), \tag{3.14}$$

$$y_{sj} = \frac{r_t}{z_{sc}^H}(r_t - 1). \tag{3.15}$$

And by using the short-circuit impedance of the transformer in p.u. (in the transformer bases), i.e. z_{scT}, the nodal equations and the components of the π-equivalent model turn out to be the same as the ones in the previous case, (3.7) - (3.10). Indeed, it follows that

$$\begin{bmatrix} i_H \\ i_L \end{bmatrix} = \begin{bmatrix} \frac{S_T}{v_{TH}^2 z_{scT}} & \frac{-S_T}{v_{TH} v_{TL} z_{scT}} \\ \frac{-S_T}{v_{TH} v_{TL} z_{scT}} & \frac{S_T}{v_{TL}^2 z_{scT}} \end{bmatrix} \begin{bmatrix} v_H \\ v_L \end{bmatrix}. \tag{3.16}$$

And the components of the π-equivalent model are

$$y_{ij} = \frac{S_T}{v_{TH} v_{TL} z_{scT}}, \tag{3.17}$$

$$y_{si} = \frac{S_T}{v_{TH} z_{scT}}\left(\frac{1}{v_{TH}} - \frac{1}{v_{TL}}\right), \tag{3.18}$$

$$y_{sj} = \frac{S_T}{v_{TL} z_{scT}}\left(\frac{1}{v_{TL}} - \frac{1}{v_{TH}}\right). \tag{3.19}$$

3.2.1.3 Short-circuit Impedance Distributed at Both Sides

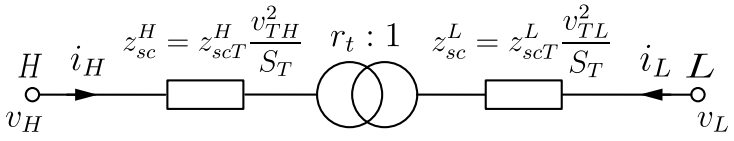

Fig. 3.3 Tap-changing transformer with short-circuit impedance at both sides

Now suppose that the short-circuit impedance of the transformer, expressed in p.u . in its own bases, is distributed between off-nominal and nominal, in such a way that

$$z_{scT} = z_{scT}^H + z_{scT}^L. \tag{3.20}$$

Then, as it can be seen from chapter 2, k, the p.u. impedance ratio is

$$k = \frac{z_{scT}^{L}}{z_{scT}^{H}}. \tag{3.21}$$

And the impedances to each side, in physical values can be calculated as

$$Z_{sc}^{H} = Z_{scT}^{H}\frac{v_{TH}^{2}}{S_T}, \tag{3.22}$$

$$Z_{sc}^{L} = Z_{scT}^{L}\frac{v_{TL}^{2}}{S_T}. \tag{3.23}$$

This concept of consistent transformer model is shown in Fig. 3.3. The nodal equations can thus be expresses as

$$\begin{bmatrix} i_H \\ i_L \end{bmatrix} = \begin{bmatrix} \frac{1}{r_t^2 z_{sc}^{L} + z_{sc}^{H}} & \frac{-r_t}{r_t^2 z_{sc}^{L} + z_{sc}^{H}} \\ \frac{-r_t}{r_t^2 z_{sc}^{L} + z_{sc}^{H}} & \frac{r_t^2}{r_t^2 z_{sc}^{L} + z_{sc}^{H}} \end{bmatrix} \begin{bmatrix} v_H \\ v_L \end{bmatrix}. \tag{3.24}$$

So, the components of the π-equivalent model are

$$y_{ij} = \frac{r_t}{r_t^2 z_{sc}^{L} + z_{sc}^{H}}, \tag{3.25}$$

$$y_{si} = \frac{1 - r_t}{r_t^2 z_{sc}^{L} + z_{sc}^{H}}, \tag{3.26}$$

$$y_{sj} = \frac{r_t(r_t - 1)}{r_t^2 z_{sc}^{L} + z_{sc}^{H}}. \tag{3.27}$$

Substituting the physical quantities, z_{sc}^{L} and z_{sc}^{H} in (3.24), by their corresponding p.u. quantities (at the transformer base), z_{scT}^{L} and z_{scT}^{H}, which are in fact the two components of total p.u. impedance z_{scT}, it follows that

$$\begin{bmatrix} i_H \\ i_L \end{bmatrix} = \begin{bmatrix} \frac{S_T}{v_{TH}^2 z_{scT}} & \frac{-S_T}{v_{TH} v_{TL} z_{scT}} \\ \frac{-S_T}{v_{TH} v_{TL} z_{scT}} & \frac{S_T}{v_{TL}^2 z_{scT}} \end{bmatrix} \begin{bmatrix} v_H \\ v_L \end{bmatrix}. \tag{3.28}$$

So again, the components of the π-equivalent model are

$$y_{ij} = \frac{S_T}{v_{TH} v_{TL} z_{scT}}, \tag{3.29}$$

$$y_{si} = \frac{S_T}{v_{TH} z_{scT}}\left(\frac{1}{v_{TH}} - \frac{1}{v_{TL}}\right), \tag{3.30}$$

$$y_{sj} = \frac{S_T}{v_{TL} z_{scT}}\left(\frac{1}{v_{TL}} - \frac{1}{v_{TH}}\right). \tag{3.31}$$

Thus, it can be concluded that if the short-circuit impedance is expressed in p.u. values in terms of transformer bases, z_{scT}, and while the transformer operates at the nominal turn-ratio, the nodal equations, and the components of the π-equivalent model are the same in all three forms of the tap-changing transformer model.

3.2.2 In the Per-Unit System

In this subsection, the form of transformer model as in (3.28) - (3.31) will be extended into p.u. systems. In this case, even if the transformer is still operated at a nominal turns-ratio, the model varies depending on the values of the quantities selected as system bases (which are not forced here to be the same as the transformer bases).

Let the chosen bases for the study of the system be v_{BH}, v_{BL}, and S_B. Note that these bases may not respond to the transformation ratio, hence, in general

$$r_t = \frac{v_{TH}}{v_{TL}} \neq \frac{v_{BH}}{v_{BL}}. \tag{3.32}$$

So the nodal equations can be expressed as

$$\begin{bmatrix} i_{Hpu} \\ i_{Lpu} \end{bmatrix} = \begin{bmatrix} Y_{HH} & Y_{HL} \\ Y_{LH} & Y_{LL} \end{bmatrix} \begin{bmatrix} v_{Hpu} \\ v_{Lpu} \end{bmatrix}, \tag{3.33}$$

where

$$Y_{HH} = \left(\frac{v_{BH}}{v_{TH}}\right)^2 \frac{S_T}{S_B} \frac{1}{z_{scT}}, \tag{3.34}$$

$$Y_{HL} = Y_{LH} = \frac{-v_{BH}v_{BL}}{v_{TH}v_{TL}} \frac{S_T}{S_B} \frac{1}{z_{scT}}, \tag{3.35}$$

$$Y_{LL} = \left(\frac{v_{BL}}{v_{TL}}\right)^2 \frac{S_T}{S_B} \frac{1}{z_{scT}}. \tag{3.36}$$

If the short-circuit impedance of the transformer is expressed in the bases of the system, two possibilities arise: to use the base voltage of the off-nominal side or the base voltage of the nominal side. In this case, let us opt for the latter case so that

$$z^L_{scpu} = z_{scT} \left(\frac{v_{TL}}{v_{BL}}\right)^2 \frac{S_B}{S_T}. \tag{3.37}$$

Let us call the ratio between the voltage bases of the off-nominal and nominal as r_B, so that

$$r_B = \frac{v_{BH}}{v_{BL}}. \tag{3.38}$$

With this denotation, it turns out to be

$$Y_{HH} = \left(\frac{v_{BH}}{v_{BL}}\right)^2 \frac{1}{r_t^2 z^L_{scpu}}, \tag{3.39}$$

$$Y_{HL} = Y_{LH} = \frac{-v_{BH}}{v_{BL}} \frac{1}{r_t z^L_{scpu}}, \tag{3.40}$$

$$Y_{LL} = \frac{1}{z^L_{scpu}}. \tag{3.41}$$

The components of the corresponding π-equivalent model is

$$y_{ij} = \frac{v_{BH}}{v_{BL}} \frac{1}{r_t z^L_{scpu}} = \frac{r_B}{r_t z^L_{scpu}}, \tag{3.42}$$

$$y_{si} = \frac{v_{BH}}{v_{BL}} \frac{1}{r_t z^L_{scpu}} \left(\frac{v_{BH}}{v_{BL}} \frac{1}{r_t} - 1 \right) = \frac{r_B}{r_t z^L_{scpu}} \left(\frac{r_B}{r_t} - 1 \right), \tag{3.43}$$

$$y_{sj} = \frac{1}{z^L_{scpu}} \left(1 - \frac{v_{BH}}{v_{BL}} \frac{1}{r_t} \right) = \frac{1}{z^L_{scpu}} \left(1 - \frac{r_B}{r_t} \right). \tag{3.44}$$

Notice that in this derivation the transformer bases do not explicitly appear in the model; however, the model depends on the side of the transformer used to refer the short-circuit impedance.

If the short-circuit impedance is referred to the nominal side, thus, instead of that of the secondary, this derivation would become

$$z^H_{scpu} = z_{scT} \left(\frac{v_{TH}}{v_{BH}} \right)^2 \frac{S_B}{S_T}. \tag{3.45}$$

Then, again, denoting r_B as the ratio between the voltage bases of the off-nominal and nominal, it follows that

$$Y_{HH} = \frac{1}{z^H_{scpu}}, \tag{3.46}$$

$$Y_{HL} = Y_{LH} = \frac{-v_{BL}}{v_{BH}} \frac{r_t}{z^H_{scpu}} = \frac{-r_t}{r_B z^H_{scpu}}, \tag{3.47}$$

$$Y_{LL} = \left(\frac{v_{BL}}{v_{BH}} \right)^2 \frac{r_t^2}{z^H_{scpu}} = \frac{r_t^2}{r_B^2 z^H_{scpu}}. \tag{3.48}$$

Components of the corresponding π-equivalent model are

$$y_{ij} = \frac{v_{BL}}{v_{BH}} \frac{r_t}{z^H_{scpu}} = \frac{r_t}{r_B z^H_{scpu}}, \tag{3.49}$$

$$y_{si} = \frac{1}{z^H_{scpu}} \left(1 - \frac{v_{BL}}{v_{BH}} r_t \right) = \frac{1}{z^H_{scpu}} \left(1 - \frac{r_t}{r_B} \right), \tag{3.50}$$

$$y_{sj} = \frac{v_{BL}}{v_{BH}} \frac{r_t}{z^H_{scpu}} \left(\frac{v_{BL}}{v_{BH}} r_t - 1 \right) = \frac{r_t}{r_B z^H_{scpu}} \left(\frac{r_t}{r_B} - 1 \right). \tag{3.51}$$

As a convenient strategy, if the short-circuit impedance is defined so as to take into account both transformer sides as of the transformer at the base of the system in this way

$$z'_{scpu} = z_{scT} \frac{v_{TH}}{v_{BH}} \frac{v_{TL}}{v_{BL}} \frac{S_B}{S_T}, \tag{3.52}$$

a compact alternative model can be derived, where

$$Y_{HH} = \frac{r_B}{r_t}\frac{1}{z'_{scpu}}, \tag{3.53}$$

$$Y_{HL} = Y_{LH} = \frac{-1}{z'_{scpu}}, \tag{3.54}$$

$$Y_{LL} = \frac{r_t}{r_B}\frac{1}{z'_{scpu}}. \tag{3.55}$$

And the well-known π-equivalent model for the transformer with fixed turns-ratio is obtained

$$y_{ij} = \frac{1}{z'_{scpu}}, \tag{3.56}$$

$$y_{si} = \frac{1}{z'_{scpu}}\left(\frac{r_B}{r_t} - 1\right), \tag{3.57}$$

$$y_{sj} = \frac{1}{z'_{scpu}}\left(\frac{r_t}{r_B} - 1\right). \tag{3.58}$$

If the chosen base voltages are the same as those of the transformer, there are no more different cases since $z^H_{scpu} = z^L_{scpu} = z'_{scpu}$, which can be designated as z_{scpu}, and the model then reduces to

$$Y_{HH} = \frac{1}{z_{scpu}}, \tag{3.59}$$

$$Y_{HL} = Y_{LH} = \frac{-1}{z_{scpu}}, \tag{3.60}$$

$$Y_{LL} = \frac{1}{z_{scpu}}. \tag{3.61}$$

Components of the corresponding π-equivalent model are

$$y_{ij} = \frac{1}{z_{scpu}}, \tag{3.62}$$

$$y_{si} = 0, \tag{3.63}$$

$$y_{sj} = 0. \tag{3.64}$$

3.3 Single-phase Transformer Model at Off-nominal Turn-ratios

In this section, the models of the tap-changing transformer at off-nominal turn-rations is generalized, including the possibility of using a base for the system different from the one used for the transformer.

3.3.1 In Physical Quantities

In this sub-section, the model of the single-phase transformer at off-nominal taps is derived in physical quantities. As the two traditional models are just particular cases of the consensus model, only this are taken into account in the following. Nonetheless, the short-circuit impedance expressed in p.u. in terms of the bases of the transformer, z_{scT}, is still used as a data.

Let us assume that the short-circuit impedance expressed in p.u. at the bases of the transformer, z_{scT}, is divided between the off-nominal and nominal sides, in the same way as in (3.20). Let us also assume that the definition of k, the p.u. impedance ratio is the same as in (3.21). Let us define the transformer tap as

$$a = \frac{1}{1 + \frac{t}{100}}, \tag{3.65}$$

where t is the percentage of variation of the secondary voltage in %. In this way, the off-nominal transformation ratio is

$$r'_t = \frac{v_{TH}}{v_{TL}\left(1 + \frac{t}{100}\right)} = a\frac{v_{TH}}{v_{TL}} = ar_t. \tag{3.66}$$

So the nodal equations become

$$\begin{bmatrix} i_H \\ i_L \end{bmatrix} = \begin{bmatrix} \frac{1+k}{1+ka^2}\frac{S_T}{v_{TH}^2 z_{scT}} & \frac{a(1+k)}{1+ka^2}\frac{-S_T}{v_{TH}v_{TL}z_{scT}} \\ \frac{a(1+k)}{1+ka^2}\frac{-S_T}{v_{TH}v_{TL}z_{scT}} & \frac{a^2(1+k)}{1+ka^2}\frac{S_T}{v_{TL}^2 z_{scT}} \end{bmatrix} \begin{bmatrix} v_H \\ v_L \end{bmatrix}. \tag{3.67}$$

The components of the π-equivalent model can then be expressed as

$$y_{ij} = \frac{a(1+k)}{1+ka^2}\frac{S_T}{v_{TH}v_{TL}z_{scT}}, \tag{3.68}$$

$$y_{si} = \frac{1+k}{1+ka^2}\frac{S_T}{v_{TH}z_{scT}}\left(\frac{1}{v_{TH}} - \frac{a}{v_{TL}}\right), \tag{3.69}$$

$$y_{sj} = \frac{a(1+k)}{1+ka^2}\frac{S_T}{v_{TL}z_{scT}}\left(\frac{a}{v_{TL}} - \frac{1}{v_{TH}}\right). \tag{3.70}$$

3.3.2 In the Per-Unit System

Again, let the bases chosen for the study of the system be v_{BH}, v_{BL}, and S_B. Note that these bases may not respond to the transformation ratio, as previously expressed in (3.32). Let us call again the voltage ratio between the bases r_B as defined in (3.38). Similarly, the nodal equations can be expressed as in (3.33).

If the voltage bases on the nominal side are used to express the short-circuit impedance, the following expression is obtained

$$z_{scpu}^L = z_{scT}\left(\frac{v_{TL}}{v_{BL}}\right)^2\frac{S_B}{S_T}, \tag{3.71}$$

whereas

$$Y_{HH} = \frac{1+k}{1+ka^2}\left(\frac{r_B}{r_t}\right)^2 \frac{1}{z^L_{scpu}}, \tag{3.72}$$

$$Y_{HL} = Y_{LH} = \frac{-a(1+k)}{1+ka^2}\frac{r_B}{r_t}\frac{1}{z^L_{scpu}}, \tag{3.73}$$

$$Y_{LL} = \frac{a^2(1+k)}{1+ka^2}\frac{1}{z^L_{scpu}}. \tag{3.74}$$

Thus, the components of the corresponding π-equivalent model are

$$y_{ij} = \frac{a(1+k)}{1+ka^2}\frac{r_B}{r_t}\frac{1}{z^L_{scpu}}, \tag{3.75}$$

$$y_{si} = \frac{1+k}{1+ka^2}\frac{r_B}{r_t}\frac{1}{z^L_{scpu}}\left(\frac{r_B}{r_t} - a\right), \tag{3.76}$$

$$y_{sj} = \frac{a(1+k)}{1+ka^2}\frac{1}{z^L_{scpu}}\left(a - \frac{r_B}{r_t}\right). \tag{3.77}$$

Conversely, if the voltage bases on the off-nominal side are used to express the short-circuit impedance, then

$$z^H_{scpu} = z_{scT}\left(\frac{v_{TH}}{v_{BH}}\right)^2 \frac{S_B}{S_T}, \tag{3.78}$$

and the nodal equations turn out to be

$$Y_{HH} = \frac{1+k}{1+ka^2}\frac{1}{z^H_{scpu}}, \tag{3.79}$$

$$Y_{HL} = Y_{LH} = \frac{-a(1+k)}{1+ka^2}\frac{r_t}{r_B}\frac{1}{z^H_{scpu}}, \tag{3.80}$$

$$Y_{LL} = \frac{a^2(1+k)}{1+ka^2}\left(\frac{r_t}{r_B}\right)^2 \frac{1}{z^H_{scpu}}. \tag{3.81}$$

Thus, components of the corresponding π-equivalent model are

$$y_{ij} = \frac{a(1+k)}{1+ka^2}\frac{r_t}{r_B}\frac{1}{z^H_{scpu}}, \tag{3.82}$$

$$y_{si} = \frac{1+k}{1+ka^2}\frac{1}{z^H_{scpu}}\left(1 - a\frac{r_t}{r_B}\right), \tag{3.83}$$

$$y_{sj} = \frac{a(1+k)}{1+ka^2}\frac{r_t}{r_B}\frac{1}{z^H_{scpu}}\left(a\frac{r_t}{r_B} - 1\right). \tag{3.84}$$

If the impedance of the transformer at the base of the system is defined in the same way as in (3.52), an alternative model can be derived which would be

$$Y_{HH} = \frac{1+k}{1+ka^2}\frac{r_B}{r_t}\frac{1}{z'_{scpu}}, \tag{3.85}$$

$$Y_{HL} = Y_{LH} = \frac{-a(1+k)}{1+ka^2}\frac{1}{z'_{scpu}}, \tag{3.86}$$

$$Y_{LL} = \frac{a^2(1+k)}{1+ka^2}\frac{r_t}{r_B}\frac{1}{z'_{scpu}}. \tag{3.87}$$

Components of the corresponding π-equivalent model are

$$y_{ij} = \frac{a(1+k)}{1+ka^2}\frac{1}{z'_{scpu}}, \tag{3.88}$$

$$y_{si} = \frac{1+k}{1+ka^2}\frac{1}{z'_{scpu}}\left(\frac{r_B}{r_t} - a\right), \tag{3.89}$$

$$y_{sj} = \frac{a(1+k)}{1+ka^2}\frac{1}{z'_{scpu}}\left(a\frac{r_t}{r_B} - 1\right). \tag{3.90}$$

Although the models that emerge from the 3 cases are all correct, the model from case 3 appears to be less ambiguous, since it eliminates the uncertainty about the validity of referring to one side or the other.

If the chosen base voltages are the same as those of the transformer, there are no more different cases since $z^H_{scpu} = z^L_{scpu} = z'_{scpu}$, which can be designated as z_{scpu}, and the model then reduces to

$$Y_{HH} = \frac{1+k}{1+ka^2}\frac{1}{z_{scpu}}, \tag{3.91}$$

$$Y_{HL} = Y_{LH} = \frac{-a(1+k)}{1+ka^2}\frac{1}{z_{scpu}}, \tag{3.92}$$

$$Y_{LL} = \frac{1}{z_{scpu}}. \tag{3.93}$$

Components of the corresponding π-equivalent model are

$$y_{ij} = \frac{a(1+k)}{1+ka^2}\frac{1}{z_{scpu}}, \tag{3.94}$$

$$y_{si} = \frac{(1-a)(1+k)}{1+ka^2}\frac{1}{z_{scpu}}, \tag{3.95}$$

$$y_{sj} = \frac{a(a-1)(1+k)}{1+ka^2}\frac{1}{z_{scpu}}, \tag{3.96}$$

which turns out to be the single-phase consensus model previously presented in section 2.3

3.4 Three-phase Transformer Model at Nominal Turn-ratios

In this section, the tap-changing transformer model is extended to the three-phase case. The Dyg11 configuration which is one of the most widely used types in distribution grids, is considered here as a relevant example. Particularly in this section, three-phase models are developed while transformers are operated at nominal turn-ratios.

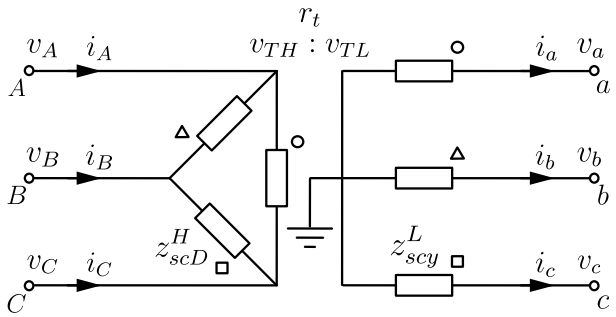

Fig. 3.4 Dyg11 transformer in physical quantities

3.4.1 In Physical Quantities

Here for the three-phase transformer (Dyg11) a generic model with a random distribution of the impedance between the windings is derived. Let z_{scT} be the short-circuit impedance of the transformer expressed in p.u. at its own bases (i.e. v_{TH}, v_{TL}, and S_T, these being the line voltages in off-nominal and nominal and the apparent power of the machine). This impedance is related to the single-phase impedances in ohms of the windings, i.e., z^H_{scD}, single-phase impedance of the delta on the off-nominal side,, and z^L_{scy} , single-phase impedance of the wye connection on the nominal side, with the following relation

$$z_{scT} = \frac{z^H_{scD}}{3}\frac{S_T}{v^2_{TH}} + z^L_{scy}\frac{S_T}{v^2_{TL}} = z^H_{scYT} + z^L_{scyT}. \tag{3.97}$$

Since v_{TD} is the rated line voltage at the off-nominal side and v_{Ty} is the rated phase-to-ground voltage at the nominal side, the transformation ratio can be obtained as,

$$r_t = \frac{v_{TH}}{v_{TL}} = \frac{v_{TD}}{\sqrt{3}v_{Ty}}. \tag{3.98}$$

Assuming that the z_{scT} is entirely provided by the nominal side, the impedance in ohms, z^L_{sc} , is calculated as

$$z^L_{sc} = \frac{v^2_{TL}}{S_T} z_{scT}. \tag{3.99}$$

Applying the KVL voltage equations in the off-nominal and nominal sides and considering that

$$r_t = \frac{-i^L_y}{\sqrt{3}i^H_D}, \tag{3.100}$$

the nodal equations of the three-phase transformer are obtained as

$$\begin{bmatrix} i_A \\ i_B \\ i_C \\ i_a \\ i_b \\ i_c \end{bmatrix} = \frac{S_T}{3z_{scT}v_{TH}^2} \begin{bmatrix} 2 & -1 & -1 & -\sqrt{3}r_t & 0 & \sqrt{3}r_t \\ -1 & 2 & -1 & \sqrt{3}r_t & -\sqrt{3}r_t & 0 \\ -1 & -1 & 2 & 0 & \sqrt{3}r_t & -\sqrt{3}r_t \\ -\sqrt{3}r_t & \sqrt{3}r_t & 0 & 3r_t^2 & 0 & 0 \\ 0 & -\sqrt{3}r_t & \sqrt{3}r_t & 0 & 3r_t^2 & 0 \\ \sqrt{3}r_t & 0 & -\sqrt{3}r_t & 0 & 0 & 3r_t^2 \end{bmatrix} = \begin{bmatrix} v_A \\ v_B \\ v_C \\ v_a \\ v_b \\ v_c \end{bmatrix}. \tag{3.101}$$

3.4.2 In the Per-Unit System

Let the bases chosen for the study of the system be v_{BH}, v_{BL}, and S_B. Note that these bases may not respond to the transformation ratio, that is, in general

$$r_t = \frac{v_{TH}}{v_{TL}} \neq \frac{v_{BH}}{v_{BL}}. \tag{3.102}$$

By expressing the short-circuit impedance of the transformer at the base of the system, as in (3.52)

$$z'_{scpu} = z_{scT}\frac{v_{TH}}{v_{BH}}\frac{v_{TL}}{v_{BL}}\frac{S_B}{S_T}, \tag{3.103}$$

the nodal equations can be expressed as

$$\begin{bmatrix} i_{Apu} \\ i_{Bpu} \\ i_{Cpu} \\ i_{apu} \\ i_{bpu} \\ i_{cpu} \end{bmatrix} = \frac{1}{3z'_{scpu}} \begin{bmatrix} 2\frac{r_B}{r_t} & -\frac{r_B}{r_t} & -\frac{r_B}{r_t} & -\sqrt{3} & 0 & \sqrt{3} \\ -\frac{r_B}{r_t} & 2\frac{r_B}{r_t} & -\frac{r_B}{r_t} & \sqrt{3} & -\sqrt{3} & 0 \\ -\frac{r_B}{r_t} & -\frac{r_B}{r_t} & 2\frac{r_B}{r_t} & 0 & \sqrt{3} & -\sqrt{3} \\ -\sqrt{3} & \sqrt{3} & 0 & 3\frac{r_t}{r_B} & 0 & 0 \\ 0 & -\sqrt{3} & \sqrt{3} & 0 & 3\frac{r_t}{r_B} & 0 \\ \sqrt{3} & 0 & -\sqrt{3} & 0 & 0 & 3\frac{r_t}{r_B} \end{bmatrix} = \begin{bmatrix} v_{Apu} \\ v_{Bpu} \\ v_{Cpu} \\ v_{apu} \\ v_{bpu} \\ v_{cpu} \end{bmatrix}. \tag{3.104}$$

And if the chosen base voltages are the same as those of the transformer, the model reduces to

$$\begin{bmatrix} i_{Apu} \\ i_{Bpu} \\ i_{Cpu} \\ i_{apu} \\ i_{bpu} \\ i_{cpu} \end{bmatrix} = \frac{1}{3z_{scT}} \begin{bmatrix} 2 & -1 & -1 & -\sqrt{3} & 0 & \sqrt{3} \\ -1 & 2 & -1 & \sqrt{3} & -\sqrt{3} & 0 \\ -1 & -1 & 2 & 0 & \sqrt{3} & -\sqrt{3} \\ -\sqrt{3} & \sqrt{3} & 0 & 3 & 0 & 0 \\ 0 & -\sqrt{3} & \sqrt{3} & 0 & 3 & 0 \\ \sqrt{3} & 0 & -\sqrt{3} & 0 & 0 & 3 \end{bmatrix} = \begin{bmatrix} v_{Apu} \\ v_{Bpu} \\ v_{Cpu} \\ v_{apu} \\ v_{bpu} \\ v_{cpu} \end{bmatrix}. \tag{3.105}$$

3.5 Three-phase Transformer Model at Off-nominal Turn-ratios

In this section, the three-phase transformer model of the Dyg11 connection (as a relevant example in distribution systems) is extended to the case of off-nominal turns-ratio operation.

3.5.1 In Physical Quantities

Here again, for the three-phase transformer (Dyg11)a generic model with a random distribution of the impedance between the windings is derived. As before, be the single-phase impedance of the transformer expressed in p.u. at its own bases (i.e. v_{TH}, v_{TL}, and S_T). This impedance is related to the impedances in ohms of the windings, z^H_{scD}, single-phase impedance of the delta on the off-nominal side, and z^L_{scy} , single-phase impedance of the wye connection on the nominal side. Thus,

$$z_{scT} = \frac{z^H_{scD}}{3}\frac{S_T}{v^2_{TH}} + z^L_{scy}\frac{S_T}{v^2_{TL}} = z^H_{scYT} + z^L_{scyT}. \tag{3.106}$$

Since v_{TD} is the rated line voltage at the off-nominal side and v_{Ty} is the rated phase-to-ground voltage at the nominal side, the transformation ratio can be obtained as,

$$r_t = \frac{v_{TH}}{v_{TL}} = \frac{v_{TD}}{\sqrt{3}v_{Ty}}. \tag{3.107}$$

Considering off-nominal operation, the transformation ratio turns out to be

$$r'_t = \frac{v_{tD}}{v_{TL}} = a\frac{v_{TD}}{\sqrt{3}v_{Ty}} = ar_t. \tag{3.108}$$

Assuming that the impedance is entirely provided by the nominal side, the impedance in ohms, z^L_{sc} , is calculated as

$$z^L_{sc} = \frac{v^2_{TL}}{S_T} z_{scT}. \tag{3.109}$$

Then, applying the KVL voltage equations in the off-nominal and nominal sides and considering that

$$r'_t = ar_t = \frac{-i^L_y}{\sqrt{3}i^H_D}, \tag{3.110}$$

the nodal equations of the three-phase transformer can be derived as

$$\begin{bmatrix} i_A \\ i_B \\ i_C \\ i_a \\ i_b \\ i_c \end{bmatrix} = \frac{S_T}{3z_{scT}v_{TH}^2} \begin{bmatrix} 2 & -1 & -1 & -\sqrt{3}r_t & 0 & \sqrt{3}r_t \\ -1 & 2 & -1 & \sqrt{3}r_t & -\sqrt{3}r_t & 0 \\ -1 & -1 & 2 & 0 & \sqrt{3}r_t & -\sqrt{3}r_t \\ -\sqrt{3}r_t & \sqrt{3}r_t & 0 & 3r_t^2 & 0 & 0 \\ 0 & -\sqrt{3}r_t & \sqrt{3}r_t & 0 & 3r_t^2 & 0 \\ \sqrt{3}r_t & 0 & -\sqrt{3}r_t & 0 & 0 & 3r_t^2 \end{bmatrix} = \begin{bmatrix} v_A \\ v_B \\ v_C \\ v_a \\ v_b \\ v_c \end{bmatrix}. \tag{3.111}$$

3.5.2 In the Per-Unit System

Here again, let the bases chosen for the study of the system be v_{BH}, v_{BL}, and S_B. Note that these bases may not respond to the transformation ratio, that is, in general

$$r_t = \frac{v_{TH}}{v_{TL}} \neq \frac{v_{BH}}{v_{BL}}. \tag{3.112}$$

By expressing the short-circuit impedance of the transformer as follows

$$z'_{scpu} = z_{scT}\frac{v_{TH}}{v_{BH}}\frac{v_{TL}}{v_{BL}}\frac{S_B}{S_T}, \tag{3.113}$$

the nodal equations can now be expressed as

$$\begin{bmatrix} i_{Apu} \\ i_{Bpu} \\ i_{Cpu} \\ i_{apu} \\ i_{bpu} \\ i_{cpu} \end{bmatrix} = \frac{1+k}{3z'_{scpu}(1+ka^2)} \begin{bmatrix} 2\frac{r_B}{r_t} & -\frac{r_B}{r_t} & -\frac{r_B}{r_t} & -a\sqrt{3} & 0 & a\sqrt{3} \\ -\frac{r_B}{r_t} & 2\frac{r_B}{r_t} & -\frac{r_B}{r_t} & a\sqrt{3} & -a\sqrt{3} & 0 \\ -\frac{r_B}{r_t} & -\frac{r_B}{r_t} & 2\frac{r_B}{r_t} & 0 & a\sqrt{3} & -a\sqrt{3} \\ -a\sqrt{3} & a\sqrt{3} & 0 & 3a^2\frac{r_t}{r_B} & 0 & 0 \\ 0 & -a\sqrt{3} & a\sqrt{3} & 0 & 3a^2\frac{r_t}{r_B} & 0 \\ a\sqrt{3} & 0 & -a\sqrt{3} & 0 & 0 & 3a^2\frac{r_t}{r_B} \end{bmatrix} = \begin{bmatrix} v_{Apu} \\ v_{Bpu} \\ v_{Cpu} \\ v_{apu} \\ v_{bpu} \\ v_{cpu} \end{bmatrix}. \tag{3.114}$$

And if the chosen base voltages are the same as those of the transformer, the model reduces to

$$\begin{bmatrix} i_{Apu} \\ i_{Bpu} \\ i_{Cpu} \\ i_{apu} \\ i_{bpu} \\ i_{cpu} \end{bmatrix} = \frac{1+k}{3z_{scT}(1+ka^2)} \begin{bmatrix} 2 & -1 & -1 & -a\sqrt{3} & 0 & a\sqrt{3} \\ -1 & 2 & -1 & a\sqrt{3} & -a\sqrt{3} & 0 \\ -1 & -1 & 2 & 0 & a\sqrt{3} & -a\sqrt{3} \\ -a\sqrt{3} & a\sqrt{3} & 0 & 3a^2 & 0 & 0 \\ 0 & -a\sqrt{3} & a\sqrt{3} & 0 & 3a^2 & 0 \\ a\sqrt{3} & 0 & -a\sqrt{3} & 0 & 0 & 3a^2 \end{bmatrix} = \begin{bmatrix} v_{Apu} \\ v_{Bpu} \\ v_{Cpu} \\ v_{apu} \\ v_{bpu} \\ v_{cpu} \end{bmatrix}. \tag{3.115}$$

3.6 Conclusion

In this chapter, a powerful methodology for modeling tap-changing transformer is derived which removes any ambiguity. Thereby, tap-changing transformer models, both conventional and consistent, have been extended to possible variations depending on their mode of operation, systems of expression, chosen bases, and number of phases to be considered. Also, this modeling approach has been extended for the three-phase case and can assume system bases different from the bases of the transformer. In this way, this chapter addresses and resolves the ambiguity around tap-changing transformer modeling.

Chapter 4

Reconciling Phase-shifting Transformer Models

The model of regulating transformers used in classic power system studies, such as load flow analysis or state estimation, is still debatable. As it is demonstrated in chapter 2, the two alternative tap-changing transformer models usually found in the literature and power system simulation software packages may lead to important discrepancies, especially at extreme tap positions. In the present chapter, the model developed in chapter 2 is extended to the case of the phase-shifting transformers (PST). This chapter demonstrates that prevailing formulations of PST, particularly of the asymmetrical type, may also lead to important discrepancies when operating far from the nominal tap, with a different impact depending on the power factor of the power flowing through the device. Furthermore, a general model for the PST is proposed in this contribution. The new model uses the same data available in conventional formulations leading to improved results and avoiding any ambiguity.

4.1 Introduction

With the deregulation of the electricity market, control of power flows over transmission lines and tie lines has become an important concern. Moreover, uneven loading of parallel transmission lines is a recurring problem to solve during the transmission of energy. The use of phase shifting transformers (PST) is a well-established solution to provide control of real power flows through transmission lines. Several PSTs, as in the case of asymmetrical types, offer also some control over the magnitude of output voltage, thus providing regulation of the reactive power flows up to a certain limit [42].

The quality of the results of classic power system studies such as power flow and optimal power flow analysis, state estimation, etc. are highly dependent on the accuracy of the models used to describe system components. However, simplified models are typically

used in these algorithms, due to the complexity and magnitude of the problems and also because of the scarce information generally available for the engineering practitioner in charge of these tasks. The nameplate of the transformer is usually the exclusive data source used in PST modeling.

In literature and practical implementations, as also described in 1.6.2, two alternative phase-shifting transformer models can be found [32, 6, 33, 8]. Similar to the tap-changing transformer, the differences in these models arise from the fact that they consider the short-circuit impedance either provided exclusively by the nominal or off-nominal turns side winding of the device. These extreme assumptions cause that both models yield different results and thus, the users can be misled trying to validate their results with different tools. This fact was originally observed in [43], but the authors chose one of those models and focused their efforts on the manipulations needed on the other model to reach the same results. However, in [9] as well as in chapter 2, those discrepancies were fully explained and a reconciled solution was proposed. Furthermore, [9] and chapter 2 demonstrate that even if the differences between the two models are trivial at the principal tap, significant mismatches take place at distant tap positions. Similarly, this lack of consistency also exists in the representation of PST through the two conventional models typically used in power system studies [44, 45, 38]. The aim of this contribution is to addressed this problem precisely by extending the applicability of [9] and chapter 2 to PSTs.

This chapter demonstrates that the two available models also yield different results for asymmetrical PSTs, which is misleading. Though these discrepancies from two models can be considered trivial at the principal tap, the inconsistency can lead to huge differences at distant tappings.

In this chapter, a new model of the PST is proposed in Section 4.2 in order to explain the causes of the discrepancies between the two existing models and with the aim of reaching a reconciled solution free of any ambiguity. Furthermore, the new model opens the door to a more accurate description of the device. Section 4.3 describes the conventional models and demonstrates that they are degenerate cases of the new proposal. Section 4.4 presents a theoretical assessment of the discrepancies caused by conventional models and relates them with the solution offered by the new model. A case study is presented in Section 4.5 in order to highlight the importance of the new proposal. Finally, the conclusions of this study are drawn in section 4.6.

4.2 Description of the New Model

Neglecting the shunt admittances of the detailed model of PSTs (i.e. those responsible for the magnetizing current and core losses) is a common practice in power system studies. This fact, simplifies the analysis, as the internal bus of the detailed model is removed from the problem. If the PST operates at nominal turns ratios, no further assumption is needed,

as the specific contribution of each transformer winding to the short-circuit impedance is irrelevant in that case. However, as is demonstrated in the following, this is far from being true when the PST works at an off-nominal tap position. Let us consider a PST with off-nominal turns ratio $|a|\, e^{j\theta}$ as depicted in Fig. 4.1.

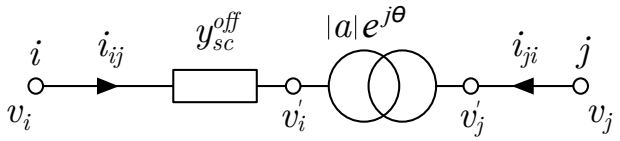

Fig. 4.1 Model of the phase shifting transformer with short-circuit impedance at the off-nominal turns side

The fundamental equations of a PST can be formulated as

$$\frac{v_i'}{v_j'} = a = |a|\, e^{j\theta}, \tag{4.1}$$

$$\frac{i_{ij}}{i_{ji}} = -\frac{1}{a^*} = -\frac{1}{|a|\, e^{-j\theta}}. \tag{4.2}$$

Then, though these parameters are not normally known by the user, let k be the ratio between the per p.u. impedance in the nominal winding, z_j and tapped winding, z_i (for the sake of simplicity, the same ratio is considered for resistance and leakage reactance). So, from (4.1) and (4.2), z_j can be referred to the off-nominal turns side as

$$z_j^{off} = \frac{v_i'}{v_j'}\frac{-i_{ij}}{i_{ji}} z_j = aa^* z_j = |a|^2\, z_j. \tag{4.3}$$

Therefore, considering the new ratio k together with (4.3), the series transformer admittance, as seen from the off-nominal side, can be calculated as

$$y_{sc}^{off} = \frac{1}{z_i + |a|^2\, z_j} = \frac{1}{z_i(1 + |a|^2\, k)}. \tag{4.4}$$

Typically, the data provided to the engineering practitioner in order to model the PST is the short-circuit impedance of the transformer, z_{sc}, which is also available at the nameplate of the device. This data is obtained from the short-circuit test, which is conducted, at least, at the nominal tap (i.e. $|a| = 1$). Thus, the rated short-circuit admittance of the PST, y_{sc}, can be expressed as

$$y_{sc} = \frac{1}{z_i + z_j}. \tag{4.5}$$

From (4.5) and the definition of k, the contribution of the winding at the off-nominal side to the short-circuit impedance, z_i, can be calculated as

$$z_i = \frac{1}{y_{sc}(1 + k)}, \tag{4.6}$$

Using this value in (4.4) yields

$$y_{sc}^{off} = \frac{1+k}{1+k\left|a\right|^2} y_{sc}. \tag{4.7}$$

Considering KVL, the nodal equations of the PST can now be written as

$$\begin{bmatrix} i_{ij} \\ i_{ji} \end{bmatrix} = \begin{bmatrix} Y_{ii} & Y_{ij} \\ Y_{ji} & Y_{jj} \end{bmatrix} \begin{bmatrix} v_i \\ v_j \end{bmatrix}, \tag{4.8}$$

where

$$Y_{ii} = y_{sc}^{off} = \frac{1+k}{1+k\left|a\right|^2} y_{sc}, \tag{4.9}$$

$$Y_{ij} = -a y_{sc}^{off} = -\frac{a\left(1+k\right)}{1+k\left|a\right|^2} y_{sc}, \tag{4.10}$$

$$Y_{ji} = -a^* y_{sc}^{off} = -\frac{a^*\left(1+k\right)}{1+k\left|a\right|^2} y_{sc}, \tag{4.11}$$

$$Y_{jj} = \left|a\right|^2 y_{sc}^{off} = \frac{\left|a\right|^2\left(1+k\right)}{1+k\left|a\right|^2} y_{sc}. \tag{4.12}$$

It is important to note that the Y_bus matrix of the nodal equations for PST is not symmetrical as $Y_{ij} \neq Y_{ji}$. Therefore forming a π-equivalent model for PST is not straightforward; rather the model will have two different branch admittances depending on the current under consideration (i_{ij} or i_{ji}). Keeping this fact in mind, the parameters of a pseudo π-equivalent model for the PST, which has been depicted in Fig. 4.2, can be derived from (4.9)–(4.12), as

$$y_{ij} = -Y_{ij} = \frac{a\left(1+k\right)}{1+k\left|a\right|^2} y_{sc}, \tag{4.13}$$

$$y_{ji} = -Y_{ji} = \frac{a^*\left(1+k\right)}{1+k\left|a\right|^2} y_{sc}, \tag{4.14}$$

$$y_{si} = Y_{ii} + Y_{ij} = \frac{\left(1-a\right)\left(1+k\right)}{1+k\left|a\right|^2} y_{sc}, \tag{4.15}$$

$$y_{sj} = Y_{jj} + Y_{ji} = \frac{\left(\left|a\right|^2 - a^*\right)\left(1+k\right)}{1+k\left|a\right|^2} y_{sc}. \tag{4.16}$$

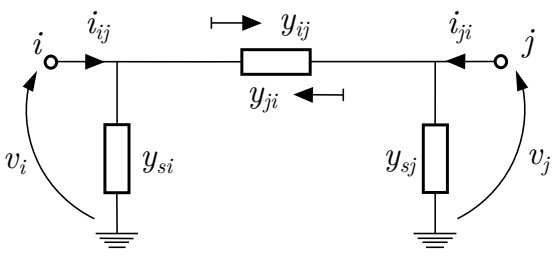

Fig. 4.2 A pseudo π-equivalent model of PST

4.3 Reconciliation of Previous Models

It can be easily derived that the two PST models most extensively used in the literature and practical implementations, correspond to the particular cases of making the parameter k equal to 0 and ∞ in (4.7), and thus in (4.9)–(4.16). The version with $k = 0$ corresponds to the assumption that all the short-circuit impedance of the PST is provided by the winding at the off-nominal turns side. In this case, the off-nominal admittance of the PST, y_{sc}^{off}, turns to be the same as the rated short-circuit admittance, y_{sc}, and the parameters of the pseudo π-equivalent circuit shown in Fig. 4.3(a) are obtained. On the other hand, considering $k = \infty$, corresponds to the assumption that all the short-circuit impedance of the PST is provided by the winding at the nominal turns side. Thus, y_{sc}^{off} turns to be $y_{sc}/|a|^2$, and the set of parameters of the pseudo π-equivalent circuit shown in Fig. 4.3(b) is reached.

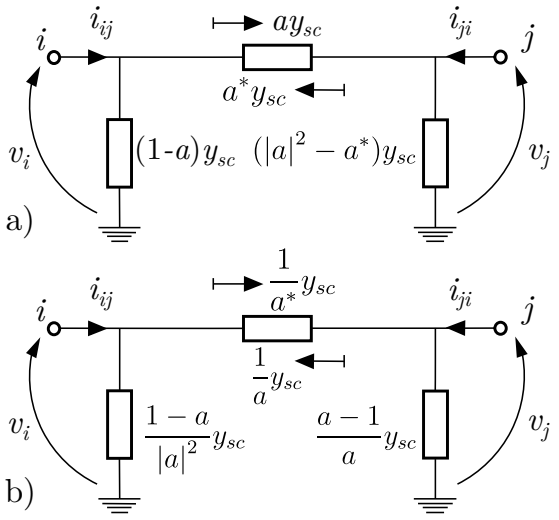

Fig. 4.3 The π-equivalent conventional models of the phase shifting transformer. (a) $k = 0$, and (b) $k = \infty$

It is interesting to note that the lack of consistency between the results offered by the two conventional alternatives of the PST models was initially identified in [43]. However, this publication focused on the adjustments needed to make them yield the same results and, thus, appropriately pointed out that the model in Fig. 4.3(a) turns to be the same as the one in Fig 4.3(b) if all the admittances are divided by $|a|^2$. The problem of taking this approach lies on the fact that all the short-circuit impedance of the device is still being assigned to one specific side of the transformer which, as is demonstrated in this contribution, can lead to important errors. Conversely, the new model is capable of describing the cause of the discrepancies and allows for a description of the device free of any ambiguity, provided that the specific value of k used in the analysis is reported.

It is important to highlight that the new PST model presented here, opens the door to obtain accurate results if k is known (e.g. being provided by the manufacturer or estimated from off-line field measurements). But, even if this is not the case, much more realistic estimates can be obtained if k is set to 1, which stands for an equal contribution of each

winding of the transformer to the short-circuit impedance. In fact, this is a common engineering practice, typically used when a detailed model of the transformer is to be used [38, 37]. While the benefits of using $k = 1$ in the case of the tap-changing transformer model was previously discussed in chapter 2, this chapter analyzes the advantage of making the same assumption for the case of PSTs.

4.4 Error Assessment

By using the new PST model proposed in Section 4.2, the voltage at the nominal turns side of the PST, v_j, can be determined if the variables at the off-nominal turns side, v_i and i_{ij}, are provided. Indeed, using the nodal equation of the PST displayed in (4.8), v_j can be calculated as

$$v_j = \frac{i_{ij} - Y_{ii} v_i}{Y_{ij}}. \tag{4.17}$$

Let us designate the voltage at the nominal turns side for a generic value of k as v_j^k. Thus, the discrepancies between the conventional models and the consensus model, can be assessed, by just considering the values obtained for $k = 0$ and $k = \infty$, i.e. v_j^0 and v_j^∞. Indeed, using (4.17) according to the values of Y_{ii} and Y_{ij} in (4.9) and (4.10), yields,

$$\Delta v_j^0 = v_j^0 - v_j^k = \frac{k(|a|^2 - 1) i_{ij}}{a(1+k) y_{sc}}, \tag{4.18}$$

$$\Delta v_j^\infty = v_j^\infty - v_j^k = \frac{(1 - |a|^2) i_{ij}}{a(1+k) y_{sc}}. \tag{4.19}$$

As it is immediately derived from (4.18) and (4.19), the discrepancies grow with the load level of the transformer as well as with the value of the rated short-circuit impedance. Moreover, those equations imply that the mismatch does not take place when $|a| = 1$, which is the case of symmetrical PSTs (i.e. those causing a pure phase-angle shift but with no effect on voltage magnitudes). In this specific case, the proposed model cannot contribute to provide better results. In fact, both the conventional and new models turn to be the same under that particular circumstances.

However, many asymmetrical PSTs are also used in power system applications. The proposed model can highly contribute to their modeling and simulation. According to [46], there exist three types of asymmetrical PSTs. For the widely-used quadrature booster, shown in Fig. 4.4(a), the regulating winding is connected at ±90 deg., whereas for other asymmetric PSTs, as the one shown in Fig. 4.4(b), the regulating winding can be connected at different angles, $0 < \delta < 180$. For the asymmetrical PST with in-phase transformer, as in Fig. 4.4(c), voltages on both primary and secondary side can be boosted with a common ratio r while the regulating winding remains connected with same angle, δ. As $|a| \neq 1$ in those cases, conventional models cause inconsistent results and the new model may effectively solve this problem.

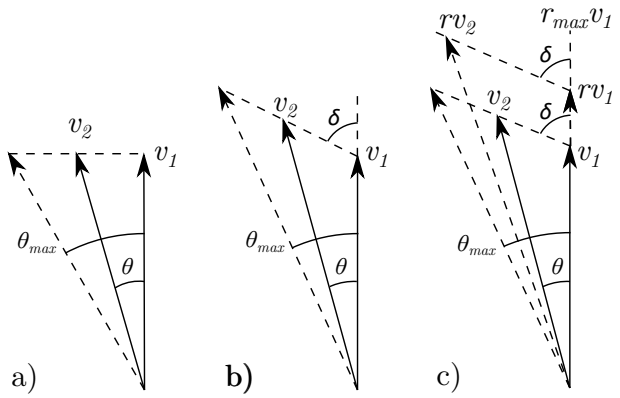

Fig. 4.4 Phasor diagrams of PSTs. (a) Quadrature booster (b) Asymmetrical PST, (c) In-phase transformer and asymmetrical PST

Notice that the new model is also useful to account for voltage magnitude tap-changing transformers provided that their vector group causes a non-zero phase-shift. In those cases, the discrepancies can be exacerbated by extreme tap positions, due to the high differences between $|a|$ and 1 that can be found in this type of devices.

4.5 Case Study

The voltage deviations from the different models according to the transformer operating conditions are assessed in subsections 4.5.1 and 4.5.2. Two case studies are presented here in order to point out the inconsistencies implied by the use of the conventional PST models shown in Fig. 4.3. Furthermore, these case studies demonstrate that the new PST model, proposed in this contribution and depicted in Fig. 4.2, can solve this problem assuring certainty in reporting results.

From Fig. 4.4, it can be easily seen that, for any of these asymmetric PSTs, there are general relations between the tap position, n, neutral tap position, n_0, phase shift, θ, magnitude of the off-nominal p.u. turns ratio, $|a|$, regulating winding connection angle, δ, and p.u. voltage step increment per tap change of the regulating winding, du. The general relations, including the effect of r, are well documented in [46, 47]. For the particular case of the asymmetrical PST, which is considered in the present case study, those relations, according to Fig. 4.4(b), can be expressed as

$$\theta = -\arctan\left(\frac{(n-n_0)du\sin\delta}{1+(n-n_0)du\cos\delta}\right), \tag{4.20}$$

$$|a| = \frac{1}{\sqrt{((n-n_0)du\sin\delta)^2+(1+(n-n_0)du\cos\delta)^2}}. \tag{4.21}$$

Even if the manufacturer can provide different short-circuit impedance values for different tap positions, this fact is omitted in the following, not to obscure the core of the proposal.

Let us consider an 80 MVA, 50 Hz, 220/132 kV, asymmetric PST, with a nameplate short-circuit impedance, z_{sc}, of $0.01 + 0.12j$ and a maximum no-load phase shift, θ_{max}, of -4.715 deg. The regulating winding connection angle, δ, is at 60 deg. and the tap changer, located on the higher voltage side, has 11 positions (from the neutral tap, $n_0 = 0$, to $n = 10$) and a voltage step increment per tap change, du, of 1%.

4.5.1 Voltage Deviations for Different Tap Positions and Power Factors

The effect of the tap position in the deviations caused by conventional models is studied in this case. The voltage at the off-nominal turns side of the PST, v_i is fixed at 1 p.u. as well as the current at the same side, i_{ij}, which is also forced to supply the rated current of the transformer. Two different power factors are used in this analysis: (a) a unity power factor, $\varphi = 0$ deg., i.e. i_{ij} is in-phase with v_i, and (b) a pure capacitive case, $\varphi = 90$ deg. in which i_{ij} leads v_i in this amount. Thus, the voltage at the nominal turns side of the transformer, v_j, can be calculated using the different models. Fig. 4.5 shows the results for the conventional versions, i.e. $k = 0$ and $k = \infty$, together with those obtained using the new model and assuming an equal contribution of both windings to the short-circuit impedance, i.e. $k = 1$. Although the setting of k in this way is not necessarily exact, it is according to well-accepted engineering practices, and is a more sensible estimation than the one derived from the extreme assumptions made in the conventional models.

The discrepancies in the magnitude of voltage at the nominal turns side of the transformer can be observed in Fig. 4.5(a). While they can be practically neglected at high power factors, the inconsistency is exacerbated in the capacitive case. Furthermore, and in agreement with (4.18) and (4.19), the mismatch grows when moving to distant positions from the neutral tap. In the same vein, the phase angle of the voltage at the nominal turns side (the voltage at the off-nominal side is taken as a reference) is depicted in Fig. 4.5(b) Unlike in the previous case, the discrepancies appear now magnified at high power factors and tend to be negligible with pure capacitive loads. As it is concluded from Fig. 4.5, the model proposed in this contribution offers a consensus estimate even if k is not accurately known and, more importantly, it removes any ambiguity from the results if the value of k used in the analysis is provided.

4.5.2 Maximum Voltage Deviations

In order to obtain the maximum deviations taking place in using the different models of the PST under study, the equivalent circuits of the conventional ($k = 0$ and $k = \infty$) and new model (setup with $k = 1$) were used to calculate the nominal turns side voltage at every tap position, n, and with every possible power factor (i.e. letting φ vary in the full range, which includes reverse power flow) while operating the transformer at rated values on the off-nominal side. The results obtained with the new model, v_j^1, were taken

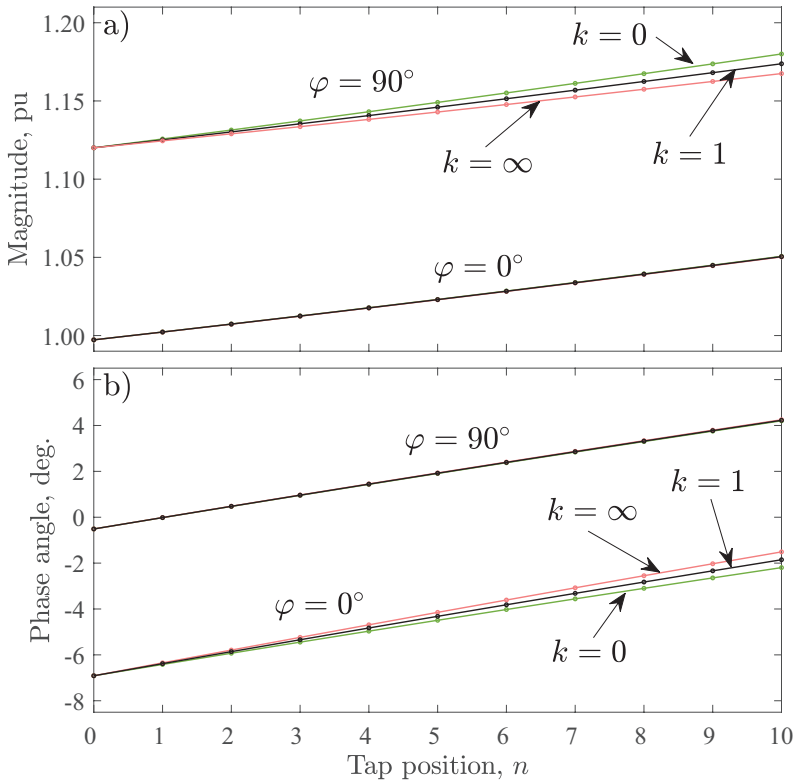

Fig. 4.5 Nominal-turns side voltage at different tap positions for the different PST models. The PST is operated at rated values at the off-nominal turns side at two different power factors: unity ($\varphi = 0$ deg.) and pure capacitive ($\varphi = 90$ deg.). (a) Voltage magnitude, and (b) Voltage phase angle

as a reference. Thus, Fig. 4.6(a) represents the differences in voltage magnitude between the conventional models and the present proposal, i.e. $\left|v_j^0\right| - \left|v_j^1\right|$ and $\left|v_j^\infty\right| - \left|v_j^1\right|$. The maximum difference reaches a value of 0.63% which is, in fact, a significant discrepancy. Notice that the mismatch between the conventional models doubles the previous result, being as high as 1.26%. The same differences are depicted in Fig. 4.6(b) for the case of the phase angle of the nominal turns side voltage. The mismatch reaches in this case 0.69 deg. between the conventional models, being reduced to 0.35 deg. when compared with the new model. Noticeably, these inconsistencies in the calculation of voltage phase angle can have a deep impact in the regulation of power flows by means of PST in real grids. The same results can be directly obtained from (4.18) and (4.19).

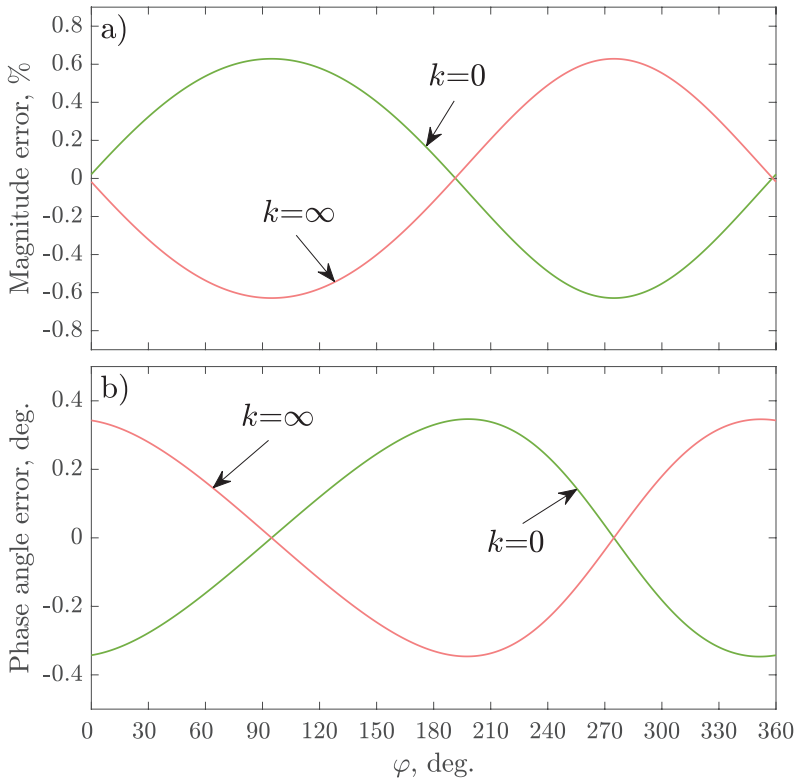

Fig. 4.6 Maximum deviation in the calculation of the nominal-turns side voltage at rated current. (a) Voltage magnitude, (b) Voltage phase angle

4.6 Conclusion

The use of simplified single-phase models of PSTs is standard practice in the execution of steady-state balanced power system studies. Although the specific contribution of each of the transformer windings to the short-circuit impedance can be completely neglected in untapped devices or when the operation takes place at the nominal tap, the same does not hold true at different tap positions. Conventional models of voltage-magnitude regulating transformers and PSTs are based on the assumption that all the short-circuit impedance is fully provided either by the winding at the nominal or off-nominal side, leading to two alternative models that yield different results. This may have strong implications, not only in the accuracy but also on the consistency of the outcomes from different tools. Although this problem does not appear in symmetrical PSTs, it can be a serious issue in asymmetrical PSTs or in voltage-magnitude regulating transformers with a non-zero vector group. Indeed, this chapter demonstrates that, in those cases, the mismatch of the results from those conventional models may be relevant, especially at extreme tap positions. These discrepancies appear both in voltage phase and voltage magnitude, depending on the power factor of the power flow handled by the device. Furthermore, this contribution proposes a consensus model of the PST which fully explains the aforementioned differences. The new model includes a new parameter that takes into account the contribution of each transformer winding to the short-circuit impedance. The use of this model gets rid of any

ambiguity provided that the value of this parameter is reported within the data of the study. Moreover, the new model can boost the accuracy of the results if good estimates for the new parameter are available. Even if this is not the case, a sensible setup, as the one derived from the assumption of an equal contribution of each transformer winding to the short-circuit impedance, provides a more reliable outcome than those obtained from the extreme assumptions of the conventional models. Thus, the inclusion of the proposed PST model in power system software packages has the potential to significantly improve the consistency of power system studies with embedded PSTs.

Chapter 5

Estimation of Impedance Ratio Parameters for Consistent Modeling

Previous chapters have shown that two widely used formulations of the tap-changing transformer model are controversial, as they generate dissimilar results depending on the selected tap and operating point. In those chapters, a new model was proposed and its consistency was demonstrated to reconcile this debate. There a novel parameter was introduced that stands for the ratio between the impedances of the nominal and tapped winding of the transformer. However, this parameter is not provided with and cannot be obtained from standard datasheets, which compels the users to rely on rough approximations. To overcome this problem, an offline state-vector-augmented parameter estimation method capable of providing accurate estimates of transformer impedance ratios is proposed in this chapter. Subsequently, this chapter demonstrates that the use of these precise parameters can effectively lead state estimators to better estimates of system states. This chapter also contributes with the derivatives of the different measurement functions in terms of the impedance ratios, which are essential tools for this or any other linearized state estimator. A multi-snapshot implementation is used to obtain a twofold advantage — increased measurement redundancy and improved accuracy of the estimated parameters. A detailed formulation of the implementation and several case studies are presented to demonstrate the validity of the proposal.

5.1 Introduction

Several power system studies, such as power flow, optimal power flow or state estimation (SE), are crucial today to ensure safety and optimality in the operation of modern grids. In this context, tap-changing transformers serve at the vanguard for voltage regulation

in power systems, and thus, accurate models of these devices are needed when they are present in the network under study.

The two most widely spread tap-changing transformer models found both in literature and software packages [31, 33] have been demonstrated to be inconsistent [43, 9, 10]. One of the models assumes that the transformer impedance, obtained through the well-known short-circuit test, is totally provided by the nominal winding, whereas the other model allocates it exclusively to the off-nominal side. This fact was first reported in [43]; however, the authors of that work selected one of the alternatives and proposed a method to shape the other so as to converge into the same results. Later, in [9, 10], it was established that, while the two models produce similar results near the central tap, they lead to significant differences at extreme tap positions. The power factor of the power flowing through the transformer primarily determines whether this divergence appears in voltage magnitude or phase angle. Analytical formulations and case studies demonstrating this inconsistency were presented in chapter 2.

To reconcile this dispute, a consistent model of tap-changing transformer was proposed in chapter 2 which reflects that the short-circuit impedance is in fact shared by both sides of the transformer [9, 10]. The new model introduces a parameter, k, which stands for the per-unit (p.u.) impedance ratio between the nominal winding and tapped winding of the tap-changing transformer. However, admittedly, the user cannot obtain the value of this parameter from standard transformer data sheets or even through straight-forward calculations. In response to that, it was argued and demonstrated that if this parameter is not available, assuming k=1, i.e. considering an equal share of the p.u. impedance at both sides of the transformer, produces results which minimizes the maximum expected error. Nonetheless, the accuracy and consistency of the results of power system studies with embedded tap-changing transformers can be obviously improved if the actual value of k is determined through a parameter estimation process utilizing historical sets of measurements. Thus, the estimation of k is pursued in the present chapter.

In a broad classification, SE methods are either recursive or static. However, static state estimators constitute a comparatively mature technology widely used by utilities for power system monitoring. While there are other possibilities, most of the static estimators minimize the weighted least squares (WLS) of residuals from a single snapshot of measurements to provide estimates of the current states of the system [6, 32]. For static SE, several alternative formulations are available in literature in order to overcome some deficiencies of the seminal algorithms, increasing numerical capabilities or adding some practical advantages. Many of these formulations are well documented in [6, 32]. In the present proposal, a widely used and suitable WLS-based formulation is extended further to cope with the objectives of this chapter.

In addition to providing estimates of the state variables, other functions and associated routines are integral parts of power system state estimators, such as observability analysis, bad data detection and identification, topology error processing and parameter estimation.

Among these, the latter can be pointed out as the key tool to address the problem of estimating the p.u. impedance ratios of tap-changing transformers. Network parameter estimation methods are broadly classified in two groups—residual sensitivity-based analysis and state vector augmentation [6]. Residual sensitivity-based analysis is efficient for parameter error identification which is not required for the purpose of this chapter, as transformer impedance ratios are objectively included in the suspicious set. As the name suggests, in state vector augmentation methods, the suspected parameters are included in the state vector and estimated together with the system state variables [48–53]. Importantly, for the sole purpose of parameter estimation, state vector augmentation methods are considered to deliver superior performance due to the fact that all the surrounding measurements get involved in the estimation [54]. Therefore, the state vector augmentation method has been selected and implemented in this section to provide accurate estimates of the parameters of interest.

The estimation of transformer tap positions has been a central issue for parameter estimation methods in power systems [50, 53]. In fact, estimation of unmeasured or erroneous transformer taps is today a regular or online function of state estimators. On the contrary, due to the non-varying nature of impedance ratio parameters, which may change only in the event of a fault or a complete replacement of a transformer, their estimation is required in very long time intervals. It is not worth including the estimation of these parameters in an online state estimator, as this may deteriorate the performance of the algorithm in terms of speed without a practical improvement. Therefore, an offline parameter estimator, designed to be run periodically, with a low cadence, is proposed in this chapter. In this concept, the online estimator used in the operation of the grid is in charge of the estimation of transformer tap positions at each snapshot; then, the offline parameter estimator, executed in long time periods, uses those tap positions together with the raw measurements at different snapshots to provide accurate estimates of the transformer impedance ratios. Certainly, the updated estimates of these parameters can now be fed into the online state estimator to increase its accuracy, as a consequence of the improvement of the model.

Finally, it is important to discuss the potential hindrances of assessing the transformer p.u. impedance ratios through parameter estimation techniques. If a large number of tap-changing transformers are embedded in the grid under study, the new variables to be included in the augmented state vector could significantly deteriorate the redundancy of the measurements. Moreover, as in any other SE application, the noise of field measurements has an impact on the quality of the estimation of the parameters. However, even more important for this particular problem is that the sensitivity of the measurement functions with respect to p.u. impedance ratios are significantly lower than the sensitivities with respect to the other state variables. As a consequence, measurement noise is likely to conceal the biases of erroneous estimation of impedance ratios throughout the process. The above-mentioned difficulties turn the estimation of the desired transformer parameters

into a challenging task. Nonetheless, one expedient feature of transformer impedance ratios can help to overcome these obstacles: they can be considered time-invariant, at least for a reasonable time span. Thus, the method proposed in this chapter can be fed with multiple snapshots of measurements, i.e. with historical data collected along a reasonable time period. Multi-snapshots usage has clear advantages in parameter estimation, as has been previously reported by other authors [6, 51, 49]. Therefore, a multi-snapshot implementation has been embraced in this proposal.

The consistent tap-changing transformer model, and thereby, the emergence of the impedance ratio parameter, was introduced in chapter 2. Then, an advantageous equality-constrained SE method is briefly described in section 5.2. Section 5.3 articulates the derivation and integration details of the estimation of p.u. impedance ratios. A set of case studies are included in section 5.4 to validate and demonstrate the advantages of the proposal. Finally, the conclusions of this study are gathered in section 5.5.

5.2 Equality-constrained SE

The Normal Equations (NE) formulation of WLS SE in its application to power system studies may lead to some well-known problems, such as ill-conditioning or divergence. This is especially critical when using zero-injection buses as virtual measurements. Therefore, several proposals have been made to overcome the shortcomings of the basic NE formulation [6]. Among these propositions, appear numerical techniques such as the Lower Upper (LU) factorization and orthogonal (QR) factorization of the gain matrix. More advantageously, there are some restructured formulations called equality-constrained SE which take advantage of the Lagrangian of equality-constrained optimization problems [6, 55]. In the present chapter, an equality-constrained SE algorithm called augmented matrix method [56, 6] was extended to the particular parameter estimation problem of interest. In this method, both the virtual and regular measurement equations are taken as equality constraints in order to improve the condition number of the Hachtel's matrix. According to this method, the following set of linearized equations describes the SE problem

$$\begin{bmatrix} R & H & 0 \\ H^T & 0 & C^T \\ 0 & C & 0 \end{bmatrix} \begin{bmatrix} \mu \\ \Delta x \\ \lambda \end{bmatrix} = \begin{bmatrix} \Delta z \\ 0 \\ -c(x) \end{bmatrix}, \tag{5.1}$$

where,

- R is the covariance matrix having variances of regular measurement errors at its diagonal elements,
- H is the matrix for derivatives of regular measurements,
- C is the matrix for derivatives of virtual measurements,

- μ is the vector of Lagrange multipliers for regular measurements,
- λ is the vector of Lagrange multipliers for virtual measurements,
- Δx is the vector for deviations of state variables,
- Δz is the vector for measurement residuals, i.e., the difference between regular field measurements and their theoretical values calculated from the current estimation of state variables,
- and $c(x)$ is the vector for virtual measurement residuals.

5.3 Estimation of Transformer Impedance Ratios

Most SE methods are linearized formulations which require the derivatives of the measurement functions, h, in terms of the state variables. As power system static SE is a well-developed and mature technique, the derivatives of general measurement functions in terms of commonly used state variables and parameters are widely used and readily available in the literature [6]. However, the consistent tap-changing transformer model is a state-of-the-art concept which has not been implemented before in power system SE algorithms. Hence, no work has yet introduced the derivatives of measurement functions in terms of the impedance transformer ratio, k, which are required for the estimation of these parameters.

In a standard SE formulation, the state vector, x, includes bus voltage magnitudes, V, and phase angles, θ, except for the phase angle reference, as state variables. In this proposal, the state vector is augmented by including the k parameters of the tap-changing transformers embedded in the network under study. Thus, as an important contribution of this chapter, the derivatives of general field measurement types such as bus voltage magnitudes, active and reactive bus power injections and active and reactive branch power flows, in terms of the impedance ratio, are presented. These derivatives are crucial for the construction of both the H and C matrices included in (5.1). Finally, for the problem-specific requirements, the present work integrates these new derivatives into a single snapshot and a multi-snapshot augmented matrix SE algorithm.

5.3.1 Derivatives of Measurement Functions with Respect to k

For aiding in visualization, let us consider a tap-changing transformer with off-nominal turns ratio $a : 1$ and again depict it in Fig. 5.1.

5.3.1.1 Bus Voltage Magnitudes

The measurement function of voltage magnitude at bus i reduce itself to its corresponding voltage magnitude, V_i, which is a state variable on its own. Therefore, these functions are

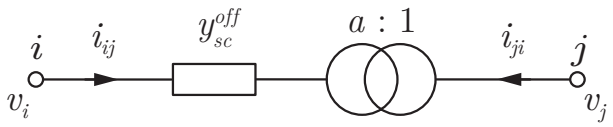

Fig. 5.1 Model of the tap-changing transformer with short-circuit impedance at the off-nominal turns side.

independent of tap-changing transformer impedance ratios, k. So, it can be stated that

$$\frac{\partial V_i}{\partial k} = 0. \tag{5.2}$$

5.3.1.2 Power Injections

The measurement functions for the active and reactive power injections, P_i and Q_i, at a specific bus i, are well-known in power system analysis, being formulated as [6]

$$P_i = V_i \sum_{n=1}^{N} V_n [G_{in} \cos\theta_{in} + B_{in} \sin\theta_{in}], \tag{5.3}$$

$$Q_i = V_i \sum_{n=1}^{N} V_n [G_{in} \sin\theta_{in} - B_{in} \cos\theta_{in}], \tag{5.4}$$

where n stands for each of the total number of buses in the network, N. Likewise, G_{in}, B_{in} are the conductance and susceptance of the element Y_{in} of the system bus admittance matrix. Finally, θ_{in} stands for the phase angle between buses i and n.

As it can be immediately concluded from (5.3) and (5.4), if bus i is not directly connected to a tap-changing transformer, none of the terms of these equations depend on the impedance ratio of that specific device. Thus, the derivatives of those active and reactive power injections in terms of the impedance ratio of that transformer equal zero. On the other hand, if there is a tap-changing transformer located between buses i and j, with an impedance ratio k, the admittance of the transformer impacts the calculation of power injections through the addends corresponding to $n = i$ and $n = j$. Thus, the parts of P_i and Q_i impacted by k, which are the only ones of interest for the calculation of the derivatives, can be designated as P_i^k and Q_i^k and may be evaluated as

$$P_i^k = V_i^2 G_{ii}^k + V_i V_j [G_{ij} \cos\theta_{ij} + B_{ij} \sin\theta_{ij}], \tag{5.5}$$

$$Q_i^k = -V_i^2 B_{ii}^k + V_i V_j [G_{ij} \sin\theta_{ij} - B_{ij} \cos\theta_{ij}], \tag{5.6}$$

where, G_{ii}^k and B_{ii}^k contain the addends of the diagonal elements of the bus admittance matrix which are a function of k, i.e. those provided by the series and shunt branch of the tap-changing transformer model connected at bus i.

At this point, two cases should be taken into consideration. On the one hand, if the tapped winding of the transformer is connected to bus i, as shown in Fig. 5.1, (2.8) and (2.9) allow to express the elements of the bus admittance matrix in (5.5) and (5.6) as a function of k and the conductance, g_{sc}, and susceptance, b_{sc}, of the short-circuit

admittance, y_{sc}, of the transformer. Thus,

$$G_{ii}^k = \frac{1+k}{1+ka^2} g_{sc}, \qquad B_{ii}^k = \frac{1+k}{1+ka^2} b_{sc}, \tag{5.7}$$

$$G_{ij} = -\frac{a(1+k)}{1+ka^2} g_{sc}, \quad B_{ij} = -\frac{a(1+k)}{1+ka^2} b_{sc}. \tag{5.8}$$

The substitution of (5.7) and (5.8) in (5.5) and (5.6) leads to

$$P_i^k = \frac{1+k}{1+ka^2} \left[V_i^2 g_{sc} - aV_iV_j \left(g_{sc} \cos\theta_{ij} + b_{sc} \sin\theta_{ij} \right) \right], \tag{5.9}$$

$$Q_i^k = \frac{1+k}{1+ka^2} \left[-V_i^2 b_{sc} - aV_iV_j \left(g_{sc} \sin\theta_{ij} - b_{sc} \cos\theta_{ij} \right) \right]. \tag{5.10}$$

By applying the quotient rule to (5.9) and (5.10), the derivatives of P_i and Q_i in terms of k can be obtained as

$$\frac{\partial P_i}{\partial k} = \frac{1+ka^2-a^2(1+k)}{(1+ka^2)^2} \times ... \left[V_i^2 g_{sc} - aV_iV_j \left(g_{sc} \cos\theta_{ij} + b_{sc} \sin\theta_{ij} \right) \right], \tag{5.11}$$

$$\frac{\partial Q_i}{\partial k} = \frac{1+ka^2-a^2(1+k)}{(1+ka^2)^2} \times ... \left[-V_i^2 b_{sc} - aV_iV_j \left(g_{sc} \sin\theta_{ij} - b_{sc} \cos\theta_{ij} \right) \right]. \tag{5.12}$$

On the other hand, if bus i is connected to the untapped winding of the transformer, (2.10) should be used instead of (2.8) to formulate the diagonal elements of the bus admittance matrix impacted by k, G_{ii}^k and B_{ii}^k, in (5.5) and (5.6). Thus,

$$G_{ii}^k = \frac{a^2(1+k)}{1+ka^2} g_{sc}, \quad B_{ii}^k = \frac{a^2(1+k)}{1+ka^2} b_{sc}. \tag{5.13}$$

The substitution of (5.8) and (5.13) in (5.5) and (5.6) leads to

$$P_i^k = \frac{a(1+k)}{1+ka^2} \left[aV_i^2 g_{sc} - V_iV_j \left(g_{sc} \cos\theta_{ij} + b_{sc} \sin\theta_{ij} \right) \right], \tag{5.14}$$

$$Q_i^k = \frac{a(1+k)}{1+ka^2} \left[-aV_i^2 b_{sc} - V_iV_j \left(g_{sc} \sin\theta_{ij} - b_{sc} \cos\theta_{ij} \right) \right]. \tag{5.15}$$

And the derivatives of P_i and Q_i in terms of k in this second case turn out to be

$$\frac{\partial P_i}{\partial k} = \frac{a(1+ka^2) - a^3(1+k)}{(1+ka^2)^2} \times ... \\ \left[aV_i^2 g_{sc} - V_i V_j \left(g_{sc}\cos\theta_{ij} + b_{sc}\sin\theta_{ij}\right)\right], \tag{5.16}$$

$$\frac{\partial Q_i}{\partial k} = \frac{a(1+ka^2) - a^3(1+k)}{(1+ka^2)^2} \times ... \\ \left[-aV_i^2 b_{sc} - V_i V_j \left(g_{sc}\sin\theta_{ij} - b_{sc}\cos\theta_{ij}\right)\right]. \tag{5.17}$$

5.3.1.3 Power Flows

Note that the π-equivalent model depicted in Fig. 2.3(a) is not only valid for a tap-changing transformer but also for a line. Thus, the measurement functions of active and reactive power, P_{ij}, Q_{ij}, flowing from bus i to bus j and measured at the sending end can be expressed for both types of elements as [6]

$$P_{ij} = V_i^2(g_{si} + g_{ij}) - V_i V_j(g_{ij}\cos\theta_{ij} + b_{ij}\sin\theta_{ij}), \tag{5.18}$$

$$Q_{ij} = -V_i^2(b_{si} + b_{ij}) - V_i V_j(g_{ij}\sin\theta_{ij} - b_{ij}\cos\theta_{ij}), \tag{5.19}$$

where, g_{si} and b_{si} are the conductance and susceptance of the shunt leg at bus i, and g_{ij} and b_{ij} stand for the conductance and susceptance of the series admittance.

From (5.18) and (5.19), it can be immediately concluded that, if a power flow measurement between the adjacent buses i and j does not flow through a tap-changing transformer, none of the elements of these equations are affected by the impedance ratio of the device. Thus, the derivatives of those active or reactive power flows in terms of k equal zero. However, when a tap-changing transformer connects buses i and j, the admittances in those equations are a function of the impedance ratio, k. Again, two different cases need to be addressed. On the one hand, if the measuring location, i.e. bus i, is connected to the tapped winding, as in Fig. 5.1, the conductances and susceptances can be directly taken from (2.11) and (2.12). Thus,

$$g_{si} + g_{ij} = \frac{1+k}{1+ka^2} g_{sc}, \qquad b_{si} + b_{ij} = \frac{1+k}{1+ka^2} b_{sc}, \tag{5.20}$$

$$g_{ij} = \frac{a(1+k)}{1+ka^2} g_{sc}, \qquad b_{ij} = \frac{a(1+k)}{1+ka^2} b_{sc}. \tag{5.21}$$

The substitution of (5.20) and (5.21) in (5.18) and (5.19) leads to

$$P_{ij} = \frac{1+k}{1+ka^2}\left[V_i^2 g_{sc} - aV_i V_j \left(g_{sc}\cos\theta_{ij} + b_{sc}\sin\theta_{ij}\right)\right], \tag{5.22}$$

$$Q_{ij} = \frac{1+k}{1+ka^2}\left[-V_i^2 b_{sc} - aV_i V_j \left(g_{sc}\sin\theta_{ij} - b_{sc}\cos\theta_{ij}\right)\right]. \tag{5.23}$$

By applying the quotient rule to (5.22) and (5.23), the derivatives of P_{ij} and Q_{ij} in terms of k can be obtained as

$$\frac{\partial P_{ij}}{\partial k} = \frac{1 + ka^2 - a^2(1+k)}{(1+ka^2)^2} \times ... \\ \left[V_i^2 g_{sc} - aV_iV_j \left(g_{sc}\cos\theta_{ij} + b_{sc}\sin\theta_{ij}\right)\right], \tag{5.24}$$

$$\frac{\partial Q_{ij}}{\partial k} = \frac{1 + ka^2 - a^2(1+k)}{(1+ka^2)^2} \times ... \\ \left[-V_i^2 b_{sc} - aV_iV_j \left(g_{sc}\sin\theta_{ij} - b_{sc}\cos\theta_{ij}\right)\right]. \tag{5.25}$$

On the other hand, if the measuring location, i.e. bus i, is connected to the untapped winding, (2.13) should be used instead of (2.12) to obtain the conductances and susceptances used in (5.22) and (5.23). Thus,

$$g_{si} + g_{ij} = \frac{a^2(1+k)}{1+ka^2} g_{sc}, \quad b_{si} + b_{ij} = \frac{a^2(1+k)}{1+ka^2} b_{sc}. \tag{5.26}$$

The substitution of (5.21) and (5.26) in (5.22) and (5.23) leads to

$$P_{ij} = \frac{a(1+k)}{1+ka^2}\left[aV_i^2 g_{sc} - V_iV_j\left(g_{sc}\cos\theta_{ij} + b_{sc}\sin\theta_{ij}\right)\right], \tag{5.27}$$

$$Q_{ij} = \frac{a(1+k)}{1+ka^2}\left[-aV_i^2 b_{sc} - V_iV_j\left(g_{sc}\sin\theta_{ij} - b_{sc}\cos\theta_{ij}\right)\right]. \tag{5.28}$$

And the derivatives of P_{ij} and Q_{ij} in terms of k in this second case can be expressed as

$$\frac{\partial P_{ij}}{\partial k} = \frac{a(1+ka^2) - a^3(1+k)}{(1+ka^2)^2} \times ... \\ \left[aV_i^2 g_{sc} - V_iV_j \left(g_{sc}\cos\theta_{ij} + b_{sc}\sin\theta_{ij}\right)\right], \tag{5.29}$$

$$\frac{\partial Q_{ij}}{\partial k} = \frac{a(1+ka^2) - a^3(1+k)}{(1+ka^2)^2} \times ... \\ \left[-aV_i^2 b_{sc} - V_iV_j \left(g_{sc}\sin\theta_{ij} - b_{sc}\cos\theta_{ij}\right)\right]. \tag{5.30}$$

5.3.2 Formation of Jacobian Matrices for the SE Process

In the formulation of the augmented matrix approach for SE [6, 55], the derivatives of the h_z–functions of a set of L regular measurements, z_r, reside in the H matrix, while the derivatives of the c_z–functions of a set of M virtual measurements, z_v, reside in the C matrix shown in (5.1). Both matrices are augmented in this proposal with a new set of state variables, k, corresponding to the transformer impedance ratios of the T tapped-transformers embedded in the grid under study.

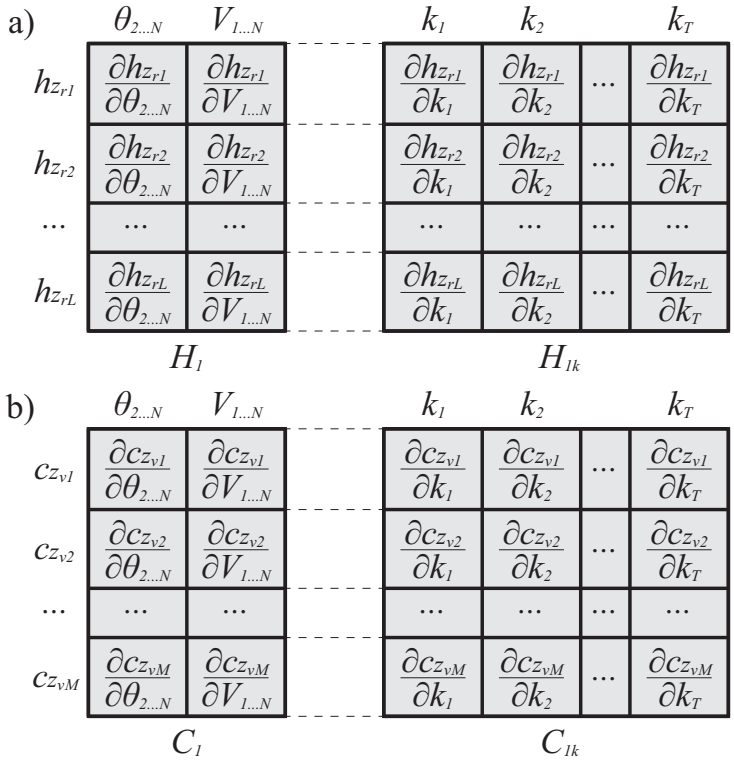

Fig. 5.2 Formation of the augmented Jacobian matrices for a single snapshot. a) H matrix, and b) C matrix.

If the estimation of k is carried out considering just a single snapshot of measurements, the extension of the Jacobian matrices is rather straightforward. In this case, a new column has to be added, both to the H and C matrices, to account for each of the T elements of k. Thus, the use of the new derivatives described in Section 5.3.1 together with the classical set [6], allows to form the augmented H and C matrices as depicted in Fig. 5.2. Notice that in this figure and w.l.o.g, the phase angle at bus 1, θ_1, has been taken as reference, and thus, excluded from the set of state variables. This is a similar approach to other augmentation techniques such as those previously presented in [48–53]

According to Fig. 5.2, two parts can be distinguished in the new H and C matrices: H_1 and C_1, that account for the derivatives of regular and virtual measurements with respect to the conventional state variables, and H_{1k} and C_{1k}, that hold the derivatives of regular and virtual measurements in terms of the transformer impedance ratios, k. The final H and C matrices are formed by horizontal concatenation of H_1, H_{1k} and C_1, C_{1k} respectively.

The difficulties of estimating the p.u. impedance ratios of tap-changing transformers from a single snapshot of measurements have been previously discussed in section 5.1. As it was pointed out, an adaptation of a multi-snapshot of measurements is proposed in this chapter to overcome those obstacles. This is a suitable approach for the estimation of the parameters under study, which can be considered time-invariant during long periods.

Indeed, parameter estimation, conducted as an offline task, can sacrifice computation time in favor of the accuracy of the estimation.

In SE theory, measurement redundancy is defined as the ratio between the number of measurements and the number of state variables. Hence, as L is the number of regular measurements and M is the number of virtual measurements, the base case redundancy of the problem, ε_0, i.e., the one in which p.u. impedance ratios are not included as state variables, can be calculated as

$$\varepsilon_0 = \frac{L+M}{2N-1}. \tag{5.31}$$

In a single snapshot or multi-snapshot implementation of the augmented problem, in which Q snapshots and T time-invariant transformer impedance ratios are included as additional state variables, the redundancy level is deteriorated according to

$$\varepsilon_Q = \frac{Q(L+M)}{Q(2N-1)+T} = \frac{L+M}{2N-1+\frac{T}{Q}}. \tag{5.32}$$

From (5.32), it can be concluded that, increasing the number of snapshots in the estimation process, allows to move the redundancy level of the augmented problem as close as desired to the redundancy of the base case. Thus, provided that a sufficient number of snapshots are included into the problem, the application of the augmented approach cannot be blamed for deteriorating the redundancy level.

The formation of the augmented matrices, H and C, for the case of the multi-snapshot problem is depicted in Fig. 5.3. Each snapshot q involves a specific set of conventional state variables, $[V\theta]_q$, together with a specific set of h–functions, $[h_{zr}]_q$, and c–functions, $[c_{zv}]_q$, associated with regular and virtual measurements, respectively. Notice that the conventional state variables change at each snapshot but the augmented ones, k, remain always the same. Thus, the parts of the Jacobian matrices linked to conventional state variables are augmented diagonally by means of H_q and C_q, while the parts associated with the transformer impedance ratios are augmented vertically by means of H_{qk} and C_{qk}.

It is worth noting that, in order to apply (5.1) in the multisnapshot context, the covariance matrix, R, should be formed by diagonal augmentation of the respective covariance matrices of each snapshot. Likewise, Δz and Δx vectors are respectively formed by vertical concatenation of measurement residuals and state variable deviations from each snapshot.

Equation (5.1) can now be iteratively solved to provide estimates of the full set of state variables. Among them, the final values of k constitute the estimated parameters of the p.u. impedance ratios of the tap-changing transformers.

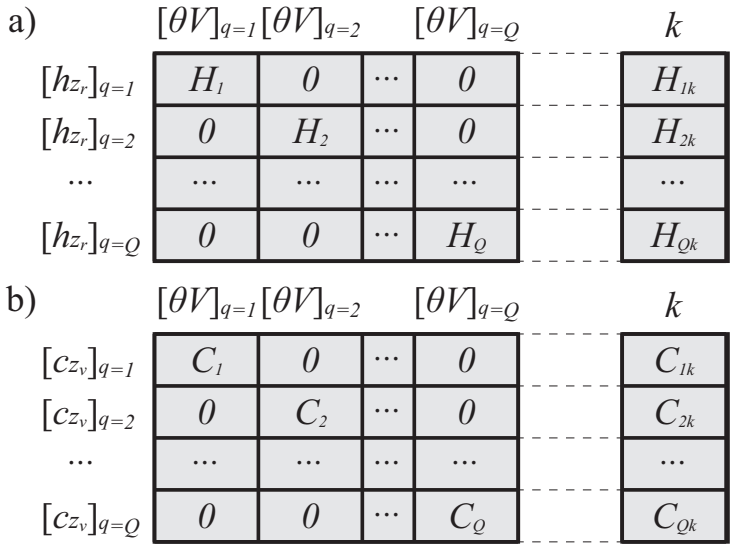

Fig. 5.3 Formation of the augmented Jacobian matrices in a multi-snapshot problem. a) H matrix, and b) C matrix.

5.3.3 Treatment of Bad Data

The treatment of bad data is a crucial concern for any state estimator. However, as it is pointed out in section 5.1, the parameter estimator proposed in this chapter is designed to work offline. Thus, it uses historical data comprised of measurement snapshots in which any possible bad data has been already detected, identified and removed by the online state estimator used in the operation of the grid. Of course, removal of bad data may reduce the redundancy of the measurement set. However, as it is shown in the case studies presented in section 5.4, the proposed algorithm converges to the solution even in low redundancy scenarios. In summary, as the bad data is pre-treated by the online state estimator, the proposed offline parameter estimator does not need further filtering of the input measurements.

Nevertheless, it is interesting to point out that model inaccuracies, such as those that may appear during the initialization process (i.e. when k=1 is adopted as an educated guess of the transformer impedance ratios), can lead the online state estimator to an undesired removal of measurements (erroneously flagged as bad data). The influence of this aspect on the proper estimation of the parameters is studied in section 5.4.5.

5.3.4 Initialization and Pseudomeasurement Strategy

The initialization of the iterative process presented in (5.1) is conducted considering a flat profile, i.e. all the bus voltage magnitudes are set to 1 p.u. and all the bus voltage phase angles are set to 0 deg. For the case of transformer impedance ratios, k, they are set to 1, which is a sensible educated guess according to [9]. Nonetheless, once the algorithm has been run for the first time in a particular grid, the initialization of the transformer

impedance ratios can be changed to adopt the estimated parameters provided as an output by the last execution.

As it is analysed in subsection 5.3.2, adding new elements to the state vector reduces measurement redundancy. To counteract this fact, a general practice was common in parameter estimation methods: the inclusion of the last available estimates of the suspicious parameters as pseudomeasurements in the problem. This practice can be applied to the case of the estimation of transformer impedance ratios; however, this strategy has been argued as controversial [6, 54]. Certainly, if the system is not observable without the pseudomeasurements, then the parameters become critical and their estimates become equal to the initialization values. On the other hand, if the pseudomeasurements are not critical, but redundant, the arbitrary weights assigned to them can lead to largely biased results. For this reason, transformer impedance ratios have not been included as pseudomeasurements in the present implementation.

It is important to note that, if pseudomeasurements of the estimated parameters are not used, as in the case of the present proposal, initiating the iterative process from a flat start leads to the singularity of the Jacobian matrix at the first iteration. Certainly, all the derivatives with respect to the parameters become zero at this operating point. This problem can be easily counteracted by including the parameters in the state vector only after the first iteration [6]. This is the strategy adopted in the present study.

5.4 Case Studies

A well-tested industrial power system, previously used in [57], has been adopted in these case studies to validate and analyze the proposal. The topology of the network, which includes four tap-changing transformers, together with the voltage levels are depicted in Fig. 5.4. The specific data of the lines, transformers and loads are summarized in Table 5.1.

In order to generate data for the multi-snapshot scenario, the tap position of the transformers and the value of the loads are randomly assigned at each instant. All the transformers provide a voltage regulating range of $\pm 7\%$, with a regulating step, ΔU, of 1%. Thus, each p.u. turns ratio is calculated at every snapshot according to

$$a = \frac{1}{1 + \Delta U \times I}, \tag{5.33}$$

with I being a random integer which follows a uniform discrete distribution in the range -7 to $+7$. It is worth mentioning that, according to (2.8)–(2.13), at central taps, i.e. a=1, the impedance ratio, k, has no effect on the impedance values of the π-equivalent transformer model. Thus, any snapshot with one or more transformers operating at the central tap positions does not aid in the estimation of the impedance ratio of those particular machines. However, provided that there is not a transformer in the grid permanently connected

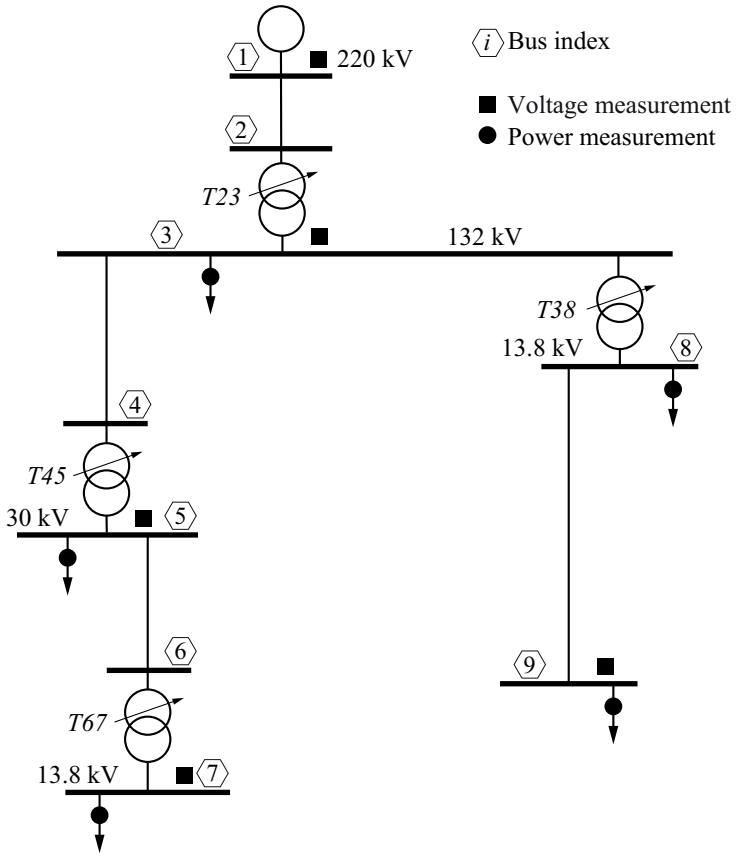

Fig. 5.4 9-bus test grid. The specific set of measurements used in the case study shown in section 5.4.4 is highlighted in this figure.

at the central tap position (i.e. during the T snapshots considered in the problem), the measurement sets include information on every transformer impedance ratio, and thus, all those parameters become observable. The diversity of each snapshot is further guaranteed by assigning random values to each active and reactive power injection. Thus, a random value from a continuous uniform distribution within the range of -50% to $+50\%$ is added to the mean value of each of the loads shown in Table 5.1. In this way, the case studies presented in this section incorporate the possible influence of the variation of the transformer load level in the performance of the parameter estimation algorithm.

With the aim of emulating the measurement acquisition process, the topological information and assigned values for taps and loads were used to conduct a power flow of the grid for each snapshot. The system states, which were verified with OpenDSS [34], were used to calculate the full set of ideal measurements: bus voltages magnitudes, active and reactive power injections and active and reactive line power flows. Eventually, Gaussian noise was added to these measurements in order to obtain a set of corrupted regular measurements which, together with virtual measurements (from zero injection buses), were included in the SE process. According to [6], sensible values for the standard deviation of the measurements can be selected as $\sigma = 0.1 \cdot \gamma \cdot FS$ for voltage measurements and as $\sigma = \gamma \cdot FS$ for power measurements, where γ stands for the accuracy class of the measurement device and FS stands for the full scale value in accordance with the largest

Table 5.1 Parameters of the 9-Bus Test Grid

Line Data

From bus	To bus	Length [km]	Impedance [Ω/km]
1	2	4.7	$0.025 + 0.240i$
3	4	1.5	$0.161 + 0.151i$
5	6	0.3	$0.568 + 0.133i$
8	9	1.8	$0.161 + 0.112i$

Transformer Data

No.	a-range[1] [p.u.]	Rating[2] [MVA]	R_{sc} [%]	X_{sc} [%]	k [p.u.]
T23	0.934 : 1.075	2×270	0.90	12.97	0.75
T45	0.934 : 1.075	3×37.5	0.90	8.95	1.25
T67	0.934 : 1.075	10	0.95	4.76	0.70
T38	0.934 : 1.075	3×50	0.92	7.95	1.35

Load Data - Mean values[3]

Bus	P [MW]	Q [Mvar]	Bus	P [MW]	Q [Mvar]
3	84.0	26.0	8	52.0	39.0
5	34.0	12.0	9	1.7	1.5
7	7.5	5.0	–	–	–

[1] Taps are randomly selected within this range.

[2] Preceded by the number of transformers connected in parallel.

[3] Load data are randomly generated around the mean values.

magnitude expected at the respective measurement point. In the present proposal, devices of accuracy class 0.1 according to [58] were considered and, for the sake of simplicity, the value of the corresponding ideal measurement was adopted as the full scale value.

5.4.1 Validation of the Proposal

For an initial validation of the proposal, a full redundancy scenario is considered. This includes measurements for bus voltage magnitudes, sending and receiving branch power flows, and power injections at each bus (except for bus 1 that is taken as the slack). According to (5.31), a redundancy of 3.35 corresponds to this base case. However, considering (5.32), the inclusion of k parameters in a single-snapshot implementation of the augmented SE problem reduces the redundancy level to 2.71. To recover most of the redundancy of the base case, 20 snapshots are considered in this initial study, which, according to (5.32), increases its level to 3.31. In this full redundancy scenario, the algorithm converges in 7 iterations using a threshold of $1e-8$ for the maximum absolute value of the state variable deviations, Δx. The conventional state variables, not shown here for the sake of clarity, are found to be very close to the actual values, previously obtained from the power flow analysis. Finally, the estimated values of the transformer

Table 5.2 Comparison of Actual and Estimated Impedance Ratios - Full Redundancy - 20 Snapshots

Transformer p.u. Impedance Ratios			
No.	k^{AC} [p.u.]	k^{SE} [p.u.]	$\|e\|$ [%]
T23	0.7500	0.7396	1.04
T45	1.2500	1.2471	0.29
T67	0.7000	0.6994	0.06
T38	1.3500	1.3306	1.94

p.u. impedance ratios, k^{SE}, are presented in Table 5.2, together with their actual values, k^{AC}, and absolute errors, $|e|$. A maximum absolute error (MAE) of 1.94% and an average absolute error (AAE) of 0.83% allow to demonstrate the validity of the proposal.

5.4.2 Improvement in SE Results

In [9, 10], through several case studies, the advantages of using the new transformer model with an educated guess of k=1, was established. However, as the present proposal allows for the offline estimation of accurate values of transformer p.u. impedance ratios, it is interesting to assess the expected improvement in the accuracy of SE results, as those provided by an online state estimator, as a consequence of this refinement. With this aim, a single snapshot standard WLS augmented matrix state estimator was used to calculate the state variables of the grid in Fig. 5.4 for the 20 measurement snapshots considered in the previous case study (i.e. the one shown in subsection 5.4.1). This test was carried out with two different setups of the transformer impedance ratios: Case A) uses the educated guess proposed in [4], [5], i.e. all the parameters are assumed as equal to 1; conversely, in Case B) the estimated parameters shown in the 3$^{\text{rd}}$ column of Table 5.2 were used along the SE process.

As it is highlighted in [9, 10], the errors derived from the use of an inaccurate value of k become more significant at extreme tap positions and are highly dependent on the power factor of the power flow. As the case study reported in subsection 5.4.1 uses both load values and tap positions randomly generated, a diverse influence of the errors caused by k is assured. Two figures of merit have been used to assess the comparison: (1) the MAE of bus voltage magnitudes and phase angles with respect to the true state, calculated considering the full set of buses and snapshots, and (2), the average value of the sum of variances over Q snapshots, defined as

$$\sigma_{av}^2 = \frac{1}{Q}\sum_{q=1}^{Q}\left[\frac{1}{S}\sum_{s=1}^{S}(\hat{x}_{sq} - x_{sq})^2\right], \tag{5.34}$$

with $\hat{x}_{sq}$ and x_{sq} being the estimated and true state of the s-th state variable of the system at snapshot q, which has been used with this aim in similar studies [59]. The true state of the system was previously obtained for each snapshot by using a power flow algorithm

Table 5.3 Comparison of Estimation Errors in State Variables - A) Using an Educated Guess, k_t=1, B) Using Estimates of k_t

	σ^2_{av}	$MAE(V), [\%]$	$MAE(\theta), [deg.]$
Case A	1.2776 e-4	0.0438	0.0449
Case B	0.0106 e-4	0.0078	0.0049

with the true values of k, i.e, those shown in the 2$^{\text{nd}}$ column of Table 5.2. The results in Table 5.3 show the values of the aforementioned figures of merit.

From Table 5.3, it becomes evident that the errors in the estimated states are significantly reduced with the use of accurate estimates of transformer impedance ratios. This result ensures the practical usefulness of the proposal.

5.4.3 Influence of the Number of Snapshots

As it is stated in (5.32), using a large number of snapshots should return the redundancy of the SE problem close to the one from the base case. However, it is still interesting to analyze if the quality of the estimates of the transformer impedance ratios keeps improving with the number of snapshots or if, from a certain point, adding more snapshots is not really worthy. This case study is designed to test this specific feature, and for that, the same base case of subsection 5.4.1 is used. However, now, the test is repeated with an increasing number of snapshots, Q, ranging from 1 to 60. The quality of these multi-snapshot estimates is assessed by using different figures of merit. Thus, Figure 5.5 represents the value of the MAE, AAE and root mean square error (RMSE). The definitions of these figures of merit, in the context of this test, are included in the legend of the figure. Note that k_t^{AC} and k_t^{SE} are the actual and estimated values of p.u. impedance ratios, t, and T being the particular and the total number of transformer impedance ratios to be estimated.

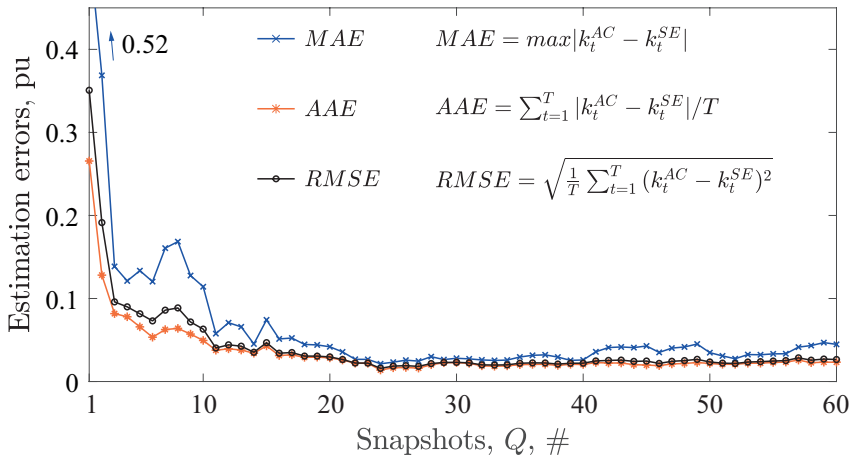

Fig. 5.5 Estimation errors of transformer impedance ratios vs. number of snapshots - full redundancy.

From Fig. 5.5, it can be concluded that using a very low number of snapshots is not feasible, as Q in ranges from 1 to 11 may lead to gross errors in the estimation of the parameters. On the other hand, the graph shows that these errors decline very fast as new information is included into the problem by increasing the number of snapshots. In this case study, the MAE is always lower than 5% when 12 or more snapshots are included into the problem, and lower than 3.5% if Q is raised to 17. Regarding the RMSE, it is always lower than 5% if at least 11 snapshots are used and lower than 3.5% if more than 12 snapshots are included. Similarly, 9 and 11 snapshots are enough to assure an AAE under 5% and 3.5%, respectively.

It is also interesting to note that, from a certain number of Q, the benefit of adding new snapshots is only marginally significant. Thus, none of the p.u. impedance ratio estimation shows an error higher than 5% (compared with the actual values) when the number of snapshots included in the problem is at least 20. This comparison is presented in Table 5.4. In any case, a compromise between accuracy and computational burden should be assumed by the user.

Table 5.4 Comparison of Actual and Estimated Values - Full Redundancy - Different Snapshots

Transformer p.u. Impedance Ratios					
		$Q = 20$		$Q = 60$	
No.	k^{AC} [p.u.]	k^{SE} [p.u.]	$\|e\|$ [%]	k^{SE} [p.u.]	$\|e\|$ [%]
T23	0.7500	0.7429	0.71	0.7354	1.46
T45	1.2500	1.2309	1.91	1.2194	3.06
T67	0.7000	0.6812	1.88	0.6889	1.11
T38	1.3500	1.3342	1.57	1.3333	1.67

5.4.4 Influence of the Redundancy Level

An interesting concern related to the utilisation of the proposed methodology, is to analyze the influence of the redundancy level on its capability to provide accurate estimates of the transformer impedance ratios. With this aim, the base case used in section 5.4.1 is downgraded now by removing some of the measurements, down to the point in which the system is just observable with a single snapshot. In this minimum redundancy case study, the 17 state variables and 4 parameters to be estimated in the single snapshot scenario, are obtained from a set of 21 measurements, thus leading, according to (5.32), to a redundancy level of 1 for a single-snapshot implementation, i.e. ε_1=1. Specifically, all the power flow measurements, less common at certain parts of the grid, have been completely removed. On the other hand, 5 of the 9 bus voltage magnitudes as well as the full set of power injection measurements are retained. For the benefit of the reader, the specific set of measurements considered in the problem is depicted in Fig. 5.4.

The same multi-snapshot analysis previously conducted in section 5.4.3 for the full redundancy case, has been carried out here for the new minimum redundancy scenario. Fig. 5.6 shows the values of the different figures of merit, i.e. MAE, AAE and RMSE for the different number of snapshots included into the problem, ranging from 1 to 60. Thus, according to (5.32), the maximum redundancy level considered along the test is limited to ε_{60}=1.23.

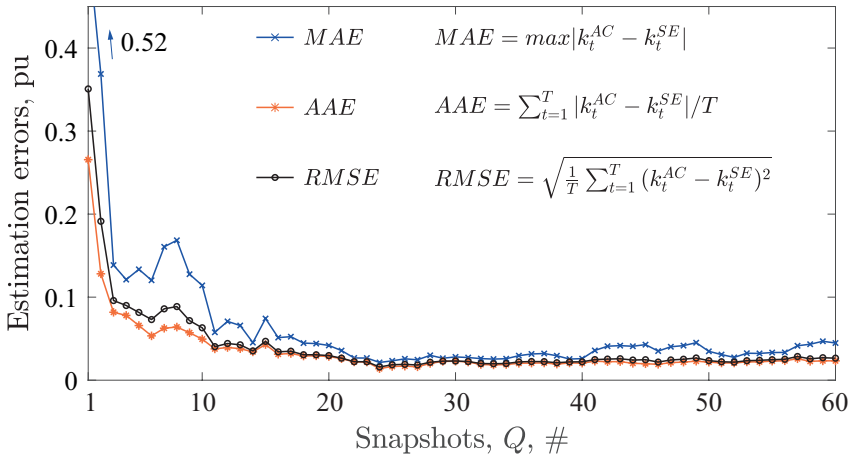

Fig. 5.6 Estimation errors of transformer impedance ratios vs. number of snapshots - minimum redundancy.

Table 5.5 Comparison of Actual and Estimated Values - Minimum Redundancy - Different Snapshots

Transformer p.u. Impedance Ratios					
		$Q = 30$		$Q = 60$	
No.	k^{AC} [p.u.]	k^{SE} [p.u.]	$\|e\|$ [%]	k^{SE} [p.u.]	$\|e\|$ [%]
T23	0.7500	0.7735	2.35	0.7626	1.26
T45	1.2500	1.2220	2.80	1.2052	4.48
T67	0.7000	0.6779	2.21	0.6841	1.59
T38	1.3500	1.3324	1.76	1.3301	1.99

As it can be seen in Fig. 5.6, a similar pattern to the one derived from the full redundancy scenario is obtained, though slightly higher errors arise in this case. However, it is important to highlight that the convergence ratio of the problem is not deteriorated and not more than 8 iterations are needed to solve the SE for any value of Q. This is an important observation for those parts of the grid where full redundancy is typically far from the reality of standard infrastructures. Specifically, the MAE needs at least 18 snapshots to drop under 5%. For the case of the RMSE, 11 snapshots are needed to go under this error threshold. Finally, just 10 snapshots are enough to reduce the AAE under 5%. Estimations from specific snapshots are presented in Table 5.5 for the minimum redundancy case. This allows to conclude that, in order to achieve similar accuracy levels, the user should be aware of including a higher number of snapshots when redundancy is

compromised. Indeed, this observation is aligned with the nature of the problem, as fewer information about the system is being provided if this compensation is not conducted.

5.4.5 Influence of Bad Data

As it was stated in Section 5.3.3, the proposed parameter estimation algorithm is designed to work offline, and thus, a conventional online state estimator is responsible for the detection, identification and removal of bad data. However, using inaccurate values of the transformer impedance ratios (as during the initialization process in which an educated guess is used, k=1), can lead the online state estimator to erroneously flag and remove measurements as bad data. The present case study analyses if the removal of these measurements from the data set could have a significant influence on the estimation of transformer impedance ratios by the offline algorithm.

To replicate the performance of an online state estimator, a single snapshot standard WLS augmented matrix algorithm was applied to the 60 snapshots considered in the full redundancy case study analysed in Section 5.4.3. A value of k=1 was assigned to the impedance ratio of each of the four tapped transformers in Fig. 5.4. The normalized residual test, with a threshold level of 4, was used to detect, identify and remove bad data. The estimation process and bad data test are sequentially repeated until the complete filtering of the input data. As a result, bad data was identified in 28 of the 60 snapshots. Up to a maximum of 4 measurements had to be removed from a single snapshot to reach a set of fully filtered data.

The parameter estimation algorithm proposed in this chapter was applied to the filtered set of measurements for an increasing number of snapshots (from 1 to 60). Fig. 5.7 compares the value of the average absolute error of the estimated parameters with those obtained in section 5.4.3. As can be observed in Fig. 5.7, the removal of measurements can lead to a slight increase in parameter estimation errors when a low number of snapshots are used as input data. However, this effect is practically obliterated by the addition of more snapshots.

It is important to highlight that this situation is only expected during the first execution of the algorithm in a particular grid. Once a realistic approximation to the values of k is available for the online estimator, erroneous bad data detections due to transformer model inaccuracies are not likely to occur. Thus, using a larger number of snapshots during the initialization can be considered a sensible recommendation.

Finally, in a context of lower redundancy, the same pattern shown in Section 5.4.4 is expected. Notice that if the removal of bad data causes the loss of observability, the corresponding snapshot would just not be provided by the online estimator, and thus, it will not have any influence on the parameter estimation algorithm.

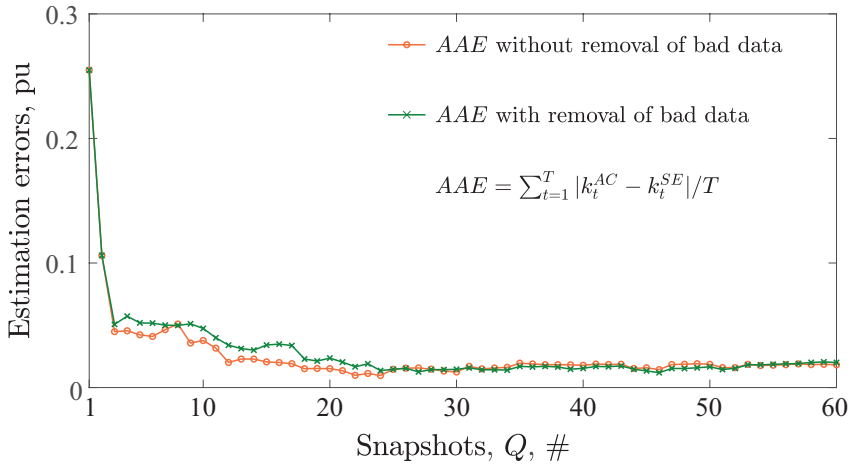

Fig. 5.7 Estimation errors of transformer impedance ratios vs. number of snapshots - influence of bad data.

5.5 Conclusion

An offline state-vector-augmented parameter estimation method, capable of providing accurate estimates of transformer impedance ratios, is proposed, validated, and analyzed in this chapter. Moreover, the derivatives of the different measurement functions in terms of the new parameter, which are essential tools for this or any other linearized state estimator, are provided as a contribution. This study, calls attention to the hindrances found in the estimation of these parameters, such as the significantly lower sensitivity of the measurement functions with respect to p.u. impedance ratios and the reduction of redundancy that their inclusion causes in the state estimation problem. To overcome these difficulties, a method based on the use of a multi-snapshots scenario is proposed and validated in this chapter. A set of case studies are presented in order to validate and demonstrate the usefulness of the proposal, including an analysis of the effect of the number of snapshots and the redundancy level on the accuracy of the estimation. These case studies allow to conclude that, a lower number of snapshots, in the range 1 to 10, are not enough to derive accurate results regardless of the redundancy level. However, the inclusion of a higher number of snapshots always allows to reach acceptable estimates. Though a low measurement redundancy level requires a higher number of snapshots to reach the same accuracy, this chapter demonstrates that even those systems close to the limit of observability can be handled successfully by the proposed algorithm.

Chapter 6

Step Voltage Regulator Modeling and Standard Test System

This chapter delivers two main contributions; first, the development of a general, exact and standardized step voltage regulator model considering all possible configurations, and second, the proposal of a 4-node test system for testing and evaluating three-phase step voltage regulator connections. Although the 4-node test feeder for testing three-phase transformer configurations is already available in the literature, there is no such model for the inclusion, testing, and validation of Step Voltage Regulators in a test feeder. With the contribution presented in this chapter, a new test system will be available to evaluate and benchmark programs or algorithms that attempt to include different configurations of step voltage regulators. The formulation is stated for all three-phase step voltage regulators; i.e. wye, close-delta, and open-delta connections, both type A and B regulators, in raise or lower positions. Subsequently, these models are included in a 4-node test feeder to obtain several power flow solutions. All obtained results are presented here to assist power system software developers.

6.1 Introduction

Step Voltage Regulators (SVRs) have been employed in power feeders for many decades [13–16]. Its modeling posses particular importance in power flow studies of unbalanced distribution networks [17–19] and is gaining even more importance in distribution feeders with the proliferation of distributed generation (DG) [20]; several voltage control possibilities can be achieved by coordinating the small generators and storage units installed near customers and the well-known switched capacitors and step voltage regulators [60]. As an example, the authors in [61] proposed a coordinated control of energy storage systems with SVRs to mitigate the voltage rise caused for high penetration levels of photovoltaic systems. Similar applications can be found in [62] or [63]. In both works

the combination of SVRs, static VAR compensators (SVC) and shunt capacitors (SC) are applied to achieve voltage control in distribution feeders including DG. In [64] the control schedules of SVRs are updated according to wind power predictions to compensate voltage variations derived from high penetration of wind power plants. Many other works related to coordination of SVRs in distributed systems with DG can be found in the literature [65–68]. In [65] a voltage estimation is used to control overvoltages in residential networks with varying PV penetrations. In [66] the authors coordinate the location of reactive power injections from the PV inverters with transformer tap positions in a distributed system as a way to constrain voltage variations. In [67] an unbalanced power flow is used to obtain the influence of SVRs and DG penetration in power losses and voltage profiles. In [68] an optimal control method of distribution voltage with coordination of distributed installations, such as on load tap changers (OLTC), SVR, SC, shunt reactor (ShR), and SVC is proposed.

In [69] a robust, low-cost and high-efficiency voltage regulator is designed for rural networks with serial voltage compensation. In [70] the authors propose distributed voltage control for multiple voltage regulation devices: on-load tap changers, step voltage regulators and switched capacitors in the presence of PV. They tested the scheme in a medium voltage feeder in California. In [71] detailed models for open-delta connected SVR are presented. The authors developed a bus admittance model suitable for unbalanced power flow studies.

Regarding the optimization of tap positions, in [72] an algorithm to set the positions of regulating transformers is proposed. The algorithm is valid for unbalanced and distributed systems. In [73], the authors propose a linear power flow formulation to optimally configure a distribution system using, among other control variables, the tap positions in voltage regulators. In [74], also the tap positions of transformers are included, among others, as optimization variables.

Directly related to SVR modeling, a brief description of a SVR model, to be included in an unbalanced power flow formulation based on the current injection method, can be found in [75]. In [76] the authors are capable of designing dynamic SVRs, but the model they considered is single-phase. From their point of view, this model can be used into a three-phase system taking into account that each phase works independently, so they do not considered closed delta or open-delta configurations. In [77, 2] Kersting addressed the modeling of some SVR configurations to study some of their applications. Those works cover the distribution system modeling in *abc* reference frame, the SVR control mechanism by estimating R and X line settings and other applications of SVRs in distribution systems.

Looking at this literature review we can conclude that SVR modeling and testing are of great importance for distribution systems and power flow studies and are expected to be even more present with the proliferation of DG. However, although there are many extensive works dealing with SVR inclusion in power flow studies, there is not any work

presenting general models and results for all possible configurations. This work might be also used as a benchmark for other researchers.

Reviewing the IEEE test feeders [78] of the IEEE PES Distribution System Analysis Subcommittee's Distribution Test Feeder Working Group, a set of common data for testing and validating software for distribution systems analysis can be found. More specifically, the 4-bus test feeder offers a set of comparison results to deal with transformers of various configurations [79].

In this chapter, the IEEE 4-node test system in [78] will be modified: the transformer is removed to introduce SVRs instead. Thus, a general model for SVR is proposed together with a modified 4-node test feeder. These tools are available for designers and power system software developers as a test standard system with detailed SVR modeling and results.

The chapter is structured as follows. In section 6.2, advantages of the chosen power flow method [80] for unbalanced power flow study is discussed. Then, importantly, a general matrix formulation is stated in section 6.3 for all possible configurations: 2 grounded-wye connections (type A and B regulators), 2 close-delta connections (type A and B), and 6 open-delta connections depending on the selection of phases (3 cases for type A and 3 other cases for type B). The regulators can be at raise or at lower positions. In section 6.4, all these SVR configurations defined a 4-node test feeder that has been formulated in the $\alpha\beta 0$ frame, following the procedure in [80], but adapted for SVRs. Then, in the same section, power flow formulation is presented for balanced and unbalanced loading at different tap positions. In section 6.5, basic data for describing the 4-node test feeder with SVRs are presented. Finally, the problem is solved and the results are presented through section 6.6, 6.7 and appendix A with the Backward Forward Sweep (BFS) algorithm in [81] to obtain the results for all possible configurations. Thereby, section 6.6 describes the formation of study cases whereas section 6.7 and appendix A respectively analyze and present all the results. In section 6.8, a summary of the work is drawn.

6.2 Unbalanced Power Flow in Distribution Systems

Distribution systems are generally unbalanced; therefore, multi-phase power flow methods are required to study such systems. In this dissertation, for validating the SVR models in unbalanced distribution systems, a suitable unbalanced power flow method using the complex theory in $\alpha\beta 0$ stationary reference frame [80] has been carefully chosen. It is a formulation which conjugates the use of the $\alpha\beta 0$ coordinates and the node incidence matrix instead of the admittance matrix. This model is very advantageous as it is ready to incorporate any device. For instance, this model is very adaptive so that the developed regulator models in this dissertation could be incorporated. Also, any other device controlled into the same reference frame can be incorporated into the model as

well. Furthermore, the power flow method used here has three major advantages described below.

6.2.1 Advantage of Node Incidence Matrix

The use of the node incidence matrix, instead of the admittance matrix in the power flow method used here prevents some serious drawbacks such as [82, 80]:

- When using the admittance matrix, it is not possible to unambiguously go back to the line and transformer parameters, as the admittance matrix merges together all parallel lines and shunt devices. However, with the power flow method used, the information regarding the system parameters and topology is separately organized.
- Any change in the topology of the system or in any parameter requires rebuilding the whole admittance matrix. However, in the power flow method used here, any system parameter can be independently modified without restoring the node incidence matrix.

6.2.2 Advantage of $\alpha\beta 0$ Reference over $dq0$ Reference Frame

In unbalanced systems, currents are unbalanced so that, in three-phase reference frame, current and voltage quantities are not phase apart at an angle of 120 degrees to each other. According to Fortescue theorem [83], this three-phase asymmetrical system of phasors will be decomposed into three symmetrical systems of positive, negative and zero sequence, respectively.

The application of $dq0$ reference frame in power flow formulation is not new [84], and it has been recently used in microgrid steady-state modeling [85], and in unified AC/DC power flow analysis [86]. However, in those cases, the $dq0$ reference frame was applied to balanced systems, so the components are constant in steady-state analysis. This is not a valid assumption when working with unbalanced systems [80].

In [5], the $dq0$ reference frame was employed to solve the power flow problem in unbalanced three-phase power systems containing PWM converters. However, in that case, the zero and negative sequences caused pulsating terms to appear which causes the obtained expressions to be quite intricate. Hence, regarding the unbalanced three-phase power flow problem, the use of the $\alpha\beta 0$ reference frame and a complex vector model are proposed in [80]. The use of this reference frame includes the benefits provided by an orthogonal reference frame, avoiding the pulsating terms derived from the existence of sequence components [80].

6.2.3 Advantage in Terms of Network Reconfiguration

In Conventional power flow methods, changes in the location of loads or generators require the recalculation of big matrices. However, a great advantage of the power flow method

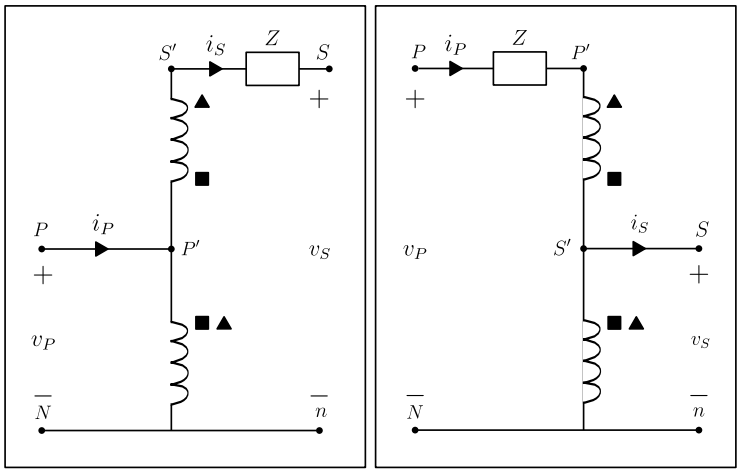

(a) Single-Phase Type A (b) Single-Phase Type B

Fig. 6.1 SVR: Single-phase connections.
▲ Raise position. ■ Lower position.

Table 6.1 Equations for Ideal Single-phase SVRs.

	Operator $\oplus$		a_R	$\frac{v_{P'}}{v_{S'}}$	$\frac{i_P}{i_S}$
Type	Lower	Raise			
A	-	+	$1 \oplus \frac{N_2}{N_1}$	$\frac{1}{a_R}$	a_R
B	+	-		a_R	$\frac{1}{a_R}$

used here is that the general matrix **M** at (6.83) and the grid equation (6.81) depend only on the grid interconnections (nodes and lines). As it will be explained later, any change in the location of loads or generators does not modify these matrices [80].

6.3 SVR modeling

6.3.1 Single-Phase Step Voltage Regulator

A model for an ideal single-phase regulator can be derived from [2]. If the series impedance is to be considered, then, that ideal model needs to be modified. In Fig. 6.1 the single-phase configurations are displayed. P stands for primary (or source side) and S stands for secondary (load side). For the sake of simplicity, as it will be justified later, the series impedance is concentrated at the secondary side for type A configurations and at the primary side for type B configurations. The relationships between voltages and currents for the ideal SVR are summarized in Table 6.1, where N_1 and N_2 are the number of turns of the shunt and series windings, respectively. a_R is the effective turns ratio and is defined in a different way depending on the type of regulator, as it is shown in the Table. From Fig. 6.1 it can be deduced that $P = P'$ for type A and $S = S'$ for type B regulators.

The relationship between the primary and secondary voltages for type A, single-phase regulators can then be written as follows

$$v_{P'} = v_{S'}\frac{1}{a_R}, \tag{6.1}$$
$$v_{P'} = v_P, \tag{6.2}$$
$$v_{S'} = v_S + Z\, i_S. \tag{6.3}$$

Then replacing (6.2) and (6.3) into (6.1) and taking v_P apart, it becomes

$$v_P = \frac{1}{a_R}v_S + \frac{1}{a_R}Z\, i_S. \tag{6.4}$$

For type A regulators, the primary and secondary currents can be related by

$$i_P = a_R\, i_S. \tag{6.5}$$

The corresponding equations for type B, single-phase regulators, with impedance on the primary side are stated as

$$v_{P'} = v_{S'}\, a_R, \tag{6.6}$$
$$v_{S'} = v_S, \tag{6.7}$$
$$v_P = Zi_P + v_{P'}. \tag{6.8}$$

Then, replacing (6.6) and (6.7) into (6.8) it is deduced that

$$v_P = a_R v_S + Zi_P. \tag{6.9}$$

And finally, the primary and secondary currents for type B regulators can be related by

$$i_P = \frac{1}{a_R}i_S. \tag{6.10}$$

Single-phase equations (6.4),(6.5) for type A regulators and (6.9), (6.10) for type B regulators are the baseline for the definition of the three-phase configurations.

6.3.2 Three-phase Connections

Three-phase configurations to be considered are wye, close-delta and open-delta. In following subsections, upper case letters are used for primary (or source) side and lower case letters represent secondary (or load) side. In the present chapter, type A regulators have been chosen for three-phase connections. However, the same procedure can be extended to type B regulators. For the power flow calculations, the mathematical model in [80] and a BFS algorithm are going to be used. The formulation is valid for any transformer

connection, and the algorithm in $\alpha\beta 0$ frame solves the problems of some transformer connections including three-wire configurations (Δ and ungrounded wye) in the *abc* frame; especially $Y_g\Delta$ connection. These problems are solved by means of the zero components of voltages and currents that are always available in $\alpha\beta 0$ frame [80].

There are three general equations that represent all three-phase connections, which are

$$\left[\mathbf{V}\right]^{\mathrm{P}}_{\alpha\beta 0} = \mathbf{N}_{\mathbf{II}_{\alpha\beta 0}} \left[\mathbf{V}\right]^{\mathrm{S}}_{\alpha\beta 0} \quad + \quad Z\,\mathbf{N}_{\mathbf{I}_{\alpha\beta 0}} \left[\mathbf{I}\right]^{\mathrm{PS}}_{\alpha\beta 0}, \tag{6.11}$$

$$\left[0\right] = -\left[\mathbf{I}\right]^{\mathrm{P}}_{\alpha\beta 0} \quad + \quad \mathbf{N}_{\mathbf{IV}_{\alpha\beta 0}} \left[\mathbf{I}\right]^{\mathrm{PS}}_{\alpha\beta 0}, \tag{6.12}$$

$$\left[0\right] = \left[\mathbf{I}\right]^{\mathrm{S}}_{\alpha\beta 0} \quad + \quad \mathbf{N}_{\mathbf{III}_{\alpha\beta 0}} \left[\mathbf{I}\right]^{\mathrm{PS}}_{\alpha\beta 0}. \tag{6.13}$$

The sub-index $\alpha\beta 0$ are used in the expressions because all the elements in brackets are three-phase $\alpha\beta 0$ components (voltages or currents). The super-indexes P and S stand for the primary and secondary, respectively. The super-index PS stands for primary or secondary, depending on the transformer connection. Equations (6.11), (6.12) and (6.13) comprise an exact model for three-phase transformers, so it can be directly included in the power flow solver. The matrices $\mathbf{N}_{\mathrm{I}_{\alpha\beta 0}}$, $\mathbf{N}_{\mathrm{II}_{\alpha\beta 0}}$, $\mathbf{N}_{\mathrm{III}_{\alpha\beta 0}}$ and $\mathbf{N}_{\mathrm{IV}_{\alpha\beta 0}}$ are different for each transformer connection. Any transformer connection is defined by these four matrices and the phase impedance Z. These equations can be also used to model SVRs, as it is demonstrated in the following.

The meaning of superscript PS changes with the type of regulator. If (6.11) is compared to (6.4) and (6.9), it seems as in the SVR case, it is easy to consider that PS stands for secondary in type A regulators and for primary in type B regulators. This fact is proven for each transformer connection. Z is the transformer impedance, that is supposed to be the same for all the phases.

In the present chapter, the matrices $\mathbf{N}_{\mathrm{I}_{\alpha\beta 0}}$, $\mathbf{N}_{\mathrm{II}_{\alpha\beta 0}}$, $\mathbf{N}_{\mathrm{III}_{\alpha\beta 0}}$ and $\mathbf{N}_{\mathrm{IV}_{\alpha\beta 0}}$ will be defined to include any type of SVR configuration in the power flow solution. These equations are firstly obtained in the *abc* frame and subsequently transformed into the $\alpha\beta 0$ frame using the transformation matrix $\mathbf{A}$, which is

$$\mathbf{A} = \sqrt{\frac{2}{3}} \begin{pmatrix} 1 & 0 & \frac{1}{\sqrt{2}} \\ -\frac{1}{2} & \frac{\sqrt{3}}{2} & \frac{1}{\sqrt{2}} \\ -\frac{1}{2} & -\frac{\sqrt{3}}{2} & \frac{1}{\sqrt{2}} \end{pmatrix}. \tag{6.14}$$

6.3.2.1 Wye-connected Regulators

Three-phase wye-connected regulators are depicted in Fig. 6.2(a) (type A) and Fig. 6.2(b) (type B). The winding polarities are shown for both raise and lower positions. The equations that relate the primary and secondary phase-to-neutral voltages are similar to

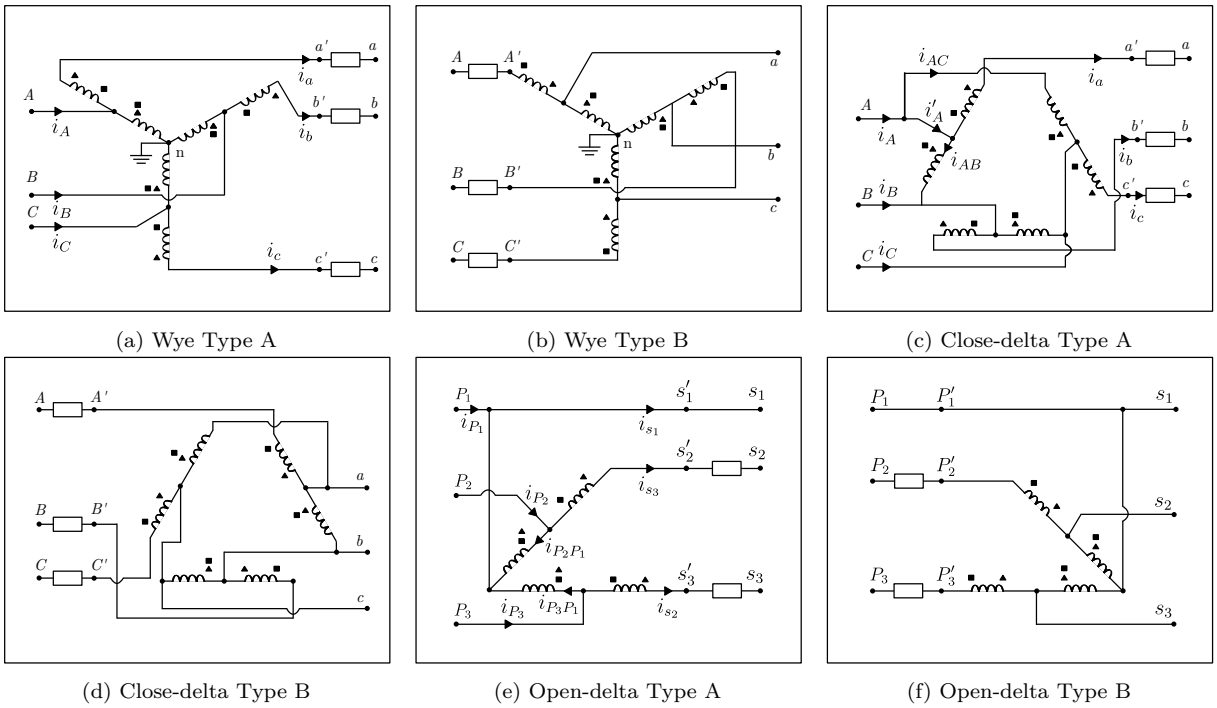

(a) Wye Type A (b) Wye Type B (c) Close-delta Type A

(d) Close-delta Type B (e) Open-delta Type A (f) Open-delta Type B

Fig. 6.2 SVR: Three-phase connections.
▲ Raise position. ■ Lower position.

those for the single-phase (6.4), but extended to the three-phase wye connection as

$$\begin{bmatrix} v_A \\ v_B \\ v_C \end{bmatrix} = \begin{pmatrix} \frac{1}{a_{R_a}} & 0 & 0 \\ 0 & \frac{1}{a_{R_b}} & 0 \\ 0 & 0 & \frac{1}{a_{R_c}} \end{pmatrix} \begin{bmatrix} v_a \\ v_b \\ v_c \end{bmatrix} + \cdots$$

$$+ \quad \cdots Z \begin{pmatrix} \frac{1}{a_{R_a}} & 0 & 0 \\ 0 & \frac{1}{a_{R_b}} & 0 \\ 0 & 0 & \frac{1}{a_{R_c}} \end{pmatrix} \begin{bmatrix} i_a \\ i_b \\ i_c \end{bmatrix}. \tag{6.15}$$

This equation can be expressed in matrix form as

$$\Big[\mathbf{V}\Big]^{\mathrm{P}}_{abc} = \mathbf{N}_{\mathrm{II}_{abc}} \Big[\mathbf{V}\Big]^{\mathrm{S}}_{abc} + Z\, \mathbf{N}_{\mathrm{I}_{abc}} \Big[\mathbf{I}\Big]^{\mathrm{S}}_{abc}, \tag{6.16}$$

where

$$\mathbf{N}_{\mathrm{I}_{abc}} = \mathbf{N}_{\mathrm{II}_{abc}} = \begin{pmatrix} \frac{1}{a_{R_a}} & 0 & 0 \\ 0 & \frac{1}{a_{R_b}} & 0 \\ 0 & 0 & \frac{1}{a_{R_c}} \end{pmatrix}. \tag{6.17}$$

Translating (6.16) into the $\alpha\beta 0$ frame, the resulting equation is

$$\mathbf{A}\Big[\mathbf{V}\Big]^{\mathrm{P}}_{\alpha\beta 0} = \mathbf{N}_{\mathrm{II}_{abc}} \mathbf{A} \Big[\mathbf{V}\Big]^{\mathrm{S}}_{\alpha\beta 0} + Z\, \mathbf{N}_{\mathrm{I}_{abc}} \mathbf{A} \Big[\mathbf{I}\Big]^{\mathrm{S}}_{\alpha\beta 0}, \tag{6.18}$$

and taking $\left[\mathbf{V}\right]^{\mathrm{P}}_{\alpha\beta 0}$ apart, the following equation applies

$$\left[\mathbf{V}\right]^{\mathrm{P}}_{\alpha\beta 0} = \mathbf{N}_{\mathbf{II}_{\alpha\beta 0}} \left[\mathbf{V}\right]^{\mathrm{S}}_{\alpha\beta 0} + Z\, \mathbf{N}_{\mathbf{I}_{\alpha\beta 0}} \left[\mathbf{I}\right]^{\mathrm{S}}_{\alpha\beta 0}, \tag{6.19}$$

where two of the four generalized matrices are defined as

$$\mathbf{N}_{\mathrm{I}_{\alpha\beta 0}} = \mathbf{A}^{-1}\mathbf{N}_{\mathrm{I}_{abc}}\mathbf{A}, \tag{6.20}$$

$$\mathbf{N}_{\mathrm{II}_{\alpha\beta 0}} = \mathbf{A}^{-1}\mathbf{N}_{\mathrm{II}_{abc}}\mathbf{A}. \tag{6.21}$$

Equation (6.19) is already of the same form as (6.11), proving that $[\mathbf{I}]^{\mathrm{PS}}_{\alpha\beta 0}$ are secondary currents for wye type A configurations. For the case of type B regulators, primary currents are needed instead.

To derive the relationships between the primary and secondary currents, from (6.5) the resulting three-phase equation is

$$\begin{bmatrix} i_A \\ i_B \\ i_C \end{bmatrix} = \begin{pmatrix} a_{R_a} & 0 & 0 \\ 0 & a_{R_b} & 0 \\ 0 & 0 & a_{R_c} \end{pmatrix} \begin{bmatrix} i_a \\ i_b \\ i_c \end{bmatrix}. \tag{6.22}$$

This equation can be rewritten in matrix form as

$$\left[\mathbf{I}\right]^{\mathrm{P}}_{abc} = \mathbf{N}_{\mathrm{IV}_{abc}} \left[\mathbf{I}\right]^{\mathrm{S}}_{abc}, \tag{6.23}$$

where

$$\mathbf{N}_{\mathrm{IV}_{abc}} = \begin{pmatrix} a_{R_a} & 0 & 0 \\ 0 & a_{R_b} & 0 \\ 0 & 0 & a_{R_c} \end{pmatrix}. \tag{6.24}$$

Translating this equation into the $\alpha\beta 0$ frame and taking all terms to the right, (6.25) can be reached as

$$[0] = -\left[\mathbf{I}\right]^{\mathrm{P}}_{\alpha\beta 0} + \mathbf{N}_{\mathrm{IV}_{\alpha\beta 0}} \left[\mathbf{I}\right]^{\mathrm{S}}_{\alpha\beta 0}. \tag{6.25}$$

Equation (6.25) can be now identified with (6.12), being $[\mathbf{I}]^{\mathrm{PS}}_{\alpha\beta 0}$ equal to $[\mathbf{I}]^{\mathrm{S}}_{\alpha\beta 0}$ in this case. From (6.25) another generalized matrix in the $\alpha\beta 0$ frame can be derived as

$$\mathbf{N}_{\mathrm{IV}_{\alpha\beta 0}} = \mathbf{A}^{-1}\mathbf{N}_{\mathrm{IV}_{abc}}\mathbf{A}. \tag{6.26}$$

To obtain the last generalized matrix $\mathbf{N}_{\mathrm{III}_{\alpha\beta 0}}$, an equation similar to (6.13) has to be written. First, it has to be assured that (6.27) is checked as

$$[0] = \left[\mathbf{I}\right]^{\mathrm{S}}_{abc} - \left[\mathbf{I}\right]^{\mathrm{S}}_{abc}. \tag{6.27}$$

Then, introducing matrix $\mathbf{N}_{\mathrm{III}_{abc}}$ in (6.28)

$$\mathbf{N}_{\mathrm{III}_{abc}} = -\begin{pmatrix} 1\,0\,0 \\ 0\,1\,0 \\ 0\,0\,1 \end{pmatrix}, \tag{6.28}$$

(6.27) becomes

$$\left[0\right] = \left[\mathbf{I}\right]^{\mathrm{S}}_{abc} + \mathbf{N}_{\mathrm{III}_{abc}} \left[\mathbf{I}\right]^{\mathrm{S}}_{abc}. \tag{6.29}$$

If 6.29 is transformed into the $\alpha\beta 0$ reference frame it leads to

$$\left[0\right] = \left[\mathbf{I}\right]^{\mathrm{S}}_{\alpha\beta 0} + \mathbf{N}_{\mathrm{III}_{\alpha\beta 0}} \left[\mathbf{I}\right]^{\mathrm{S}}_{\alpha\beta 0}, \tag{6.30}$$

where

$$\mathbf{N}_{\mathrm{III}_{\alpha\beta 0}} = \mathbf{A}^{-1}\mathbf{N}_{\mathrm{III}_{abc}}\mathbf{A}. \tag{6.31}$$

Considering in this case that $[\mathbf{I}]^{\mathrm{PS}}_{\alpha\beta 0}$ are secondary currents, (6.30) is of the same form as (6.13), so the model is feasible to be introduced into the power flow formulation of [80].

The four equations (6.20), (6.21), (6.26) and (6.31) demonstrate that for a generic matrix in the *abc* frame, $\mathbf{N}_{abc}$, the corresponding matrix in the $\alpha\beta 0$ frame, $\mathbf{N}_{\alpha\beta 0}$, can be computed as

$$\mathbf{N}_{\alpha\beta 0} = \mathbf{A}^{-1}\mathbf{N}_{abc}\mathbf{A}. \tag{6.32}$$

The four matrices $\mathbf{N}_{\mathrm{I}_{abc}}$,$\mathbf{N}_{\mathrm{II}_{abc}}$,$\mathbf{N}_{\mathrm{III}_{abc}}$ and $\mathbf{N}_{\mathrm{IV}_{abc}}$ are presented in Table 6.4 for this connection and also for subsequent connections. $i_{d(3\times 3)}$ stands for the identity matrix with dimensions (3×3). Because all matrices are defined in terms of effective turns ratio instead of number of turns, they are valid for both raise and lower positions.

6.3.2.2 Close Delta-connected Regulators

Three single-phase regulators can be connected in close-delta configurations as shown in Figs. 6.2(c) (type A) and 6.2(d) (type B). Both lower and raise positions give different polarities in the windings, as it is also depicted in those figures. For close-delta connections line-to-line voltages have to be considered. The relationship between the primary and secondary line voltages in type A close-delta case, is given by (refer to Fig. 6.2(c))

$$v_{AB} + v_{Bb'} + v_{b'a'} + v_{a'A} = 0. \tag{6.33}$$

So secondary voltage $v_{a'b'}$ can be written as

$$v_{a'b'} = v_{AB} + v_{Bb'} + v_{a'A}. \tag{6.34}$$

The voltages v_{AB} and $v_{a'A}$ are related by the effective turns ratio for the regulator connected between phases A and B [2]. The same assumption can be made for voltages v_{BC} and $v_{b'B}$.

If the shunt winding has a number of turns N_1, the series winding has a number of turns N_2 and the raise position is taken in consideration then these can be derived

$$\frac{v_{AB}}{v_{a'A}} = \frac{N_1}{N_2}, \tag{6.35}$$

$$\frac{v_{BC}}{v_{b'B}} = \frac{N_1}{N_2}. \tag{6.36}$$

If $v_{Bb'}$ and $v_{a'A}$ are replaced into (6.34) by their relations to v_{AB} and v_{BC} using (6.35) and (6.36) it is deduced that

$$v_{a'b'} = v_{AB}(1 + \frac{N_2}{N_1}) + v_{BC}(-\frac{N_2}{N_1}). \tag{6.37}$$

If the reversing switches of all regulators are in raise position, this equation can be rewritten in terms of the effective turns ratios (see Table 6.1); i.e. $a_{R_{ab}}$ (for the regulator between phases A and B) and $a_{R_{bc}}$ (for the regulator between phases B and C), as

$$v_{a'b'} = a_{R_{ab}}\, v_{AB} + (1 - a_{R_{bc}})\, v_{BC}. \tag{6.38}$$

If the same procedure is followed for obtaining the voltages $v_{b'c'}$ and $v_{c'a'}$, the resulting three-phase equation can be expressed as

$$\begin{bmatrix} v_{a'b'} \\ v_{b'c'} \\ v_{c'a'} \end{bmatrix} = \begin{pmatrix} a_{R_{ab}} & 1 - a_{R_{bc}} & 0 \\ 0 & a_{R_{bc}} & 1 - a_{R_{ca}} \\ 1 - a_{R_{ab}} & 0 & a_{R_{ca}} \end{pmatrix} \begin{bmatrix} v_{AB} \\ v_{BC} \\ v_{CA} \end{bmatrix}. \tag{6.39}$$

With a similar reasoning for lower positions in the regulators, the same expression would be derived, so regardless of whether the regulators are raising or lowering the voltages, the same (6.39) applies.

If the matrix in the first term of the right-hand side of (6.39) is renamed as $\mathbf{A}_{R_V}$ (which is non-singular and invertible) the primary voltages are obtained as

$$\left[\mathbf{V}\right]_{abc}^{\text{S'}} = \mathbf{A}_{R_V} \left[\mathbf{V}\right]_{abc}^{\text{P}}. \tag{6.40}$$

As it was explained in the previous subsection, being the regulators of type A, the impedances must be considered into the secondary side. Then, the matrix equation that includes the voltage drop across those impedances is given by

$$\begin{bmatrix} v_{a'a} \\ v_{b'b} \\ v_{c'c} \end{bmatrix} = Z \begin{bmatrix} i_a \\ i_b \\ i_c \end{bmatrix}. \tag{6.41}$$

The line voltages in the secondary side are then computed as

$$\begin{bmatrix} v_{a'b'} \\ v_{b'c'} \\ v_{c'a'} \end{bmatrix} = \begin{bmatrix} v_{ab} \\ v_{bc} \\ v_{ca} \end{bmatrix} + \begin{pmatrix} 1 & -1 & 0 \\ 0 & 1 & -1 \\ -1 & 0 & 1 \end{pmatrix} \begin{bmatrix} v_{a'a} \\ v_{b'b} \\ v_{c'c} \end{bmatrix}. \tag{6.42}$$

The matrix in the second term of the right-hand side of (6.42), which is singular, can be labeled as $\mathbf{T}_{\mathrm{DY}}$. It is a singular matrix. Substituting (6.41) into (6.42) and it can be written into matrix form as

$$\Big[\mathbf{V}\Big]^{\mathrm{S'}}_{abc} = \Big[\mathbf{V}\Big]^{\mathrm{S}}_{abc} + Z\,\mathbf{T}_{DY}\,\Big[\mathbf{I}\Big]^{\mathrm{S}}_{abc}. \tag{6.43}$$

Merging equations (6.40) and (6.43) and taking primary voltages apart, the resulting equation is

$$\Big[\mathbf{V}\Big]^{\mathrm{P}}_{abc} = \mathbf{A}^{-1}_{R_V}\Big[\mathbf{V}\Big]^{\mathrm{S}}_{abc} + \mathbf{A}^{-1}_{R_V}\,Z\,\mathbf{T}_{\mathrm{DY}}\Big[\mathbf{I}\Big]^{\mathrm{S}}_{abc} \tag{6.44}$$

Equation (6.44) might be written in the same form of (6.11). A comparison between both equations reveals

$$\mathbf{N}_{\mathbf{I}_{abc}} = \mathbf{A}^{-1}_{R_V}\,\mathbf{T}_{\mathrm{DY}}, \tag{6.45}$$

$$\mathbf{N}_{\mathbf{II}_{abc}} = \mathbf{A}^{-1}_{R_V}. \tag{6.46}$$

To derive the relationships between the primary and secondary currents, if current references are taken as shown in Fig. 6.2(c), it can be assured that

$$i_A = i_{A'} + i_{AC}, \tag{6.47}$$

$$i_{A'} = i_a + i_{AB}. \tag{6.48}$$

Again, the relationship between currents through shunt and series windings can be computed in terms of the turns ratio

$$\frac{i_{AC}}{i_c} = -\frac{N_2}{N_1}, \tag{6.49}$$

$$\frac{i_{AB}}{i_a} = \frac{N_2}{N_1}. \tag{6.50}$$

Merging equations (6.47), (6.48), (6.49) and (6.50) into a single equation, it can be formulated that

$$i_A = i_a\,(1 + \frac{N_2}{N_1}) + i_c\,(-\frac{N_2}{N_1}). \tag{6.51}$$

Because the regulators are in raise position, (6.51) can be written as (see Table 6.1)

$$i_A = a_{R_{ab}}\,i_a + (1 - a_{R_{ca}})i_c. \tag{6.52}$$

Table 6.2 Terminals Notation for Open Delta Connections.

Regulators	**Case a** *ab & ca*		**Case b** *bc & ab*		**Case c** *ca & bc*	
Type	**A**	**B**	**A**	**B**	**A**	**B**
$P_1\ P_2\ P_3$	$A\ B\ C$	$A\ B\ C$	$B\ C\ A$	$B\ C\ A$	$C\ A\ B$	$C\ A\ B$
$P_1'\ P_2'\ P_3'$	–	$A'\ B'\ B'$	–	$B'\ B'\ A'$	–	$B'\ A'\ B'$
$s_1\ s_2\ s_3$	$a\ b\ c$	$a\ b\ c$	$b\ c\ a$	$b'\ c'\ a'$	$c\ a\ b$	$c'\ a'\ b'$
$s_1'\ s_2'\ s_3'$	$a'\ b'\ c'$	–	$b'\ c'\ a'$	–	$c'\ a'\ b'$	–

In a similar manner, the primary currents i_B and i_C can be also expressed in terms of secondary currents and effective turns ratios. The generalized matrix equation that relates the primary and secondary currents is finally given by

$$\begin{bmatrix} i_A \\ i_B \\ i_C \end{bmatrix} = \begin{pmatrix} a_{R_{ab}} & 0 & 1-a_{R_{ca}} \\ 1-a_{R_{ab}} & a_{R_{bc}} & 0 \\ 0 & 1-a_{R_{bc}} & 0 \end{pmatrix} \begin{bmatrix} i_a \\ i_b \\ i_c \end{bmatrix}. \tag{6.53}$$

Labeling the matrix of the first term in the right-hand side of (6.53) as A_{R_I}, the expression becomes

$$\left[\mathbf{I}\right]_{abc}^{\mathrm{P}} = \mathbf{A}_{R_I} \left[\mathbf{I}\right]_{abc}^{\mathrm{S}}. \tag{6.54}$$

Equation (6.54) is written in the same form as (6.12) so matrix $\mathbf{N}_{\mathrm{IV}_{abc}}$ is already known as

$$\mathbf{N}_{\mathrm{IV}_{abc}} = \mathbf{A}_{R_I}. \tag{6.55}$$

In this case, (6.29) also applies, so matrix $\mathbf{N}_{\mathrm{III}_{abc}}$ is the same as in (6.28).

The four matrices $\mathbf{N}_{\mathrm{I}_{abc}}$, $\mathbf{N}_{\mathrm{II}_{abc}}$, $\mathbf{N}_{\mathrm{III}_{abc}}$ and $\mathbf{N}_{\mathrm{IV}_{abc}}$ are included in Table 6.4 for both close-delta connections (type A and B). All these matrices are defined again in terms of turns ratios, so they are the same for both raise and lower positions.

6.3.2.3 Open-delta Connections

Two single-phase regulators can be connected giving rise to a three-phase configuration. This is an open-delta connection. Because there are two regulators to be connected between three phases, there are three different connections (or cases). In this chapter, the notation case a, case b and case c is going to be used. All configurations are depicted in Fig. 6.2(c) for type A regulators and in Fig. 6.2(f) for type B regulators. As in previous connections, the impedances are considered in the primary side for type B and in the secondary side for type A regulators.

In Figs. 6.2(c) and 6.2(f), characters P_1, P_2, P_3, P_1', P_2' and P_3' are used in the primary side and s_1, s_2, s_3, s_1', s_2' and s_3' denote secondary side. The schemes are general for all open-delta configurations; the meaning of each character in both figures depends on the considered case, as it is detailed in Table 6.2. For instance, in case b the two regulators are connected between phases *bc* and *ab*. As before, upper case letters are employed for the terminals at primary side and lower case letters are used for secondary side. The

meaning of each character P_1, P_2 and P_3 are B, C and A, respectively for both types of regulators. P_1', P_2' and P_3' stand for B', C' and A' for type B regulators and has no meaning for type A because those points do not exist in open-delta connected type A regulators (see Fig. 6.2(c)).

In this section, the open-delta connection, case a with type A regulators has been chosen as the case to explain the open-delta general model. The regulators are supposed to be in raise position. The matrices needed for the power flow problem are going to be deduced for this specific case, but with the general notation of Figs. 6.2(c) and 6.2(f) and Table 6.2.The same reasoning may be applied to any other open-delta configuration.

First, it has to be noted for the studied configuration that phase A in the primary and phase a in the secondary are directly connected, so it can be written $A = a'$. From Fig. 6.2(c) the voltages through the first regulator are related by

$$v_{a'b'} = v_{Ab'} = v_{AB} + v_{Bb'}. \tag{6.56}$$

Being N_1 the turns number for the shunt winding and N_2 the turns number for the series winding (in the regulator connected to phases ab), the voltages v_{AB} and $v_{Bb'}$ can be related as

$$\frac{v_{Bb'}}{v_{AB}} = \frac{N_2}{N_1}. \tag{6.57}$$

Merging (6.56) and (6.57) into a single equation, the following expression is obtained

$$v_{a'b'} = v_{AB} + v_{AB}\frac{N_2}{N_1} = v_{AB}\,(1 + \frac{N_2}{N_1}). \tag{6.58}$$

Being the type A regulators in raise position and according to Table 6.1, 6.58 becomes

$$v_{a'b'} = a_{R_{ab}}\, v_{AB}. \tag{6.59}$$

For voltage $v_{c'a'}$ the same procedure can be followed to obtain these expressions

$$v_{c'a'} = v_{c'C} + v_{CA}, \tag{6.60}$$

$$\frac{v_{c'C}}{v_{CA}} = \frac{N_2}{N_1}, \tag{6.61}$$

$$v_{c'a'} = v_{CA}\,\frac{N_2}{N_1} + v_{CA}, \tag{6.62}$$

$$v_{c'a'} = v_{CA}\,(1 + \frac{N_2}{N_1}), \tag{6.63}$$

$$v_{c'a'} = a_{R_{ca}}\, v_{CA}. \tag{6.64}$$

In matrix form, primary voltages as a function of secondary voltages are now obtained from the combination of (6.59) and (6.64) and taking into account that for three-phase three-wire configurations the primary voltages have to satisfy $v_{AB} + v_{BC} + v_{CA} = 0$, it can

be derived that

$$\begin{bmatrix} v_{AB} \\ v_{BC} \\ v_{CA} \end{bmatrix} = \begin{pmatrix} \frac{1}{a_{R_{ab}}} & 0 & 0 \\ -\frac{1}{a_{R_{ab}}} & 0 & -\frac{1}{a_{R_{ca}}} \\ 0 & 0 & \frac{1}{a_{R_{ca}}} \end{pmatrix} \begin{bmatrix} v_{a'b'} \\ v_{b'c'} \\ v_{c'a'} \end{bmatrix}. \tag{6.65}$$

Here, the number of turns have been replaced by the effective turns ratios of the regulators, as used before with the previous cases.

If the same reasoning is carried out for lower positions, the same matrix appearing in the first term of the right-hand side of (6.65) is also obtained. If this matrix is called $\mathbf{A}_{R_{v2}}$, the equation can be written in compact form as

$$\left[\mathbf{V}\right]_{abc}^{\mathrm{P}} = \mathbf{A}_{R_{v2}} \left[\mathbf{V}\right]_{abc}^{\mathrm{S'}}. \tag{6.66}$$

For the studied connection, the voltage drops across the secondary side impedances are given as

$$\begin{bmatrix} v_{a'a} \\ v_{b'a} \\ v_{c'c} \end{bmatrix} = Z \begin{pmatrix} 0\,0\,0 \\ 0\,1\,0 \\ 0\,0\,1 \end{pmatrix} \begin{bmatrix} i_a \\ i_b \\ i_c \end{bmatrix}. \tag{6.67}$$

There is no voltage drop due to current i_a because of the connection of the regulators (from Fig. 6.2(c) it easily deduced that $A = a = a'$).

Equation (6.42) must be also satisfied in this case, so merging equations (6.42) and (6.67), the secondary voltages can be deduced as

$$\begin{bmatrix} v_{a'b'} \\ v_{b'c'} \\ v_{c'a'} \end{bmatrix} = \begin{bmatrix} v_{ab} \\ v_{bc} \\ v_{ca} \end{bmatrix} + Z\,\mathbf{T}_{\mathrm{DY}} \begin{pmatrix} 0\,0\,0 \\ 0\,1\,0 \\ 0\,0\,1 \end{pmatrix} \begin{bmatrix} i_a \\ i_b \\ i_c \end{bmatrix}. \tag{6.68}$$

Substituting (6.68) into (6.65), and writing the new equation in compact form, the following expression is obtained

$$\left[\mathbf{V}\right]_{abc}^{\mathrm{P}} = \mathbf{A}_{R_{v2}} \left[\mathbf{V}\right]_{abc}^{\mathrm{S}} + Z\,\mathbf{A}_{R_{v2}} \mathbf{T}_{\mathrm{DY}a} \left[\mathbf{I}\right]_{abc}^{\mathrm{S}}, \tag{6.69}$$

where

$$\mathbf{T}_{\mathrm{DY}a} = \begin{pmatrix} 0 & -1 & 0 \\ 0 & 1 & -1 \\ 0 & 0 & 1 \end{pmatrix}. \tag{6.70}$$

Matrix $\mathbf{T}_{\mathrm{DY}a}$ in (6.70) is the same matrix as $\mathbf{T}_{\mathrm{DY}}$ in (6.43)), except that the first column is replaced by zeros. For open-delta configurations case b and case c, the matrices $\mathbf{T}_{\mathrm{DY}b}$

and $\mathbf{T}_{\mathrm{DY}c}$ can be obtained. In the former, the second column in $\mathbf{T}_{\mathrm{DY}}$ should be replaced by zeros, and the same should be done in the latter with the third column$\mathbf{T}_{\mathrm{DY}}$ has been replaced by zeros and in the latter the third column in $\mathbf{T}_{\mathrm{DY}}$ is changed by zeros.

To derive the relationship between the primary and secondary currents in Fig. 6.2(c), the depicted current references as well as the corresponding phases shown in Table 6.2 are needed. From the Fig. these can be derived

$$i_B = i_b + i_{BA}, \tag{6.71}$$

$$i_C = i_c + i_{CA}. \tag{6.72}$$

If for both regulators the numbers of turns are N_1 and N_2 for the shunt and series wingdings, respectively, and the raise position is considered, then it can be assured that

$$\frac{i_{BA}}{i_b} = \frac{N_2}{N_1}, \tag{6.73}$$

$$\frac{i_{CA}}{i_c} = \frac{N_2}{N_1}. \tag{6.74}$$

Merging (6.71)-(6.74), and writing them in terms of turns ratios, it follows that

$$i_B = i_b\,(1 + \frac{N_2}{N_1}) = a_{R_{ab}}\, i_b, \tag{6.75}$$

$$i_C = i_c\,(1 + \frac{N_2}{N_1}) = a_{R_{ca}}\, i_c. \tag{6.76}$$

Merging (6.75) and (6.76) and taking into account that for a three-phase three-wire connection the constraint $i_A + i_B + i_C = 0$ must be satisfied, a matrix equation is obtained as

$$\begin{bmatrix} i_A \\ i_B \\ i_C \end{bmatrix} = \begin{pmatrix} 0 & -a_{R_{ab}} & -a_{R_{ca}} \\ 0 & a_{R_{ab}} & 0 \\ 0 & 0 & a_{R_{ca}} \end{pmatrix} \begin{bmatrix} i_a \\ i_b \\ i_c \end{bmatrix}. \tag{6.77}$$

By assigning the name $\mathbf{A}_{R_{I2}}$ to the first term of the right-hand side of (6.77), this equation is of

$$\Big[\mathbf{I}\Big]^{\mathrm{P}}_{abc} = \mathbf{A}_{R_{I2}}\ \Big[\mathbf{I}\Big]^{\mathrm{S}}_{abc}. \tag{6.78}$$

Then, matrix $\mathbf{N}_{\mathrm{IV}_{abc}}$ can be obtained as

$$\mathbf{N}_{\mathrm{IV}_{abc}} = \mathbf{A}_{R_{I2}}. \tag{6.79}$$

In this case, (6.29) also applies, so matrix $\mathbf{N}_{\mathrm{III}_{abc}}$ is the same matrix as in (6.28).

Matrices $\mathbf{N}_{\mathrm{I}_{abc}}$, $\mathbf{N}_{\mathrm{II}_{abc}}$, $\mathbf{N}_{\mathrm{III}_{abc}}$ and $\mathbf{N}_{\mathrm{IV}_{abc}}$ are included in Table 6.4 for all open-delta configurations (cases a, b and c, type A and B regulators). They are defined in terms of effective turns ratios, so they are the same for both raise and lower positions. To obtain

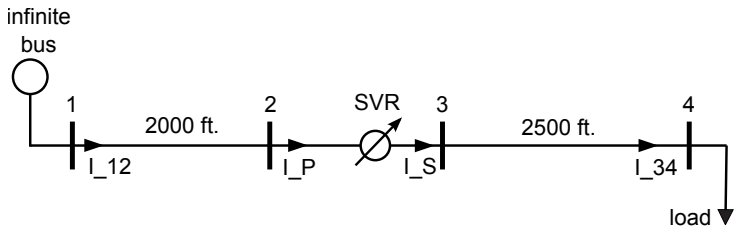

Fig. 6.3 4-node test feeder system

the corresponding $\alpha\beta 0$ frame matrices, the same transformation that was used for previous connections may be applicable as in (6.32).

With the generalized matrices detailed in Table 6.4, the SVR models are prepared for the power flow solver. All the configurations in the Table were simulated in the proposed 4-node test feeder, as it is explained in section 6.6.

6.3.3 Comparison to Previous Works

There are several related works in the literature that present similar SVR models, however, none of them includes all possible configurations. In Table 6.3 a comparison with the models described in previous works is summarized. It can be seen that the type B regulators are usually considered due to the fact they are mainly installed in distribution systems. The present work aims to include not only the most common configurations, but all of them. Thus, a general model is proposed in this chapter, allowing the inclusion of any SVR configuration in power flow analysis.

Table 6.3 Comparison to Previous Modeling Works

reference	connection	type	frame
[60]	**OΔ**	not specified	abc
[62]	**YY**	B	abc
[67]	**YY**	B	abc
[71]	**OΔ**, case b	B	abc
[77]	**YY**	B	abc
[2]	**YY, ΔΔ,OΔ, case b**	B	abc
present work	all	A and B	abc / $\alpha\beta 0$

6.4 4-node Test Feeder Including SVRs

To introduce SVRs in the 4-node test feeder [78], the transformer is replaced by a SVR. The power flow problem to be solved is the one in which the transformer matrices $\mathbf{N}_{\mathrm{I}}$, $\mathbf{N}_{\mathrm{II}}$, $\mathbf{N}_{\mathrm{III}}$ and $\mathbf{N}_{\mathrm{IV}}$ are taken from Table 6.4 for each specific SVR configuration. The matrices in this Table are defined in the *abc* frame, so they need to be transformed into the $\alpha\beta 0$ frame by means of (6.32).

Table 6.4 Matrices for All SVR Configurations.

	$\mathbf{N}_{\mathrm{I}_{abc}}$	$\mathbf{N}_{\mathrm{II}_{abc}}$	$\mathbf{N}_{\mathrm{III}_{abc}}$	$\mathbf{N}_{\mathrm{IV}_{abc}}$
YY type A	$\begin{pmatrix} \frac{1}{a_{R_a}} & 0 & 0 \\ 0 & \frac{1}{a_{R_b}} & 0 \\ 0 & 0 & \frac{1}{a_{R_c}} \end{pmatrix}$	$\begin{pmatrix} \frac{1}{a_{R_a}} & 0 & 0 \\ 0 & \frac{1}{a_{R_b}} & 0 \\ 0 & 0 & \frac{1}{a_{R_c}} \end{pmatrix}$	$-\mathbf{I}_{d\,(3\times3)}$	$\begin{pmatrix} a_{R_a} & 0 & 0 \\ 0 & a_{R_b} & 0 \\ 0 & 0 & a_{R_c} \end{pmatrix}$
YY type B	$\mathbf{I}_{d\,(3\times3)}$	$\begin{pmatrix} a_{R_a} & 0 & 0 \\ 0 & a_{R_b} & 0 \\ 0 & 0 & a_{R_c} \end{pmatrix}$	$-\begin{pmatrix} a_{R_a} & 0 & 0 \\ 0 & a_{R_b} & 0 \\ 0 & 0 & a_{R_c} \end{pmatrix}$	$\mathbf{I}_{d\,(3\times3)}$
ΔΔ type A	$\begin{pmatrix} a_{R_{ab}} & 1-a_{R_{bc}} & 0 \\ 0 & a_{R_{bc}} & 1-a_{R_{ca}} \\ 1-a_{R_{ab}} & 0 & a_{R_{ca}} \end{pmatrix}^{-1}.\mathbf{T_{DY}}$	$\begin{pmatrix} a_{R_{ab}} & 1-a_{R_{bc}} & 0 \\ 0 & a_{R_{bc}} & 1-a_{R_{ca}} \\ 1-a_{R_{ab}} & 0 & a_{R_{ca}} \end{pmatrix}^{-1}$	$-\mathbf{I}_{d\,(3\times3)}$	$\begin{pmatrix} a_{R_{ab}} & 0 & 1-a_{R_{ca}} \\ 1-a_{R_{ab}} & a_{R_{bc}} & 0 \\ 0 & 1-a_{R_{bc}} & a_{R_{ca}} \end{pmatrix}$
ΔΔ type B	$\mathbf{T_{DY}}$	$\begin{pmatrix} a_{R_{ab}} & 1-a_{R_{bc}} & 0 \\ 0 & a_{R_{bc}} & 1-a_{R_{ca}} \\ 1-a_{R_{ab}} & 0 & a_{R_{ca}} \end{pmatrix}$	$-\begin{pmatrix} a_{R_{ab}} & 0 & 1-a_{R_{ca}} \\ 1-a_{R_{ab}} & a_{R_{bc}} & 0 \\ 0 & 1-a_{R_{bc}} & a_{R_{ca}} \end{pmatrix}$	$\mathbf{I}_{d\,(3\times3)}$
OΔ type A case a	$\begin{pmatrix} \frac{1}{a_{R_{ab}}} & 0 & 0 \\ -\frac{1}{a_{R_{ab}}} & 0 & -\frac{1}{a_{R_{ca}}} \\ 0 & 0 & \frac{1}{a_{R_{ca}}} \end{pmatrix}.\mathbf{T_{DY}}_a$	$\begin{pmatrix} \frac{1}{a_{R_{ab}}} & 0 & 0 \\ -\frac{1}{a_{R_{ab}}} & 0 & -\frac{1}{a_{R_{ca}}} \\ 0 & 0 & \frac{1}{a_{R_{ca}}} \end{pmatrix}$	$-\mathbf{I}_{d\,(3\times3)}$	$\begin{pmatrix} 0 & -a_{R_{ab}} & -a_{R_{ca}} \\ 0 & a_{R_{ab}} & 0 \\ 0 & 0 & a_{R_{ca}} \end{pmatrix}$
OΔ type A case b	$\begin{pmatrix} \frac{1}{a_{R_{ab}}} & 0 & 0 \\ 0 & \frac{1}{a_{R_{bc}}} & 0 \\ -\frac{1}{a_{R_{ab}}} & -\frac{1}{a_{R_{bc}}} & 0 \end{pmatrix}.\mathbf{T_{DY}}_b$	$\begin{pmatrix} \frac{1}{a_{R_{ab}}} & 0 & 0 \\ 0 & \frac{1}{a_{R_{bc}}} & 0 \\ -\frac{1}{a_{R_{ab}}} & -\frac{1}{a_{R_{bc}}} & 0 \end{pmatrix}$	$-\mathbf{I}_{d\,(3\times3)}$	$\begin{pmatrix} a_{R_{ab}} & 0 & 0 \\ -a_{R_{ab}} & 0 & -a_{R_{bc}} \\ 0 & 0 & a_{R_{bc}} \end{pmatrix}$
OΔ type A case c	$\begin{pmatrix} 0 & -\frac{1}{a_{R_{bc}}} & -\frac{1}{a_{R_{ca}}} \\ 0 & \frac{1}{a_{R_{bc}}} & 0 \\ 0 & 0 & \frac{1}{a_{R_{ca}}} \end{pmatrix}.\mathbf{T_{DY}}_c$	$\begin{pmatrix} 0 & -\frac{1}{a_{R_{bc}}} & -\frac{1}{a_{R_{ca}}} \\ 0 & \frac{1}{a_{R_{bc}}} & 0 \\ 0 & 0 & \frac{1}{a_{R_{ca}}} \end{pmatrix}$	$-\mathbf{I}_{d\,(3\times3)}$	$\begin{pmatrix} a_{R_{bc}} & 0 & 0 \\ 0 & a_{R_{ca}} & 0 \\ -a_{R_{bc}} & -a_{R_{ca}} & 0 \end{pmatrix}$
OΔ type B case a	$\mathbf{T_{DY}}_a$	$\begin{pmatrix} a_{R_{ab}} & 0 & 0 \\ -a_{R_{ab}} & 0 & -a_{R_{ca}} \\ 0 & 0 & a_{R_{ca}} \end{pmatrix}$	$-\begin{pmatrix} 0 & -\frac{1}{a_{R_{ab}}} & -\frac{1}{a_{R_{ca}}} \\ 0 & \frac{1}{a_{R_{ab}}} & 0 \\ 0 & 0 & \frac{1}{a_{R_{ca}}} \end{pmatrix}$	$\mathbf{I}_{d\,(3\times3)}$
OΔ type B case b	$\mathbf{T_{DY}}_b$	$\begin{pmatrix} a_{R_{ab}} & 0 & 0 \\ 0 & a_{R_{bc}} & 0 \\ -a_{R_{ab}} & -a_{R_{bc}} & 0 \end{pmatrix}$	$-\begin{pmatrix} \frac{1}{a_{R_{ab}}} & 0 & 0 \\ -\frac{1}{a_{R_{ab}}} & 0 & -\frac{1}{a_{R_{bc}}} \\ 0 & 0 & \frac{1}{a_{R_{bc}}} \end{pmatrix}$	$\mathbf{I}_{d\,(3\times3)}$
OΔ type B case c	$\mathbf{T_{DY}}_c$	$\begin{pmatrix} 0 & -a_{R_{bc}} & -a_{R_{ca}} \\ 0 & a_{R_{bc}} & 0 \\ 0 & 0 & a_{R_{ca}} \end{pmatrix}$	$-\begin{pmatrix} \frac{1}{a_{R_{ca}}} & 0 & 0 \\ 0 & \frac{1}{a_{R_{bc}}} & 0 \\ -\frac{1}{a_{R_{ca}}} & -\frac{1}{a_{R_{bc}}} & 0 \end{pmatrix}$	$\mathbf{I}_{d\,(3\times3)}$

Where **Δ** stands for Delta, **Y** for wye and **OΔ** for open-delta.

Several configurations were solved for defining a benchmark of results. The effective turns ratios for the different regulators were taken considering that most of the SVRs have a reversing switch enabling ±10% regulator range in 32 steps (16 in raise and 16 in lower positions). That means a change of 0.625 per-unit per step. With these numbers, the effective turns ratio in terms of number of turns might be replaced by expression [2] (see section 7.4.1.2)

$$a_R = 1 \oplus 0.00625 \text{ Tap}, \tag{6.80}$$

where Tap has a value between 0 and 16, depending on the tap position and where the operator $\oplus$ has to be taken from Table 6.1. The model has been defined in such a way that for wye and close-delta configurations three single-phase regulators are connected together. That implies that the taps of each regulator can change separately, and thus, different values for the effective turns ratio per phase can appear. Nevertheless, three-phase regulators (in which taps are constrained to ganged operation) might be also modeled by choosing the same values of a_R in the three phases. For open-delta connections only single-phase regulators are used, so the values for the different turns ratio a_R can be different.

The resulting 4-node test feeder including a SVR is depicted in Fig. 6.3. The SVR is always connected between nodes 2 and 3, while node 1 behaves as an infinite or slack bus and the load is connected at node 4. Line configurations and load types are inherited from the conventional test feeder [78]. In this case, since the transformer has been replaced by a SVR, the rated voltage is the same in the primary and secondary sides of the regulator. This value has been chosen as 12.47 kV which corresponds to the rated voltage value at the load side in the original test feeder.

An unbalanced BFS solver is used in this section [2]. The linear equations are defined in matrix form including all system KVL and KCL relationships as

$$\mathbf{M}\,\mathbf{z}^T = 0. \tag{6.81}$$

The vector $\mathbf{z}$ contains all complex, three-phase system voltages and currents as follows

$$\mathbf{z} = \left[\mathbf{I}_{12}\ \ \mathbf{I}_{23}\ \ \mathbf{I}_{34}\ \ \mathbf{I}_{\mathbf{Load}_4}\ \ \mathbf{I}_{\mathbf{G}_1}\ \ \mathbf{V}_1\ \ \mathbf{V}_2\ \ \mathbf{V}_3\ \ \mathbf{V}_4\ \right]_{\alpha\beta 0}, \tag{6.82}$$

where $\mathbf{I}_{12}$ and $\mathbf{I}_{34}$ are the line currents depicted in Fig. 6.3, $\mathbf{I}_{G_1}$ are the currents drawn from the infinite bus (the only generator), $\mathbf{I}_{Load_4}$ are the load currents and $\mathbf{I}_{23}$ are the SVR primary or secondary currents depending on its configuration. The structure of $\mathbf{M}$ is shown in the following

$$\mathbf{M} = \left(\begin{array}{c|c|c|c} \mathbf{Z}_{\alpha\beta 0} & 0 & 0 & -\mathbf{\Gamma} \\ \hline \mathbf{\Gamma}^T & \mathbf{I}_d & -\mathbf{I}_d & 0 \end{array}\right), \tag{6.83}$$

where the $\mathbf{\Gamma}$ and $\mathbf{\Gamma}^{\boldsymbol{T}}$ are the modified node incidence matrices in which the SVR matrices $\mathbf{N}_{\mathrm{I}}$, $\mathbf{N}_{\mathrm{II}}$, $\mathbf{N}_{\mathrm{III}}$ and $\mathbf{N}_{\mathrm{IV}}$ are included at the corresponding positions. This is the same procedure that the one for transformers described in [80].

The load adds the following non-linear equations

$$\mathbf{P}_{abc} = \mathrm{real}\left(\mathbf{AV}_{\alpha\beta 0} \circ \mathrm{conj}\left[\mathbf{AI}_{L_{\alpha\beta 0}}\right]\right), \tag{6.84}$$

$$\mathbf{Q}_{abc} = \mathrm{imag}\left(\mathbf{AV}_{\alpha\beta 0} \circ \mathrm{conj}\left[\mathbf{AI}_{L_{\alpha\beta 0}}\right]\right), \tag{6.85}$$

where the operator $\circ$ is the Hadamard (element-wise) product.

To test the different configurations for the regulators in lower and raise positions, both types of loads: capacitive and inductive, are considered. A good convergence was shown by the algorithm in all the analyzed cases.

6.5 4-node Test Feeder Data

The data for describing loads, lines and SVR are inherited from those described in the 4-node test feeder with transformers [78] but with some modifications needed to replace the transformer by a SVR.

6.5.1 Step Voltage Regulators

The SVR configurations used in this chapter were taken from [2] (see section 7.4.2). Depending on the way that the single-phase regulators are connected, the resulting configurations are different. In wye and close-delta there are 3 regulators, but in case of open-delta there are only 2 regulators. In open-delta, 3 different connections (cases a, b and c) are defined: In case a, the regulators are connected to phases ab and ca, in case b to phases ab and ca and finally, in case c to phases ab and ca. There is only a four-wire configuration: wye-grounded connection. Notice that close-delta and open-delta are three-wire configurations. That implies that the lines connected to a wye-grounded SVR have to be four-wire, while they must be three-wire in the other four cases.

The rated values of the 3-phase SVR are: 6 MVA, 12.47 kV, R=1% and X=6%.

6.5.2 Loads

A 3-phase load is connected to node 4. Depending on the SVR connection and the line configuration between nodes 3 and 4, the load is wye-grounded or delta type. Loads are given in terms of constant active and reactive power (PQ). Different loading scenarios are considered trying to achieve different tap positions (both in the raise and lower modes). The loads are defined in Table 6.5. For each balanced or unbalanced loading scenario two possibilities are considered: lag and lead power factor. In the Table, there is no reference to phases a, b and c as the nomenclature phase 1, 2 and 3 is employed instead. This is

Table 6.5 Loads

		Balanced	Unbalanced
phase 1	**P (kW)**	1800	1275
	power factor	0.9 lag/lead	0.85 lag/lead
phase 2	**P (kW)**	1800	1800
	power factor	0.9 lag/lead	0.9 lag/lead
phase 3	**P (kW)**	1800	2375
	power factor	0.9 lag/lead	0.95 lag/lead

because the spot loads are not always connected to a given phase: in 3-wire lines loads are connected line-to-line while in 4-wire lines loads are connected between a phase and the neutral conductor.

6.5.3 Lines

The lines were chosen to be exactly the same configurations and lengths as in the 4-node test feeder.

The line corresponds to the exact segment model described in [2]. The matrices derived from Carson's equations and Kron's reduction are always of dimensions 3×3 and are available in the web site [78] for both three-wire and four-wire configurations.

6.6 Study Cases

The cases have been selected in such a way that each SVR configuration (type A and type B regulators) has been tested under several conditions: balanced and unbalanced, inductive (lag power factor) and capacitive (lead power factor) loading and two different cases of before and after optimization. Apart from a neutral central connection, each regulator has 32 taps: 16 for raise positions and 16 for lower positions. Two scenarios are considered: in the first one, the SVR is in fixed at the neutral position, while in a second (optimized state), voltage regulation is conducted in order to achieve the minimum voltage magnitude in the grid which complies with the voltage constraints.

The load can be inductive or capacitive, so the taps need to be in raise or lower positions depending on the operating point. The different combinations between connections, regulator types and loading scenarios, as well as the cases before/after optimization have given rise to 80 different cases.

For wye and close-delta connections there are 3 taps per regulator, that can be changed independently, but in case of open-delta there are only 2 tap changers per regulator, which means one less degree of freedom for optimization.

A per-unit value of 0.95 was selected as a constraint for the minimum voltage of the grid. That means a minimum line voltage of 11847 V and a minimum phase-to-neutral voltage

of 6840 V. There was no need to set a maximum voltage value, because the optimization aims to find the minimum voltage profile that satisfies the constraint.

Since the system is radial, the furthest node from the slack is node 4. As a result, it happened for all inductive loading scenarios that the minimum voltage magnitudes are obtained at that node, so if the minimum voltage constraint is satisfied at this location, it is satisfied at any other. Then, the optimization algorithm is expected to search for a power flow solution that meets the minimum voltage profile per phase (0.95 pu) at node 4 in inductive cases. For capacitive loading cases the voltage profile changes, and thus, node 4 does not always present the minimum voltage per phase in the network.

6.7 Results

The results to the 80 cases in 16 scenario are presented in appendix A below and they have been organized in tables. As each Table presents 5 cases of SVR configurations in one different scenario, there are 16 tables in total from Table A.1 to A.16. The organization of scenarios and cases into tables are presented in Table 6.6.

Table 6.6 Structure of Tables in Annex 1

	Type		**Loading**				**Optimization state**	
TABLE	**A**	**B**	**Balanc.**	**Unbalanc.**	**Induct.**	**Capacit.**	**Before**	**After**
A.1	X		X		X		X	
A.2	X		X		X			X
A.3	X		X			X	X	
A.4	X		X			X		X
A.5	X			X	X		X	
A.6	X			X	X			X
A.7	X			X		X	X	
A.8	X			X		X		X
A.9		X	X		X		X	
A.10		X	X		X			X
A.11		X	X			X	X	
A.12		X	X			X		X
A.13		X		X	X		X	
A.14		X		X	X			X
A.15		X		X		X	X	
A.16		X		X		X		X

Each of these tables includes three-phase voltages in nodes 2, 3 and 4 and three-phase currents in lines 1 (from node 1 to 2) and line 2 (from node 3 to 4). Line voltages are shown for 3-wire nodes while phase-to-neutral voltages are shown for 4-wire nodes. Each single current or voltage is represented by its magnitude in Amps or Volts and its angle in degrees. The columns correspond to the different connections: wye grounded (Y_gY_g),

close delta ($\Delta\Delta$) and open-delta ($O\Delta$), respectively. All the results in an individual table correspond to the defined loading scenario and optimization state.

For each connection, a vector named *Taps* is included in the second row of the tables. It represents the tap positions for the different regulators. A zero in *Taps* means neutral position. A positive value corresponds to a raise position, varying form 1 to 16, and a negative value is obtained for lower positions, varying from -1 to -16. As it can be seen, this vector includes 3 values for wye and close-delta connections (1 regulator per phase) and 2 values for open-delta configurations (2 regulators for three phases). There is always an empty position in *Taps* for the open-delta cases, which corresponds to the phase without regulator. As an example, consider case a: the 2 regulators are connected between phases ab and ca (first and third positions), so the corresponding vector *Taps* is of the form $[0, -, 0]$. There is no regulator between phases bc, so the second position of vector *Taps* is empty. The same reasoning applies to open-delta cases b and c.

Looking at the tables, a number of analyses can be done. Most importantly, comparing the voltage profiles for any specific case before and after optimization, it can be seen that the minimum voltage constraint is met after optimization of taps. For example, in Table A.1, for Y_gY_g case, the voltage level at node 4 is violating the voltage constraint (minimum 6840 V) in all the 3 phases, but after optimization, as shown in Table A.2, the constraint is not violated in any phase. A similar observation can be reached to closed-delta and open-delta connections. In fact, it can be observed that in all cases of closed-delta and open-delta connections, the voltage constraint (minimum 11847 V) is fulfilled in all the phases.

Then, interestingly, in balanced loading cases with wye and close-delta connections, the tap positions are quiet similar among different phases but not exactly the same because of the unbalanced nature of the lines. In contrast, open-delta connections give rise to great differences among taps because the SVR itself is not symmetric (two regulators for three phases), so even for a balanced loading scenario one regulator can be at raise position while the other can be at lower position.

Finally, for unbalanced loading cases it can be seen that the SVRs, not only improves the voltage in magnitude but also leads to a more balanced scenario. This strengthens the concept that with the optimization of tap positions, SVRs can aid in reducing unbalance in such cases.

6.8 Conclusion

This chapter provides for the theoretical background, the model description and the diagrams needed for the inclusion of step voltage regulators into a general, there phase and unbalanced power flow problem. The general model for three-phase SVRs has been included in a 4-node test feeder and solved by means of an unbalanced Backward-Forward Sweep solver. The obtained results are presented as a benchmark. The main contribution

of this chapter is, besides the guidelines for the SVR model development, the proposal of a new 4-node test system for testing and evaluation of three-phase SVRs connections. The software developers will be able to test their software using the model and data presented in this chapter. All results are included in appendix A.

Chapter 7

Transformer Models and Direct Approach Method

This chapter is intended to extend the field of application of an extremely efficient power flow algorithm used in radial and weakly meshed grids, the so-called Direct Approach (DA) method. With this contribution, the method is broadened with the possibility of handling shunt admittances, transformers with taps, and phase-shifting transformers. While the integration of the two former elements in the DA solver is quite straightforward, the use of phase-shifting transformers is far from obvious due to their inherent non-symmetrical admittance matrix. Thus, two new models of phase-shifting transformers, one extended from its conventional model and another extended from its consistent model, are proposed in this contribution, which allows the use of the DA method in grids that include such devices. A set of case studies is conducted in the context of a balanced industrial grid and a standard test-bed to demonstrate the validity of the proposal.

7.1 Introduction

Power flow solvers are an essential tool in the operation and planning of power systems. They allow the assessment of voltage profiles, power flows and losses in the grid, and thus, they are crucial to detect unacceptable voltage deviations and identify overloaded components. Furthermore, power flow algorithms are used to conduct reliability studies and foresee the impact of future demand [22, 87].

The most conventional power flow methods such as Newton-Raphson and Gauss-Seidel, used widely in transmission systems, do not offer the best performance and robustness when applied to the distribution level [88]. This is due to the especial nature of the distribution network, characterized by a radial or weakly meshed topology and a high R/X ratio. Several approaches have been proposed in order to deal with these particular features,

such as the implicit Z-bus Gauss method [89] and backward-forward sweep methods [90], [2]. In the latter group, a very efficient formulation called the direct approach (DA) was proposed in [21]. The DA method avoids the time-consuming tasks of LU factorization and forward and backward substitution of the Jacobian or admittance matrices, which are a commonplace in conventional formulations. The characteristics of DA method make it ideal for real-time applications in the smart grid context. In [91], the DA solver is used in the core of an optimal power flow (OPF) algorithm to provide references to a distribution FACTS in an industrial grid. High update rates are needed in this type of applications and the DA solver accommodates perfectly to this requirement.

The three-phase approach used in [21] takes series self-impedances and mutual couplings into consideration; however, shunt admittances are neglected. Even if that assumption can be enough to run a power flow analysis at the lowest voltage levels of the distribution grid, characterized by short-length lines and untapped transformers, ignoring shunt admittances strongly limits the application of the method to higher voltage levels. The extension of the method to accommodate medium-length lines and transformers with tap changers in a balanced environment is presented in this chapter. Though no previous references to this use have been found, its application is fairly straightforward.

In a pure radial grid, a post-processing of the voltage phase angles after the application of the power flow solver is enough to account for the transformer phase shift. However, if a weakly meshed grid is to be considered, this method is no longer valid. Thus, a model of the phase-shifting transformer, both to consider specific devices used to control the active power flow in the loop and to include the phase shift of common power transformers, is mandatory. Modeling of phase-shifting transformers in power flow studies is a non-trivial problem, as they cannot be represented by a π-equivalent component due to their inherent asymmetric admittance matrix [22]. A set of different phase-shifting transformer models is available for application in various fields of study, to both steady state [23–27] and transient simulation [28]. In [29], a survey on phase-shifting transformer models for steady state analysis is presented; however, none of them are expressed in a suitable form to be embedded in the DA solver. In this chapter, two new models of phase-shifting transformers, one extended from its conventional model and another extended from its consistent model, are proposed to overcome this limitation.

The DA method, as described in [21], is presented in Section 7.2 for the benefit of the reader. Section 7.3 presents a straightforward method to include shunt admittances in the DA solver. Thus, those components capable of being represented by π-equivalent models, such as medium-length lines and transformers with tap changers, can be easily included in the problem. In Section 7.4, the new phase-shifting transformer models are presented together with minor modifications to be performed in the DA algorithm. Three case studies are presented in Section 7.5 in order to illustrate the implementation procedure and demonstrate the validity of the proposal. Finally, Section 7.6 summarizes the most important results of this study.

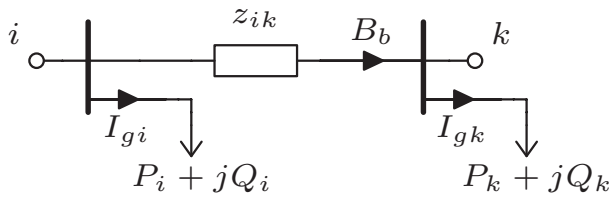

Fig. 7.1 Scheme used in the DA method

7.2 Direct Approach Power Flow

The method to be proposed in this contribution is based on the DA formulation of the power flow problem [21]. This is a technique, especially designed for radial networks, inspired by well-known backward-forward sweep methods such as Ladder Iterative Technique [2]. DA provides a very compact vectorized formulation with excellent computational and convergence characteristics.

In the application of DA to balanced grids, lines and transformers are modeled as series impedances, z_{ik}, as it is shown in Fig. 7.1. The equivalent bus current injection vector, $\boldsymbol{I_g}$, is calculated from the power injection at each bus, i, given the estimation of the bus voltage vector $\boldsymbol{V}$ at iteration (n) as

$$I_{gi}^{(n)} = \frac{P_i - jQ_i}{conj(V_i^{(n)})}. \tag{7.1}$$

Assuming a radial grid, the branch current vector can be calculated as

$$\boldsymbol{B}^{(n)} = \mathbf{BIBC} \cdot \boldsymbol{I_g}^{(n)}, \tag{7.2}$$

where **BIBC** is the so-called bus-injection to branch-current matrix. The entry $BIBC_{bi}$ equals 1 if the current injection of node i contributes to the branch current B_b, and equals 0 otherwise. Finally, a better approximation to the voltage profile can be obtained from

$$\boldsymbol{\Delta V}^{(n+1)} = \mathbf{BCBV} \cdot \boldsymbol{B}^{(n)}, \tag{7.3}$$

where **BCBV** is the branch-current to bus-voltage matrix. The entry $BCBV_{ib}$ equals the series impedance of branch b if that branch is in the path from node i to the slack bus, and equals 0 otherwise. $\boldsymbol{\Delta V}$ is a vector with the voltage of the slack bus referred to the different bus voltages. An improved approximation to the state variables is subsequently obtained by

$$\boldsymbol{V}^{(n+1)} = \boldsymbol{V_s} - \boldsymbol{\Delta V}^{(n+1)}, \tag{7.4}$$

where $\boldsymbol{V_s}$ is a column vector with the slack bus voltage at each entry.

Starting from a flat voltage profile, the solution of the distribution power flow is reached by solving (7.1)–(7.4) iteratively up to a specified convergence threshold.

In order to include the treatment of meshes in the network, Teng [21] proposes minor modifications to be conducted in the definition of **BIBC** and **BCBV** and in the solution technique. A brief summary of these changes can be described as:

- Specific branches are selected to break the meshed grid into a radial network. Then, new entries are included in the current injection vector to account for the currents at the selected branches, i.e. $[\boldsymbol{I_g B}_{\text{new}}]^T$.

- The **BIBC** matrix is built as in the base case, by considering the currents of the branches used to break the network as additional current injections. However, entries with the value -1 appear now to account for the contribution of the receiving node of the branches used to break the network due to the inverted current reference. Notice that the double-sided contribution of the sending and receiving nodes of a branch used to break the network, B_c, to the current of those branches upstream from the first common parent node, B_b, is null, as they have the same value but opposite references.

  Additionally, new rows are added to the **BIBC** matrix with a single non-null entry in order to identify the currents of the branches used to break the network. Taking all this into account, (7.2) can now be expressed as

$$\begin{bmatrix} \boldsymbol{B} \\ \boldsymbol{B}_{\text{new}} \end{bmatrix}^{(n)} = \mathbf{BIBC} \cdot \begin{bmatrix} \boldsymbol{I_g} \\ \boldsymbol{B}_{\text{new}} \end{bmatrix}^{(n)}. \tag{7.5}$$

- The **BCBV** matrix is built as in the base case, but a new row is added for each loop in the grid to account for KVL. The impedances included in the entries of the new rows of the matrix are signed positive or negative according to the reference of the current at the different branches. Then, (7.3) is reformulated as

$$\begin{bmatrix} \boldsymbol{\Delta V} \\ 0 \end{bmatrix}^{(n+1)} = \mathbf{BCBV} \cdot \begin{bmatrix} \boldsymbol{B} \\ \boldsymbol{B}_{\text{new}} \end{bmatrix}^{(n)}. \tag{7.6}$$

- By using (7.5) and (7.6) and rewriting the resulting matrix, it follows that

$$\begin{aligned} \begin{bmatrix} \boldsymbol{\Delta V} \\ 0 \end{bmatrix}^{(n+1)} &= \mathbf{BCBV} \cdot \mathbf{BIBC} \cdot \begin{bmatrix} \boldsymbol{I_g} \\ \boldsymbol{B}_{\text{new}} \end{bmatrix}^{(n)} \\ &= \begin{bmatrix} \boldsymbol{A} & \boldsymbol{M}^T \\ \boldsymbol{M} & \boldsymbol{N} \end{bmatrix} \begin{bmatrix} \boldsymbol{I_g} \\ \boldsymbol{B}_{\text{new}} \end{bmatrix}^{(n)}. \end{aligned} \tag{7.7}$$

  The application of Kron reduction to (7.7) leads to

$$\boldsymbol{\Delta V}^{(n+1)} = (\boldsymbol{A} - \boldsymbol{M}^T \boldsymbol{N}^{-1} \boldsymbol{M}) \boldsymbol{I_g}^{(n)}. \tag{7.8}$$

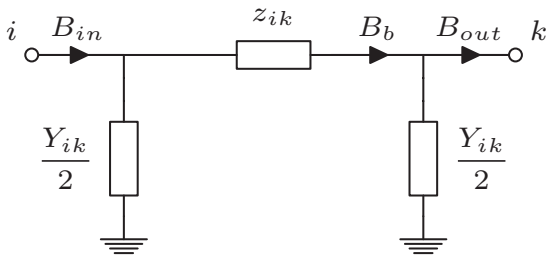

Fig. 7.2 The π-equivalent line model

The iterative use of (7.1), (7.8) and (7.4), in this order, allows the application of the DA method to weakly meshed grids.

7.3 Including π-equivalent Models

The DA method in [21] models the lines and transformers in balanced systems by simple series impedances. While this is acceptable for short-length lines and untapped transformers, minor modifications must be included in the method in order to deal with other common device models.

By considering a π-equivalent model as the one shown in Fig. 7.2, medium-length lines with series impedance z_{ik} and total lumped shunt admittance Y_{ik} can be included in the DA method. In this case, an intermediate variable arises, B_b, which is to be included in the branch current matrix $\boldsymbol{B}$. The current injection vector, $\boldsymbol{I_g}$, is now replaced in (7.2) by an augmented vector $\boldsymbol{I}$ that includes the currents drawn by the shunt admittances as

$$\boldsymbol{I}^{(n)} = \boldsymbol{I_g}^{(n)} + \mathbf{Y_B} \circ \boldsymbol{V}^{(n)}, \tag{7.9}$$

where $\circ$ is the Hadamard product and $\mathbf{Y_B}$ is the bus admittance vector. The sending and receiving end currents, B_{in} and B_{out}, do not appear explicitly in the formulation, but can be subsequently obtained from the state variables by

$$B_{in} = B_b + \frac{Y_{ik}}{2} V_i, \tag{7.10}$$

$$B_{out} = B_b - \frac{Y_{ik}}{2} V_k. \tag{7.11}$$

Once the structure in Fig. 7.3 is adopted, no further modifications are required in the DA method if z_{ik} is used within the **BCBV** matrix.

Even more important than medium-length lines in radial grids is the inclusion of tap-changing transformers in the DA solver. The latter devices are massively used along the power system and are of particular importance in the regulation of voltages in radial grids, to which the DA method is specifically devoted.

Considering the consistent tap-changing transformer model presented in chapter 2, which assumes that both nominal and off-nominal side shares the short-circuit impedance

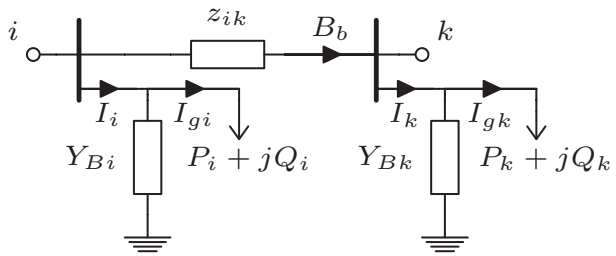

Fig. 7.3 Modified scheme for the DA method

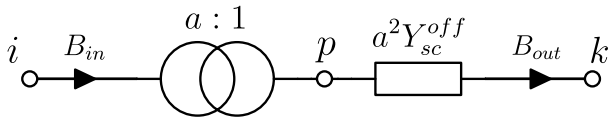

Fig. 7.4 Equivalent circuit of the consistent tap-changing transformer model

and both shares are referred to off-nominal side as depicted in Fig. 7.4. Here, it is to be noted from (2.7) that

$$Y_{sc}^{off} = \frac{1+k}{1+k\,|a|^2} Y_{sc}, \tag{7.12}$$

where k is the p.u. impedance ratio, the new parameter as described in chapter 2. Then the fundamental equations of such a machine can be written as

$$V_i = aV_p = a\left(\frac{B_{out}}{|a|^2 Y_{sc}^{off}} + V_k\right), \tag{7.13}$$

$$B_{out} = aB_{in}. \tag{7.14}$$

As it is well established in chapter 2, from (7.13) and (7.14) the tap-changing transformer can be represented through a π-equivalent model as in Fig. 7.5, which accounts for the nodal equations of the machine

$$B_{in} = Y_{sc}^{off} V_i - aY_{sc}^{off} V_k, \tag{7.15}$$

$$-B_{out} = -aY_{sc}^{off} V_i + |a|^2 Y_{sc}^{off} V_k. \tag{7.16}$$

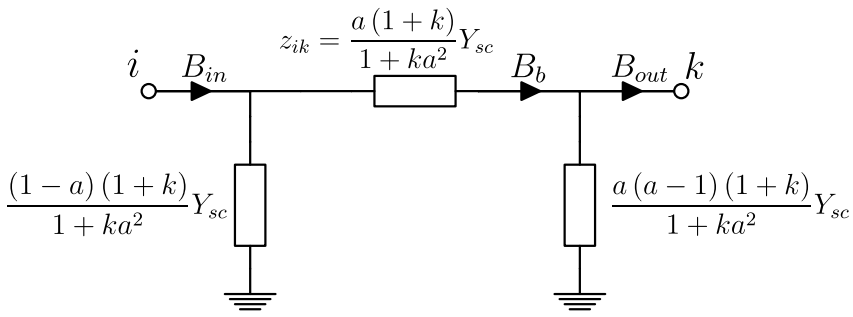

Fig. 7.5 π-equivalent model of the consistent tap-changing transformer

Using the same methodology described for π-equivalent lines, the inclusion of tap-changing transformers in the DA method is thus achieved. Notice that, in this case, the input and output currents of the transformer can be derived from the state variables as

$$B_{in} = B_b + \frac{(1-a)(1+k)}{1+ka^2} Y_{sc} V_i, \tag{7.17}$$

$$B_{out} = B_b - \frac{a(a-1)(1+k)}{1+ka^2} Y_{sc} V_k. \tag{7.18}$$

It is noteworthy that, from this π-equivalent model of the consistent tap-changing transformer, π-equivalent models of two conventional tap-changing transformer formulations can also be derived by simply putting, $k = 0$ or $k = \infty$, as discussed in chapter 2.

7.4 Phase-shifting Transformer Model

Phase-shifting transformers cannot be represented through a π-equivalent model due to the asymmetry of its admittance matrix. As a consequence, the methodology described in Section 7.3 is not valid for the integration of these devices within the DA method. However, in this section we present alternative pseudo π-equivalent models both for the conventional and consistent phase-shifting transformer models, which are suitable to be used with the DA method provided that slight modifications are included.

7.4.1 Pseudo π-equivalent of Conventional Model

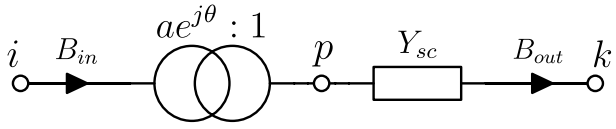

Fig. 7.6 Equivalent circuit of the conventional phase-shifting transformer model with all the short-circuit impedance provided by the nominal side

The equivalent circuit of one of the two alternative conventional phase-shifting transformer models is depicted in Fig. 7.6 with all the short-circuit impedance provided by the nominal side, provided that a is now a complex number, i.e. $a = |a|e^{j\theta}$, $|a|$ being the regulation between the primary and secondary voltage magnitudes and θ being the phase shift. The fundamental equations of such a machine can be written as

$$V_i = aV_p = a\left(\frac{B_{out}}{Y_{sc}} + V_k\right), \tag{7.19}$$

$$B_{out} = a^* B_{in}, \tag{7.20}$$

where a^* is the complex conjugate of a.

The nodal equations of a phase-shifting transformer can be derived from (7.19) and (7.20) as

$$B_{in} = \frac{1}{a\,a^*} Y_{sc} V_i - \frac{1}{a^*} Y_{sc} V_k, \tag{7.21}$$

$$-B_{out} = -\frac{1}{a} Y_{sc} V_i + Y_{sc} V_k, \tag{7.22}$$

where the asymmetry of the admittance matrix becomes clear.

In order to comply with the principles of the DA method, a suitable equivalent of the phase-shifting transformer should maintain the structure of (7.3). From (7.19) and (7.20), it can be derived that

$$\begin{aligned} V_i - V_k &= \frac{a}{Y_{sc}} B_{out} + a V_k - V_k \\ &= \frac{a}{Y_{sc}} \left(B_{out} + \frac{a-1}{a} Y_{sc} V_k \right) \\ &= \frac{a}{Y_{sc}} B_b, \end{aligned} \tag{7.23}$$

where B_b, defined as

$$B_b = B_{out} + \frac{a-1}{a} Y_{sc} V_k, \tag{7.24}$$

is an intermediate variable used to calculate the voltage between nodes i and k. Finally, using (7.19), (7.20) and (7.23), the input current to the transformer can be formulated as

$$\begin{aligned} B_{in} &= \frac{Y_{sc}}{a^*} \left[\frac{1}{a} V_i - V_k \right] \\ &= \frac{Y_{sc}}{a^*} \left[V_i - V_k + \frac{1-a}{a} V_i \right] \\ &= \frac{Y_{sc}}{a^*} \left[\frac{a}{Y_{sc}} B_b + \frac{1-a}{a} V_i \right] \\ &= \frac{a}{a^*} B_b + \frac{1-a}{|a|^2} Y_{sc} V_i \\ &= e^{j2\theta} B_b + \frac{1-a}{|a|^2} Y_{sc} V_i. \end{aligned} \tag{7.25}$$

The equivalent circuit shown in Fig. 7.7 meets the set of equations (7.23)–(7.25) and constitutes the conventional phase-shifting transformer model proposed in this contribution. It is noteworthy that a third shunt leg is introduced here which compensates for

$$B_b - e^{j2\theta} B_b = \frac{a^* - a}{a^*} B_b. \tag{7.26}$$

Though it is obviously not a pure π-equivalent circuit, it is especially suited to be embedded in the DA power flow method, as is demonstrated in section 7.4.3.

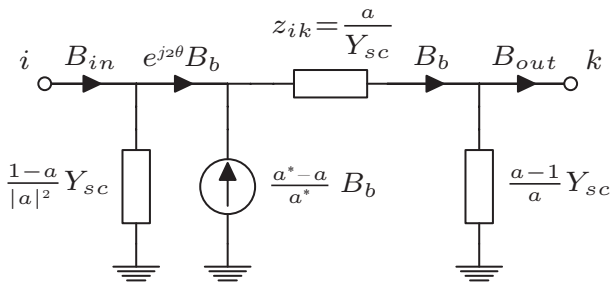

Fig. 7.7 Pseudo π-equivalent model of the phase-shifting transformer's conventional model

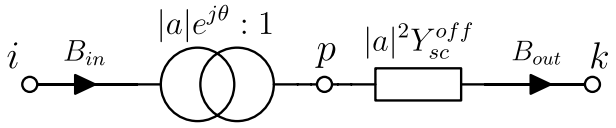

Fig. 7.8 Equivalent circuit for the consistent phase-shifting transformer model

7.4.2 Pseudo π-equivalent of Consistent Model

The equivalent circuit shown in Fig. 7.6 is not valid to represent a consistent phase-shifting transformer model as all the short-circuit impedance is considered there on one side (the nominal side). Rather the equivalent circuit for the consistent phase-shifting transformer model is shown in Fig. 7.8. Here, it is to be noted from (4.7) that

$$Y_{sc}^{off} = \frac{1+k}{1+k\,|a|^2} Y_{sc}, \tag{7.27}$$

where k is the p.u. impedance ratio, the new parameter as described in chapter 4. Then the fundamental equations of such a machine can be written as

$$V_i = aV_p = a\left(\frac{B_{out}}{|a|^2 Y_{sc}^{off}} + V_k\right), \tag{7.28}$$

$$B_{out} = a^* B_{in}, \tag{7.29}$$

where a^* is the complex conjugate of a.

The nodal equations of a consistent phase-shifting transformer model can be derived from (7.28) and (7.29) as

$$B_{in} = Y_{sc}^{off} V_i - aY_{sc}^{off} V_k, \tag{7.30}$$

$$-B_{out} = -a^* Y_{sc}^{off} V_i + |a|^2 Y_{sc}^{off} V_k, \tag{7.31}$$

where the asymmetry of the admittance matrix becomes clear.

In order to comply with the principles of the DA method, a suitable equivalent of the phase-shifting transformer should maintain the structure of (7.3). From (7.28) and (7.29),

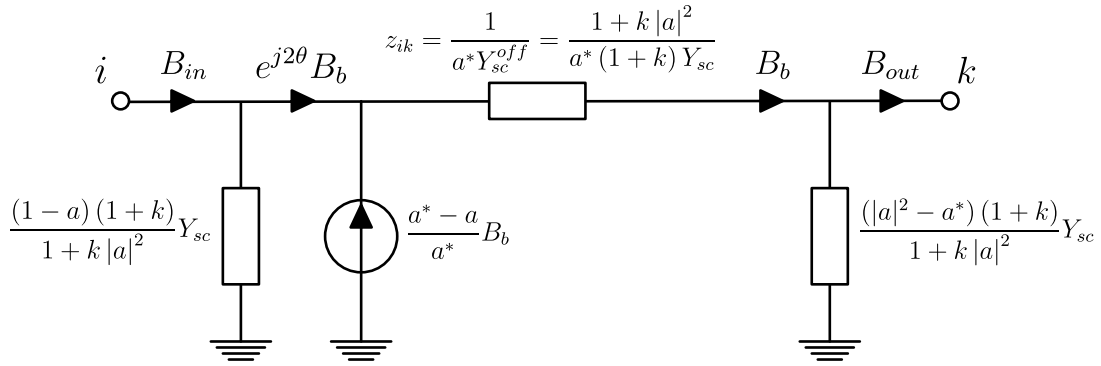

Fig. 7.9 Pseudo π-equivalent model of the phase-shifting transformer's consistent model

it can be derived that

$$\begin{aligned} V_i - V_k &= \frac{a}{|a|^2 Y_{sc}^{off}} B_{out} + aV_k - V_k \\ &= \frac{a}{|a|^2 Y_{sc}^{off}} \left(B_{out} + \frac{|a|^2\,(a-1)}{a} Y_{sc}^{off} V_k \right) \\ &= \frac{1}{a^* Y_{sc}^{off}} \left(B_{out} + \left(|a|^2 - a^* \right) Y_{sc}^{off} V_k \right) \\ &= \frac{1}{a^* Y_{sc}^{off}} B_b, \end{aligned} \tag{7.32}$$

where B_b, from (7.32) and (7.27), can be defined as

$$B_b = B_{out} + \left(|a|^2 - a^* \right) Y_{sc}^{off} V_k = B_{out} + \frac{(|a|^2 - a^*)\,(1+k)}{1+k\,|a|^2} Y_{sc} V_k, \tag{7.33}$$

which is an intermediate variable used to calculate the voltage between nodes i and k. Finally, using (7.27), (7.28), (7.29) and (7.32), the input current to the transformer can be formulated as

$$\begin{aligned} B_{in} &= Y_{sc}^{off} \left[a \left(\frac{1}{a} V_i - V_k \right) \right] \\ &= a Y_{sc}^{off} \left[V_i - V_k + \frac{1-a}{a} V_i \right] \\ &= a Y_{sc}^{off} \left[\frac{1}{a^* Y_{sc}^{off}} B_b + \frac{1-a}{a} V_i \right] \\ &= \frac{a}{a^*} B_b + (1-a)\, Y_{sc}^{off} V_i \\ &= e^{j2\theta} B_b + \frac{(1-a)\,(1+k)}{1+k\,|a|^2} Y_{sc} V_i. \end{aligned} \tag{7.34}$$

The equivalent circuit shown in Fig. 7.9 meets the set of equations (7.32)–(7.34) and constitutes the consistent phase-shifting transformer model proposed in this contribution. Though it is obviously not a pure π-equivalent circuit, it is especially suited to be embedded in the DA power flow method, as is demonstrated in section 7.4.3.

7.4.3 Integration of the Model in the DA Method

Slight modifications in the application of the DA method have to be conducted in order to integrate the pseudo π-equivalent circuis of the phase-shifting transformer into the DA power flow calculation method. These modifications will be similar for both pseudo π-equivalent circuits from the conventional and the consistent method. The first two considerations are in fact extensions from the conclusions drawn in Section 7.3 for the inclusion of π-equivalent models:

- The series impedance z_{ik} shown in Fig. 7.7 and 7.9 is respectively used for the conventional and the consistent model to represent the impedance between nodes i and k within the BCBV matrix.
- In the calculation of the current injection augmented vector $\boldsymbol{I}$ according to (7.9), $\mathbf{Y_B}$ has to include new shunt admittance terms at the sending bus, i, and receiving bus, k, according to Fig. 7.7 or 7.9 respectively for the conventional and consistent method.

The third consideration requires the modification of the **BIBC** matrix and this modification will be same for both the conventional and consistent models. As is depicted in Fig. 7.10(a), let i', k' and b' be the sending node, receiving node and branch index of a phase-shifting transformer. In the same way, let b be the index of a branch located upstream from that transformer. According to (7.25) and Fig. 7.7 (or (7.34) and Fig. 7.9 for the consensus model), the effect of all the augmented current injections of the nodes downstream from i' on the branch current, B_b, can be evaluated as $e^{j2\theta}B_{b'}$. This fact can be easily considered by modifying the entries $BIBC_{bi}$ of the matrix. If node i is now downstream from the receiving node of branch b, the following term,

$$BIBC_{bi} = \prod_t e^{j2\theta_t} = e^{j2\sum_t \theta_t}, \tag{7.35}$$

applies instead of 1, with t being the different phase-shifting transformers between the receiving node of branch b and node i, and θ_t being their corresponding phase angle shifts. Fig. 7.10 illustrates the process for the cases of one phase-shifting transformer, example (a), and two series connected phase-shifting transformers, example (b).

7.4.4 Dealing with Weakly Meshed Grids

Additional changes, apart from those described in Section 7.2, must be conducted to include the proposed phase-shifting transformer models, both the conventional and consistent, in the DA method in the context of weakly meshed topologies. Those modifications can be summarized in the following aspects:

- The double-sided contribution of the current of a branch used to break the network, B_c, to a branch current upstream from the first common parent node, B_b, is no

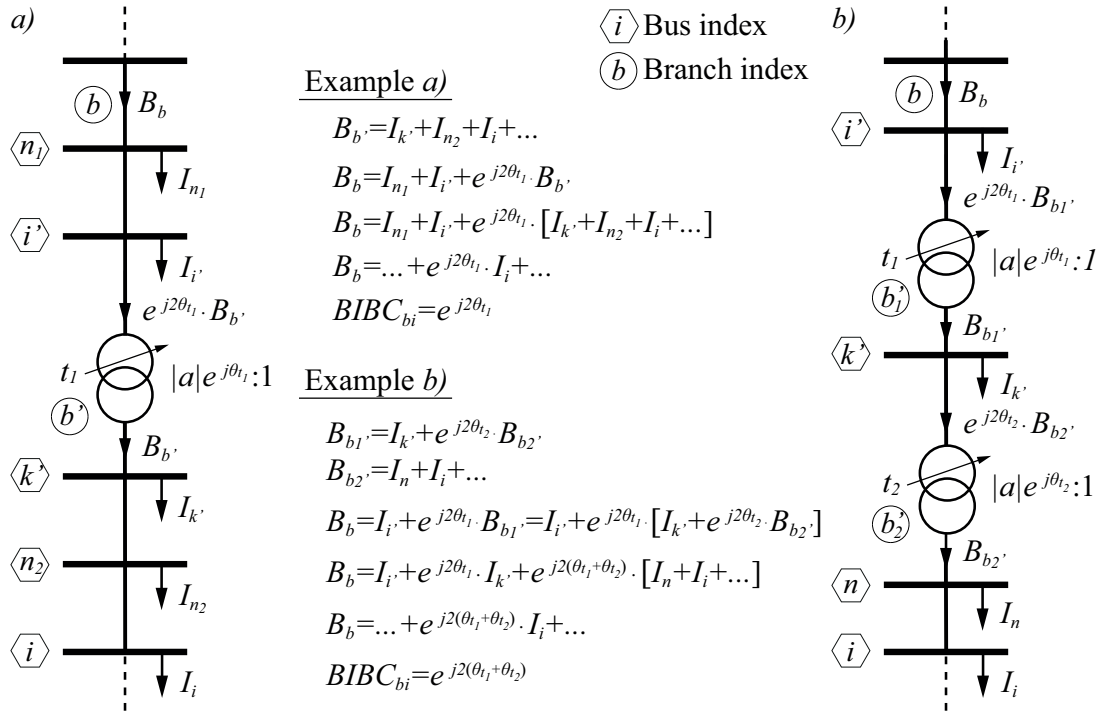

Fig. 7.10 Building process of the **BIBC** matrix for grids with embedded phase-shifting transformers. (a) Example with one phase-shifting transformer, and (b) Example with two phase-shifting transformers

longer canceled in this case, as it is shown in Fig. 7.11. Notice that even if B_c arises with different current references in each path, both sides can be affected by different phase angle jumps. As a consequence, a minor modification of the **BIBC** matrix is required. For those branches, b, upstream from the first common parent node, the contribution of a branch used to break the network, c, whose current branch is at position i in the augmented injection vector $[\boldsymbol{I_g B}_{\text{new}}]^T$, is evaluated by the term

$$BIBC_{bi} = \prod_{t_s} e^{j2\theta_{ts}} - \prod_{t_r} e^{j2\theta_{tr}} = e^{j2\sum_{ts}\theta_{ts}} - e^{j2\sum_{tr}\theta_{tr}}. \tag{7.36}$$

In (7.36) t_s stands for the different phase-shifting transformers found in the path between the receiving node of branch b and the receiving node of branch c that includes the sending node of branch c. In the same way, t_r stands for the different phase-shifting transformers found in the path between the receiving node of branch b and the receiving node of branch c that does not include the sending node of branch c. Finally, θ_{ts} and θ_{tr} account for their corresponding phase angle shifts. The example shown in Fig. 7.11 illustrates this situation using a simple network. Notice that, in this example, one phase-shifting transformer exists between node n and the receiving node k' of branch c along the path that includes the sending node of branch c. However, no phase-shifting transformers exist along the alternative path connecting the same pair of nodes, which obviously leads to -1 in the second addend of (7.36).

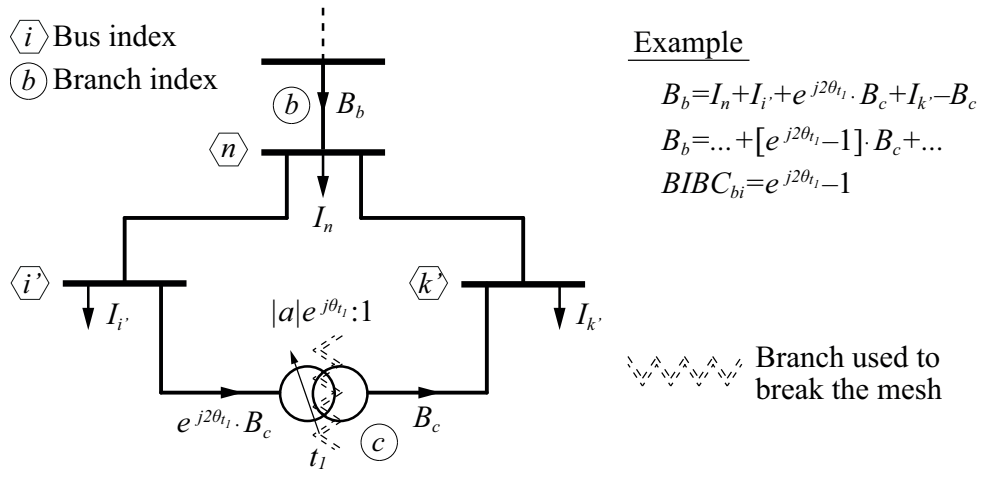

Fig. 7.11 Example of the building process of the **BIBC** matrix for weakly meshed grids with embedded phase-shifting transformers

- From the application of (7.5) and (7.6) to this case, it follows that

$$\begin{bmatrix} \boldsymbol{\Delta V} \\ 0 \end{bmatrix}^{(n+1)} = \mathbf{BCBV} \cdot \mathbf{BIBC} \cdot \begin{bmatrix} \boldsymbol{I} \\ \boldsymbol{B}_{\text{new}} \end{bmatrix}^{(n)} = \begin{bmatrix} \boldsymbol{A} & \boldsymbol{P} \\ \boldsymbol{M} & \boldsymbol{N} \end{bmatrix} \begin{bmatrix} \boldsymbol{I} \\ \boldsymbol{B}_{\text{new}} \end{bmatrix}^{(n)}. \tag{7.37}$$

  Notice that the symmetry found in (7.7) does not appear in (7.37). In any case, the application of Kron reduction leads to

$$\boldsymbol{\Delta V}^{(n+1)} = (\boldsymbol{A} - \boldsymbol{P}\boldsymbol{N}^{-1}\boldsymbol{M})\boldsymbol{I}^{(n)}. \tag{7.38}$$

The iterative use of (7.1), (7.9), (7.38) and (7.4), in this order, allows the application of the DA method to weakly meshed grids including phase-shifting transformers.

7.5 Case Studies

To demonstrate the validity of the proposed methodology, three case studies are carried out in this section. In the first one, the DA method is applied to a radial network in which the phase shifts associated to the embedded power transformers are considered. In the second case study, the same radial grid is turned into a weakly meshed grid by using a phase-shifting transformer. While the first two case studies take advantage of the low number of nodes of an industrial grid to give insight into the matrices building process, the third case study is used to demonstrate the good convergence characteristics of the method in a standard medium-size testbed.

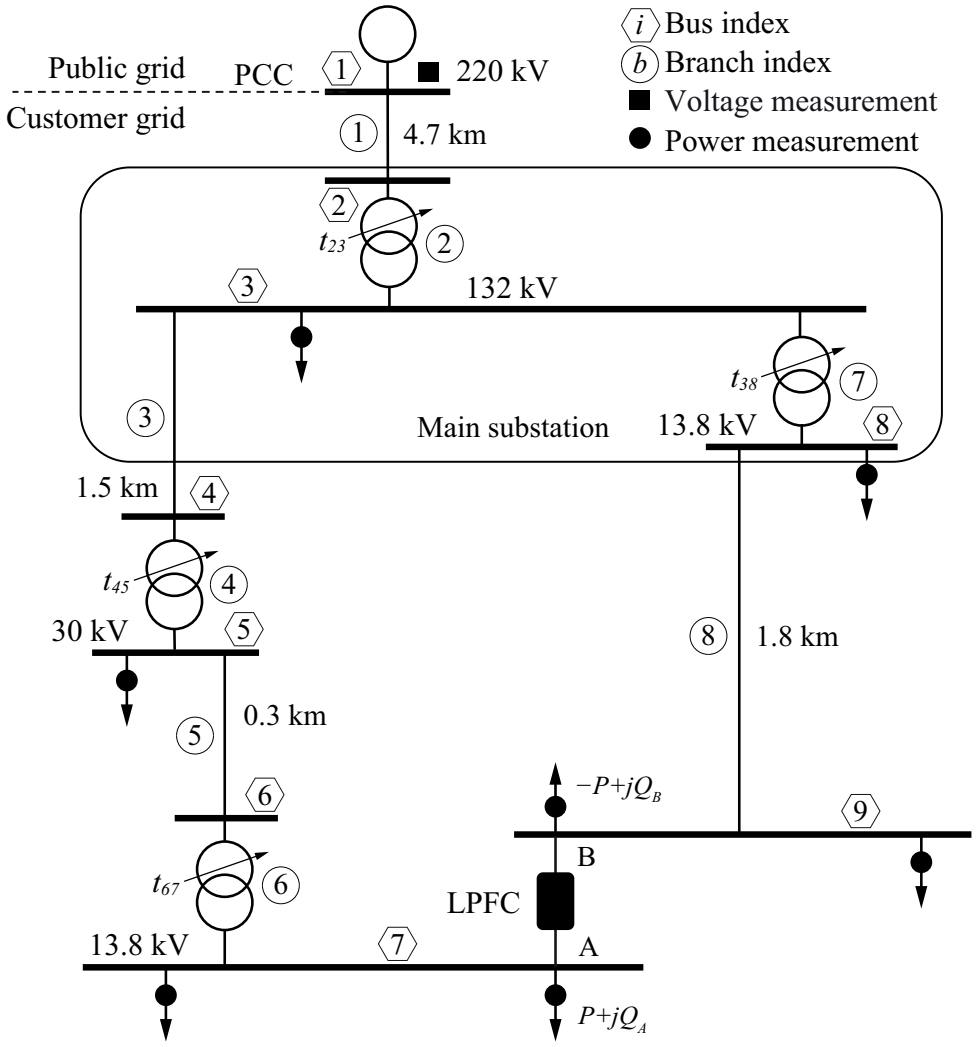

Fig. 7.12 Industrial installation with a distribution-FACTS-based mesh

7.5.1 Case 1: Radial Network

A simplified version of the customer owned grid of a steelworks in the north of Spain, already tested in previous works [91], is considered in this case study. The grid is shown in Fig. 7.12 and the parameters and configuration of the embedded transformers are listed in Table 7.1. Table 7.2 shows the lengths and per km impedances of the lines according to Fig. 7.2.

In [91], a proposal aimed to improve the efficiency of the grid and provide dynamic voltage support to the facility was presented. This objective is conducted through the application of a distribution FACTS usually known as Loop Power Flow Controller (LPFC). The real-time optimization of the device is based on a heuristic algorithm out of the scope of this chapter. However, the proper operation of that heuristic algorithm relies upon the availability of a fast power flow algorithm, compatible with such a real-time application. Even if other algorithms were considered, the DA method shows very good performance in this environment, characterized by a small number of nodes and radial nature. The controller uses the DA power flow algorithm to analyze the effect of different power

Table 7.1 Transformer Parameters

Transf. #	S_n [MVA]	R_{sc} [%]	X_{sc} [%]	a [pu]	θ [deg.]	k [pu]
t_{23}	2x270	0.90	12.90	1.0125	−30	1
t_{45}	3x37.5	0.90	9.00	0.9875	0	1
t_{67}	10	0.95	4.80	0.9250	30	1
t_{38}	3x50	0.92	8.50	0.9750	30	1

Table 7.2 Branch Parameters

Branch #	Length [km]	z_{line} [Ω/km]	z_{ik} [pu]
1	4.7	$0.025 + j0.240$	$2.428\text{e}{-5} + j2.331\text{e}{-4}$
3	1.5	$0.161 + j0.151$	$1.386\text{e}{-4} + j1.300\text{e}{-4}$
5	0.3	$0.568 + j0.133$	$1.893\text{e}{-3} + j4.433\text{e}{-4}$
8	1.8	$0.161 + j0.112$	$1.522\text{e}{-2} + j1.059\text{e}{-2}$

injections at the power converter terminals (i.e. the real power, P, flowing from terminal A to B in Fig. 7.12, and the decoupled reactive power injections at both terminals, Q_A and Q_B). The addition of these values to the rest of the power injections at buses 7 and 9 turns the power flow problem into a pure radial case, despite of the mesh created by the distribution FACTS. Table 7.3 shows the specific power injection values considered in this case study. Note that the negative value of the reactive power injection in bus 9 is due to the reactive power supply of the LPFC at terminal B for the current operation point. The voltage at the slack bus is taken as 1.0 pu and as the origin of phase angles.

The use of the phase-shifting model proposed in this contribution for the tapped transformers in such a radial network is not really mandatory, as it would be in Case 2. This is due to the fact that, in a radial network, the phase shift of the transformers can be initially disregarded and later taken into account on a subsequent post-processing of the results that would correct the phase angle jump in each voltage area. Nevertheless, the use of the proposed phase-shifting transformer models is applied in this case study in order to avoid any post-processing of the results. Foremostly, the goal of this case study is

Table 7.3 Power Injections

Bus #	Real power, P_i [MW]	Reactive power, Q_i, [Mvar]
2	0.0	0.0
3	84.0	26.0
4	0.0	0.0
5	34.0	12.0
6	0.0	0.0
7	4.9	12.6
8	52.0	39.0
9	2.7	−3.4

$$\begin{bmatrix} 1 & e^{j2\theta_{23}} & e^{j2\theta_{23}} & e^{j2(\theta_{23}+\theta_{45})} & e^{j2(\theta_{23}+\theta_{45})} & e^{j2(\theta_{23}+\theta_{45}+\theta_{67})} & e^{j2(\theta_{23}+\theta_{38})} & e^{j2(\theta_{23}+\theta_{38})} \\ 0 & 1 & 1 & e^{j2\theta_{45}} & e^{j2\theta_{45}} & e^{j2(\theta_{45}+\theta_{67})} & e^{j2\theta_{38}} & e^{j2\theta_{38}} \\ 0 & 0 & 1 & e^{j2\theta_{45}} & e^{j2\theta_{45}} & e^{j2(\theta_{45}+\theta_{67})} & 0 & 0 \\ 0 & 0 & 0 & 1 & 1 & e^{j2\theta_{67}} & 0 & 0 \\ 0 & 0 & 0 & 0 & 1 & e^{j2\theta_{67}} & 0 & 0 \\ 0 & 0 & 0 & 0 & 0 & 1 & 0 & 0 \\ 0 & 0 & 0 & 0 & 0 & 0 & 1 & 1 \\ 0 & 0 & 0 & 0 & 0 & 0 & 0 & 1 \end{bmatrix} \tag{7.39}$$

$$\begin{bmatrix} z_{12} & 0 & 0 & 0 & 0 & 0 & 0 & 0 \\ z_{12} & z_{23} & 0 & 0 & 0 & 0 & 0 & 0 \\ z_{12} & z_{23} & z_{34} & 0 & 0 & 0 & 0 & 0 \\ z_{12} & z_{23} & z_{34} & z_{45} & 0 & 0 & 0 & 0 \\ z_{12} & z_{23} & z_{34} & z_{45} & z_{56} & 0 & 0 & 0 \\ z_{12} & z_{23} & z_{34} & z_{45} & z_{56} & z_{67} & 0 & 0 \\ z_{12} & z_{23} & 0 & 0 & 0 & 0 & z_{38} & 0 \\ z_{12} & z_{23} & 0 & 0 & 0 & 0 & z_{38} & z_{89} \end{bmatrix} \tag{7.40}$$

to validate the concept of integrating pseudo π-equivalent forms of both conventional and consistent models of phase-shifting transformer. Hence, in this case study, simulations are first run with the pseudo π -equivalent form of the conventional phase-shifting transformer model and, subsequently, the results are compared with those obtained with the pseudo π -equivalent form of the consistent phase-shifting transformer model. The **BIBC** and **BCBV** matrices are calculated according to the considerations disclosed in sub-section 7.4.3. Their structure is shown in (7.39) and (7.40) for the sake of clarity. A flat voltage profile is considered for the initial iteration step. The set (7.1)–(7.4) is applied iteratively together with (7.9) to account for the augmented current injection vector, until a threshold of $1e-6$ is reached in the maximum absolute deviation of two consecutive entries in $\boldsymbol{V}$. The voltages at the different buses, as state variables of the grid, are presented in Table 7.4 for pseudo π-equivalent form of conventional model and in Table 7.5 for pseudo π-equivalent form of consistent model. It can be seen from these tables, that, both of the pseudo π-equivalent forms of phase-shifting transformer is functioning well and resulting in close results. Finally, the system has also been implemented in the PowerWorld$^{\text{TM}}$ Simulator software to crosscheck and demonstrate the validity of the results. Even if this tool uses a Newton-Raphson approach and the conventional model of transformer with all the impedance assigned to the nominal side to solve the system, the results are identical up to the threshold level. Hence the validity of the concept and pseudo π-equivalent forms are validated.

Table 7.4 Case 1 – Results for the Pseudo π-equivalent of the Conventional Model

Bus #	$\lvert V_i\rvert$ [pu]	θ_i [deg.]	Bus #	$\lvert V_i\rvert$ [pu]	θ_i [deg.]
2	0.9972	−0.226	6	0.9419	25.588
3	0.9579	27.278	7	0.9496	−5.097
4	0.9570	27.270	8	0.9574	−4.478
5	0.9436	25.436	9	0.9569	−4.980

Table 7.5 Case 1 – Results for the Pseudo π-equivalent of the Consistent Model

Bus #	$\lvert V_i\rvert$ [pu]	θ_i [deg.]	Bus #	$\lvert V_i\rvert$ [pu]	θ_i [deg.]
2	0.9972	−0.226	6	0.9418	25.596
3	0.9582	27.310	7	0.9432	−5.151
4	0.9573	27.302	8	0.9571	−4.493
5	0.9435	25.444	9	0.9565	−4.995

7.5.2 Case 2: Weakly Meshed Grid

In this case study, the industrial network considered in the previous subsection is used to verify the correct performance of the DA method with embedded phase-shifting transformers in the context of a weakly meshed grid. With this aim, a similar role as the one played by the LPFC in Case 1 is played by a tapped phase-shifting transformer, simulated with its pseudo π-equivalent model of conventional formulation presented in Fig. 7.7. This device regulates the power flow between nodes 7 and 9. The new setup is depicted in Fig. 7.13. The parameters and selected tap of the phase-shifting transformer used to mesh the grid is shown in Table 7.6 and Table 7.7 displays the series impedance, z_{79}, of the new branch according to the model shown in Fig. 7.7.

Only the proposal presented in this chapter allows the application of the efficient DA method to this type of system. Notice that in this case a post-processing of the phase-angle jumps of the transformers is not possible, due to the coupling between both sides of the grid downstream from the first common parent node. The new branch, $c = 9$, is selected to break the mesh, though any other branch within the loop (i.e. 3 to 8) could be used with this aim. According to Section 7.2 and Sub-section 7.4.4, once the selection is made, this branch is treated as an additional source of current injection at nodes 7 and 9. However, the use of Kron reduction allows a straightforward consideration of the mesh, i.e. no additional iterative processes are involved. For clarity purposes, the same power injections considered in Case 1 are adopted here and once again the voltage at the slack bus is taken as 1.0 pu and as the origin of phase angles.

Table 7.6 Phase-Shifting Transformer Parameters

Transf. #	S_n [MVA]	R_{sc} [%]	X_{sc} [%]	a [pu]	θ [deg.]
t_{79}	10	0.95	4.80	1.0000	5

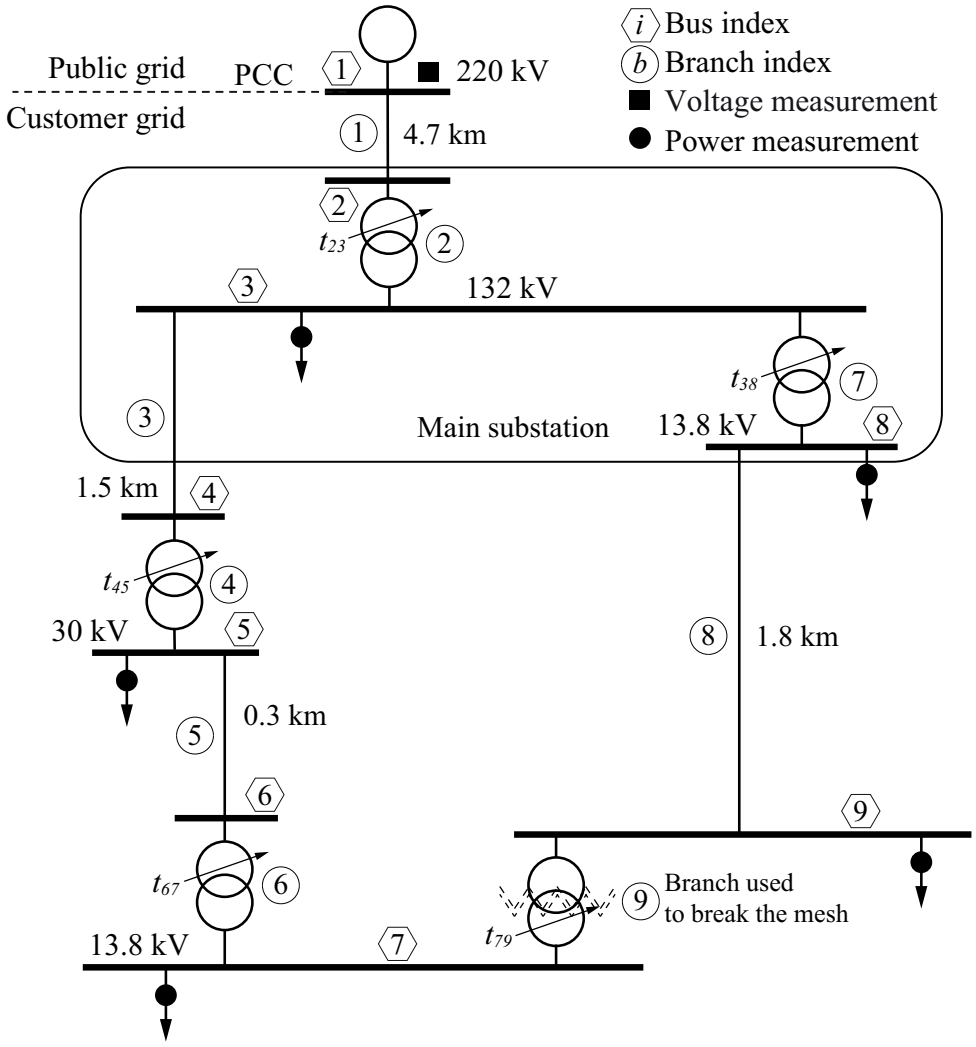

Fig. 7.13 Industrial installation meshed through a phase-shifting transformer

In this case study, the pseudo π-equivalent form for the conventional phase-shifting transformer is used. The **BIBC** and **BCBV** matrices are calculated according to the specific considerations described in sub-section 7.4.4. Their structure is shown in (7.41) and (7.42). The entries $BIBC_{19}$ and $BIBC_{29}$ account for the double contribution of B_9 to the branch currents B_1 and B_2, respectively. Notice, as an example, that for $BIBC_{19}$ the phase shifts to be considered fit $t_r = [t_{23}, t_{45}, t_{67}, t_{79}]^T$ and $t_s = [t_{23}, t_{38}]^T$. It should be highlighted that both $BIBC_{19}$ and $BIBC_{29}$ would be zero in a meshed network not including phase-shifting transformers, as the contribution of both sides would be canceled upstream from the first common parent node in such a case.

Table 7.7 New Branch Parameters

Branch #	Length [km]	z_{line} [Ω/km]	z_{ik} [pu]
9	–	–	$5.280\text{e}{-3} + j4.865\text{e}{-2}$

$$\begin{bmatrix}
1 & e^{j2\theta_{23}} & e^{j2\theta_{23}} & e^{j2(\theta_{23}+\theta_{45})} & e^{j2(\theta_{23}+\theta_{45})} & e^{j2(\theta_{23}+\theta_{45}+\theta_{67})} & e^{j2(\theta_{23}+\theta_{38})} & e^{j2(\theta_{23}+\theta_{38})} & e^{j2(\theta_{23}+\theta_{45}+\theta_{67}+\theta_{79})} - e^{j2(\theta_{23}+\theta_{38})} \\
0 & 1 & 1 & e^{j2\theta_{45}} & e^{j2\theta_{45}} & e^{j2(\theta_{45}+\theta_{67})} & e^{j2\theta_{38}} & e^{j2\theta_{38}} & e^{j2(\theta_{45}+\theta_{67}+\theta_{79})} - e^{j2\theta_{38}} \\
0 & 0 & 1 & e^{j2\theta_{45}} & e^{j2\theta_{45}} & e^{j2(\theta_{45}+\theta_{67})} & 0 & 0 & e^{j2(\theta_{45}+\theta_{67}+\theta_{79})} \\
0 & 0 & 0 & 1 & 1 & e^{j2\theta_{67}} & 0 & 0 & e^{j2(\theta_{67}+\theta_{79})} \\
0 & 0 & 0 & 0 & 1 & e^{j2\theta_{67}} & 0 & 0 & e^{j2(\theta_{67}+\theta_{79})} \\
0 & 0 & 0 & 0 & 0 & 1 & 0 & 0 & e^{j2\theta_{79}} \\
0 & 0 & 0 & 0 & 0 & 0 & 1 & 1 & -1 \\
0 & 0 & 0 & 0 & 0 & 0 & 0 & 1 & -1 \\
0 & 0 & 0 & 0 & 0 & 0 & 0 & 0 & 1
\end{bmatrix} \tag{7.41}$$

$$\begin{bmatrix}
z_{12} & 0 & 0 & 0 & 0 & 0 & 0 & 0 & 0 \\
z_{12} & z_{23} & 0 & 0 & 0 & 0 & 0 & 0 & 0 \\
z_{12} & z_{23} & z_{34} & 0 & 0 & 0 & 0 & 0 & 0 \\
z_{12} & z_{23} & z_{34} & z_{45} & 0 & 0 & 0 & 0 & 0 \\
z_{12} & z_{23} & z_{34} & z_{45} & z_{56} & 0 & 0 & 0 & 0 \\
z_{12} & z_{23} & z_{34} & z_{45} & z_{56} & z_{67} & 0 & 0 & 0 \\
z_{12} & z_{23} & 0 & 0 & 0 & 0 & z_{38} & 0 & 0 \\
z_{12} & z_{23} & 0 & 0 & 0 & 0 & z_{38} & z_{89} & 0 \\
0 & 0 & z_{34} & z_{45} & z_{56} & z_{67} & -z_{38} & -z_{89} & z_{79}
\end{bmatrix} \tag{7.42}$$

As in the previous case study, a flat voltage profile is considered for the initial iteration step. The set (7.1), (7.9), (7.38) and (7.4) is applied iteratively in this order until convergence. With this aim, a threshold of $1e-6$ in the maximum absolute deviation of two consecutive values in $\boldsymbol{V}$ is considered. The solution of the power flow problem, in the form of the bus voltages taken as state variables of the system, is presented in Table 7.8. The new setup was also implemented in the PowerWorld$^{\text{TM}}$ Simulator software package to demonstrate the validity of the results. As in the previous case study, those results are not showed here, due to a perfect match with the proposed methodology.

7.5.3 Case 3: Standard test grid

The IEEE 33-bus test distribution system [92] is used in this case study to assess the impact of the inclusion of the proposed phase-shifting transformer model as in Fig. 7.7 on the convergence characteristics of the DA method. This standard testbed describes a radial grid with 33 buses and 5 tie lines. A modified version of this testbed is presented in this contribution in order to test the proposed model. The modified version, shown in Fig. 7.14, uses two of the existing tie lines to mesh the network through phase-shifting

Table 7.8 Case 2 – Results: State Variables

Bus #	$\lvert V_i\rvert$ [pu]	θ_i [deg.]	Bus #	$\lvert V_i\rvert$ [pu]	θ_i [deg.]
2	0.9972	−0.223	6	0.9423	25.955
3	0.9578	27.275	7	0.9485	−2.824
4	0.9569	27.273	8	0.9574	−4.714
5	0.9428	25.766	9	0.9478	−5.775

Table 7.9 Phase-shifting Transformer Parameters

Transf. #	S_n [kVA]	R_{sc} [%]	X_{sc} [%]	a [pu]	θ [deg.]
$t_{12\text{-}34}$	250	0.95	4.80	1.0000	5
$t_{18\text{-}35}$	400	0.95	4.80	1.0000	-3

transformers. With this aim, two additional buses, 34 and 35, are added to the standard system. The power injections and line parameters of the IEEE 33-bus test distribution system can be found in [92]. The parameters of the phase-shifting transformers, which are the only data of the modified topology not presented in the original testbed, are shown in Table 7.9.

While the original version is solved using the conventional DA formulation [21], only the proposal included in this chapter allows the DA method to solve the modified testbed. In this case study, the pseudo π-equivalent form for the conventional phase-shifting transformer is used. The results for both cases are shown in Table 7.10 and Table 7.11. The validity of these results was checked by using PowerWorld$^{\text{TM}}$ Simulator software. System losses are reduced from 211.00 kW to 183.14 kW thanks to the control of the power flows offered by the use of phase-shifting transformers. Furthermore, the minimum bus voltage in the grid increases from 0.9038 pu to 0.9203 pu, which illustrates the voltage support capability of the modified topology. A threshold of $1e-6$ in the maximum absolute deviation of two consecutive values in $\boldsymbol{V}$ was considered and, starting from a flat voltage profile, only 6 iterations were needed to reach convergence in both topologies. This fact proves that the excellent convergence characteristics of the DA method persist with the inclusion of the proposed phase-shifting transformer model.

In order to generalize this result, a set of $10,000$ cases was solved with the aim of putting additional stress on the convergence test. With this purpose, the power injections of the 33-bus testbed were randomly varied using independent normal distribution functions for each real power and reactive power. The mean of these distribution functions was set to their corresponding values in the original testbed, P_i and Q_i, and the standard deviation to 40% of these values, i.e. $N(P_i, (0.4P_i)^2)$ and $N(Q_i, (0.4Q_i)^2)$. The set was solved by applying the conventional DA formulation to the original testbed topology, and by applying the formulation proposed in this chapter to the modified topology. Table 7.12 shows the key results of this demanding test. The average and maximum number of iterations were not increased by the use of the phase-shifting transformer model even when the meshed configuration used in the modified version results in a more complex topology. In fact, the average number of iterations is slightly reduced, as the voltage support capability of the phase-shifting transformers leads to solutions closer to the flat voltage profile used as an initial iteration point. The time required for these calculations was estimated by averaging the results over the full set of simulation runs, which were carried out in an Intel Core i5 - 2467M - CPU 1.60 GHz. This time increases from 1.4 ms to 3.6 ms, which is due to the higher number of buses used in the modified topology, 35

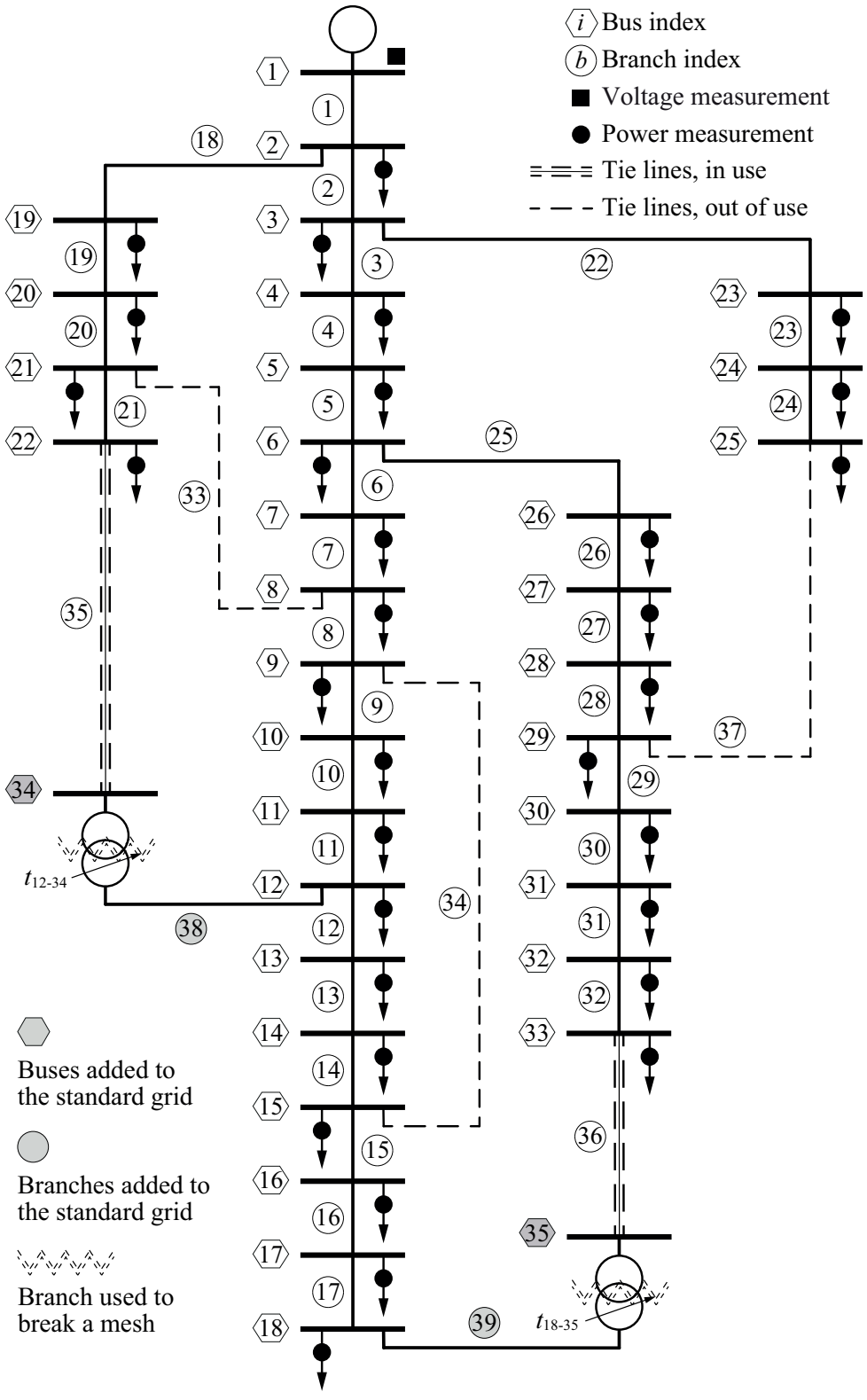

Fig. 7.14 Modified IEEE 33-bus test distribution system

Table 7.10 Case 3 – IEEE 33-bus System: State Variables

Bus #	$\lvert V_i \rvert$ [pu]	θ_i [deg.]	Bus #	$\lvert V_i \rvert$ [pu]	θ_i [deg.]
2	0.9970	0.015	19	0.9965	0.004
3	0.9829	0.097	20	0.9929	−0.063
4	0.9754	0.163	21	0.9922	−0.083
5	0.9680	0.230	22	0.9916	−0.103
6	0.9495	0.136	23	0.9793	0.066
7	0.9460	−0.096	24	0.9726	−0.023
8	0.9323	−0.249	25	0.9693	−0.067
9	0.9260	−0.324	26	0.9475	0.175
10	0.9201	−0.388	27	0.9450	0.232
11	0.9192	−0.380	28	0.9335	0.315
12	0.9177	−0.368	29	0.9253	0.393
13	0.9115	−0.462	30	0.9218	0.498
14	0.9092	−0.542	31	0.9176	0.413
15	0.9078	−0.580	32	0.9167	0.390
16	0.9064	−0.604	33	0.9164	0.383
17	0.9044	−0.683	34	—	—
18	0.9038	−0.693	35	—	—

Table 7.11 Case 3 – Modified IEEE 33-bus System: State Variables

Bus #	$\lvert V_i \rvert$ [pu]	θ_i [deg.]	Bus #	$\lvert V_i \rvert$ [pu]	θ_i [deg.]
2	0.9970	0.016	19	0.9959	−0.010
3	0.9845	0.116	20	0.9873	−0.204
4	0.9781	0.196	21	0.9851	−0.275
5	0.9719	0.277	22	0.9819	−0.401
6	0.9562	0.263	23	0.9809	0.085
7	0.9537	0.088	24	0.9742	−0.003
8	0.9445	−0.043	25	0.9709	−0.047
9	0.9409	−0.104	26	0.9544	0.313
10	0.9377	−0.155	27	0.9520	0.384
11	0.9372	−0.154	28	0.9412	0.545
12	0.9365	−0.154	29	0.9334	0.683
13	0.9296	−0.347	30	0.9302	0.815
14	0.9272	−0.480	31	0.9266	0.814
15	0.9255	−0.563	32	0.9258	0.821
16	0.9237	−0.637	33	0.9255	0.853
17	0.9213	−0.847	34	0.9750	−0.605
18	0.9203	−0.909	35	0.9257	0.896

Table 7.12 Convergence Characteristics: Set of 10,000 Simulations

Topology	Av. iter. #	Max. iter. #	Av. sim. time [ms]
Base case	6.0244	7	1.4019
Modified version	5.9528	7	3.5503

vs. 33, and particularly, to the additional matrix manipulations involved in the treatment of meshed grids, according to Subsection 7.4.4. This test clearly demonstrates that the convergence characteristics of the DA method are not negatively affected by the inclusion of the phase-shifting model proposed in this contribution.

7.6 Concluding Remarks

This chapter proposes an extension of the well-known DA power flow method applied to balanced networks in order to allow its use with common grid components not previously considered in the existing formulation. The inclusion of π-equivalent line models and transformer tap changers is quite straightforward, and only a formal formulation of the considerations needed to use these components is stated in this chapter. However, the inclusion of phase-shifting transformer models in the DA method is far from obvious, due to the inherent asymmetry of their admittance matrix. Only a custom model of these devices can allow the application of the DA method in weakly meshed networks, where the phase angle of transformers cannot be corrected by post-processing. Thus, this proposal introduces two new models of phase-shifting transformers, one extended from its conventional model and another extended from its consistent model (proposed as a contribution of this dissertation), together with a set of slight modifications to be included in the standard DA power flow formulation. Two case studies in the context of the application of fast power flow algorithms to industrial networks are presented. Those cases allow to demonstrate the validity of the proposal both with radial and weakly-meshed topologies. A third case study is carried out in a medium-size test system in order to prove that the excellent convergence characteristics of the DA method are not deteriorated by the inclusion of the new phase-shifting transformer model. In each case, the results are compared with those obtained from a popular software package that uses a different approach, leading to a perfect match.

Conclusions and Future Work

Accurate models of power system components are today an essential tool for the operation and planning of power systems. The new paradigm of smart grids, with an increasing penetration of distributed generation and electric vehicles, makes the role of voltage regulating transformers increasingly important at all levels of the electrical infrastructure.

In chapter 2, it has been established that the practice of neglecting the fact that the short-circuit impedance is the result of contributions from two different windings can lead to unacceptable discrepancies in the formulation of the tap-changing transformer model. This doctoral work thereby proposes a new general model which includes the contribution of each winding to the short-circuit impedance. If data is not available or cannot be estimated, the new model allows to consider a fair contribution (50/50) of both windings, which is an accepted practice in engineering.

The new models presented in chapters 2, and 3, can be tuned to match the results from conventional alternatives, which consider the short-circuit impedance is provided by only one of the transformer windings, either the off-nominal or nominal turns side. This fact makes the new model useful to understand the basis of each formulation, providing a clear perspective on the influence of the underlying assumptions.

In chapters 2, the works demonstrate that the discrepancies caused by conventional models of tap-changing transformer can be unacceptable at extreme tap positions and are greatly influenced by the operating point of the transformer. The studies conducted there demonstrate that those discrepancies can be significant even in the case of a well-known standard grid, which is illustrated by a power flow analysis and a stability analysis. The inclusion of the proposed tap-changing transformer model in power system software packages, tuned with the 50/50 values, can significantly help to improve the consistency of power system studies without the need to provide additional data.

In chapter 3, several variations of the consistent model of tap-changing transformer are presented in order to suit different requirements, depending on the operational setup, chosen bases, and the number of phases to be considered. This way, the ambiguity around tap-changing transformer modeling has been addressed and resolved.

Also, in chapter 4, consistent models have been developed for asymmetrical phase-shifting transformers reaching similar conclusions.

In chapter 5, to make the consistent modeling approach more accurate, an offline state-vector-augmented multi-snapshot-based parameter estimation method, capable of providing accurate estimates of transformer impedance ratios, was proposed, validated,

and analyzed. The case studies there, allow to conclude that a lower number of snapshots, in the range 1 to 10, are not enough to derive accurate results regardless of the redundancy level. However, the inclusion of a higher number of snapshots always allows to reach acceptable estimates. Though a low measurement redundancy level requires a higher number of snapshots to reach the same accuracy, this work demonstrates that even those systems close to the limit of observability can be handled successfully by the proposed algorithm. Importantly, the case studies conducted in this work clearly demonstrate that the procurement of accurate estimates for the transformer short-circuit impedance ratio can positively impact the accuracy of critical tools such as online power system state estimators.

Moreover, in chapter 6, this doctoral work extended its contributions by providing the models needed for the inclusion of step voltage regulators (of all configurations) into a general, three-phase, and unbalanced power flow problem. The general model for three-phase step voltage regulators is included in a 4-node test feeder and solved by means of an unbalanced Backward-Forward Sweep solver. The results obtained are presented as a benchmark to allow researchers and power system software developers to test their algorithms in a well-proven environment.

Finally, in chapter 7, this work proposed an extension of the well-known DA power flow method applied to balanced networks in order to allow its use with common grid components not previously considered in the existing formulation. It was found that the inclusion of π-equivalent line models and transformer tap changers is quite straightforward, and only a formal formulation of the considerations needed to use these components was included in this work. However, the inclusion of phase-shifting transformer models in the DA method is far from obvious, due to the inherent asymmetry of their admittance matrix. Only a custom model of these devices can allow the application of the DA method in weakly meshed networks, where the phase angle of transformers cannot be corrected by post-processing. Thus, this work introduces two new models of phase-shifting transformers, one extended from its conventional model and another extended from the consistent model introduced in this dissertation, together with a set of slight modifications to be included in the standard DA power flow formulation. Case studies allowed to demonstrate the validity of the proposal both with radial and weakly-meshed topologies. It was also tested that the excellent convergence characteristics of the DA method are not deteriorated by the inclusion of the new phase-shifting transformer model. This work, therefore, opens the possibility of using the DA power flow method in grids with embedded phase-shifting transformers.

The work presented in this dissertation opens the door to a wide range of interesting research possibilities. Some of these lines correspond to ongoing activities, while others are just schedule as future work. Among them, it is worth to mention:

- A study of the impact of phasor measurement units (PMU) in the estimation of transformer impedance ratio is ongoing. As it is discussed in chapter 5, there

are some hindrances that make the estimation of transformer impedance ratio a challenging task. Thus, the study of the impact and expected benefit of including PMU measurements in the parameter estimation algorithm seems promising.

- The development of a Kalman filter-based online parameter estimator for the short-circuit impedance ratio, as an improvement of the off-line multi-snapshot technique presented in this work, has been scheduled as future work. Interestingly, Kalman based estimation methods can include past measurements with varying weights in the estimation process. Thus a Kalman filter implementation will be able to overcome the difficulties discussed in chapter 5 and deliver the continuous estimation of transformer impedance ratio as an online estimator.

- A study of the advantage in bad data detection with the estimated values of transformer impedance ratio is ongoing. Better models and accurate parameter always aids in the bad data detection function of state estimation. Thus, it is interesting to further study how the estimates of transformer impedance ratio within the context of the consistent transformer model would aid in the improvement of the bad data detection function.

Conclusiones y Trabajos Futuros

Disponer de modelos precisos de los componentes del sistema eléctrico es hoy en día un asunto esencial para la correcta operación y planificación de las redes eléctricas. El nuevo paradigma que constituyen las redes inteligentes, con una creciente penetración de la generación distribuida y los vehículos eléctricos, hace que el papel de los transformadores reguladores de tensión sea cada vez más importante en todos los niveles de la infraestructura eléctrica.

El capítulo 2 de este trabajo demuestra que la práctica de despreciar el hecho de que la impedancia de cortocircuito es el resultado de las contribuciones de dos devanados diferentes puede conducir a discrepancias inaceptables en la formulación del modelo del transformador con tomas. Por ello, este documento propone un nuevo modelo general que incluye la contribución de cada devanado a la impedancia de cortocircuito. Si no se dispone de datos específicos sobre este aspecto o tal contribución no se puede estimar, el nuevo modelo permite considerar una contribución equitativa (50/50) de ambos devanados, lo que resulta ser una práctica aceptada en ingeniería.

Los nuevos modelos presentados en los capítulos 2 y 3 pueden ajustarse a los resultados de las alternativas convencionales, que consideran que la impedancia de cortocircuito es proporcionada por uno solo de los devanados del transformador, ya sea el nominal o el devanado con tomas. Este hecho hace que el nuevo modelo sea útil para entender la base de cada formulación, proporcionando una perspectiva clara sobre la influencia de las suposiciones subyacentes.

En el capítulo 2, el trabajo demuestra que las discrepancias causadas por los modelos convencionales de transformador con tomas pueden ser inaceptables en las posiciones extremas del cambiador, y que la forma en que aparecen, es muy influenciada por el punto de funcionamiento de la máquina. Los estudios realizados en este capítulo demuestran que esas discrepancias pueden ser significativas incluso en el caso de análisis de redes estándar bien conocidas, lo que se ilustra con un estudio de flujo de cargas y un análisis de estabilidad. La inclusión del modelo de transformador con tomas propuesto en este trabajo en los paquetes de software de análisis de sistemas de potencia, aun simplemente ajustado con los valores 50/50, puede ayudar significativamente a mejorar la consistencia de estos estudios sin necesidad de proporcionar datos adicionales.

En el capítulo 3 se presentan distintas variaciones del modelo consistente del transformador con tomas propuesto en este trabajo con el fin de adaptarse a diferentes requisitos, dependiendo de la configuración operativa, las bases elegidas y el número de fases a con-

siderar. De este modo, se abordada y resuelve cualquier ambigüedad en torno al modelado de este dispositivo. En el capítulo 4 el modelo consistente propuesto se extiende al estudio de los transformadores desfasadores asimétricos, alcanzándose conclusiones similares.

En el capítulo 5, y de cara a aumentar la precisión del modelo consistente presentado en este trabajo, se ha propuesto, validado y analizado un método de estimación de parámetros offline basado en vectores de estado aumentados con instantes múltiples, capaz de proporcionar estimaciones precisas de las ratios de impedancia de cortocircuito de los transformadores. Los casos estudiados permiten concluir que la inclusión de medidas de un número bajo de instantes, en el rango de 1 a 10, no es suficiente para dar lugar a resultados precisos, independientemente del nivel de redundancia del sistema. Sin embargo, la inclusión de un número mayor de instantes siempre permite alcanzar estimaciones aceptables. Aunque un bajo nivel de redundancia de las medidas requiere un mayor número de instantes para alcanzar la misma precisión, este trabajo demuestra que incluso aquellos sistemas cercanos al límite de observabilidad pueden ser manejados con éxito por el algoritmo propuesto. Es importante destacar que los casos de estudio analizados en este trabajo demuestran claramente que la obtención de estimaciones precisas de la ratio de impedancia de cortocircuito del transformador puede influir positivamente en la precisión de herramientas críticas como los estimadores de estado online.

Además, en el capítulo 6, este trabajo doctoral amplía sus aportaciones proporcionando los modelos necesarios para la inclusión de reguladores de tensión en cualquier de sus configuraciones en el análisis de flujos de carga trifásicos desequilibrados. El modelo general alcanzado para estos dispositivos se incluye en una red de prueba de 4 nudos que ser resuelve mediante un algoritmo Backward-Forward Sweep desequilibrado. Los resultados obtenidos se presentan como referencia para que los investigadores y desarrolladores de software de sistemas de potencia puedan validar sus algoritmos en un entorno bien probado.

Por último, en el capítulo 7, este trabajo propone una extensión del conocido método de flujo de cargas de Aproximación Directa (DA) para redes equilibradas, de cara a permitir su uso con componentes comunes de la red no considerados hasta la fecha en la formulación existente. Este trabajo demuestra que la extensión del método para la inclusión de modelos de líneas en π o transformadores con tomas es bastante sencilla, por lo que el documento se limita a establecer consideraciones formales sobre su aplicación. Sin embargo, la inclusión en el método DA de los modelos de transformadores desfasadores no es en absoluto trivial debido a la asimetría inherente a su matriz de admitancias. Sólo un modelo personalizado de estos dispositivos puede permitir la aplicación del método DA en redes débilmente malladas, en las que el ángulo de fase de los transformadores no puede corregirse mediante postprocesamiento. Así, este trabajo introduce dos nuevos modelos de transformadores desfasadores, uno que surge del modelo convencional y otro del modelo consistente aquí propuesto. La aplicación de estos modelos junto con una serie de ligeras modificaciones a incluir en la formulación estándar de flujo de cargas DA permite la aplicación de este algoritmo a redes que incluyen este tipo de dispositivos. Un conjunto de casos de estudio

permite demostrar la validez de la propuesta tanto con topologías radiales como débilmente malladas. El trabajo demuestra también que las excelentes características de convergencia del método DA no se ven deterioradas por la inclusión del nuevo modelo de transformador desfasador.

El trabajo presentado en esta tesis abre la puerta a un amplio abanico de interesantes posibilidades de investigación. Algunas de estas líneas corresponden a actividades en curso, mientras que otras sólo están programadas como trabajos futuros. Entre ellas, cabe destacar:

- En la actualidad, se está explorando el impacto que los sincrofasores (phasor-measurement units, PMU) pueden tener en la estimación de la ratio de impedancia de cortocircuito de los transformadores. Tal como se apunta en el capítulo 5, diversos obstáculos hacen compleja la estimación precisa de este parámetro. El beneficio esperado a partir de la inclusión de las medidas aportadas por estos nuevos dispositivos resulta prometedor y merece ser explorado en profundidad.

- Se ha dejado como trabajo futuro el desarrollo de un estimador de parámetros online basado en filtros de Kalman para la determinación de la ratio de impedancia de cortocircuito. Esta técnica puede aportar mejoras sobre la aproximación offline basada en instantes múltiples presentada aquí. Resulta interesante que los métodos de estimación basados en filtros de Kalman puedan incluir mediciones pasadas con pesos variables en el proceso de estimación. Por lo tanto, una implementación de este tipo podría superar algunas de las dificultades discutidas en el capítulo 5 y ofrecer una estimación continua de la ratio de impedancia capaz de ser integrada directamente en un estimador de estado online.

- En la actualidad, se está estudiando la ventaja que, para la detección de datos erróneos, puede tener el uso de valores estimados de la ratio de impedancia de cortocircuito del transformador. El uso de modelos mejorados y parámetros precisos tiene sin duda un efecto positivo en la función de detección de datos erróneos por parte de los estimadores de estado. El impacto concreto que las mejoras introducidas en este trabajo pueden tener en estos aspectos merecen ser estudiadas en profundidad.

References

[1] Arthur Eugene Fitzgerald, Charles Kingsley, Stephen D Umans, and B James. *Electric machinery*, volume 5. McGraw-Hill New York, 2003.

[2] William H Kersting. *Distribution system modeling and analysis*. CRC press, 2012.

[3] The International Electrotechnical Commission. Power transformers - part 1: General, IEC 60076-1:2011, 2011.

[4] Luciano V. Barboza, Hans H. Zürn, and Roberto Salgado. Load tap change transformers: A modeling reminder. *IEEE Power Engineering Review*, 21(2):51–52, Feb. 2001.

[5] A. Monticelli. *State Estimation in Electric Power Systems. A Generalized Approach*. Kluwer Academic Publishers, Norwell, MA, 1 edition, 1999.

[6] Ali Abur and Antonio Gomez Exposito. *Power system state estimation: theory and implementation*. CRC press, 2004.

[7] PowerWorld Corporation. *PowerWorld User's Guide*, 2011. [Online]. Available: http://www.powerworld.com.

[8] Carlos Grande-Moran. Phase-shifting transformer modeling in PSS®E. *Siemens Power Technology*, 1(111):1–7, Mar. 2012.

[9] Jose M Cano, Md Rejwanur Rashid Mojumdar, and Gonzalo Alonso Orcajo. Reconciling tap-changing transformer models. *IEEE Transactions on Power Delivery*, 34(6):2266–2268, 2019.

[10] Jose M Cano, Md Rejwanur Rashid Mojumdar, and Gonzalo A. Orcajo. On the consistency of tap-changing transformer models in power system studies. In *2020 IEEE Power & Energy Society General Meeting*. IEEE, Aug. 2020.

[11] Md Rejwanur R Mojumdar, Jose M Cano, Mohsen Assadi, and Gonzalo A Orcajo. Consensus phase shifting transformer model. In *2020 IEEE Power & Energy Society General Meeting (PESGM)*, pages 1–5. IEEE, 2020.

[12] Md Rejwanur Rashid Mojumdar, Jose M Cano, and Gonzalo Alonso Orcajo. Estimation of impedance ratio parameters for consistent modeling of tap-changing transformers. *IEEE Transactions on Power Systems*, 2021.

[13] J. E. Hobson and W. A. Lewis. Regulating transformers in power-system analysis. *Electrical Engineering*, 58(11):874–886, Nov 1939.

[14] L. H. Hill. Step type feeder voltage regulators. *Electrical Engineering*, 54(2):154–158, Feb 1935.

[15] M. Saidy and F.M. Hughes. A predictive integrated voltage regulator and power system stabilizer. *International Journal of Electrical Power and Energy Systems*, 17(2):101–111, 1995. cited By 8.

[16] I. Dzafic, R. A. Jabr, E. Halilovic, and B. C. Pal. A sensitivity approach to model local voltage controllers in distribution networks. *IEEE Transactions on Power Systems*, 29(3):1419–1428, May 2014.

[17] C.A.N. Pereira and C.A. Castro. Optimal placement of voltage regulators in distribution systems. In *PowerTech, 2009 IEEE Bucharest*, pages 1–5, June 2009.

[18] J. D. Watson, N. R. Watson, and B. Das. Effectiveness of power electronic voltage regulators in the distribution network. *IET Generation, Transmission Distribution*, 10(15):3816–3823, 2016.

[19] M. E. C. Brito, L. R. Limongi, M. C. Cavalcanti, F. A. S. Neves, and G. M. S. Azevedo. A step-dynamic voltage regulator based on cascaded reduced-power series transformers. *Electric Power Systems Research*, 108:245–253, 2014. Cited By :3.

[20] T. Senjyu, Y. Miyazato, A. Yona, N. Urasaki, and T. Funabashi. Optimal distribution voltage control and coordination with distributed generation. *IEEE Trans. on Power Delivery*, 23(2):1236–1242, April 2008.

[21] Jen-Hao Teng. A direct approach for distribution system load flow solutions. *IEEE Transactions on Power Delivery*, 18(3):882–887, July 2003.

[22] C. Cañizares A. Gómez-Expósito, A. J. Conejo. *Electric Energy Systems. Analysis and Operation*. CRC Press LLC, Boca Raton, FL, 1 edition, 2009.

[23] J. Bandler, M. El-Kady, and H. Grewal. An application of complex branch modeling to nonreciprocal power transmission elements. *IEEE Transactions on Circuits and Systems*, 32(12):1292–1295, Dec. 1985.

[24] J. C. Jimenez and C. O. Nwankpa. Circuit model of a phase-shifting transformer for analog power flow emulation. In *2011 IEEE International Symposium of Circuits and Systems (ISCAS)*, pages 1864–1867, May 2011.

[25] R. D. Youssef. Phase-shifting transformers in load flow and short-circuit analysis: modelling and control. *IEE Proceedings C - Generation, Transmission and Distribution*, 140(4):331–336, July 1993.

[26] E. Acha, H. Ambriz-Perez, and C. R. Fuerte-Esquivel. Advanced transformer control modeling in an optimal power flow using newton's method. *IEEE Transactions on Power Systems*, 15(1):290–298, Feb. 2000.

[27] S. A. Nabavi Niaki. A novel steady-state model and principles of operation of phase-shifting transformer comparable with facts new devices. In *Proceedings. International Conference on Power System Technology*, volume 3, pages 1450–1457, Oct. 2002.

[28] D. A. Tziouvaras and R. Jimenez. 138 kv phase shifting transformer protection: Emtp modeling and model power system testing. In *2004 Eighth IEE International Conference on Developments in Power System Protection*, volume 1, pages 343–347, April 2004.

[29] T. Okon and K. Wilkosz. Phase shifter models for steady state analysis. In *2016 17th International Scientific Conference on Electric Power Engineering (EPE)*, pages 1–6, May 2016.

[30] John Okyere Attia. *Electronics and circuit analysis using MATLAB*. CRC press, 2018.

[31] J Duncan Glover, Mulukutla S Sarma, and Thomas Overbye. *Power system analysis & design, SI version*. Cengage Learning, 2012.

[32] Alcir Monticelli. *State estimation in electric power systems: a generalized approach*. Springer Science & Business Media, 2012.

[33] Powerworld user's guide, 2011.

[34] R. C. Dugan and D. Montenegro. *The Open Distribution System Simulator (OpenDSS): Reference guide*. EPRI, program rev. 8.6.1 edition, June 2019.

[35] Institute of Electrical and Electronics Engineers. IEEE standard for general requirements for liquid-immersed distribution, power, and regulating transformers. *IEEE Std C57.12.00-2015 (Revision of IEEE Std C57.12.00-2010)*, pages 1–74, May 2016.

[36] K. Karsai, D. Kerényi, and L. Kiss. *Large Power Transformers*, volume 25 of *Studies in Electrical and Electronic Engineering*. Elsevier Science Ltd., Amsterdam, NL, 1 edition, 1987.

[37] Satish V Kulkarni and Shrikrishna A Khaparde. *Transformer engineering: design, technology, and diagnostics*. CRC press, 2017.

[38] K. Shaarbafi. Transformer modelling guide. Technical report, Alberta Electric System Operator, Jul. 2014.

[39] Ali R. Al-Roomi. Power Flow Test Systems Repository, 2015.

[40] R. D. Zimmerman, C. E. Murillo-Sánchez, and R. J. Thomas. MATPOWER: Steady-state operations, planning, and analysis tools for power systems research and education. *IEEE Transactions on Power Systems*, 26(1):12–19, Feb 2011.

[41] R. D. Zimmerman and C. E. Murillo-Sánchez. *MATPOWER User's Manual*, version 7.0 edition, 2019. [Online]. Available: https://matpower.org/docs/MATPOWER-manual-7.0.pdf.

[42] IEEE. IEEE guide for the application, specification, and testing of phase-shifting transformers - redline. *IEEE Std C57.135-2011 (Revision of IEEE Std C57.135-2001) - Redline*, pages 1–71, 2011.

[43] Luciano V Barboza, HH Zurn, and Roberto Salgado. Load tap change transformers: A modeling reminder. *parameters*, 1:5, 2001.

[44] RD Youssef. Phase-shifting transformers in load flow and short-circuit analysis: modelling and control. In *IEE Proceedings C (Generation, Transmission and Distribution)*, volume 140, pages 331–336. IET, 1993.

[45] José M Cano, Md Rejwanur R Mojumdar, Joaquín G Norniella, and Gonzalo A Orcajo. Phase shifting transformer model for direct approach power flow studies. *International Journal of Electrical Power & Energy Systems*, 91:71–79, 2017.

[46] ENTSO-E. Phase shift transformers modelling, 2014.

[47] Jody Verboomen, Dirk Van Hertem, Pieter H Schavemaker, Wil L Kling, and Ronnie Belmans. Phase shifting transformers: principles and applications. In *2005 International Conference on Future Power Systems*, pages 6–pp. IEEE, 2005.

[48] O Alsac, N Vempati, B Stott, and A Monticelli. Generalized state estimation. *IEEE Transactions on power systems*, 13(3):1069–1075, 1998.

[49] MRM Castillo, JBA London Jr, and NG Bretas. Identification and estimation of power system branch parameter error. In *2009 IEEE Power & Energy Society General Meeting*, pages 1–8. IEEE, 2009.

[50] PAUL A Teixeira, STEVEN R Brammer, William L Rutz, WC Merritt, and JL Salmonsen. State estimation of voltage and phase-shift transformer tap settings. *IEEE transactions on power systems*, 7(3):1386–1393, 1992.

[51] Yuzhang Lin and Ali Abur. Enhancing network parameter error detection and correction via multiple measurement scans. *IEEE Transactions on Power Systems*, 32(3):2417–2425, 2016.

[52] Y. Lin and A. Abur. Robust state estimation against measurement and network parameter errors. *IEEE Transactions on Power Systems*, 33(5):4751–4759, 2018.

[53] George N Korres, Peter J Katsikas, and George C Contaxis. Transformer tap setting observability in state estimation. *IEEE Transactions on Power Systems*, 19(2):699–706, 2004.

[54] Pedro Zarco and Antonio Gomez Exposito. Power system parameter estimation: a survey. *IEEE Transactions on power systems*, 15(1):216–222, 2000.

[55] FC Aschmoneit, NM Peterson, and EC Adrian. State estimation with equality constraints. In *Tenth PICA Conference Proceedings*, pages 427–430, 1977.

[56] Anders Gjelsvik, Sverre Aam, and Lars Holten. Hachtel's augmented matrix method-a rapid method improving numerical stability in power system static state estimation. *IEEE Transactions on Power Apparatus and Systems*, 1985.

[57] Md Rejwanur R Mojumdar, Jose M Cano, Shahid Jaman, and Gonzalo A Orcajo. Smoothing parameter optimization routine for high-quality a priori estimates in forecasting-aided state estimation. In *2018 IEEE Power & Energy Society General Meeting (PESGM)*, pages 1–5. IEEE, 2018.

[58] American National Standards Institute. ANSI C12.20-2015, Electricity meters, 0.1, 0.2 and 0.5 accuracy classes. Standard, ANSI, Washington, D.C., 2015.

[59] S. Chakrabarti, E. Kyriakides, G. Ledwich, and A. Ghosh. Inclusion of pmu current phasor measurements in a power system state estimator. *IET Generation, Transmission Distribution*, 4(10):1104–1115, 2010.

[60] M. I. Hossain, R. Yan, and T. K. Saha. Investigation of the interaction between step voltage regulators and large-scale photovoltaic systems regarding voltage regulation and unbalance. *IET Renewable Power Generation*, 10(3):299–309, 2016.

[61] Xiaohu Liu, A. Aichhorn, Liming Liu, and Hui Li. Coordinated control of distributed energy storage system with tap changer transformers for voltage rise mitigation under high photovoltaic penetration. *IEEE Trans. on Smart Grid*, 3(2):897–906, June 2012.

[62] K. H. Youssef. A new method for online sensitivity-based distributed voltage control and short circuit analysis of unbalanced distribution feeders. *IEEE Transactions on Smart Grid*, 6(3):1253–1260, May 2015.

[63] H. Rahbarimagham, M. J. Sanjari, A. Tavakoli, G. B. Gharehpetian, and R. Jafari. Emission reduction in a micro grid including pv considering voltage profile improvement. In *2013 Smart Grid Conference (SGC)*, pages 219–224, Dec 2013.

[64] Z. Tang, D. Hill, T. Liu, and H. Ma. Hierarchical voltage control of weak subtransmission networks with high penetration of wind power. *IEEE Transactions on Power Systems*, PP(99):1–1, 2017.

[65] K. M. Murphy and N. K. C. Nair. Voltage control in distribution networks with penetration of solar pv: Estimated voltages as a control input. In *2016 IEEE Power and Energy Society General Meeting (PESGM)*, pages 1–5, July 2016.

[66] O. Ceylan, A. Dimitrovski, M. Starke, and K. Tomsovic. Optimal reactive power allocation for photovoltaic inverters to limit transformer tap changes. In *2016 IEEE Power and Energy Society General Meeting (PESGM)*, pages 1–5, July 2016.

[67] H.E. Farag, E.F. El-Saadany, R. El Shatshat, and A. Zidan. A generalized power flow analysis for distribution systems with high penetration of distributed generation. *Electric Power Systems Research*, 81(7):1499–1506, 2011. cited By 35.

[68] M. Oshiro, K. Tanaka, A. Uehara, T. Senjyu, Y. Miyazato, A. Yona, and T. Funabashi. Optimal voltage control in distribution systems with coordination of distribution installations. *International Journal of Electrical Power and Energy Systems*, 32(10):1125–1134, 2010. cited By 26.

[69] P. Frias, C. A. Platero, D. Soler, and F. Blazquez. High-efficiency voltage regulator for rural networks. *IEEE Transactions on Power Delivery*, 25(3):1666–1672, July 2010.

[70] M. Chamana, B. H. Chowdhury, and F. Jahanbakhsh. Distributed control of voltage regulating devices in the presence of high pv penetration to mitigate ramp-rate issues. *IEEE Transactions on Smart Grid*, PP(99):1–1, 2017.

[71] R. Yan, Y. Li, T. Saha, L. Wang, and M. Hossain. Modelling and analysis of open-delta step voltage regulators for unbalanced distribution network with photovoltaic power generation. *IEEE Transactions on Smart Grid*, PP(99):1–1, 2017.

[72] B. A. Robbins, H. Zhu, and A. D. Domínguez-García. Optimal tap setting of voltage regulation transformers in unbalanced distribution systems. *IEEE Transactions on Power Systems*, 31(1):256–267, Jan 2016.

[73] H. Ahmadi and J. R. Martí. Distribution system optimization based on a linear power-flow formulation. *IEEE Transactions on Power Delivery*, 30(1):25–33, Feb 2015.

[74] L. R. Araujo, D. R. R. Penido, S. Carneiro, and J. L. R. Pereira. A three-phase optimal power-flow algorithm to mitigate voltage unbalance. *IEEE Transactions on Power Delivery*, 28(4):2394–2402, Oct 2013.

[75] Ujjwal Ghatak and V. Mukherjee. An improved load flow technique based on load current injection for modern distribution system. *International Journal of Electrical Power & Energy Systems*, 84:168 – 181, 2017.

[76] J. W. Liu, S. S. Choi, and S. Chen. Design of step dynamic voltage regulator for power quality enhancement. *IEEE Transactions on Power Delivery*, 18(4):1403–1409, Oct 2003.

[77] W. H. Kersting. The modeling and application of step voltage regulators. In *2009 IEEE/PES Power Systems Conference and Exposition*, pages 1–8, March 2009.

[78] Distribution Test Feeders, IEEE PES Distribution System Analysis Subcommittee's. Distribution Test Feeder Working Group. [On-line]. Available: http://ewh.ieee.org/soc/pes/dsacom/testfeeders/.

[79] William H Kersting. Transformer model test system. In *Transmission and Distribution Conference and Exposition, 2003 IEEE PES*, volume 3, pages 1022–1026. IEEE, 2003.

[80] P. Arboleya, C. Gonzalez-Moran, and M. Coto. Unbalanced power flow in distribution systems with embedded transformers using the complex theory in $\alpha\beta 0$ stationary reference frame. *Power Systems, IEEE Transactions on*, 29(3):1012–1022, May 2014.

[81] Cristina González-Morán, Pablo Arboleya, and Bassam Mohamed. Matrix backward forward sweep for unbalanced power flow in Î±Î²0 frame. *Electric Power Systems Research*, 148:273 – 281, 2017.

[82] Federico Milano. *Power system modelling and scripting*. Springer, 2010.

[83] Charles L Fortescue. Method of symmetrical co-ordinates applied to the solution of polyphase networks. *American Institute of Electrical Engineers, Transactions of the*, 37(2):1027–1140, 1918.

[84] JM Uudrill. Dynamic stability calculations for an arbitrary number of interconnected synchronous machines. *Power Apparatus and Systems, IEEE Transactions on*, (3):835–844, 1968.

[85] Guzmán Díaz and Cristina Gonzalez-Moran. Fischer-burmeister-based method for calculating equilibrium points of droop-regulated microgrids. *Power Systems, IEEE Transactions on*, 27(2):959–967, 2012.

[86] Pablo Arboleya, Guzman Diaz, and Manuel Coto. Unified ac/dc power flow for traction systems: A new concept. *Vehicular Technology, IEEE Transactions on*, 61(6):2421–2430, 2012.

[87] J. A. Martinez and J. Mahseredjian. Load flow calculations in distribution systems with distributed resources. a review. In *2011 IEEE Power and Energy Society General Meeting*, pages 1–8, July 2011.

[88] D. Das, D. P. Kothari, and A. Kalam. Simple and efficient method for load flow solution of radial distribution networks. *International Journal of Electrical Power & Energy Systems*, 17(5):335–346, Oct. 1995.

[89] T. H. Chen, M. S. Chen, K. J. Hwang, P. Kotas, and E. A. Chebli. Distribution system power flow analysis-a rigid approach. *IEEE Transactions on Power Delivery*, 6(3):1146–1152, July 1991.

[90] D. Shirmohammadi, H. W. Hong, A. Semlyen, and G. X. Luo. A compensation-based power flow method for weakly meshed distribution and transmission networks. *IEEE Transactions on Power Systems*, 3(2):753–762, May 1988.

[91] J. M. Cano, J. G. Norniella, C. H. Rojas, G. A. Orcajo, and J. Jatskevich. Application of loop power flow controllers for power demand optimization at industrial customer sites. In *2015 IEEE Power Energy Society General Meeting*, pages 1–5, July 2015.

[92] M. E. Baran and F. F. Wu. Network reconfiguration in distribution systems for loss reduction and load balancing. *IEEE Transactions on Power Delivery*, 4(2):1401–1407, Apr. 1989.

Appendix A

Full Set of Results for the 4-node Test Feeder

The result Tables as described in Section 6.6 are included here.

Table A.1 Type A Regulators. Inductive Balanced Loading. Before Optimization

		Y_gY_g	$\Delta\Delta$	OΔ case a	OΔ case b	OΔ case c
	Taps	[0 0 0]	[0 0 0]	[0 — 0]	[0 0 —]	[— 0 0]
Node 2	V_1	$7125\angle -0.3°$	$12360\angle 29.7°$	$12364\angle 29.7°$	$12365\angle 29.7°$	$12362\angle 29.7°$
	V_2	$7145\angle -120.4°$	$12370\angle -120.4°$	$12375\angle -90.4°$	$12376\angle -90.4°$	$12373\angle -90.4°$
	V_3	$7136\angle 119.6°$	$12346\angle 149.6°$	$12351\angle 149.6°$	$12353\angle 149.6°$	$12349\angle 149.6°$
Node 3	V_1	$6842\angle -4°$	$11870\angle 26.7°$	$12364\angle 29.7°$	$11951\angle 28.8°$	$11891\angle 26.7°$
	V_2	$6863\angle -123.4°$	$11882\angle -93.4°$	$12125\angle -93.0°$	$12194\angle -89.8°$	$11950\angle -91.2°$
	V_3	$6854\angle 116.6°$	$11857\angle 146.6°$	$11749\angle 149.4°$	$12330\angle 148.6°$	$12296\angle 147.5°$
Node 4	V_1	$6752\angle -3.8°$	$11737\angle 26.3°$	$12231\angle 29.3°$	$11821\angle 28.4°$	$11762\angle 26.3°$
	V_2	$6798\angle -123.9°$	$11764\angle -94.0°$	$12012\angle -93.5°$	$12077\angle -90.3°$	$11832\angle -91.8°$
	V_3	$6778\angle 116.0°$	$11709\angle 146.0°$	$11601\angle 148.9°$	$12187\angle 148.0°$	$12150\angle 147.0°$
Line 12	I_a	$296.2\angle -29.7°$	$295.2\angle -29.7°$	$290.3\angle -27.6°$	$288.1\angle -27.1°$	$290.9\angle -28.7°$
	I_b	$294.2\angle -149.7°$	$295.2\angle -149.7°$	$289.8\angle -147.7°$	$288.0\angle -147.1°$	$290.7\angle -148.7°$
	I_c	$295.1\angle 90.2°$	$295.2\angle 90.3°$	$290.0\angle 92.4°$	$288.0\angle 92.9°$	$290.8\angle 91.4°$
Line 34	I_a	$296.2\angle -29.7°$	$295.2\angle -29.7°$	$290.3\angle -27.6°$	$288.1\angle -27.1°$	$290.9\angle -28.7°$
	I_b	$294.2\angle -149.7°$	$295.2\angle -149.7°$	$289.8\angle -147.7°$	$288.0\angle -147.1°$	$290.7\angle -148.7°$
	I_c	$295.1\angle 90.2°$	$295.2\angle 90.3°$	$290.0\angle 92.4°$	$288.0\angle 92.9°$	$290.8\angle 91.4°$

Where V_1, V_2 and V_3 are phase-to-neutral voltages in wye connections and line voltages in the others.

Table A.2 Type A Regulators. Inductive Balanced Loading. After Optimization

		Y_gY_g	$\Delta\Delta$	OΔ case a	OΔ case b	OΔ case c
	Taps	[2 1 2]	[2 1 2]	[-5 — 4]	[1 -3 —]	[— 1 2]
Node 2	V_1	$7125\angle -0.3°$	$12360\angle 29.7°$	$12365\angle 29.7°$	$12363\angle 29.7°$	$12362\angle 29.7°$
	V_2	$7145\angle -120.3°$	$12371\angle -90.4°$	$12377\angle -90.4°$	$12377\angle -90.4°$	$12373\angle -90.4°$
	V_3	$7136\angle 119.6°$	$12346\angle 149.6°$	$12347\angle 149.6°$	$12354\angle 149.6°$	$12349\angle 149.6°$
Node 3	V_1	$6936\angle -3.3°$	$12075\angle 27.1°$	$11979\angle 29.7°$	$12025\angle 28.8°$	$12015\angle 26.4°$
	V_2	$6910\angle -123.3°$	$12046\angle -92.7°$	$12070\angle -90.2°$	$11965\angle -89.8°$	$12031\angle -91.2°$
	V_3	$6947\angle 116.7°$	$12098\angle 147.3°$	$12040\angle 149.4°$	$12253\angle 149.8°$	$12450\angle 147.6°$
Node 4	V_1	$6847\angle -3.7°$	$11944\angle 26.7°$	$11847\angle 29.3°$	$11895\angle 28.4°$	$11887\angle 26.0°$
	V_2	$6845\angle -123.8°$	$11930\angle -93.2°$	$11953\angle -90.7°$	$11848\angle -90.3°$	$11914\angle -91.7°$
	V_3	$6873\angle 116.1°$	$11952\angle 146.8°$	$11894\angle 148.9°$	$12107\angle 149.2°$	$12305\angle 147.0°$
Line 12	I_a	$295.8\angle -29.6°$	$295.5\angle -29.7°$	$290.6\angle -29.5°$	$291.7\angle -26.7°$	$289.8\angle -28.8°$
	I_b	$294.0\angle -149.7°$	$293.7\angle -149.7°$	$282.1\angle -146.7°$	$288.1\angle -148.0°$	$291.3\angle -148.7°$
	I_c	$294.6\angle 90.3°$	$294.6\angle 90.6°$	$298.4\angle 93.3°$	$284.5\angle 93.3°$	$290.6\angle 91.0°$
Line 34	I_a	$292.1\angle -29.6°$	$290.1\angle -29.1°$	$291.1\angle -29.7°$	$289.9\angle -26.7°$	$288.0\angle -28.8°$
	I_b	$292.2\angle -149.7°$	$290.1\angle -149.1°$	$291.2\angle -146.7°$	$289.9\angle -146.7°$	$287.7\angle -148.7°$
	I_c	$291.0\angle 90.3°$	$290.1\angle 90.9°$	$291.1\angle 93.3°$	$289.9\angle 93.3°$	$288.0\angle 91.3°$

Where V_1, V_2 and V_3 are phase-to-neutral voltages in wye connections and line voltages in the others.

Table A.3 Type A Regulators. Capacitive Balanced Loading. Before Optimization

		Y_gY_g	$\Delta\Delta$	OΔ case a	OΔ case b	OΔ case c
	Taps	[0 0 0]	[0 0 0]	[0 — 0]	[0 0 —]	[— 0 0]
Node 2	V_1	$7184\angle -0.6°$	$12451\angle 29.5°$	$12454\angle 29.5°$	$12455\angle 29.5°$	$12453\angle 29.5°$
	V_2	$7199\angle -120.5°$	$12473\angle -90.6°$	$12477\angle -90.6°$	$12478\angle -90.6°$	$12475\angle -90.6°$
	V_3	$7198\angle 119.4°$	$12457\angle 149.4°$	$12461\angle 149.4°$	$12463\angle 149.4°$	$12460\angle 149.4°$
Node 3	V_1	$7289\angle -3.9°$	$12631\angle 26.1°$	$12454\angle 29.5°$	$12346\angle 27.5°$	$12648\angle 26.2°$
	V_2	$7304\angle -123.8°$	$12654\angle -93.9°$	$12733\angle -92.9°$	$12265\angle -90.8°$	$12358\angle -92.5°$
	V_3	$7303\angle 116.1°$	$12639\angle 146.1°$	$12138\angle 147.1°$	$12619\angle 148.6°$	$12762\angle 148.0°$
Node 4	V_1	$7277\angle -4.7°$	$12617\angle 25.5°$	$12436\angle 28.8°$	$12334\angle 26.8°$	$12637\angle 25.5°$
	V_2	$7309\angle -124.5°$	$12667\angle -94.6°$	$12749\angle -93.6°$	$12277\angle -91.5°$	$12371\angle -93.2°$
	V_3	$7308\angle 115.4°$	$12636\angle 145.3°$	$12136\angle 146.3°$	$12614\angle 147.8°$	$12756\angle 147.2°$
Line 12	I_a	$274.9\angle 21.1°$	$274.1\angle 21.2°$	$278.4\angle 22.9°$	$279.2\angle 23.5°$	$275.1\angle 22.3°$
	I_b	$273.7\angle -98.6°$	$274.1\angle -98.8°$	$278.4\angle -97.0°$	$279.1\angle -96.5°$	$275.2\angle -97.7°$
	I_c	$273.7\angle 141.2°$	$274.1\angle 141.2°$	$278.7\angle 143.0°$	$279.3\angle 143.6°$	$275.3\angle 142.3°$
Line 34	I_a	$274.9\angle 21.1°$	$274.1\angle 21.2°$	$278.4\angle 22.9°$	$279.2\angle 23.5°$	$275.1\angle 22.3°$
	I_b	$273.7\angle -98.6°$	$274.1\angle -98.8°$	$278.4\angle -97.0°$	$279.1\angle -96.5°$	$275.2\angle -97.7°$
	I_c	$273.7\angle 141.2°$	$274.1\angle 141.2°$	$278.7\angle 143.0°$	$279.3\angle 143.6°$	$275.3\angle 142.3°$

Where V_1, V_2 and V_3 are phase-to-neutral voltages in wye connections and line voltages in the others.

Table A.4 Type A Regulators. Capacitive Balanced Loading. After Optimization

		Y_gY_g	$\Delta\Delta$	OΔ case a	OΔ case b	OΔ case c
	Taps	[-9 -10 -10]	[-6 -6 -6]	[-7 — -3]	[-6 -5 —]	[— -6 -11]
Node 2	V_1	$7184\angle -0.6°$	$12450\angle 29.5°$	$12453\angle 29.5°$	$12455\angle 29.5°$	$12452\angle 29.5°$
	V_2	$7198\angle -120.5°$	$12472\angle -90.6°$	$12478\angle -90.6°$	$12478\angle -90.6°$	$12478\angle -90.6°$
	V_3	$7198\angle 119.4°$	$12456\angle 149.4°$	$12460\angle 149.4°$	$12462\angle 149.4°$	$12463\angle 149.4°$
Node 3	V_1	$6888\angle -4.4°$	$11943\angle 23.8°$	$11908\angle 29.5°$	$11873\angle 27.3°$	$11986\angle 27.4°$
	V_2	$6858\angle -124.3°$	$11964\angle -96.2°$	$12346\angle -91.9°$	$11865\angle -90.9°$	$11889\angle -92.7°$
	V_3	$6856\angle 115.7°$	$11952\angle 143.7°$	$11889\angle 147.0°$	$12195\angle 148.3°$	$11927\angle 147.8°$
Node 4	V_1	$6875\angle -5.2°$	$11928\angle 23.0°$	$11890\angle 28.7°$	$11861\angle 26.6°$	$11971\angle 26.7°$
	V_2	$6863\angle -125.0°$	$11979\angle -97.0°$	$12360\angle -92.6°$	$11877\angle -91.6°$	$11904\angle -93.4°$
	V_3	$6862\angle 114.8°$	$11948\angle 142.8°$	$11889\angle 146.1°$	$12190\angle 147.4°$	$11922\angle 146.9°$
Line 12	I_a	$274.5\angle 20.6°$	$273.7\angle 20.8°$	$278.5\angle 22.0°$	$278.5\angle 23.3°$	$279.4\angle 22.5°$
	I_b	$273.2\angle -99.2°$	$273.7\angle -99.2°$	$275.1\angle -96.7°$	$279.2\angle -96.4°$	$270.4\angle -97.5°$
	I_c	$273.3\angle 140.7°$	$273.7\angle 140.8°$	$282.3\angle 143.2°$	$280.3\angle 143.3°$	$275.0\angle 144.2°$
Line 34	I_a	$290.9\angle 20.6°$	$289.8\angle 18.8°$	$287.4\angle 23.2°$	$289.3\angle 23.3°$	$290.3\angle 22.5°$
	I_b	$291.4\angle -99.2°$	$289.8\angle -101.2°$	$287.7\angle -96.7°$	$289.2\angle -96.7°$	$290.3\angle -97.5°$
	I_c	$291.5\angle 140.7°$	$289.9\angle 138.8°$	$287.7\angle 143.2°$	$289.3\angle 143.3°$	$290.3\angle 142.5°$

Where V_1, V_2 and V_3 are phase-to-neutral voltages in wye connections and line voltages in the others.

Table A.5 Type A Regulators. Inductive Unbalanced Loading. Before Optimization

		Y_gY_g	$\Delta\Delta$	OΔ case a	OΔ case b	OΔ case c
	Taps	[0 0 0]	[0 0 0]	[0 — 0]	[0 0 —]	[— 0 0]
Node 2	V_1	$7161\angle -0.1°$	$12361\angle 29.8°$	$12364\angle 29.8°$	$12366\angle 29.8°$	$12364\angle 29.8°$
	V_2	$7119\angle -120.3°$	$12391\angle -90.5°$	$12396\angle -90.5°$	$12397\angle -90.5°$	$12394\angle -90.5°$
	V_3	$7125\angle 119.3°$	$12332\angle 150.0°$	$12338\angle 149.5°$	$12340\angle 149.5°$	$12337\angle 149.5°$
Node 3	V_1	$6929\angle -2.2°$	$11846\angle 27.3°$	$12364\angle 29.8°$	$11907\angle 29.0°$	$11873\angle 27.2°$
	V_2	$6836\angle -123.3°$	$12040\angle -93.6°$	$12247\angle -93.2°$	$12217\angle -89.7°$	$12042\angle -91.2°$
	V_3	$6826\angle 115.1°$	$11793\angle 146.0°$	$11759\angle 148.8°$	$12294\angle 148.4°$	$12236\angle 147.3°$
Node 4	V_1	$6881\angle -2.3°$	$11713\angle 26.9°$	$12232\angle 29.5°$	$11779\angle 28.7°$	$11744\angle 26.9°$
	V_2	$6739\angle -123.7°$	$11949\angle -94.2°$	$12161\angle -93.8°$	$12125\angle -90.3°$	$11949\angle -91.8°$
	V_3	$6744\angle 114.1°$	$11630\angle 145.4°$	$11597\angle 148.2°$	$12135\angle 147.9°$	$12076\angle 146.7°$
Line 12	I_a	$218.0\angle -34.1°$	$315.4\angle -35.3°$	$311.6\angle -33.1°$	$307.0\angle -32.6°$	$309.0\angle -34.0°$
	I_b	$296.8\angle -149.5°$	$250.3\angle -147.6°$	$246.1\angle -146.0°$	$244.7\angle -144.7°$	$246.7\angle -146.2°$
	I_c	$370.7\angle 95.9°$	$319.6\angle 98.3°$	$313.5\angle 100.5°$	$312.4\angle 100.8°$	$314.4\angle 99.4°$
Line 34	I_a	$218.0\angle -34.1°$	$315.4\angle -35.3°$	$311.6\angle -33.1°$	$307.0\angle -32.6°$	$309.0\angle -34.0°$
	I_b	$296.8\angle -149.5°$	$250.3\angle -147.6°$	$246.1\angle -146.0°$	$244.7\angle -144.7°$	$246.7\angle -146.2°$
	I_c	$370.7\angle 95.9°$	$319.6\angle 98.3°$	$313.5\angle 100.5°$	$312.4\angle 100.8°$	$314.4\angle 99.4°$

Where V_1, V_2 and V_3 are phase-to-neutral voltages in wye connections and line voltages in the others.

Table A.6 Type A Regulators. Inductive Unbalanced Loading. After Optimization

		Y_gY_g	$\Delta\Delta$	OΔ case a	OΔ case b	OΔ case c
	Taps	[0 3 3]	[3 -2 2]	[-5 — 4]	[1 -3 —]	[— -1 4]
Node 2	V_1	$7161\angle -0.1°$	$12360\angle 29.8°$	$12365\angle 29.8°$	$12364\angle 29.8°$	$12365\angle 29.8°$
	V_2	$7120\angle -120.3°$	$12393\angle -90.5°$	$12398\angle -90.5°$	$12398\angle -90.5°$	$12390\angle -90.4°$
	V_3	$7126\angle 119.3°$	$12333\angle 149.5°$	$12334\angle 149.5°$	$12342\angle 149.5°$	$12337\angle 149.6°$
Node 3	V_1	$6929\angle -2.2°$	$12017\angle 26.7°$	$11979\angle 29.8°$	$11981\angle 29.0°$	$12011\angle 25.7°$
	V_2	$6976\angle -123.2°$	$11966\angle -93.0°$	$12191\angle -90.4°$	$11987\angle -89.7°$	$11963\angle -91.2°$
	V_3	$6968\angle 115.3°$	$12065\angle 147.1°$	$12052\angle 148.8°$	$12216\angle 149.6°$	$12543\angle 147.4°$
Node 4	V_1	$6880\angle -2.3°$	$11887\angle 26.3°$	$11848\angle 29.5°$	$11853\angle 28.7°$	$11886\angle 25.4°$
	V_2	$6882\angle -123.6°$	$11875\angle -93.6°$	$12101\angle -91.0°$	$11895\angle -90.3°$	$11871\angle -91.8°$
	V_3	$6887\angle 114.3°$	$11903\angle 146.4°$	$11892\angle 148.2°$	$12055\angle 149.0°$	$12384\angle 146.8°$
Line 12	I_a	$218.0\angle -34.1°$	$319.5\angle -35.2°$	$312.7\angle -34.8°$	$310.9\angle -32.0°$	$302.7\angle -34.3°$
	I_b	$296.1\angle -149.4°$	$247.2\angle -148.4°$	$238.7\angle -144.7°$	$245.3\angle -146.0°$	$250.5\angle -146.4°$
	I_c	$369.8\angle 96.1°$	$318.0\angle 99.1°$	$322.3\angle 101.1°$	$308.1\angle 101.3°$	$312.0\angle 97.6°$
Line 34	I_a	$218.0\angle -34.1°$	$310.9\angle -34.7°$	$309.9\angle -32.4°$	$308.9\angle -32.0°$	$304.6\angle -34.3°$
	I_b	$290.6\angle -149.4°$	$248.1\angle -147.1°$	$246.4\angle -144.7°$	$246.9\angle -144.3°$	$244.3\angle -146.4°$
	I_c	$363.0\angle 96.1°$	$315.3\angle 98.6°$	$314.4\angle 101.1°$	$313.9\angle 101.3°$	$310.6\angle 98.9°$

Where V_1, V_2 and V_3 are phase-to-neutral voltages in wye connections and line voltages in the others.

Table A.7 Type A Regulators. Capacitive Unbalanced Loading. Before Optimization

		Y_gY_g	$\Delta\Delta$	OΔ case a	OΔ case b	OΔ case c
	Taps	[0 0 0]	[0 0 0]	[0 — 0]	[0 0 —]	[— 0 0]
Node 2	V_1	$7210\angle -0.4°$	$12447\angle 29.6°$	$12448\angle 29.6°$	$12451\angle 29.6°$	$12449\angle 29.6°$
	V_2	$7179\angle -120.4°$	$12488\angle -90.6°$	$12492\angle -90.6°$	$12494\angle -90.6°$	$12491\angle -90.6°$
	V_3	$7181\angle 119.1°$	$12434\angle 149.3°$	$12437\angle 149.3°$	$12441\angle 149.3°$	$12438\angle 149.3°$
Node 3	V_1	$7324\angle -2.8°$	$12556\angle 26.8°$	$12448\angle 29.6°$	$12271\angle 27.8°$	$12577\angle 26.8°$
	V_2	$7285\angle -123.8°$	$12775\angle -94.0°$	$12825\angle -93.2°$	$12288\angle -90.7°$	$12434\angle -92.4°$
	V_3	$7233\angle 114.8°$	$12509\angle 145.5°$	$12117\angle 146.6°$	$12556\angle 148.5°$	$12662\angle 147.7°$
Node 4	V_1	$7340\angle -3.2°$	$12534\angle 26.2°$	$12422\angle 29.0°$	$12252\angle 27.2°$	$12558\angle 26.2°$
	V_2	$7264\angle -124.3°$	$12810\angle -94.8°$	$12862\angle -93.9°$	$12320\angle -91.5°$	$12468\angle -93.2°$
	V_3	$7222\angle 113.7°$	$12479\angle 144.6°$	$12087\angle 145.7°$	$12525\angle 147.6°$	$12630\angle 146.9°$
Line 12	I_a	$204.4\angle 28.6°$	$258.3\angle 9.4°$	$262.1\angle 10.6°$	$262.6\angle 12.3°$	$259.5\angle 11.2°$
	I_b	$275.3\angle -98.5°$	$247.3\angle -91.7°$	$249.6\angle -90.2°$	$252.9\angle -89.1°$	$249.3\angle -90.3°$
	I_c	$346.1\angle 131.9°$	$321.3\angle 140.4°$	$326.5\angle 141.9°$	$326.5\angle 142.9°$	$322.0\angle 141.8°$
Line 34	I_a	$204.4\angle 28.6°$	$258.3\angle 9.4°$	$262.1\angle 10.6°$	$262.6\angle 12.3°$	$259.5\angle 11.2°$
	I_b	$275.3\angle -98.5°$	$247.3\angle -91.7°$	$249.6\angle -90.2°$	$252.9\angle -89.1°$	$249.3\angle -90.3°$
	I_c	$346.2\angle 131.9°$	$321.3\angle 140.4°$	$326.5\angle 141.9°$	$326.5\angle 142.9°$	$322.0\angle 141.8°$

Where V_1, V_2 and V_3 are phase-to-neutral voltages in wye connections and line voltages in the others.

Table A.8 Type A Regulators. Capacitive Unbalanced Loading. After Optimization

		Y_gY_g	$\Delta\Delta$	OΔ case a	OΔ case b	OΔ case c
	Taps	[-10 -9 -8]	[-4 -9 -5]	[-7 — -2]	[-5 -5 —]	[— -7 -10]
Node 2	V_1	$7210\angle -0.4°$	$12445\angle 29.6°$	$12447\angle 29.6°$	$12451\angle 29.6°$	$12448\angle 29.6°$
	V_2	$7178\angle -120.4°$	$12487\angle -90.6°$	$12494\angle -90.6°$	$12494\angle -90.6°$	$12492\angle -90.6°$
	V_3	$7180\angle 119.1°$	$12443\angle 149.3°$	$12435\angle 149.3°$	$12440\angle 149.3°$	$12439\angle 149.3°$
Node 3	V_1	$6879\angle -3.1°$	$11923\angle 23.5°$	$11903\angle 29.6°$	$11875\angle 27.7°$	$11913\angle 27.4°$
	V_2	$6885\angle -124.2°$	$11891\angle -96.2°$	$12476\angle -91.8°$	$11890\angle -90.7°$	$11886\angle -92.6°$
	V_3	$6872\angle 114.3°$	$11962\angle 143.8°$	$11948\angle 146.5°$	$12171\angle 148.5°$	$11898\angle 147.6°$
Node 4	V_1	$6896\angle -3.6°$	$11901\angle 22.9°$	$11877\angle 29.0°$	$11856\angle 27.1°$	$11891\angle 26.8°$
	V_2	$6863\angle -124.8°$	$11927\angle -97.0°$	$12511\angle -92.6°$	$11924\angle -91.5°$	$11923\angle -93.4°$
	V_3	$6860\angle 113.1°$	$11929\angle 142.8°$	$11920\angle 145.5°$	$12138\angle 147.5°$	$11864\angle 146.6°$
Line 12	I_a	$203.9\angle 28.2°$	$259.6\angle 9.1°$	$263.3\angle 9.3°$	$262.7\angle 12.2°$	$262.1\angle 11.0°$
	I_b	$275.0\angle -99.0°$	$246.2\angle -92.6°$	$245.8\angle -89.7°$	$253.0\angle -89.2°$	$246.3\angle -90.4°$
	I_c	$346.2\angle 131.3°$	$319.8\angle 140.1°$	$330.8\angle 142.1°$	$326.6\angle 142.8°$	$322.3\angle 142.5°$
Line 34	I_a	$217.5\angle 28.2°$	$273.3\angle 7.3°$	$268.0\angle 11.1°$	$271.1\angle 12.2°$	$274.1\angle 11.0°$
	I_b	$291.4\angle -99.0°$	$262.2\angle -94.1°$	$257.1\angle -89.7°$	$261.2\angle -89.2°$	$262.8\angle -90.4°$
	I_c	$364.4\angle 131.3°$	$339.3\angle 138.0°$	$335.0\angle 142.1°$	$337.2\angle 142.8°$	$340.2\angle 141.8°$

Where V_1, V_2 and V_3 are phase-to-neutral voltages in wye connections and line voltages in the others.

Table A.9 Type B Regulators. Inductive Balanced Loading. Before Optimization

		Y_gY_g	$\Delta\Delta$	OΔ case a	OΔ case b	OΔ case c
	Taps	[0 0 0]	[0 0 0]	[0 — 0]	[0 0 —]	[— 0 0]
Node 2	V_1	$7125\angle -0.3°$	$12360\angle 29.7°$	$12364\angle 29.7°$	$12365\angle 29.7°$	$12362\angle 29.7°$
	V_2	$7145\angle -120.3°$	$12370\angle -90.4°$	$12375\angle -90.4°$	$12376\angle -90.4°$	$12373\angle -90.4°$
	V_3	$7136\angle 119.6°$	$12346\angle 149.6°$	$12351\angle 149.6°$	$12353\angle 149.6°$	$12349\angle 149.6°$
Node 3	V_1	$6842\angle -3.4°$	$11870\angle 26.7°$	$12364\angle 29.7°$	$11951\angle 28.8°$	$11891\angle 26.7°$
	V_2	$6863\angle -123.4°$	$11882\angle -93.4°$	$12125\angle -93.0°$	$12194\angle -89.8°$	$11950\angle -91.2°$
	V_3	$6854\angle 116.6°$	$11857\angle 146.6°$	$11749\angle 149.4°$	$12330\angle 148.6°$	$12296\angle 147.5°$
Node 4	V_1	$6752\angle -3.8°$	$11737\angle 26.3°$	$12231\angle 29.3°$	$11821\angle 28.4°$	$11762\angle 26.3°$
	V_2	$6798\angle -123.9°$	$11764\angle -94.0°$	$12012\angle -93.5°$	$12077\angle -90.3°$	$11832\angle -91.8°$
	V_3	$6778\angle 116.0°$	$11709\angle 146.0°$	$11601\angle 148.9°$	$12187\angle 148.0°$	$12150\angle 147.0°$
Line 12	I_a	$296.2\angle -29.7°$	$295.2\angle -29.7°$	$290.3\angle -27.6°$	$288.1\angle -27.1°$	$290.9\angle -28.7°$
	I_b	$294.2\angle -149.7°$	$295.2\angle -149.7°$	$289.8\angle -147.7°$	$288.0\angle -147.1°$	$290.7\angle -148.7°$
	I_c	$295.1\angle 90.2°$	$295.2\angle 90.3°$	$290.0\angle 92.4°$	$288.0\angle 93.0°$	$291.0\angle 91.3°$
Line 34	I_a	$296.2\angle -29.7°$	$295.2\angle -29.7°$	$290.3\angle -27.6°$	$288.1\angle -27.1°$	$291.0\angle -28.7°$
	I_b	$294.2\angle -149.7°$	$295.2\angle -149.7°$	$290.0\angle -147.7°$	$288.0\angle -147.1°$	$290.7\angle -148.7°$
	I_c	$295.1\angle 90.2°$	$295.2\angle 90.3°$	$290.0\angle 92.4°$	$288.0\angle 93.0°$	$290.8\angle 91.3°$

Where V_1, V_2 and V_3 are phase-to-neutral voltages in wye connections and line voltages in the others.

Table A.10 Type B Regulators. Inductive Balanced Loading. After Optimization

		Y_gY_g	$\Delta\Delta$	OΔ case a	OΔ case b	OΔ case c
	Taps	[2 1 2]	[2 1 2]	[-5 — 4]	[1 -3 —]	[— 1 2]
Node 2	V_1	$7125\angle -0.3°$	$12359\angle 29.7°$	$12364\angle 29.7°$	$12366\angle 29.7°$	$12365\angle 29.7°$
	V_2	$7145\angle -120.3°$	$12371\angle -90.4°$	$12375\angle -90.4°$	$12376\angle -90.4°$	$12374\angle -90.4°$
	V_3	$7136\angle 119.6°$	$12346\angle 149.6°$	$12358\angle 149.6°$	$12351\angle 149.6°$	$12352\angle 149.6°$
Node 3	V_1	$6929\angle -3.4°$	$12056\angle 27.0°$	$11989\angle 29.7°$	$12029\angle 28.9°$	$12018\angle 26.4°$
	V_2	$6907\angle -123.4°$	$12035\angle -92.8°$	$12078\angle -90.2°$	$11968\angle -89.8°$	$12034\angle -91.2°$
	V_3	$6941\angle 116.6°$	$12084\angle 147.2°$	$12060\angle 149.4°$	$12252\angle 149.8°$	$12454\angle 147.6°$
Node 4	V_1	$6840\angle -3.8°$	$11925\angle 26.6°$	$11858\angle 29.3°$	$11899\angle 28.4°$	$11890\angle 26.0°$
	V_2	$6841\angle -123.9°$	$11919\angle -93.3°$	$11962\angle -90.7°$	$11850\angle -90.3°$	$11916\angle -91.7°$
	V_3	$6867\angle 116.0°$	$11937\angle 146.7°$	$11914\angle 148.8°$	$12106\angle 149.2°$	$12309\angle 147.1°$
Line 12	I_a	$296.1\angle -29.7°$	$296.0\angle -29.8°$	$292.1\angle -23.9°$	$288.1\angle -26.8°$	$284.3\angle -28.7°$
	I_b	$294.2\angle -149.7°$	$294.1\angle -149.8°$	$300.0\angle -146.7°$	$291.7\angle -145.5°$	$285.8\angle -148.7°$
	I_c	$295.0\angle 90.2°$	$295.0\angle 90.5°$	$283.6\angle 93.3°$	$295.3\angle 93.3°$	$285.2\angle 91.0°$
Line 34	I_a	$292.4\angle -29.7°$	$290.4\angle -29.2°$	$290.8\angle -26.7°$	$289.9\angle -26.8°$	$287.9\angle -28.8°$
	I_b	$292.4\angle -149.7°$	$290.4\angle -149.2°$	$290.8\angle -146.7°$	$289.8\angle -146.7°$	$287.6\angle -148.7°$
	I_c	$291.3\angle 90.2°$	$290.4\angle 90.8°$	$290.8\angle 93.3°$	$289.9\angle 93.3°$	$287.8\angle 91.3°$

Where V_1, V_2 and V_3 are phase-to-neutral voltages in wye connections and line voltages in the others.

Table A.11 Type B Regulators. Capacitive Balanced Loading. Before Optimization

		Y_gY_g	$\Delta\Delta$	OΔ case a	OΔ case b	OΔ case c
	Taps	[0 0 0]	[0 0 0]	[0 — 0]	[0 0 —]	[— 0 0]
Node 2	V_1	$7184\angle -0.6°$	$12451\angle 29.5°$	$12454\angle 29.5°$	$12455\angle 29.5°$	$12453\angle 29.5°$
	V_2	$7199\angle -120.5°$	$12473\angle -90.6°$	$12477\angle -90.6°$	$12478\angle -90.6°$	$12475\angle -90.6°$
	V_3	$7198\angle 119.4°$	$12457\angle 149.4°$	$12461\angle 149.4°$	$12463\angle 149.4°$	$12460\angle 149.4°$
Node 3	V_1	$7289\angle -3.9°$	$12631\angle 26.2°$	$12454\angle 29.5°$	$12346\angle 27.5°$	$12648\angle 26.2°$
	V_2	$7304\angle -123.8°$	$12654\angle -93.9°$	$12733\angle -92.9°$	$12265\angle -90.8°$	$12358\angle -92.5°$
	V_3	$7303\angle 116.1°$	$12639\angle 146.1°$	$12138\angle 147.1°$	$12619\angle 148.6°$	$12762\angle 148.0°$
Node 4	V_1	$7277\angle -4.7°$	$12617\angle 25.5°$	$12436\angle 28.8°$	$12334\angle 26.8°$	$12637\angle 25.5°$
	V_2	$7309\angle -124.5°$	$12667\angle -94.6°$	$12749\angle -93.6°$	$12277\angle -91.5°$	$12371\angle -93.2°$
	V_3	$7308\angle 115.4°$	$12636\angle 145.3°$	$12136\angle 146.3°$	$12614\angle 147.8°$	$12756\angle 147.2°$
Line 12	I_a	$274.9\angle -21.1°$	$274.1\angle -21.2°$	$278.4\angle 22.9°$	$279.2\angle 23.5°$	$275.1\angle 22.3°$
	I_b	$273.7\angle -98.6°$	$274.1\angle -98.8°$	$278.4\angle -97.0°$	$279.1\angle -96.5°$	$275.2\angle -97.7°$
	I_c	$273.7\angle 141.2°$	$274.1\angle 141.2°$	$278.7\angle 143.0°$	$279.3\angle 143.6°$	$275.3\angle 142.3°$
Line 34	I_a	$274.8\angle 21.1°$	$274.1\angle 21.4°$	$278.4\angle 22.9°$	$279.2\angle 23.5°$	$275.1\angle 22.3°$
	I_b	$273.6\angle -98.6°$	$274.1\angle -98.8°$	$278.4\angle -97.0°$	$279.1\angle -96.5°$	$275.2\angle -97.7°$
	I_c	$273.7\angle 141.2°$	$274.1\angle 141.2°$	$278.7\angle 143.0°$	$279.3\angle 143.5°$	$275.3\angle 142.3°$

Where V_1, V_2 and V_3 are phase-to-neutral voltages in wye connections and line voltages in the others.

Table A.12 Type B Regulators. Capacitive Balanced Loading. After Optimization

		Y_gY_g	$\Delta\Delta$	OΔ case a	OΔ case b	OΔ case c
	Taps	[-10 -10 -10]	[-6 -6 -6]	[-7 — -3]	[-6 -5 —]	[— -6 -12]
Node 2	V_1	$7184\angle -0.6°$	$12450\angle 29.5°$	$12455\angle 29.4°$	$12453\angle 29.4°$	$12450\angle 29.4°$
	V_2	$7199\angle -120.5°$	$12472\angle -90.6°$	$12476\angle -90.6°$	$12477\angle -90.6°$	$12479\angle -90.6°$
	V_3	$7198\angle 119.4°$	$12457\angle 149.4°$	$12463\angle 149.3°$	$12462\angle 149.3°$	$12463\angle 149.3°$
Node 3	V_1	$6859\angle -3.9°$	$11951\angle 24.4°$	$11933\angle 29.4°$	$11888\angle 27.3°$	$11985\angle 27.5°$
	V_2	$6874\angle -123.8°$	$11973\angle -95.6°$	$12358\angle -92.0°$	$11877\angle -90.9°$	$11908\angle -92.7°$
	V_3	$6872\angle 116.1°$	$11960\angle 144.3°$	$11897\angle 146.9°$	$12209\angle 148.3°$	$11914\angle 147.7°$
Node 4	V_1	$6846\angle -4.8°$	$11936\angle 23.6°$	$11915\angle 28.7°$	$11876\angle 26.6°$	$11970\angle 26.7°$
	V_2	$6879\angle -124.6°$	$11987\angle -96.4°$	$12372\angle -92.7°$	$11889\angle -91.6°$	$11923\angle -93.5°$
	V_3	$6877\angle 115.3°$	$11956\angle 143.4°$	$11897\angle 146.1°$	$12204\angle 147.4°$	$11909\angle 146.8°$
Line 12	I_a	$274.9\angle 21.0°$	$274.1\angle 21.2°$	$296.1\angle 24.4°$	$299.8\angle 23.3°$	$312.0\angle 22.5°$
	I_b	$273.7\angle -98.7°$	$274.1\angle -98.8°$	$299.9\angle -97.0°$	$298.8\angle -97.0°$	$301.2\angle -97.5°$
	I_c	$273.7\angle 141.1°$	$274.1\angle 141.2°$	$292.7\angle 143.2°$	$298.0\angle 143.3°$	$306.7\angle 144.3°$
Line 34	I_a	$292.1\angle 21.1°$	$289.6\angle 19.4°$	$287.1\angle 23.2°$	$289.0\angle 23.3°$	$290.3\angle 22.5°$
	I_b	$290.8\angle -98.7°$	$289.6\angle -100.6°$	$287.3\angle -97.0°$	$288.9\angle -96.7°$	$290.3\angle -97.5°$
	I_c	$290.8\angle 141.1°$	$289.6\angle 139.4°$	$287.4\angle 143.2°$	$289.0\angle 143.3°$	$290.3\angle 142.5°$

Where V_1, V_2 and V_3 are phase-to-neutral voltages in wye connections and line voltages in the others.

Table A.13 Type B Regulators. Inductive Unbalanced Loading. Before Optimization

		Y_gY_g	$\Delta\Delta$	OΔ case a	OΔ case b	OΔ case c
	Taps	[0 0 0]	[0 0 0]	[0 — 0]	[0 0 —]	[— 0 0]
Node 2	V_1	$7161\angle -0.1°$	$12361\angle 29.8°$	$12364\angle 29.8°$	$12366\angle 29.8°$	$12364\angle 29.8°$
	V_2	$7119\angle -120.3°$	$12391\angle -90.5°$	$12396\angle -90.5°$	$12397\angle -90.5°$	$12394\angle -90.5°$
	V_3	$7125\angle 119.3°$	$12332\angle 149.5°$	$12338\angle 149.5°$	$12340\angle 149.5°$	$12337\angle 149.5°$
Node 3	V_1	$6929\angle -2.2°$	$11846\angle 27.3°$	$11364\angle 29.8°$	$11907\angle 29.0°$	$11873\angle 27.2°$
	V_2	$6836\angle -123.3°$	$12040\angle -93.6°$	$12247\angle -93.2°$	$12217\angle -89.7°$	$12042\angle -91.2°$
	V_3	$6826\angle 115.1°$	$11793\angle 146.0°$	$11759\angle 148.8°$	$12294\angle 148.4°$	$12236\angle 147.3°$
Node 4	V_1	$6881\angle -2.3°$	$11713\angle 26.9°$	$12232\angle 29.5°$	$11779\angle 28.7°$	$11744\angle 26.9°$
	V_2	$6739\angle -123.7°$	$11949\angle -94.2°$	$12161\angle -93.8°$	$12125\angle -90.3°$	$11949\angle -91.8°$
	V_3	$6744\angle 114.1°$	$11630\angle 144.3°$	$11597\angle 148.2°$	$12135\angle 147.8°$	$12076\angle 146.7°$
Line 12	I_a	$218.0\angle -34.1°$	$315.4\angle -35.3°$	$311.6\angle -33.1°$	$307.0\angle -32.6°$	$309.0\angle -34.0°$
	I_b	$296.8\angle -149.5°$	$250.3\angle -147.6°$	$246.1\angle -145.9°$	$244.7\angle -144.7°$	$246.7\angle -146.2°$
	I_c	$370.7\angle 95.9°$	$319.6\angle 98.3°$	$313.5\angle 100.5°$	$312.4\angle 100.8°$	$314.4\angle 99.4°$
Line 34	I_a	$218.0\angle -34.1°$	$315.4\angle -35.3°$	$311.6\angle -33.1°$	$307.0\angle -32.6°$	$309.0\angle -34.0°$
	I_b	$296.8\angle -149.5°$	$250.3\angle -147.6°$	$246.1\angle -145.9°$	$244.7\angle -144.7°$	$246.7\angle -146.2°$
	I_c	$370.7\angle 95.9°$	$319.5\angle 98.3°$	$313.5\angle 100.5°$	$312.4\angle 100.8°$	$314.4\angle 99.4°$

Where V_1, V_2 and V_3 are phase-to-neutral voltages in wye connections and line voltages in the others.

Table A.14 Type B Regulators. Inductive Unbalanced Loading. After Optimization

		Y_gY_g	$\Delta\Delta$	OΔ case a	OΔ case b	OΔ case c
	Taps	[0 3 3]	[4 -2 2]	[-5 — 4]	[1 -3 —]	[— 2 2]
Node 2	V_1	$7161\angle -0.1°$	$12359\angle 29.8°$	$12365\angle 29.8°$	$12368\angle 29.8°$	$12367\angle 29.8°$
	V_2	$7112\angle -120.3°$	$12393\angle -90.4°$	$12396\angle -90.5°$	$12397\angle -90.5°$	$12396\angle -90.4°$
	V_3	$7125\angle 119.3°$	$12333\angle 149.5°$	$12345\angle 149.5°$	$12339\angle 149.5°$	$12340\angle 149.6°$
Node 3	V_1	$6929\angle -2.2°$	$12056\angle 26.6°$	$11991\angle 29.7°$	$11985\angle 29.0°$	$12039\angle 27.3°$
	V_2	$6967\angle -123.3°$	$11976\angle -92.9°$	$12199\angle -90.4°$	$11990\angle -89.7°$	
	V_3	$6957\angle 115.1°$	$12102\angle 147.2°$	$12072\angle 148.8°$	$12216\angle 149.6°$	$12398\angle 147.4°$
Node 4	V_1	$6880\angle -2.3°$	$11926\angle 26.3°$	$11860\angle 29.4°$	$11857\angle 28.7°$	$11912\angle 27.0°$
	V_2	$6873\angle -123.7°$	$11885\angle -93.5°$	$12109\angle -91.0°$	$11899\angle -90.3°$	$12115\angle -91.8°$
	V_3	$6876\angle 114.1°$	$11940\angle 146.6°$	$11912\angle 148.2°$	$12055\angle 149.0°$	$12239\angle 146.8°$
Line 12	I_a	$218.0\angle -34.1°$	$320.9\angle -35.2°$	$307.3\angle -30.0°$	$307.0\angle -32.0°$	$301.0\angle -33.9°$
	I_b	$296.6\angle -149.5°$	$247.5\angle -148.7°$	$253.8\angle -144.7°$	$248.6\angle -142.7°$	$240.3\angle -146.1°$
	I_c	$370.5\angle 95.9°$	$317.2\angle 99.2°$	$306.2\angle 101.1°$	$319.8\angle 101.3°$	$306.3\angle 99.4°$
Line 34	I_a	$218.0\angle -34.1°$	$310.1\angle -34.6°$	$309.5\angle -32.4°$	$308.9\angle -32.0°$	$304.8\angle -33.9°$
	I_b	$291.0\angle -149.5°$	$247.5\angle -147.0°$	$246.1\angle -144.7°$	$246.8\angle -144.3°$	$243.4\angle -146.1°$
	I_c	$363.6\angle 95.9°$	$314.4\angle 98.7°$	$314.0\angle 101.1°$	$313.9\angle 101.3°$	$310.1\angle 99.4°$

Where V_1, V_2 and V_3 are phase-to-neutral voltages in wye connections and line voltages in the others.

Table A.15 Type B Regulators. Capacitive Unbalanced Loading. Before Optimization

		Y_gY_g	$\Delta\Delta$	OΔ case a	OΔ case b	OΔ case c
	Taps	[0 0 0]	[0 0 0]	[0 — 0]	[0 0 —]	[— 0 0]
Node 2	V_1	$7212\angle -0.4°$	$12447\angle 29.6°$	$12448\angle 29.6°$	$12451\angle 29.6°$	$12449\angle 29.6°$
	V_2	$7179\angle -120.4°$	$12488\angle -90.6°$	$12492\angle -90.6°$	$12494\angle -90.6°$	$12491\angle -90.6°$
	V_3	$7181\angle 119.1°$	$12434\angle 149.3°$	$12437\angle 149.3°$	$12441\angle 149.3°$	$12438\angle 149.3°$
Node 3	V_1	$7324\angle -2.8°$	$12556\angle 26.8°$	$12448\angle 29.6°$	$12271\angle 27.8°$	$12577\angle 26.8°$
	V_2	$7285\angle -124.0°$	$12775\angle -94.0°$	$12825\angle -93.2°$	$12288\angle -90.7°$	$12434\angle -92.4°$
	V_3	$7233\angle 114.8°$	$12509\angle 145.5°$	$12117\angle 146.6°$	$12556\angle 148.5°$	$12662\angle 147.7°$
Node 4	V_1	$7340\angle -3.2°$	$12534\angle 26.2°$	$12422\angle 29.0°$	$12252\angle 27.2°$	$12558\angle 26.2°$
	V_2	$7264\angle -124.3°$	$12810\angle -94.8°$	$12862\angle -94.0°$	$12320\angle -91.5°$	$12468\angle -93.2°$
	V_3	$7222\angle 113.7°$	$12479\angle 144.6°$	$12087\angle 145.7°$	$12525\angle 147.6°$	$12630\angle 146.9°$
Line 12	I_a	$204.4\angle 28.6°$	$258.3\angle 9.4°$	$262.1\angle 10.6°$	$262.6\angle 12.3°$	$259.5\angle 11.2°$
	I_b	$275.3\angle -98.5°$	$247.3\angle -91.7°$	$249.6\angle -90.2°$	$252.9\angle -89.1°$	$249.3\angle -90.3°$
	I_c	$346.1\angle 131.9°$	$321.3\angle 140.4°$	$326.5\angle 141.9°$	$326.59\angle 142.9°$	$322.0\angle 141.8°$
Line 34	I_a	$204.4\angle 28.6°$	$258.3\angle 9.4°$	$262.1\angle 10.6°$	$262.6\angle 12.3°$	$259.5\angle 11.2°$
	I_b	$275.3\angle -98.5°$	$247.3\angle -91.7°$	$249.6\angle -90.2°$	$252.9\angle -89.1°$	$249.3\angle -90.3°$
	I_c	$346.1\angle 131.9°$	$321.3\angle 140.4°$	$326.5\angle 141.9°$	$326.5\angle 142.9°$	$322.0\angle 141.8°$

Where V_1, V_2 and V_3 are phase-to-neutral voltages in wye connections and line voltages in the others.

Table A.16 Type B Regulators. Capacitive Unbalanced Loading. After Optimization

		Y_gY_g	$\Delta\Delta$	OΔ case a	OΔ case b	OΔ case c
	Taps	[0 3 3]	[4 -2 2]	[-5 — 4]	[1 -3 —]	[— 2 2]
Node 2	V_1	$7210\angle -0.4°$	$12446\angle 29.6°$	$12450\angle 29.5°$	$12450\angle 29.5°$	$12446\angle 29.5°$
	V_2	$7179\angle -120.4°$	$12487\angle -90.6°$	$12493\angle -90.7°$	$12495\angle -90.7°$	$12495\angle -90.7°$
	V_3	$7181\angle 119.1°$	$12435\angle 149.3°$	$12437\angle 149.3°$	$12438\angle 149.3°$	$12435\angle 149.2°$
Node 3	V_1	$6893\angle -2.8°$	$11910\angle 24.1°$	$11928\angle 29.5°$	$11886\angle 27.7°$	$11945\angle 27.3°$
	V_2	$6897\angle -123.8°$	$11873\angle -95.8°$	$12451\angle -92.2°$	$11904\angle -90.7°$	$11912\angle -92.64°$
	V_3	$6887\angle 114.8°$	$11914\angle 144.3°$	$11887\angle 146.4°$	$12181\angle 148.4°$	$11939\angle 147.5°$
Node 4	V_1	$6910\angle -3.3°$	$11889\angle 23.5°$	$11902\angle 28.9°$	$11867\angle 27.1°$	$11924\angle 26.7°$
	V_2	$6875\angle -124.4°$	$11909\angle -96.6°$	$12487\angle -93.0°$	$11937\angle -91.6°$	$11948\angle -93.5°$
	V_3	$6876\angle 113.5°$	$11881\angle 143.4°$	$11906\angle 146.5°$	$12148\angle 147.5°$	$12239\angle 146.8°$
Line 12	I_a	$204.3\angle 28.5°$	$259.5\angle 9.7°$	$275.3\angle 12.2°$	$279.3\angle 12.2°$	$290.4\angle 10.9°$
	I_b	$275.4\angle -98.6°$	$247.5\angle -92.2°$	$268.8\angle -89.9°$	$269.1\angle -89.2°$	$273.5\angle -90.5°$
	I_c	$346.3\angle 131.7°$	$319.5\angle 140.4°$	$342.3\angle 142.0°$	$347.4\angle 142.8°$	$357.4\angle 142.3°$
Line 34	I_a	$217.1\angle 28.5°$	$274.0\angle 7.8°$	$269.0\angle 10.8°$	$270.9\angle 12.2°$	$273.3\angle 10.9°$
	I_b	$290.9\angle -98.6°$	$262.8\angle -93.6°$	$257.5\angle -89.9°$	$260.9\angle -82.2°$	$262.0\angle -90.5°$
	I_c	$363.6\angle 131.7°$	$340.1\angle 138.6°$	$335.9\angle 142.0°$	$336.8\angle 142.8°$	$339.2\angle 141.7°$

Where V_1, V_2 and V_3 are phase-to-neutral voltages in wye connections and line voltages in the others.

Appendix B

Related Published Works

A number of works have been published through this doctoral work. Here closely related publications are listed.

- Cano, J. M., Mojumdar, M. R. R., & Orcajo, G. A. (2019). Reconciling tap-changing transformer models. *IEEE Transactions on Power Delivery*, 34(6), 2266-2268.
- Cano, J. M., Mojumdar, M. R. R., & Orcajo, G. A. (2020, August). On the consistency of tap-changing transformer models in power system studies. In *2020 IEEE Power & Energy Society General Meeting (PESGM)* (pp. 1-5). IEEE.
- Mojumdar, M. R. R., Cano, J. M., Assadi, M., & Orcajo, G. A. (2020, August). Consensus Phase Shifting Transformer Model. In *2020 IEEE Power & Energy Society General Meeting (PESGM)* (pp. 1-5). IEEE.
- Mojumdar, M. R. R., Cano, J. M., & Orcajo, G. A. (2021). Estimation of impedance ratio parameters for consistent modeling of tap-changing transformers. *IEEE Transactions on Power Systems*, 36(4), 3282-3292.
- Mojumdar, R. R., Arboleya, P., & González-Morán, C. (2015, July). Step-voltage regulator model test system. In *2015 IEEE Power & Energy Society General Meeting* (pp. 1-5). IEEE.
- González-Morán, C., Arboleya, P., Mojumdar, R. R., & Mohamed, B. (2018). 4-Node test feeder with step voltage regulators. *International Journal of Electrical Power & Energy Systems*, 94, 245-255.
- Cano, J. M., Mojumdar, M. R. R., Norniella, J. G., & Orcajo, G. A. (2017). Phase shifting transformer model for direct approach power flow studies. *International Journal of Electrical Power & Energy Systems*, 91, 71-79.
- Cano, J. M., Mojumdar, M. R. R., & Orcajo, G. A. (2021, October). Wide Voltage-Regulation Range Tap-changing Transformer Model for Power System Studies. In

2021 IEEE PES Innovative Smart Grid Technologies Europe (ISGT Europe) (pp. 1-5). IEEE.

Reconciling Tap-Changing Transformer Models

Jose M. Cano, *Member, IEEE*, Md Rejwanur Rashid Mojumdar, and Gonzalo Alonso Orcajo, *Member, IEEE*

***Abstract*—The model of the tap changing transformer used in classic power system studies, including load flow analysis or state estimation, is still somehow controversial. Two alternative formulations can be found in the literature, which have been adopted by the most important software packages. This work demonstrates that those formulations lead to similar results near the principal tap but to important discrepancies at extreme tap positions, with different impact depending on the power factor of the power flowing through the transformer. Moreover, a general model that fully explains those differences is proposed. The new model allows to adopt a third alternative that, without requiring further data than those used by traditional formulations, leads to highly improved results.**

***Index Terms*—Power transformers, tap changers, transformer models.**

I. Introduction

THE limited amount of information generally available about transformers, and specifically about tap-changing transformers, leads to the fact that a quite simplified model of these devices is used in such usual tasks as load flow analysis or state estimation. The data is obtained from the nameplate of the device and comprises the rated power and voltage values, short-circuit impedance and tap positions. Only transformers with a tapping range exceeding $\pm 5\%$ are obliged by standards to provide further information about the short-circuit impedance (at least, values for the extreme tappings are required in that case) [1].

Two different tap-changing transformer models can be found today in both the literature and practical software implementations [2]–[4]. However, these two models yield different results, which can easily mislead the user in certain tasks, as during the validation of engineering or research results with an external tool. While these discrepancies can be considered merely trivial at the principal tap, this work demonstrates that the inconsistency can lead to huge differences at extreme tap positions. This fact was previously observed by other authors [5] but, they chose one of the alternatives and focused their efforts on the manipulation of the other model to reach the same results. On the contrary, this work explains the causes of those discrepancies and proposes a reconciled solution.

Manuscript received November 13, 2018; revised February 19, 2019, May 3, 2019, and July 19, 2019; accepted August 29, 2019. Date of publication September 9, 2019; date of current version November 20, 2019. This work was supported by the Spanish Government Innovation Development and Research Office (MEC) under research Grant DPI2017-89186-R. Paper no. PESL-00253-2018. *(Corresponding author: Jose M. Cano.)*

J. M. Cano and G. A. Orcajo are with the Department of Electrical Engineering, University of Oviedo, Gijón 30013, Spain (e-mail: jmcano@uniovi.es; gonzalo@uniovi.es).

M. R. R. Mojumdar is with the Department of Energy and Petroleum Engineering, University of Stavanger, Stavanger 4036, Norway (e-mail: md.r.mojumdar@uis.no).

Color versions of one or more of the figures in this letter are available online at http://ieeexplore.ieee.org.

Digital Object Identifier 10.1109/TPWRD.2019.2940422

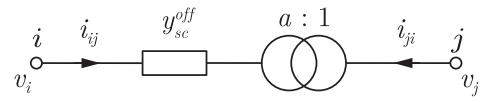

Fig. 1. Model of the tap-changing transformer with short-circuit impedance at the off-nominal turns side.

In Section II, a new model for the tap-changing transformer is proposed, which opens the door to a much more accurate description of the device. Section III uses the new model to clearly explain the reasons for the aforementioned discrepancies. An assessment of the errors caused by traditional models is presented in Section IV. Section V describes a case study to highlight the importance of the new proposal. Finally, the conclusions of this study are drawn in Section VI.

II. Description of the New Model

Power system studies do not normally require the shunt branch of the equivalent model of the transformer to be taken into account. Thus, when dealing with nominal turns ratios, the use of the detailed or simplified model of the transformer makes no difference, as in both cases the device is reduced to a series impedance. However, this is no longer true when the transformer is using an off-nominal turns ratio. As it is demonstrated in this work, the simplified model of the transformer can lead to important errors.

Let us consider a transformer with off-nominal turns ratio $a:1$ as depicted in Fig. 1. Although the following parameters are not normally known by the user, let k be the ratio between the p.u. impedance in the nominal winding, z_2, and tapped winding, z_1, (for the sake of simplicity, the same ratio is considered for resistance and leakage reactance). From the off-nominal side, the series admittance can then be calculated as

$$y_{sc}^{off} = \frac{1}{z_1 + a^2 z_2} = \frac{1+k}{1+ka^2} y_{sc}, \tag{1}$$

y_{sc} being the short-circuit admittance obtained during the short-circuit test at the principal tap (normally shown at the nameplate of the device as an impedance, z_{sc}), or at the current tap position, if further data are available.

The application of Kirchhoff Laws and the well-known relationships that apply to the ideal transformer yields

$$v_i = \frac{i_{ij}}{y_{sc}^{off}} + a v_j, \tag{2}$$

$$i_{ij} = -\frac{i_{ji}}{a}, \tag{3}$$

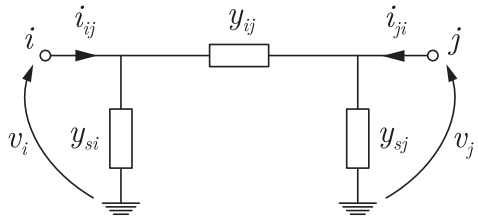

Fig. 2. π equivalent model of the tap-changing transformer.

and thus, the nodal equations of the device can be written as

$$\begin{bmatrix} i_{ij} \\ i_{ji} \end{bmatrix} = \begin{bmatrix} Y_{ii} & Y_{ij} \\ Y_{ji} & Y_{jj} \end{bmatrix} \begin{bmatrix} v_i \\ v_j \end{bmatrix}, \tag{4}$$

where

$$Y_{ii} = \frac{1+k}{1+ka^2} y_{sc}, \tag{5}$$

$$Y_{ij} = Y_{ji} = -\frac{a\,(1+k)}{1+ka^2} y_{sc}, \tag{6}$$

$$Y_{jj} = \frac{a^2\,(1+k)}{1+ka^2} y_{sc}. \tag{7}$$

Hence, the components of the π equivalent of the new model, shown in Fig. 2, can be calculated as

$$y_{ij} = -Y_{ij} = \frac{a\,(1+k)}{1+a^2k} y_{sc}, \tag{8}$$

$$y_{si} = Y_{ii} + Y_{ij} = \frac{1-a+k\,(1-a)}{1+a^2k} y_{sc}, \tag{9}$$

$$y_{sj} = Y_{jj} + Y_{ij} = \frac{a\,(a-1)\,(1+k)}{1+a^2k} y_{sc}. \tag{10}$$

III. Reconciliation of Previous Models

As it is easily proved, the two well-known models, extensively used in the literature and practical implementations, correspond to the particular cases of making the parameter k equal to 0 and ∞ in (1), and thus in (8)–(10). In particular, $k = 0$ corresponds to the option of considering all the short-circuit impedance of the transformer as being provided by the winding at the off-nominal turns side. In this case, the off-nominal admittance of the transformer, y_{sc}^{off}, turns to be the same as y_{sc}, and the well-known parameters of the π equivalent model shown in Fig. 3(a) are obtained. On the other hand, $k = \infty$ corresponds to the option of considering all the short-circuit impedance of the transformer as being provided by the winding at the nominal turns side. In this case, the off-nominal admittance of the transformer, y_{sc}^{off}, turns to be y_{sc}/a^2, and the set of parameters of the π equivalent model shown in Fig. 3(b) is reached. It is important to highlight that the new model opens the door to obtain accurate results if k is provided by the manufacturer. But, even if this is not the case, much more realistic estimates can be obtained if k is set to 1, which is a common engineering practice adopted when the detailed model of the transformer is to be used [6], [7].

Finally, notice that in [5], the authors pointed out the inconsistency of the two alternative models, and concluded that, in order to make them yield the same results the admittance in Fig. 3(a) should be previously affected by $1/a^2$. While this is a pertinent observation, this approach does not solve the fact that all the short-circuit admittance is being assigned to the nominal winding, which is far from being realistic and can lead to important errors.

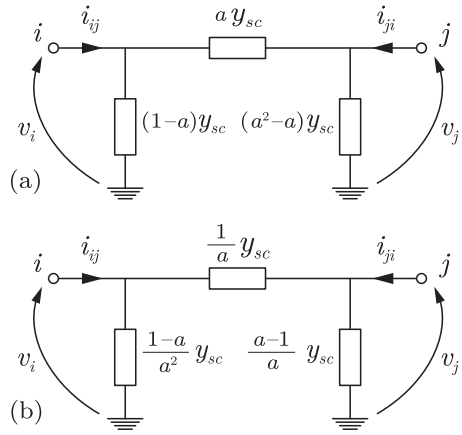

Fig. 3. π equivalent traditional models of tap-changing transformers. (a) $k = 0$, and (b) $k = \infty$.

IV. Error Assessment

For a given value of the off-nominal turns side variables, v_i and i_{ij}, the new model allows the calculation of the nominal turns side voltage v_j. If the result, for a generic value of k, v_j^k, is taken as a reference, and the calculation is repeated for the values used by traditional models, thus obtaining v_j^0 and v_j^∞, an assessment of the mismatch voltage can be obtained from (8), (9) and (10), which represent the error of these popular approaches,

$$\Delta v_j^0 = v_j^0 - v_j^k = \frac{k\left(a^2-1\right)}{a\,(1+k)} \frac{i_{ij}}{y_{sc}}, \tag{11}$$

$$\Delta v_j^\infty = v_j^\infty - v_j^k = \frac{1-a^2}{a\,(1+k)} \frac{i_{ij}}{y_{sc}}. \tag{12}$$

V. Case Study

In order to highlight the important differences that can arise when using the traditional transformer models depicted in Fig. 3 and the benefits of the newly proposed formulation, a case study is presented in this section. Let us consider an 80 MVA, 50 Hz, $220/132$ kV $\pm 10\%$ transformer with a nameplate short-circuit impedance, z_{sc}, of $0.01 + 0.12j$ and a tap changer, located on the highest voltage side, with 21 positions and a tapping step of 1%. If further data about the short-circuit impedance at extreme tap positions were available, as it should be according to [1], a different value of z_{sc} could be calculated by linear interpolation for any tap position. In any case, this straightforward task will not be used in this case study not to obscure the core of the proposal.

Fig. 4 shows the voltage of the transformer at the nominal turns side when fed by a constant voltage of 1 pu at the off-nominal turns side for each tap position available. In each case, the transformer is delivering the rated current at the off-nominal turns side. Two different power factors are considered by selecting the phase angle between v_i and i_{ij}, which is called θ in the following: (a) a unity power factor, $\theta = 0°$, and (b) a pure capacitive case, $\theta = 90°$. The voltage is calculated both for the traditional models ($k = 0$ and $k = \infty$) and for the proposed model, assuming a fair contribution of both windings to the short-circuit impedance, i.e. $k = 1$. Although this assumption is probably not exact (this data is seldom provided by the manufacturer), it is for sure a

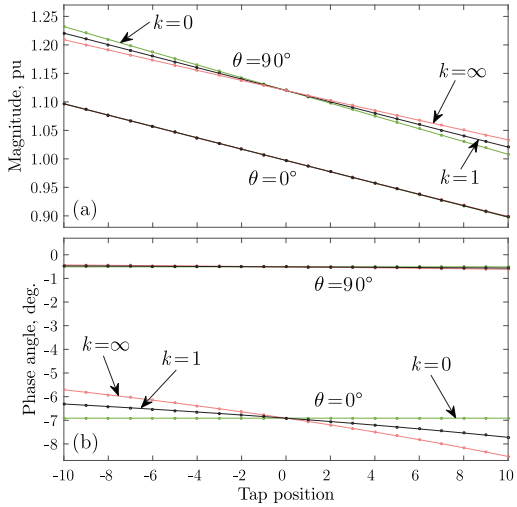

Fig. 4. Nominal-turns side voltage for the different tap positions. Transformer at rated current with two different power factors: Unity ($\theta = 0°$) and pure capacitive ($\theta = 90°$). (a) Voltage magnitude, and (b) voltage phase angle.

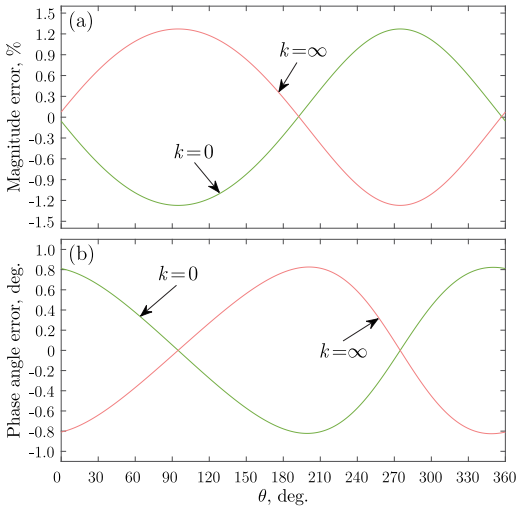

Fig. 5. Maximum deviation in the calculation of the nominal-turns side voltage at rated current. (a) Voltage magnitude, and (b) voltage phase angle.

better estimate in line with accepted engineering practices. In Fig. 4(a) the module of the voltage at the off-nominal turns side is shown. At high power factors, the differences between the alternative transformer models can be ignored. However, important discrepancies arise at poor power factors. On the other hand, Fig. 4(b) shows the phase angle of the voltage at the off-nominal turns side. The differences between the different models result evident now at high power factors. The new model offers a consensus estimate even if k is not accurately known.

The errors arisen from the use of traditional models, calculated by taking the new model as a reference (with $k = 1$), were obtained at rated current for every tap position and power factor (including reverse power flow). In Fig. 5(a) the maximum deviation of the voltage at the nominal turns side, $|v_j^0| - |v_j^1|$ and $|v_j^\infty| - |v_j^1|$, is depicted for each power factor. This graph proves that the error in the calculation of the voltage can rise to near 1.3% in extreme positions of the tap changer when dealing with poor power factors. Notice that the same result can be obtain from (11) and (12). Fig. 5(b) shows the maximum deviation of the phase angle of the voltage at the nominal turns side. Noticeably, this error evolves in the opposite direction, being maximum for high power factors, when it reaches values as high as $0.8°$, and negligible for reactive power flows. In a symmetrical tap changer, as the one considered in this work, the maximum errors are found at the highest position of the tap (and not at the lowest), as can be easily proved from (11) and (12).

VI. Conclusion

The use of the simplified equivalent model of the transformer is universally admitted when conducting power system studies, due to the low impact of the magnetizing branch and the inherent benefit of removing a useless bus from the problem. However, neglecting the fact that the short-circuit impedance is the result of contributions from two different windings can lead to unacceptable discrepancies in the formulation of the tap-changing transformer model. This work proposes a new general model which includes the contribution of each winding to the short-circuit impedance. Although this data is not generally available (and not even easy to derive from traditional tests), the new model allows to consider a fair contribution $(50/50)$ of both windings to this parameter, which is an accepted practice in engineering. The new model can be tuned to match the results from traditional alternatives, which consider the short-circuit impedance as caused by only one of the transformer windings, either the off-nominal or nominal turns side. This fact makes the new model useful to understand the basis of each formulation, providing a clear perspective on the influence of the underlying assumptions. The work demonstrates that the discrepancies caused by traditional models can be unacceptable at extreme tap positions and are greatly influenced by the operating point of the transformer. The inclusion of the proposed model in power system software packages, tuned with the recommended values shown in this work, can significantly improve the consistency of power system studies. Nonetheless, the authors are exploring methods for an accurate evaluation of the contribution of each winding based on state estimation techniques.

References

[1] *Power Transformers—Part 1: General, IEC 60076-1:2011, IEC Std.*, 2011.
[2] J. D. Glover, T. J. Overbye, and M. S. Sarma, *Power System Analysis and Design*, 6th ed. Andover, U.K.: Cengage Learning, Inc., Jul. 2016.
[3] *PowerWorld User's Guide*, PowerWorld Corporation, 2011, [Online]. Available: http://www.powerworld.com
[4] C. Grande-Moran, "Phase-shifting transformer modeling in PSSE," *Siemens Power Technol.*, vol. 1, no. 111, pp. 1–7, Mar. 2012.
[5] L. V. Barboza, H. H. Zürn, and R. Salgado, "Load tap change transformers: A modeling reminder," *IEEE Power Eng. Rev.*, vol. 21, no. 2, pp. 51–52, Feb. 2001.
[6] S. V. Kulkarni and S. A. Khaparde, *Transformer Engineering: Design, Technology and Diagnostics*, 2nd ed. Boca Raton, FL, USA: CRC Press, May 2013.
[7] K. Shaarbafi, "Transformer modelling guide," Alberta Electric System Operator, Calgary, AB, CanadaTech. Rep., Jul. 2014. [Online]. Available: https://www.aeso.ca/assets/linkfiles/4040.002-Rev02-Transformer-Modelling-Guide.pdf

On the Consistency of Tap-Changing Transformer Models in Power System Studies

José M. Cano
Electrical Engineering Dept.
University of Oviedo
Gijón, Spain
jmcano@uniovi.es

Md Rejwanur R. Mojumdar
Dept. of Energy and Petroleum Engineering
University of Stavanger
Stavanger, Norway
md.r.mojumdar@uis.no

Gonzalo A. Orcajo
Electrical Engineering Dept.
University of Oviedo
Gijón, Spain
gonzalo@uniovi.es

***Abstract*—The tap-changing transformer models used in steady-state power system studies have been recognized as somehow controversial for a long period. Indeed, discrepant versions arise depending on slightly different underlying assumptions. As a consequence, two alternative models are traditionally implemented in power system simulation software packages. A new model, recently proposed by the authors, has reconciled those versions, leading the way in removing the ensuing ambiguity. In this work, several case studies are introduced in order to highlight the important inconsistencies which can be drawn from the use of the traditional versions. Furthermore, this contribution presents a framework for the correct configuration of the new model in the usual scenario of imperfect information on transformer construction data. This work demonstrates that the adoption of the new model solves the aforementioned ambiguity, thus being a valuable tool to provide consistent results in power system studies on grids with embedded tap-changing transformers.**

***Index Terms*—power transformers, tap changers, transformer models**

I. Introduction

Tap-changing transformers are a key asset in the regulation of voltage in power systems. Thus, models of these devices are intensively used in the different fields of electric energy systems analysis and operation. Nonetheless, the models of the tap-changing transformer traditionally used in steady-state balanced studies, such as the ones conducted during power flow calculations or voltage stability analyses, have been burdened with a long-standing controversy [1]. Indeed, two alternative tap-changing transformer models can be found in the description of these devices in different books and simulation software packages [2]–[5]. Under specific operating conditions, using one model or the other can lead to results with significant differences, which produces a serious lack of consistency in reporting the outcome of the analysis of electric grids with embedded tap-changing transformers.

In [6], the authors of the present work proposed a consensus model with the aim of solving the aforementioned controversy. In this recent publication, the theoretical background that explains the differences caused by traditional models is presented. Moreover, by introducing an additional parameter, the new model allows to produce consistent results free of any ambiguity. The present contribution tries to highlight the importance of adopting the new model by state-of-the-art software packages. With this aim, the discrepancies between traditional models are theoretically assessed and the benefits of the consensus model are clearly displayed. Furthermore, a couple of case studies, based on a classical IEEE test bus system are introduced, in order to demonstrate that the differences in the outcomes offered by the traditional models cannot be neglected even in normal operating conditions.

The structure of the contribution is as follows. In Section II, the classical and newly proposed tap-changing transformer models are briefly described for the benefit of the reader. A relevant discussion on the set-up of the new model by using the limited data typically available for this type of transformers is provided in Section III, together with an assessment of the discrepancies between the different models. Section IV presents a classical power flow analysis and a voltage stability study conducted in the IEEE 57-bus system [7]. Both cases clearly highlight the importance of using the new model to provide consistency in reporting the results of power system studies.

II. Tap-Changing Transformer Models

A. Traditional Models

The most widely used traditional tap-changing transformer models are derived from two different (and not easy to justify) alternatives: either considering that all the short-circuit impedance of the transformer, z_{sc}, is provided by the winding at the off-nominal side (Type 1) or by the one at the nominal side (Type 2). Both extreme assumptions are shown in Fig. 1 for a transformer with an off-nominal turns ratio $a:1$, where y_{sc} is the short-circuit admittance of the transformer (typically provided by the manufacturer as an impedance and shown in the nameplate of the device). In this figure, the short-circuit admittance has been referred in both cases to the off-nominal side, and thus designated as y_{sc}^{off}.

The well-known relations that apply to ideal transformers, together with Kirchhoff's Laws yield

$$v_i = \frac{i_{ij}}{y_{sc}^{off}} + a v_j, \tag{1}$$

$$i_{ij} = -\frac{i_{ji}}{a}, \tag{2}$$

This work was supported by the Spanish Government Innovation Development and Research Office (MEC) under research Grant DPI2017-89186-R.

978-1-7281-5508-1/20/$31.00 ©2020 IEEE

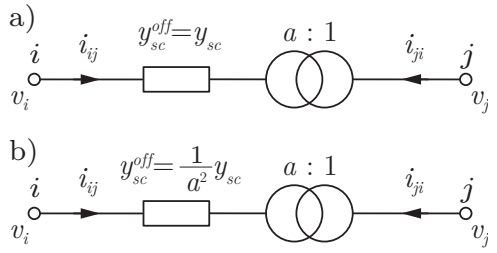

Fig. 1. Alternative assumptions made in traditional tap-changing transformer models. (a) Type 1, and (b) Type 2

and thus, the nodal equations of the device can be written in a compact form as

$$\begin{bmatrix} i_{ij} \\ i_{ji} \end{bmatrix} = \begin{bmatrix} Y_{ii} & Y_{ij} \\ Y_{ji} & Y_{jj} \end{bmatrix} \begin{bmatrix} v_i \\ v_j \end{bmatrix}. \tag{3}$$

The elements of the bus-admittance matrix, Y_{bus}, are shown in Table I for the Type 1 and Type 2 models, according to the value of y_{sc}^{off} used in each case. From those values, the parameters of the π-equivalent circuit of both transformer models can be straightforwardly derived. They have been explicitly shown in Fig. 2.

TABLE I
Y_{bus} MATRIX FOR THE DIFFERENT TAP-CHANGING TRANSFORMER MODELS

$\boldsymbol{Y_{bus}}$	**Type 1**	**Type 2**	**Type 3**	**Type 3** ($k=1$)
Y_{ii}	y_{sc}	$\frac{1}{a^2}y_{sc}$	$\frac{1+k}{1+ka^2}y_{sc}$	$\frac{2}{1+a^2}y_{sc}$
$Y_{ij}=Y_{ji}$	$-ay_{sc}$	$-\frac{1}{a}y_{sc}$	$-\frac{a(1+k)}{1+ka^2}y_{sc}$	$-\frac{2a}{1+a^2}y_{sc}$
Y_{jj}	a^2y_{sc}	y_{sc}	$\frac{a^2(1+k)}{1+ka^2}y_{sc}$	$\frac{2a^2}{1+a^2}y_{sc}$

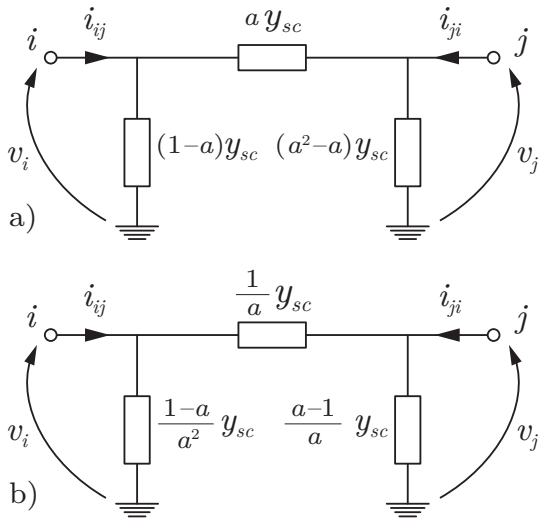

Fig. 2. π-equivalent circuit of traditional tap-changing transformer models. (a) Type 1, and (b) Type 2

B. Consensus Model

A new model, presented in [6], was proposed in order to remove any ambiguity from the results of power system studies with embedded tap-changing transformers. This model, designated in the following as Type 3, includes a new parameter in order to account for the contribution of each of the transformer windings to the short-circuit impedance. This parameter, k, is defined as the ratio between the p.u. impedance of the winding at the nominal turns side, z_j and the p.u. impedance of the tapped winding (i.e. the one at the off-nominal turns side), z_i. Thus, the short-circuit admittance referred to the off-nominal side can be calculated as

$$y_{sc}^{off} = \frac{1}{z_i + a^2 z_j} = \frac{1+k}{1+ka^2}y_{sc}. \tag{4}$$

By applying (1) and (2) to the new value of y_{sc}^{off}, the parameters of the Y_{bus} matrix in (3) can be immediately determined for the Type 3 model. They have been shown in Table I. From those values, the different admittances of the corresponding π-equivalent circuit, as depicted in Fig. 3(a), can be directly obtained as

$$y_{ij} = -Y_{ij} = \frac{a\,(1+k)}{1+a^2k}y_{sc}, \tag{5}$$

$$y_{si} = Y_{ii} + Y_{ij} = \frac{1-a+k\,(1-a)}{1+a^2k}y_{sc}, \tag{6}$$

$$y_{sj} = Y_{jj} + Y_{ij} = \frac{a\,(a-1)\,(1+k)}{1+a^2k}y_{sc}. \tag{7}$$

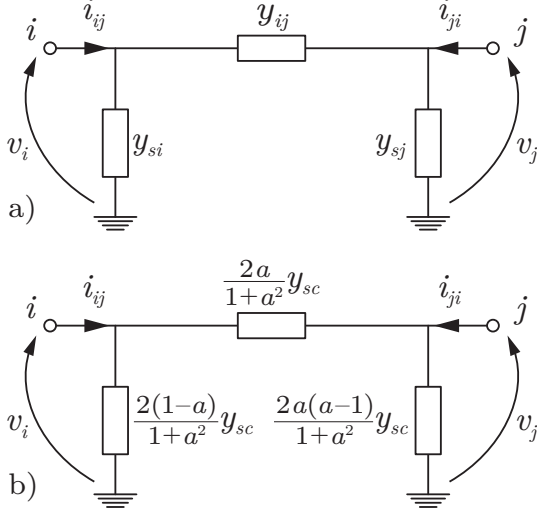

Fig. 3. Consensus model of the tap-changing transformer. (a) General model, and (b) recommended set-up

It is important to notice that the traditional models, Type 1 and Type 2, are just particular cases of the proposed general model, Type 3. Indeed, assigning the values 0 and ∞ to parameter k in (5)–(7) yields to the well-known values already presented in Fig. 2.

III. Set-up of the Consensus Model

The practical use of the new model should take into account that, usually, the data provided to the engineering practitioner in order to model the different components of the power system, and specifically, tap-changing transformers, is quite limited. The particular contribution of each transformer winding to the short-circuit impedance is not a nameplate value and, since this specification is not required by standards [8], it is seldom provided by the manufacturer. Thus, setting up the value of the new parameter, k, turns to be challenging.

As stated in [6], the discrepancy of traditional models with respect to the consensus model, assessed using the differences that arise in the voltage of the nominal winding, v_j, when the off-nominal turns side is fed at a fixed voltage, v_i, and a fixed current, i_{ij}, can be obtained, as a function of k, according to

$$\Delta v_j^0 = v_j^0 - v_j^k = \frac{k\left(a^2-1\right)}{a\left(1+k\right)}\frac{i_{ij}}{y_{sc}}, \tag{8}$$

$$\Delta v_j^\infty = v_j^\infty - v_j^k = \frac{1-a^2}{a\left(1+k\right)}\frac{i_{ij}}{y_{sc}}, \tag{9}$$

where v_j^0, v_j^∞ and v_j^k stand for the values obtained with Type 1, Type 2 and Type 3 models, respectively.

From (8) and (9), it can be concluded that the discrepancies in v_j between the different models grow with the loading of the transformer as well as with the tap position (extreme tap positions, i.e. those further from the central tap, exacerbate the differences). Due to the mainly inductive behavior of transformer short-circuit impedances, the effect of those discrepancies mostly affects the magnitude of voltage when feeding reactive loads (e.g., in that case, Δv_j^0 is close to aligned with v_j^0 and v_j^k). Conversely, resistive loads tend to magnify the differences in voltage phase angle. A detailed analysis of these facts can be found in [6].

Another interesting conclusion that can be drawn from (8) and (9) is that the particular case $k = 1$ is the midpoint between the extreme assumptions implied by traditional models. Certainly, for $k = 1$, it can be followed that $\Delta v_j^0 = -\Delta v_j^\infty$. Thus, using $k = 1$ guarantees the minimization of the maximum error caused by the lack of precise knowledge of the contribution of each transformer winding to the short-circuit impedance. The Y_{bus} elements of this recommended set-up are shown in Table I and the corresponding π-equivalent circuit is depicted in Fig. 3(b). Specifically, using $k = 1$ assures that the error is limited to

$$\Delta v_j^{max} = \pm\frac{a^2-1}{2a}\frac{i_{ij}}{y_{sc}}. \tag{10}$$

The use of $k = 1$ implies the assumption of an equal contribution of both transformer windings (expressed in per unit values) to the short-circuit impedance. In fact, this is a traditional engineering practice used in detailed transformer modeling [9]–[11], which reinforces the recommendation to use this set-up when no further data is available.

Undoubtedly, the use of parameter estimation techniques may allow to improve the quality of the set-up of tap-changing transformer models in real scenarios by obtaining accurate values of k for each specific device from the off-line analysis of field measurements. The authors are currently working in this field. However, it should be highlighted that, regardless of the accuracy of the model, which is dependent on the quality of the estimation of k, the consensus model puts an end to the lack of consistency in communicating the results of power system studies, provided that the set-up of this parameter is included in the data set.

IV. Case Studies

The discrepancies in the results provided by the traditional tap-changing transformer models are not trivial. A set of case studies are provided in this section in order to highlight this fact, and thus, to urge the adoption of the new model by power system software packages. As it is demonstrated in this section, the use of the new model can guarantee the consistency of the results obtained in such common power system studies as power flow or voltage stability analysis.

The IEEE 57-bus system, which is shown in Fig. 4, has been adopted as a test case [7]. It represents a simple approximation of the American Electric power system in the U.S. Midwest as it was in the early 1960s which has been extensively used as a test system by the power community. The IEEE 57-bus system comprises 57 buses, 7 generators, 42 loads and 17 transformers. It is important to note that 15 of these transformers are set out of the principal tap at the operating point defined by the test case. This fact makes the system especially suitable to test the new tap-changing transformer model. Table II shows the parameters and set-up of those transformers as described in the IEEE 57-bus system data files.

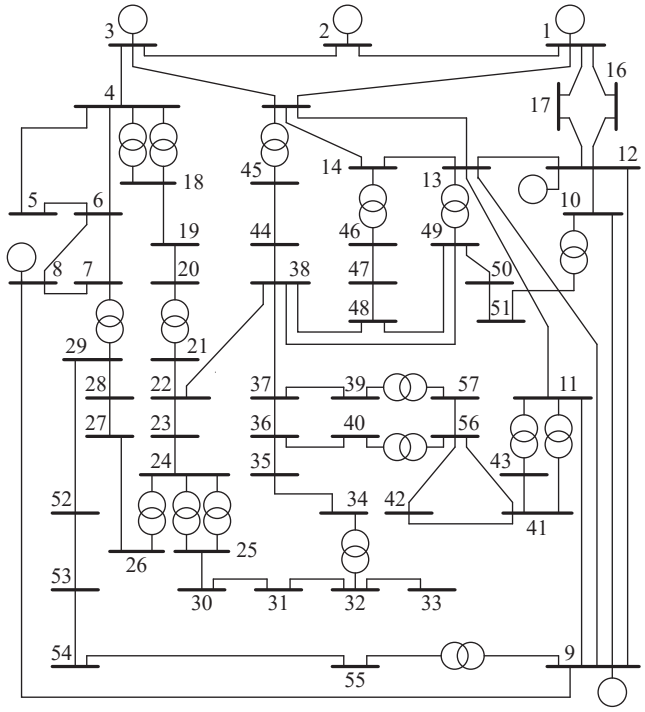

Fig. 4. IEEE 57-bus system.

TABLE II
TRANSFORMERS SET OUT OF THE PRINCIPAL TAP IN THE IEEE 57-BUS SYSTEM

From bus	To bus	R, p.u	X, p.u	Tap, a
4	18	0	0.5550	0.970
4	18	0	0.4300	0.978
21	20	0	0.7767	1.043
24	26	0	0.0473	1.043
7	29	0	0.0648	0.967
34	32	0	0.9530	0.975
11	41	0	0.7490	0.955
11	45	0	0.1042	0.955
14	46	0	0.0735	0.900
10	51	0	0.0712	0.930
13	49	0	0.1910	0.895
11	43	0	0.1530	0.958
40	56	0	1.1950	0.958
39	57	0	1.3550	0.980
9	55	0	0.1205	0.940

A. Power Flow Analysis

The state variables of the IEEE 57-bus system have been calculated by using a Newton-based power flow method for the different tap-changing transformer models under evaluation. MATPOWER [12] was used to conduct this implementation. It is important to note that this open-source electric power system simulation tool assumes one of the traditional tap-changing transformer models commented in the paper. Specifically, MATPOWER considers all the short-circuit impedance of the tap-changing transformer as being provided by the winding at the nominal turns side (i.e. $k = \infty$) [13]. The modification of those functions of the software devoted to the construction of the bus admittance matrix, has allowed the authors to test also the other alternatives (i.e, the traditional model which considers all the short-circuit impedance as provided by the off-nominal turns side, $k = 0$, and the new proposal, in which a balanced contribution is considered, $k = 1$). Those alternative transformer models can be directly implemented in MATPOWER by considering equations (5)–(7). Fig. 5 shows the resulting voltage profile of the IEEE 57-bus system according to the different tap-changing transformer models. The detailed results, for those buses showing the highest inconsistencies, are reported in Table III.

As it is shown in Table III and is also highlighted in Fig. 5, the maximum discrepancy in the calculation of voltage magnitudes between the two traditional models (i.e. $k = \infty$ and $k = 0$) takes place at bus 49. This discrepancy reaches a value of 7.63×10^{-3} p.u. (i.e. 0.763%), which can be considered a significant amount even though the transformers of the IEEE 57-bus system are not set at particularly extreme tap positions. In the same vein, the maximum discrepancy in the calculation of voltage phase angle arises at bus 33 with a value of 0.529 deg. Obviously, those differences in the state variables spread to the post-calculation of other magnitudes with an important impact on active and reactive power flows, currents, etc.

This test clearly reinforces the conclusion of the present contribution. Indeed, it confirms that the use of different tap-changing transformer models, such as the widely adopted

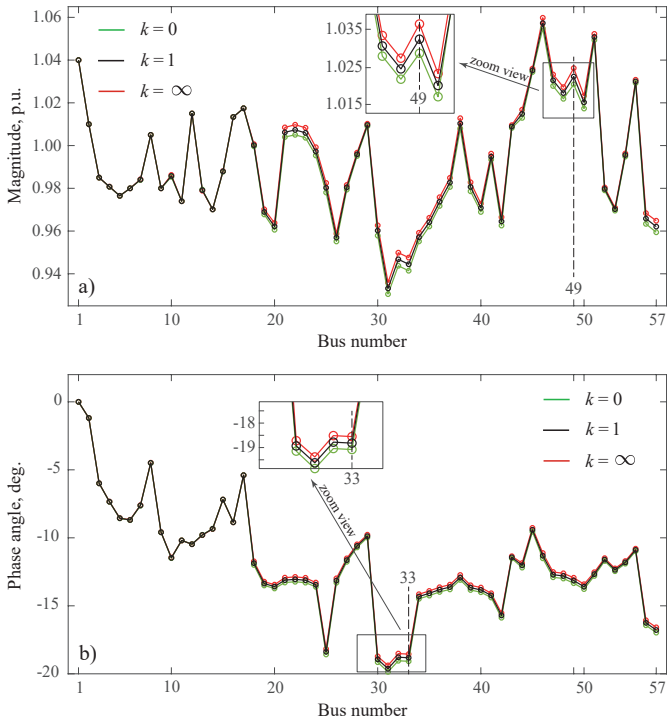

Fig. 5. Voltage profile of the IEEE 57-bus system using the traditional and new tap-changing transformer models. (a) Voltage magnitude and (b) Phase angle.

$k = 0$ (Type 1) and $k = \infty$ (Type 2) versions, leads to different and thus, inconsistent results. Conversely, the adoption of the new model by software packages for power system analysis can solve the problem, just by allowing the user to fix and report the specific value of k utilized in the study. If further information is not available to precisely determine this parameter, selecting it as $k = 1$ provides a sensible estimation that leads to results that lie between the two traditional solutions and, what is more, minimizes the maximum expected error.

B. Voltage Stability Analysis

Taking again the IEEE 57-bus system as a basis, voltage stability has been tested by gradually increasing the active power demand at bus 49. Notice that this bus was selected for the study in view of the results of the power flow analysis shown in subsection IV-A. Indeed, these results demonstrate that the voltage magnitude at bus 49 show the highest discrepancy when calculated using different traditional tap-changing transformer models.

According to [7], the active power demand at bus 49 in the IEEE 57-bus system is 18 MW. This active power was increased in steps of 1 MW and, in each case, the power flow analysis of the system was repeated for the traditional tap-changing transformer models and for the new proposed model with the recommended set-up of $k = 1$. The results, in the form of the power-voltage curve (also known as "nose" curve or P-V curve), are depicted in Fig. 6.

Notice that voltage collapse is reached at quite different values of the active power demand at bus 49. While stability

TABLE III
BUS VOLTAGES SHOWING THE HIGHEST DISCREPANCIES

	Tap-changing transformer model					
	Type 1 ($k = 0$)		**Type 2** ($k = \infty$)		**Type 3** ($k = 1$)	
Bus	**Magnitude, p.u.**	**Phase angle, deg.**	**Magnitude, p.u.**	**Phase angle, deg.**	**Magnitude, p.u.**	**Phase angle, deg.**
33	0.941	−19.081	0.948	−18.552	0.944	−18.819
49	1.029	−13.336	1.036	−12.936	1.032	−13.141

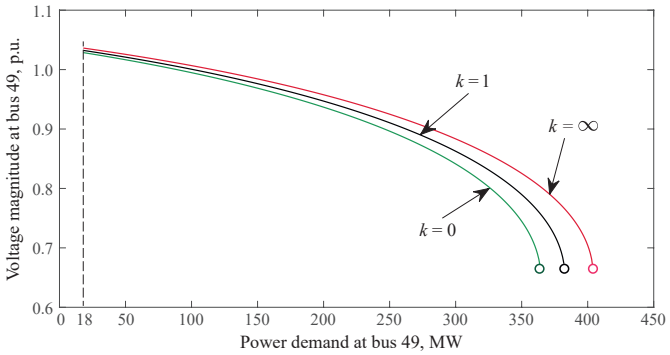

Fig. 6. Power-Voltage curves at bus 49 for the traditional tap-changing transformer models ($k = \infty$ and $k = 0$) and for the new proposed model ($k = 1$).

is lost at 364 MW in the case of $k = 0$, collapse is not reached until 404 MW if the model with $k = \infty$ is considered. The first case may be a too conservative approach while the second is certainly underestimating the voltage drop. On the contrary, the use of the new model with $k = 1$ estimates that the voltage collapse would take place at 382 MW which is certainly a sensible compromise.

Once more, this voltage stability analysis comes to emphasize the important differences that may arise from the use of the different versions of traditional tap-changing transformers. Security constraints may be compromised by using simplified assumptions, such as the ones implied in traditional models. What is more, even if $k = 1$ is a sensible estimation in a context of scarce data, a precise knowledge of this parameter could add certainty to the results obtained in this type of power system studies.

V. CONCLUSION

For decades, the different software simulation packages devoted to conduct power system studies have included one of two alternative traditional models of the tap-changing transformer. Those different models arise from the assumption of considering all the short-circuit impedance as provided by the nominal or off-nominal turns side of the transformer. Though the differences in the results offered by those models may be small at close-to-central tap positions, they can be remarkably large at extreme tap positions. Thus, the consistency in reporting results from power system studies can be compromised. The present contribution demonstrates that those discrepancies can be significant even in the case of a well-known standard grid, which is illustrated by a power flow analysis and a stability analysis. The use of a recently proposed consensus model is introduced as an ideal solution to the aforementioned problem. The new model is free from ambiguity and, whereas an additional parameter has to be provided, a sensible selection of its value can be done if accurate manufacturing data is not available.

REFERENCES

[1] L. V. Barboza, H. H. Zürn, and R. Salgado, "Load tap change transformers: A modeling reminder," *IEEE Power Engineering Review*, vol. 21, no. 2, pp. 51–52, Feb. 2001.

[2] A. Monticelli, *State Estimation in Electric Power Systems. A Generalized Approach*, 1st ed. Norwell, MA: Kluwer Academic Publishers, 1999.

[3] A. Abur and A. Gómez-Expósito, *Power System State Estimation. Theory and Implementation*, 1st ed. New York, NY: Marcel Dekker, Inc., 2004.

[4] *PowerWorld User's Guide*, PowerWorld Corporation, 2011, [Online]. Available: http://www.powerworld.com.

[5] C. Grande-Moran, "Phase-shifting transformer modeling in PSS®E," *Siemens Power Technology*, vol. 1, no. 111, pp. 1–7, Mar. 2012.

[6] J. M. Cano, M. R. R. Mojumdar, and G. A. Orcajo, "Reconciling tap-changing transformer models," *IEEE Transactions on Power Delivery*, pp. 1–3, Sep. 2019, early access.

[7] A. R. Al-Roomi, "Power Flow Test Systems Repository," Halifax, Nova Scotia, Canada, 2015. [Online]. Available: https://al-roomi.org/power-flow

[8] "IEEE standard for general requirements for liquid-immersed distribution, power, and regulating transformers," *IEEE Std C57.12.00-2015 (Revision of IEEE Std C57.12.00-2010)*, pp. 1–74, May 2016.

[9] K. Karsai, D. Kerényi, and L. Kiss, *Large Power Transformers*, 1st ed., ser. Studies in Electrical and Electronic Engineering. Amsterdam, NL: Elsevier Science Ltd., 1987, vol. 25.

[10] S. V. Kulkarni and S. A. Khaparde, *Transformer Engineering: Design, Technology and Diagnostics*, 2nd ed. Boca Raton, FL: CRC Press, 1987.

[11] K. Shaarbafi, "Transformer modelling guide," Alberta Electric System Operator, Tech. Rep., Jul. 2014.

[12] R. D. Zimmerman, C. E. Murillo-Sánchez, and R. J. Thomas, "MATPOWER: Steady-state operations, planning, and analysis tools for power systems research and education," *IEEE Transactions on Power Systems*, vol. 26, no. 1, pp. 12–19, Feb 2011.

[13] R. D. Zimmerman and C. E. Murillo-Sánchez, *MATPOWER User's Manual*, version 7.0 ed., 2019, [Online]. Available: https://matpower.org/docs/MATPOWER-manual-7.0.pdf.

Consensus Phase Shifting Transformer Model

Md Rejwanur R. Mojumdar
Dept. Energy & Petroleum Eng.
University of Stavanger
Stavanger, Norway
md.r.mojumdar@uis.no

Jose M. Cano
Dept. Electrical Eng.
University of Oviedo
Gijon, Spain
jmcano@uniovi.es

Mohsen Assadi
Dept. Energy & Petroleum Eng.
University of Stavanger
Stavanger, Norway
mohsen.assadi@uis.no

Gonzalo A. Orcajo
Dept. Electrical Eng.
University of Oviedo
Gijon, Spain
gonzalo@uniovi.es

***Abstract*—The model of regulating transformers used in classic power system studies, such as load flow analysis or state estimation, is still debatable. A recent publication has demonstrated that the two alternative tap-changing transformer models usually found in the literature and power system simulation software packages may lead to important discrepancies, especially at extreme tap positions. This work is an extension of the aforementioned publication, written by the same authors, with the aim of reconciling those models for the case of the phase shifting transformer (PST). This work demonstrates that prevailing formulations of PST, particularly of the asymmetrical type, may also lead to important discrepancies when operating far from the nominal tap, with a different impact depending on the power factor of the power flowing through the device. Furthermore, a general model for the PST is proposed in this contribution. The new model uses the same data available in traditional formulations leading to improved results and avoiding any ambiguity.**

***Index Terms*—power transformers, phase shifters, transformer models**

I. Introduction

With the deregulation of the electricity market, control of power flows over transmission lines and tie lines has become an important concern. Moreover, uneven loading of parallel transmission lines is a recurring problem to solve during the transmission of energy. The use of phase shifting transformers (PST) is a well-established solution to provide control of real power flows through transmission lines. Several PSTs, as in the case of asymmetrical types, offer also some control over the magnitude of output voltage, thus providing regulation of the reactive power flows up to a certain limit [1].

The quality of the results of classic power system studies such as power flow and optimal power flow analysis, state estimation, etc. are highly dependent on the accuracy of the models used to describe system components. However, simplified models are typically used in these algorithms, due to the complexity and magnitude of the problems and also because of the scarce information generally available for the engineering practitioner in charge of these tasks. The nameplate of the transformer is usually the exclusive data source used in PST modeling.

In literature and practical implementations, two alternative voltage-magnitude regulating transformer models can be found [2]–[5]. The differences in these models arise from the fact that they consider the short-circuit impedance either provided exclusively by the nominal or off-nominal turns side winding of the device. These extreme assumptions cause that both models yield different results and thus, the users can be misled trying to validate their results with different tools. This fact was originally observed in [6], but the authors chose one of those models and focused their efforts on the manipulations needed on the other model to reach the same results. However, in [7] those discrepancies were fully explained and a reconciled solution was proposed. Furthermore, [7] demonstrates that even if the differences between the two models are trivial at the principal tap, significant mismatches take place at distant tap positions. Similarly, this lack of consistency also exists in the representation of PST through the two traditional models typically used in power system studies [8]–[10]. The aim of this contribution is to addressed this problem precisely by extending the applicability of [7] to PSTs.

Now, in this work, the authors' objective is to demonstrate that the two available models also yield different results for asymmetrical PSTs, which is misleading. Though these discrepancies from two models can be considered trivial at the principal tap, the inconsistency can lead to huge differences at distant tappings.

In this work, a new model of the PST is proposed in Section II in order to explain the causes of the discrepancies between the two existing models and with the aim of reaching a reconciled solution free of any ambiguity. Furthermore, the new model opens the door to a more accurate description of the device. Section III describes the traditional models and demonstrates that they are degenerate cases of the new proposal. Section IV presents a theoretical assessment of the discrepancies caused by traditional models and relates them with the solution offered by the new model. A case study is presented in Section V in order to highlight the importance of the new proposal. Finally, the conclusions of this study are drawn in section VI.

II. Description of the New Model

Neglecting the shunt admittances of the detailed model of PSTs (i.e. those responsible for the magnetizing current and core losses) is a common practice in power system studies. This fact, simplifies the analysis, as the internal bus of the detailed model is removed from the problem. If the

This work was supported by the Spanish Government Innovation Development and Research Office (MEC) under research Grant DPI2017-89186-R.

978-1-7281-5508-1/20/$31.00 ©2020 IEEE

PST operates at nominal turns ratios, no further assumption is needed, as the specific contribution of each transformer winding to the short-circuit impedance is irrelevant in that case. However, as is demonstrated in the following, this is far from being true when the PST works at an off-nominal tap position. Let us consider a PST with off-nominal turns ratio $|a|e^{j\theta}$ as depicted in Fig. 1.

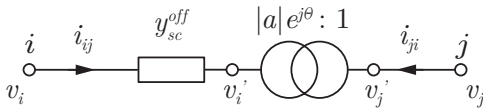

Fig. 1. Model of the phase shifting transformer with short-circuit impedance at the off-nominal turns side

The fundamental equations of a PST can be formulated as

$$\frac{v_i^{'}}{v_j^{'}} = a = |a|e^{j\theta}, \tag{1}$$

$$\frac{i_{ij}}{i_{ji}} = -\frac{1}{a^*} = -\frac{1}{|a|e^{-j\theta}}. \tag{2}$$

Then, though these parameters are not normally known by the user, let k be the ratio between the per p.u. impedance in the nominal winding, z_2 and tapped winding, z_1 (for the sake of simplicity, the same ratio is considered for resistance and leakage reactance). So, from (1) and (2), z_2 can be referred to the off-nominal turns side as

$$z_2^{off} = \frac{v_i^{'}}{v_j^{'}}\frac{-i_{ji}}{i_{ij}}z_2 = aa^*z_2 = |a|^2z_2. \tag{3}$$

Therefore, considering the new ratio k together with (3), the series transformer admittance, as seen from the off-nominal side, can be calculated as

$$y_{sc}^{off} = \frac{1}{z_1 + |a|^2 z_2} = \frac{1}{z_1\left(1 + |a|^2 k\right)}. \tag{4}$$

Typically, the data provided to the engineering practitioner in order to model the PST is the short-circuit impedance of the transformer, z_{sc}, which is also available at the nameplate of the device. This data is obtained from the short-circuit test, which is conducted, at least, at the nominal tap (i.e. $|a| = 1$). Thus, the rated short-circuit admittance of the PST, y_{sc}, can be expressed as

$$y_{sc} = \frac{1}{z_1 + z_2}. \tag{5}$$

From (5) and the definition of k, the contribution of the winding at the off-nominal side to the short-circuit impedance, z_1, can be calculated as

$$z_1 = \frac{1}{y_{sc}\left(1 + k\right)}, \tag{6}$$

Using this value in (4) yields

$$y_{sc}^{off} = \frac{1 + k}{1 + k|a|^2}y_{sc}. \tag{7}$$

Considering KVL, the nodal equations of the PST can now be written as

$$\begin{bmatrix} i_{ij} \\ i_{ji} \end{bmatrix} = \begin{bmatrix} Y_{ii} & Y_{ij} \\ Y_{ji} & Y_{jj} \end{bmatrix} \begin{bmatrix} v_i \\ v_j \end{bmatrix}, \tag{8}$$

where

$$Y_{ii} = y_{sc}^{off} = \frac{1 + k}{1 + k|a|^2}y_{sc}, \tag{9}$$

$$Y_{ij} = -ay_{sc}^{off} = -\frac{a\left(1 + k\right)}{1 + k|a|^2}y_{sc}, \tag{10}$$

$$Y_{ji} = -a^*y_{sc}^{off} = -\frac{a^*\left(1 + k\right)}{1 + k|a|^2}y_{sc}, \tag{11}$$

$$Y_{jj} = |a|^2y_{sc}^{off} = \frac{|a|^2\left(1 + k\right)}{1 + k|a|^2}y_{sc}. \tag{12}$$

It is important to note that the Y-bus matrix of the nodal equations for PST is not symmetrical as $Y_{ij} \neq Y_{ji}$. Therefore forming a π-equivalent model for PST is not straightforward; rather the model will have two different branch admittances depending on the current under consideration (i_{ij} or i_{ji}). Keeping this fact in mind, the parameters of a pseudo π-equivalent model for the PST, which has been depicted in Fig. 2, can be derived from (9)–(12), as

$$y_{ij} = -Y_{ij} = \frac{a\left(1 + k\right)}{1 + k|a|^2}y_{sc}, \tag{13}$$

$$y_{ji} = -Y_{ji} = \frac{a^*\left(1 + k\right)}{1 + k|a|^2}y_{sc}, \tag{14}$$

$$y_{si} = Y_{ii} + Y_{ij} = \frac{\left(1 - a\right)\left(1 + k\right)}{1 + k|a|^2}y_{sc}, \tag{15}$$

$$y_{sj} = Y_{jj} + Y_{ji} = \frac{\left(|a|^2 - a^*\right)\left(1 + k\right)}{1 + k|a|^2}y_{sc}. \tag{16}$$

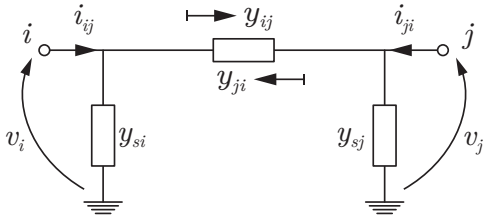

Fig. 2. A pseudo π-equivalent model of PST

III. Reconciliation of Previous Models

It can be easily derived that the two PST models most extensively used in the literature and practical implementations, correspond to the particular cases of making the parameter k equal to 0 and ∞ in (7), and thus in (9)–(16). The version with $k = 0$ corresponds to the assumption that all the short-circuit impedance of the PST is provided by the winding at the off-nominal turns side. In this case, the off-nominal admittance of the PST, y_{sc}^{off}, turns to be the same as the rated short-circuit admittance, y_{sc}, and the parameters of the pseudo π-equivalent circuit shown in Fig. 3(a) are obtained. On the other hand,

considering $k = \infty$, corresponds to the assumption that all the short-circuit impedance of the PST is provided by the winding at the nominal turns side. Thus, y_{sc}^{off} turns to be $y_{sc}/|a|^2$, and the set of parameters of the pseudo π-equivalent circuit shown in Fig. 3(b) is reached.

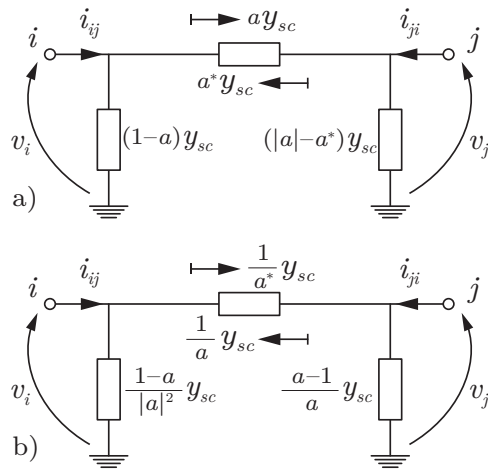

Fig. 3. π-equivalent traditional models of the phase shifting transformer. (a) $k = 0$, and (b) $k = \infty$

It is interesting to note that the lack of consistency between the results offered by the two traditional alternatives of the PST models was initially identified in [6]. However, this publication focused on the adjustments needed to make them yield the same results and, thus, appropriately pointed out that the model in Fig. 3(a) turns to be the same as the one in Fig 3(b) if all the admittances are divided by $|a|^2$. The problem of taking this approach lies on the fact that all the short-circuit impedance of the device is still being assigned to one specific side of the transformer which, as is demonstrated in this contribution, can lead to important errors. Conversely, the new model is capable of describing the cause of the discrepancies and allows for a description of the device free of any ambiguity, provided that the specific value of k used in the analysis is reported.

It is important to highlight that the new PST model presented here, opens the door to obtain accurate results if k is known (e.g. being provided by the manufacturer or estimated from off-line field measurements). But, even if this is not the case, much more realistic estimates can be obtained if k is set to 1, which stands for an equal contribution of each winding of the transformer to the short-circuit impedance. In fact, this is a common engineering practice, typically used when a detailed model of the transformer is to be used [10], [11]. While the benefits of using $k = 1$ in the case of the tap-changing transformer model was previously discussed in [7], this work analyzes the advantage of making the same assumption for the case of PSTs.

IV. Error Assessment

By using the new PST model proposed in Section II, the voltage at the nominal turns side of the PST, v_j, can be determined if the variables at the off-nominal turns side, v_i and i_{ij}, are provided. Indeed, using the nodal equation of the PST displayed in (8), v_j can be calculated as

$$v_j = \frac{i_{ij} - Y_{ii}v_i}{Y_{ij}}. \tag{17}$$

Let us designate the voltage at the nominal turns side for a generic value of k as v_j^k. Thus, the discrepancies between the traditional models and the consensus model, can be assessed, by just considering the values obtained for $k = 0$ and $k = \infty$, i.e. v_j^0 and v_j^∞. Indeed, using (17) according to the values of Y_{ii} and Y_{ij} in (9) and (10), yields,

$$\Delta v_j^0 = v_j^0 - v_j^k = \frac{k\left(|a|^2 - 1\right) i_{ij}}{a\left(1 + k\right) y_{sc}}, \tag{18}$$

$$\Delta v_j^\infty = v_j^\infty - v_j^k = \frac{\left(1 - |a|^2\right) i_{ij}}{a\left(1 + k\right) y_{sc}}. \tag{19}$$

As it is immediately derived from (18) and (19), the discrepancies grow with the load level of the transformer as well as with the value of the rated short-circuit impedance. Moreover, those equations imply that the mismatch does not take place when $|a|{=}1$, which is the case of symmetrical PSTs (i.e. those causing a pure phase-angle shift but with no effect on voltage magnitudes). In this specific case, the proposed model cannot contribute to provide better results. In fact, both the traditional and new models turn to be the same under that particular circumstances.

However, many asymmetrical PSTs are also used in power system applications. The proposed model can highly contribute to their modeling and simulation. According to [12], there exist three types of asymmetrical PSTs. For the widely-used quadrature booster, shown in Fig. 4.(a), the regulating winding is connected at ± 90 deg., whereas for other asymmetric PSTs, as the one shown in Fig. 4.(b), the regulating winding can be connected at different angles, $0{<}\delta{<}180$. For the asymmetrical PST with in-phase transformer, as in Fig. 4.(c), voltages on both primary and secondary side can be boosted with a common ratio r while the regulating winding remains connected with same angle, δ. As $|a|{\neq}1$ in those cases, traditional models cause inconsistent results and the new model may effectively solve this problem.

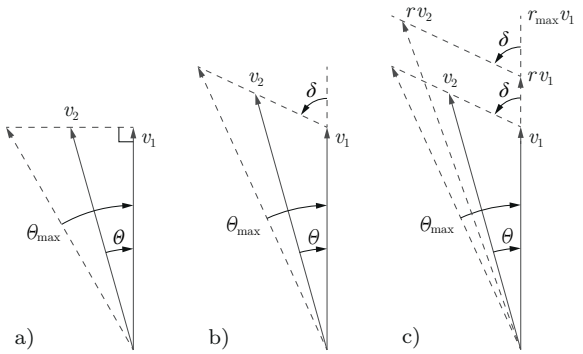

Fig. 4. Phasor diagram of PSTs. (a) Quadrature booster (b) asymmetrical PST, (c) in-phase transformer and asymmetrical PST

Notice that the new model is also useful to account for voltage magnitude tap-changing transformers provided that their vector group causes a non-zero phase-shift. In those cases, the discrepancies can be exacerbated by extreme tap positions, due to the high differences between $|a|$ and 1 that can be found in this type of devices.

V. Case Study

A case study is presented in this section in order to point out the inconsistencies implied by the use of the traditional PST models shown in Fig. 3. Furthermore, this case study demonstrates that the new PST model, proposed in this contribution and depicted in Fig. 2, can solve this problem assuring certainty in reporting results.

From Fig. 4, it can be easily seen that, for any of these asymmetric PSTs, there are general relations between the tap position, n, neutral tap position, n_0, phase shift, θ, magnitude of the off-nominal p.u. turns ratio, $|a|$, regulating winding connection angle, δ, and p.u. voltage step increment per tap change of the regulating winding, du. The general relations, including the effect of r, are well documented in [12], [13]. For the particular case of the asymmetrical PST, which is considered in the present case study, those relations, according to Fig. 4.(b), can be expressed as

$$\theta = -\arctan\left(\frac{(n-n_0)\,du\,sin\delta}{1+(n-n_0)\,du\,cos\delta}\right), \tag{20}$$

$$|a| = \frac{1}{\sqrt{\left((n-n_0)\,du\,sin\delta\right)^2+\left(1+(n-n_0)\,du\,cos\delta\right)^2}}. \tag{21}$$

Even if the manufacturer can provide different short-circuit impedance values for different tap positions, this fact is omitted in the following, not to obscure the core of the proposal.

Let us consider an 80 MVA, 50 Hz, 220/132 kV, asymmetric PST, with a nameplate short-circuit impedance, z_{sc}, of $0.01+0.12j$ and a maximum no-load phase shift, θ_{max}, of -4.715 deg. The regulating winding connection angle, δ, is at 60 deg. and the tap changer, located on the higher voltage side, has 11 positions (from the neutral tap, n_0=0, to n=10) and a voltage step increment per tap change, du, of 1%.

A. Analysis of the nominal turns side voltage deviations for different tap positions and power factors

The effect of the tap position in the deviations caused by traditional models is studied in this case. The voltage at the off-nominal turns side of the PST, v_i is fixed at 1 p.u. as well as the current at the same side, i_{ij}, which is also forced to supply the rated current of the transformer. Two different power factors are used in this analysis: (a) a unity power factor, φ=0 deg., i.e. i_{ij} is in-phase with v_i, and (b) a pure capacitive case, φ=90 deg. in which i_{ij} leads v_i in this amount. Thus, the voltage at the nominal turns side of the transformer, v_j, can be calculated using the different models. Fig. 5 shows the results for the traditional versions, i.e. k=0 and k=∞, together with those obtained using the new model and assuming an equal contribution of both windings to the short-circuit impedance, i.e. k=1. Although the setting of k in this way is not necessarily exact, it is according to well-accepted engineering practices, and is a more sensible estimation than the one derived from the extreme assumptions made in the traditional models.

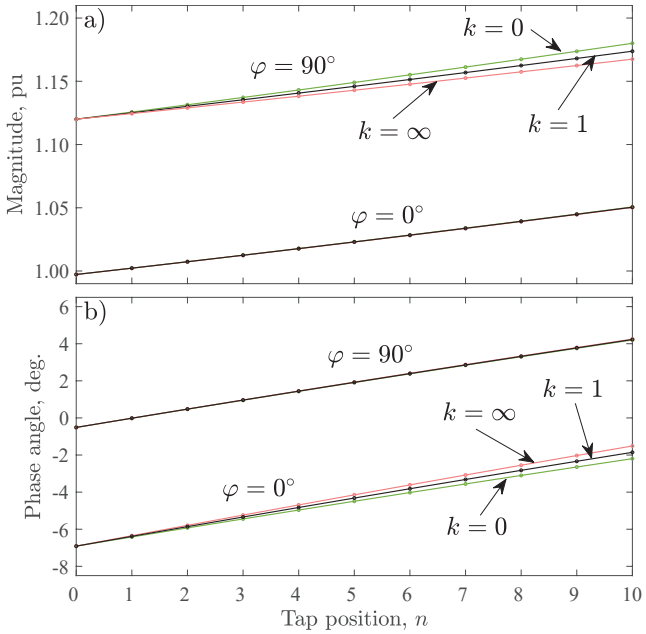

Fig. 5. Nominal-turns side voltage at different tap positions for the different PST models. The PST is operated at rated values at the off-nominal turns side at two different power factors: unity (φ = 0 deg.) and pure capacitive (φ = 90 deg.). (a) Voltage magnitude, and (b) voltage phase angle

The discrepancies in the magnitude of voltage at the nominal turns side of the transformer can be observed in Fig. 5.a. While they can be practically neglected at high power factors, the inconsistency is exacerbated in the capacitive case. Furthermore, and in agreement with (18) and (19), the mismatch grows when moving to distant positions from the neutral tap. In the same vein, the phase angle of the voltage at the nominal turns side (the voltage at the off-nominal side is taking as a reference) is depicted in Fig. 5.b. Unlike in the previous case, the discrepancies appear now magnified at high power factors and tend to be negligible with pure capacitive loads. As it is concluded from Fig. 5, the model proposed in this contribution offers a consensus estimate even if k is not accurately known and, more importantly, it removes any ambiguity from the results if the value of k used in the analysis is provided.

B. Maximum deviations in the calculation of the nominal-turns side voltage

In order to obtain the maximum deviations taking place in using the different models of the PST under study, the equivalent circuits of the traditional (k=0 and k=∞) and new model (setup with k=1) were used to calculate the nominal turns side voltage at every tap position, n, and with every possible power factor (i.e. letting φ vary in the full range, which includes reverse power flow) while operating the transformer at rated

values on the off-nominal side. The results obtained with the new model, v_j^1, were taken as a reference. Thus, Fig. 6.(a) represents the differences in voltage magnitude between the traditional models and the present proposal, i.e. $|v_j^0| - |v_j^1|$ and $|v_j^\infty| - |v_j^1|$. The maximum difference reaches a value of 0.63% which is, in fact, a significant discrepancy. Notice that the mismatch between the traditional models doubles the previous result, being as high as 1.26%. The same differences are depicted in Fig. 6.(b) for the case of the phase angle of the nominal turns side voltage. The mismatch reaches in this case 0.69 deg. between the traditional models, being reduced to 0.35 deg. when compared with the new model. Noticeably, these inconsistencies in the calculation of voltage phase angle can have a deep impact in the regulation of power flows by means of PST in real grids. The same results can be directly obtained from (18) and (19).

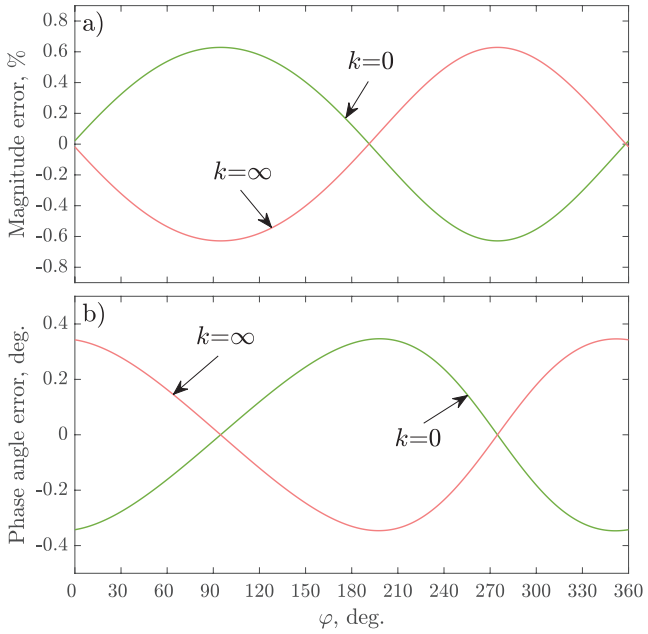

Fig. 6. Maximum deviation in the calculation of the nominal-turns side voltage at rated current. (a) Voltage magnitude, (b) voltage phase angle

VI. Conclusion

The use of simplified single-phase models of PSTs is standard practice in the execution of steady-state balanced power system studies. Although the specific contribution of each of the transformer windings to the short-circuit impedance can be completely neglected in untapped devices or when the operation takes place at the nominal tap, the same does not hold true at different tap positions. Traditional models of voltage-magnitude regulating transformers and PSTs are based on the assumption that all the short-circuit impedance is fully provided either by the winding at the nominal or off-nominal side, leading to two alternative models that yield different results. This may have strong implications, not only in the accuracy but also on the consistency of the outcomes from different tools. Although this problem does not appear in symmetrical PSTs, it can be a serious issue in asymmetrical PSTs or in voltage-magnitude regulating transformers with a non-zero vector group. Indeed, this work demonstrates that, in those cases, the mismatch of the results from those traditional models may be relevant, especially at extreme tap positions. These discrepancies appear both in voltage phase and voltage magnitude, depending on the power factor of the power flow handled by the device. Furthermore, this contribution proposes a consensus model of the PST which fully explains the aforementioned differences. The new model includes a new parameter that takes into account the contribution of each transformer winding to the short-circuit impedance. The use of this model gets rid of any ambiguity provided that the value of this parameter is reported within the data of the study. Moreover, the new model can boost the accuracy of the results if good estimates for the new parameter are available. Even if this is not the case, a sensible setup, as the one derived from the assumption of an equal contribution of each transformer winding to the short-circuit impedance, provides a more reliable outcome than those obtained from the extreme assumptions of the traditional models. Thus, the inclusion of the proposed PST model in power system software packages has the potential to significantly improve the consistency of power system studies with embedded PSTs.

References

[1] "IEEE guide for the application, specification, and testing of phase-shifting transformers - Redline," *Std C57.135-2011 (Revision of IEEE Std C57.135-2001)*, pp. 1–71, July 2011.

[2] A. Monticelli, *State Estimation in Electric Power Systems. A Generalized Approach*, 1st ed. Norwell, MA: Kluwer Academic Publishers, 1999.

[3] A. Abur and A. Gómez-Expósito, *Power System State Estimation. Theory and Implementation*, 1st ed. New York, NY: Marcel Dekker, Inc., 2004.

[4] *PowerWorld User's Guide*, PowerWorld Corporation, 2011, [Online]. Available: http://www.powerworld.com.

[5] C. Grande-Moran, "Phase-shifting transformer modeling in PSS®E," *Siemens Power Technology*, vol. 1, no. 111, pp. 1–7, Mar. 2012.

[6] L. V. Barboza, H. H. Zürn, and R. Salgado, "Load tap change transformers: A modeling reminder," *IEEE Power Engineering Review*, vol. 21, no. 2, pp. 51–52, Feb. 2001.

[7] J. M. Cano, M. R. R. Mojumdar, and G. A. Orcajo, "Reconciling tap-changing transformer models," *IEEE Transactions on Power Delivery*, pp. 1–3, Sep. 2019, early access.

[8] R. D. Youssef, "Phase-shifting transformers in load flow and short-circuit analysis: modelling and control," *IEE Proceedings C - Generation, Transmission and Distribution*, vol. 140, no. 4, pp. 331–336, July 1993.

[9] J. M. Cano, M. R. R. Mojumdar, J. G. Norniella, and G. A. Orcajo, "Phase shifting transformer model for direct approach power flow studies," *International Journal of Electrical Power & Energy Systems*, vol. 91, pp. 71 – 79, 2017.

[10] K. Shaarbafi, "Transformer modelling guide," Alberta Electric System Operator, Tech. Rep., Jul. 2014.

[11] S.V.Kulkarni and S.A.Khaparde, *Transformer Engineering: Design, Technology and Diagnostics*, 2nd ed. Boca Raton: CRC Press, May 2013.

[12] *Phase Shift Transformers Modelling, Common Grid Model Exchange Standard (CGMES) Library v2.4.14*, European Network of Transmission System Operators for Electricity (ENTSOE) Std., 2014.

[13] J. Verboomen, D. Van Hertem, P. H. Schavemaker, W. L. Kling, and R. Belmans, "Phase shifting transformers: principles and applications," in *2005 International Conference on Future Power Systems*, Nov 2005, pp. 6 pp.–6.

Estimation of Impedance Ratio Parameters for Consistent Modeling of Tap-Changing Transformers

Md Rejwanur R. Mojumdar, *Graduate Student Member, IEEE*, José M. Cano, *Senior Member, IEEE*, and Gonzalo A. Orcajo, *Member, IEEE*

***Abstract*—Recent contributions have shown that two widely used formulations of the tap-changing transformer model are controversial, as they generate dissimilar results depending on the selected tap and operating point. In recent works, the authors proposed a new model and demonstrated its consistency to reconcile this debate. It introduces a parameter which stands for the ratio between the impedances of the nominal and tapped winding of the transformer. However, this parameter is not provided with and cannot be obtained from standard datasheets, which compels the users to rely on rough approximations. To overcome this problem, an offline state-vector-augmented parameter estimation method capable of providing accurate estimates of transformer impedance ratios is proposed in this work. It is demonstrated that their use can effectively lead state estimators to better estimates of system states. This work also contributes with the derivatives of the different measurement functions in terms of the impedance ratios, which are essential for this or any other linearized state estimator. A multi-snapshot implementation is used to obtain a twofold advantage — increased measurement redundancy and improved accuracy of the estimated parameters. A detailed formulation of the implementation and several case studies are presented to demonstrate the validity of the proposal.**

***Index Terms*—Maximum likelihood estimation, parameter estimation, power transformers, tap changers, transformer models.**

I. Introduction

SEVERAL power system studies, such as power flow (PF), optimal power flow (OPF) or state estimation (SE), are crucial today to ensure safety and optimality in the operation of modern grids. In this context, tap-changing transformers serve at the vanguard for voltage regulation in power systems, and thus, accurate models of these devices are needed when they are present in the network under study.

The two most widely spread tap-changing transformer models found both in literature and software packages [1], [2] have been demonstrated to be inconsistent [3]–[5]. One of the models assumes that the transformer impedance, obtained through the well-known short-circuit test, is totally provided by the nominal winding, whereas the other model allocates it exclusively at the off-nominal side. This fact was first reported in [3]; however, the authors of this work selected one of the alternatives and proposed a method to shape the other so as to converge into the same results. Later, in [4], [5], it was established that, while the two models produce similar results near the central tap, they lead to significant differences at extreme tap positions. The power factor of the power flowing through the transformer primarily determines whether this divergence appears in voltage magnitude or phase angle. Analytical formulations and case studies demonstrating this inconsistency are presented in the aforementioned references.

To reconcile this dispute, the authors proposed a consistent model which reflects that the short-circuit impedance is in fact shared by both sides of the transformer [4], [5]. The new model introduces a parameter, k, which stands for the per-unit (p.u.) impedance ratio between the nominal winding and tapped winding of the tap-changing transformer. However, admittedly, the user cannot obtain the value of this parameter from standard transformer data sheets or even through straight-forward calculations. In response to that, the authors argued and demonstrated that if this parameter is not available, assuming $k = 1$, i.e. considering an equal share of the p.u. impedance at both sides of the transformer, produces results which minimizes the maximum expected error. Nonetheless, the authors pointed out that, to achieve accurate results, the p.u. impedance ratio could be obtained in real scenarios from the application of SE techniques. In fact, this is the main purpose of the present proposal.

In a broad classification, SE methods are either recursive or static. However, static state estimators constitute a comparatively mature technology widely used by utilities for power system monitoring. While there are other possibilities, most of the static estimators minimize the weighted least squares (WLS) of residuals from a single snapshot of measurements to provide estimates of the current states of the system [6], [7]. For static SE, several alternative formulations are available in literature in order to overcome some deficiencies of the seminal algorithms, increasing numerical capabilities or adding some practical advantages. Many of these formulations are well documented in [6], [7]. In the present proposal, a widely used and suitable WLS-based formulation is extended further to cope with the objectives of this work.

Manuscript received June 3, 2020; revised October 16, 2020 and December 24, 2020; accepted January 2, 2021. Date of publication January 12, 2021; date of current version June 18, 2021. This work was supported by the Spanish Government Innovation Development, and Research Office (MEC) under research Grant DPI2017-89186-R. Paper no. TPWRS-00922-2020. *(Corresponding author: José M. Cano.)*

Md Rejwanur R. Mojumdar is with the Electrical Control System Department, ABB AS, 4033 Stavanger, Norway (e-mail: rejwanurrashid.mojumdar@no.abb.com).

José M. Cano and Gonzalo A. Orcajo are with the Department of Electrical Engineering, University of Oviedo, 30013 Gijón, Spain (e-mail: jmcano@uniovi.es; gonzalo@uniovi.es).

Color versions of one or more figures in this article are available at https://doi.org/10.1109/TPWRS.2021.3050958.

Digital Object Identifier 10.1109/TPWRS.2021.3050958

In addition to providing estimates of the state variables, other functions and associated routines are integral parts of power system state estimators, such as observability analysis, bad data detection and identification, topology error processing and parameter estimation. Among these, the latter can be pointed out as the key tool to address the problem of estimating the p.u. impedance ratios of tap-changing transformers. Network parameter estimation methods are broadly classified in two groups-residual sensitivity-based analysis and state vector augmentation [6]. Residual sensitivity-based analysis is efficient for parameter error identification which is not required for the purpose of this work, as transformer impedance ratios are objectively included in the suspicious set. As the name suggests, in state vector augmentation methods, the suspected parameters are included in the state vector and estimated together with the system state variables [8]–[13]. Importantly, for the sole purpose of parameter estimation, state vector augmentation methods are considered to deliver superior performance due to the fact that all the surrounding measurements get involved in the estimation [14]. Therefore, the state vector augmentation method has been selected and implemented in this proposal to provide accurate estimates of the parameters of interest.

The estimation of transformer tap positions has been a central issue for parameter estimation methods in power systems [10], [13]. In fact, estimation of unmeasured or erroneous transformer taps is today a regular or online function of state estimators. On the contrary, due to the non-varying nature of impedance ratio parameters, which may change only in the event of a fault or a complete replacement of a transformer, their estimation is required in very long intervals. It is not worth including the estimation of these parameters in an online state estimator, as this may deteriorate the performance of the algorithm in terms of speed without a practical improvement. Therefore, an offline parameter estimator, designed to be run periodically, with a low cadence, is proposed in this work. In this concept, the online estimator used in the operation of the grid is in charge of the estimation of transformer tap positions at each snapshot; then, the offline parameter estimator, executed in long time periods, uses those tap positions together with the raw measurements at different snapshots to provide accurate estimates of the transformer impedance ratios. Certainly, the updated estimates of these parameters can now be fed into the online state estimator to increase its accuracy, as a consequence of the improvement of the model.

Finally, it is important to discuss the potential hindrances of assessing the transformer p.u. impedance ratios through parameter estimation techniques. If a large number of tap-changing transformers are embedded in the grid under study, the new variables to be included in the augmented state vector could significantly deteriorate the redundancy of the measurements. Moreover, as in any other SE application, the noise of field measurements has an impact on the quality of the estimation of the parameters. However, even more important for this particular problem is that the sensitivity of the measurement functions with respect to p.u. impedance ratios are significantly lower than the sensitivities with respect to the other state variables. As a consequence, measurement noise is likely to conceal the biases of erroneous estimation of impedance ratios throughout the process. The above-mentioned difficulties turn the estimation of the desired transformer parameters into a challenging task. Nonetheless, one expedient feature of transformer impedance ratios can help to overcome these obstacles: they can be considered time-invariant, at least for a reasonable time span. Thus, the method proposed in this work can be fed with multiple snapshots of measurements, i.e. with historical data collected along a reasonable time period. Multi-snapshots usage has clear advantages in parameter estimation, as has been previously reported by other authors [6], [9], [11]. Therefore, a multi-snapshot implementation has been embraced in this proposal.

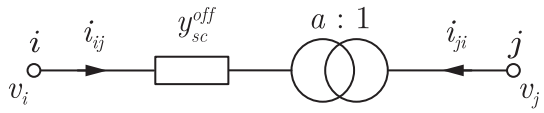

Fig. 1. Model of the tap-changing transformer with short-circuit impedance at the off-nominal turns side.

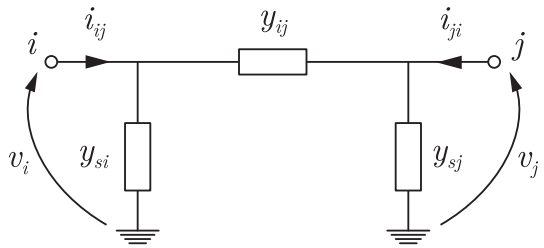

Fig. 2. Two-port π-model of a tap-changing transformer or a network branch.

In Section II, the consistent tap-changing transformer model, and thereby, the emergence of the impedance ratio parameter, is presented for the benefit of the reader. Then, an advantageous equality-constrained SE method is briefly described in Section III. Section IV articulates the derivation and integration details of the estimation of p.u. impedance ratios. A set of case studies are included in Section V to validate and demonstrate the advantages of the proposal. Finally, the conclusions of this study are gathered in Section VI.

II. Consistent Tap-Changing Transformer Model

Let us consider a tap-changing transformer with off-nominal turns ratio $a:1$ as depicted in Fig. 1. Like any network branch or in-phase transformer, a tap-changing transformer can be represented as a π-equivalent model, as shown in Fig. 2. The π-equivalent model possesses two shunt branches which induce no effect while the transformer is operated at its nominal turns ratio. However, tap-changing transformers are often operated at off-nominal turn ratios for voltage regulation purposes, and thus, the shunt branches of their π-equivalent model cannot be neglected.

As discussed in Section I, the consistent model of the tap-changing transformer was introduced in [4], [5] to reconcile the inconsistency between two widespread models. The new consistent model states that the off-nominal short-circuit admittance

at the off-nominal turns side can be calculated as

$$y_{sc}^{off} = \frac{1}{z_1 + a^2 z_2} = \frac{1+k}{1+ka^2} y_{sc}, \tag{1}$$

where y_{sc} represents the p.u. admittance of the transformer, obtained through the short-circuit test and always provided as nameplate data. Parameter k is introduced in [4] to denote the p.u. impedance ratio between the nominal winding, z_2, and tapped winding, z_1. Classical transformer models assume extreme values of this parameter ($k = 0$ and $k = \infty$). The elements of the bus admittance matrix for the consistent tap-changing transformer model are derived in [4], [5] as

$$Y_{ii} = \frac{1+k}{1+ka^2} y_{sc}, \tag{2}$$

$$Y_{ij} = Y_{ji} = -\frac{a(1+k)}{1+ka^2} y_{sc}, \tag{3}$$

$$Y_{jj} = \frac{a^2(1+k)}{1+ka^2} y_{sc}. \tag{4}$$

Then, the parameters of the π-model can be straightforwardly obtained as

$$y_{ij} = -Y_{ij} = \frac{a(1+k)}{1+ka^2} y_{sc}, \tag{5}$$

$$y_{si} = Y_{ii} + Y_{ij} = \frac{(1-a)(1+k)}{1+ka^2} y_{sc}, \tag{6}$$

$$y_{sj} = Y_{jj} + Y_{ij} = \frac{a(a-1)(1+k)}{1+ka^2} y_{sc}. \tag{7}$$

An unresolved issue of the consistent model is that the particular value of the p.u. impedance ratio, k, for a specific tap-changing transformer is a constructive parameter normally unknown for the user. Therefore, the accuracy and consistency of the results of power system studies with embedded tap-changing transformers can be obviously improved if the actual value of k is determined through a parameter estimation process utilizing historical sets of measurements. Thus, the estimation of k is pursued in the present proposal.

III. Equality-Constrained SE

The Normal Equations (NE) formulation of WLS SE in their application to power system studies may lead to some well-known problems, such as ill-conditioning or divergence. This is especially critical when using zero-injection buses as virtual measurements. Therefore, several proposals have been made to overcome the shortcomings of the basic NE formulation [6]. Among these propositions, appear numerical techniques such as the Lower Upper (LU) factorization and orthogonal (QR) factorization of the gain matrix. More advantageously, there are some restructured formulations called equality-constrained SE which take advantage of the Lagrangian of equality-constrained optimization problems [6], [15]. In the present work, an equality-constrained SE algorithm called augmented matrix method [6], [16] was extended to the particular parameter estimation problem of interest. In this method, both the virtual and regular measurement equations are taken as equality constraints in order to improve the condition number of the Hachtel's matrix. According to this method, the following set of linearized equations describes the SE problem

$$\begin{bmatrix} R & H & 0 \\ H^T & 0 & C^T \\ 0 & C & 0 \end{bmatrix} \begin{bmatrix} \mu \\ \Delta x \\ \lambda \end{bmatrix} = \begin{bmatrix} \Delta z \\ 0 \\ -c(x) \end{bmatrix}, \tag{8}$$

where,

- R is the covariance matrix having variances of regular measurement errors at its diagonal elements,
- H is the matrix for derivatives of regular measurements,
- C is the matrix for derivatives of virtual measurements,
- μ is the vector of Lagrange multipliers for regular measurements,
- λ is the vector of Lagrange multipliers for virtual measurements,
- Δx is the vector for deviations of state variables,
- Δz is the vector for measurement residuals, i.e., the difference between regular field measurements and their theoretical values calculated from the current estimation of state variables,
- and $c(x)$ is the vector for virtual measurement residuals.

IV. Estimation of Transformer Impedance Ratios

Most SE methods are linearized formulations which require the derivatives of the measurement functions, h, in terms of the state variables. As power system static SE is a well-developed and mature technique, the derivatives of general measurement functions in terms of commonly used state variables and parameters are widely used and readily available in the literature [6]. However, the consistent tap-changing transformer model is a state-of-the-art concept which has not been implemented before in power system SE algorithms. Hence, no work has yet introduced the derivatives of measurement functions in terms of the impedance transformer ratio, k, which are required for the estimation of these parameters.

In a standard SE formulation, the state vector, x, includes bus voltage magnitudes, V, and phase angles, θ, except for the phase angle reference, as state variables. In this proposal, the state vector is augmented by including the k parameters of the tap-changing transformers embedded in the network under study. Thus, as an important contribution of this work, the derivatives of general field measurement types such as bus voltage magnitudes, active and reactive bus power injections and active and reactive branch power flows, in terms of the impedance ratio, are presented. These derivatives are crucial for the construction of both the H and C matrices included in (8). Finally, for the problem-specific requirements, the authors have integrated these new derivatives into a single snapshot and a multi-snapshot augmented matrix SE algorithm.

A. Derivatives of Measurement Functions in Terms of k

1) Bus Voltage Magnitudes: The measurement function of voltage magnitude at bus i reduce itself to its corresponding voltage magnitude, V_i, which is a state variable on its own.

Therefore, these functions are independent of tap-changing transformer impedance ratios, k. So, it can be stated that

$$\frac{\partial V_i}{\partial k} = 0. \tag{9}$$

2) Power Injections: The measurement functions for the active and reactive power injections, P_i and Q_i, at a specific bus i, are well-known in power system analysis, being formulated as

$$P_i = V_i \sum_{n=1}^{N} V_n [G_{in} \cos\theta_{in} + B_{in} \sin\theta_{in}], \tag{10}$$

$$Q_i = V_i \sum_{n=1}^{N} V_n [G_{in} \sin\theta_{in} - B_{in} \cos\theta_{in}], \tag{11}$$

where n stands for each of the total number of buses in the network, N. Likewise, G_{in}, B_{in} are the conductance and susceptance of the element Y_{in} of the system bus admittance matrix. Finally, θ_{in} stands for the phase angle between buses i and n.

As it can be immediately concluded from (10) and (11), if bus i is not directly connected to a tap-changing transformer, none of the terms of these equations depend on the impedance ratio of that specific device. Thus, the derivatives of those active and reactive power injections in terms of the impedance ratio of that transformer equal zero. On the other hand, if there is a tap-changing transformer located between buses i and j, with an impedance ratio k, the admittance of the transformer impacts the calculation of power injections through the addends corresponding to $n = i$ and $n = j$. Thus, the parts of P_i and Q_i impacted by k, which are the only ones of interest for the calculation of the derivatives, can be designated as P_i^k and Q_i^k and may be evaluated as

$$P_i^k = V_i^2 G_{ii}^k + V_i V_j [G_{ij} \cos\theta_{ij} + B_{ij} \sin\theta_{ij}], \tag{12}$$

$$Q_i^k = -V_i^2 B_{ii}^k + V_i V_j [G_{ij} \sin\theta_{ij} - B_{ij} \cos\theta_{ij}], \tag{13}$$

where, G_{ii}^k and B_{ii}^k contain the addends of the diagonal elements of the bus admittance matrix which are a function of k, i.e. those provided by the series and shunt branch of the tap-changing transformer model connected at bus i.

At this point, two cases should be taken into consideration. On the one hand, if the tapped winding of the transformer is connected to bus i, as depicted in Fig. 1, (2) and (3) allow to express the elements of the bus admittance matrix in (12) and (13) as a function of k and the conductance, g_{sc}, and susceptance, b_{sc}, of the short-circuit admittance, y_{sc}, of the transformer. Thus,

$$G_{ii}^k = \frac{1+k}{1+ka^2} g_{sc}, \qquad B_{ii}^k = \frac{1+k}{1+ka^2} b_{sc}, \tag{14}$$

$$G_{ij} = -\frac{a(1+k)}{1+ka^2} g_{sc}, \quad B_{ij} = -\frac{a(1+k)}{1+ka^2} b_{sc}. \tag{15}$$

The substitution of (14) and (15) in (12) and (13) leads to

$$P_i^k = \frac{1+k}{1+ka^2} \left[V_i^2 g_{sc} - a V_i V_j \left(g_{sc} \cos\theta_{ij} + b_{sc} \sin\theta_{ij} \right) \right], \tag{16}$$

$$Q_i^k = \frac{1+k}{1+ka^2} \left[-V_i^2 b_{sc} - a V_i V_j \left(g_{sc} \sin\theta_{ij} - b_{sc} \cos\theta_{ij} \right) \right]. \tag{17}$$

By applying the quotient rule to (16) and (17), the derivatives of P_i and Q_i in terms of k can be obtained as

$$\frac{\partial P_i}{\partial k} = \frac{1+ka^2-a^2(1+k)}{(1+ka^2)^2} \times \ldots \left[V_i^2 g_{sc} - a V_i V_j \left(g_{sc} \cos\theta_{ij} + b_{sc} \sin\theta_{ij} \right) \right], \tag{18}$$

$$\frac{\partial Q_i}{\partial k} = \frac{1+ka^2-a^2(1+k)}{(1+ka^2)^2} \times \ldots \left[-V_i^2 b_{sc} - a V_i V_j \left(g_{sc} \sin\theta_{ij} - b_{sc} \cos\theta_{ij} \right) \right]. \tag{19}$$

On the other hand, if bus i is connected to the untapped winding of the transformer, (4) should be used instead of (2) to formulate the diagonal elements of the bus admittance matrix impacted by k, G_{ii}^k and B_{ii}^k, in (12) and (13). Thus,

$$G_{ii}^k = \frac{a^2(1+k)}{1+ka^2} g_{sc}, \quad B_{ii}^k = \frac{a^2(1+k)}{1+ka^2} b_{sc}. \tag{20}$$

The substitution of (15) and (20) in (12) and (13) leads to

$$P_i^k = \frac{a(1+k)}{1+ka^2} \left[a V_i^2 g_{sc} - V_i V_j \left(g_{sc} \cos\theta_{ij} + b_{sc} \sin\theta_{ij} \right) \right], \tag{21}$$

$$Q_i^k = \frac{a(1+k)}{1+ka^2} \left[-a V_i^2 b_{sc} - V_i V_j \left(g_{sc} \sin\theta_{ij} - b_{sc} \cos\theta_{ij} \right) \right]. \tag{22}$$

And the derivatives of P_i and Q_i in terms of k in this second case turn out to be

$$\frac{\partial P_i}{\partial k} = \frac{a(1+ka^2)-a^3(1+k)}{(1+ka^2)^2} \times \ldots \left[a V_i^2 g_{sc} - V_i V_j \left(g_{sc} \cos\theta_{ij} + b_{sc} \sin\theta_{ij} \right) \right], \tag{23}$$

$$\frac{\partial Q_i}{\partial k} = \frac{a(1+ka^2)-a^3(1+k)}{(1+ka^2)^2} \times \ldots \left[-a V_i^2 b_{sc} - V_i V_j \left(g_{sc} \sin\theta_{ij} - b_{sc} \cos\theta_{ij} \right) \right]. \tag{24}$$

3) Power Flows: Note that the π-equivalent model depicted in Fig. 2 is not only valid for a tap-changing transformer but also for a line. Thus, the measurement functions of active and reactive power, P_{ij}, Q_{ij}, flowing from bus i to bus j and measured at the sending end can be expressed for both types of elements as

$$P_{ij} = V_i^2 (g_{si} + g_{ij}) - V_i V_j (g_{ij} \cos\theta_{ij} + b_{ij} \sin\theta_{ij}), \tag{25}$$

$$Q_{ij} = -V_i^2 (b_{si} + b_{ij}) - V_i V_j (g_{ij} \sin\theta_{ij} - b_{ij} \cos\theta_{ij}), \tag{26}$$

where, g_{si} and b_{si} are the conductance and susceptance of the shunt leg at bus i, and g_{ij} and b_{ij} stand for the conductance and susceptance of the series admittance.

From (25) and (26), it can be immediately concluded that, if a power flow measurement between the adjacent buses i and j does not flow through a tap-changing transformer, none of the elements of these equations are affected by the impedance ratio of the device. Thus, the derivatives of those active or reactive power flows in terms of the k equal zero. However, when a tap-changing transformer connects buses i and j, the admittances in those equations are a function of the impedance ratio, k. Again, two different cases need to be addressed. On the one hand, if the measuring location, i.e. bus i, is connected to the tapped winding, as in Fig. 1, the conductances and susceptances can be directly taken from (5) and (6). Thus,

$$g_{si} + g_{ij} = \frac{1+k}{1+ka^2} g_{sc}, \qquad b_{si} + b_{ij} = \frac{1+k}{1+ka^2} b_{sc}, \quad (27)$$

$$g_{ij} = \frac{a(1+k)}{1+ka^2} g_{sc}, \qquad b_{ij} = \frac{a(1+k)}{1+ka^2} b_{sc}. \quad (28)$$

The substitution of (27) and (28) in (25) and (26) leads to

$$P_{ij} = \frac{1+k}{1+ka^2} \left[V_i^2 g_{sc} - a V_i V_j \left(g_{sc} \cos\theta_{ij} + b_{sc} \sin\theta_{ij} \right) \right], \quad (29)$$

$$Q_{ij} = \frac{1+k}{1+ka^2} \left[-V_i^2 b_{sc} - a V_i V_j \left(g_{sc} \sin\theta_{ij} - b_{sc} \cos\theta_{ij} \right) \right]. \quad (30)$$

By applying the quotient rule to (29) and (30), the derivatives of P_{ij} and Q_{ij} in terms of k can be obtained as

$$\frac{\partial P_{ij}}{\partial k} = \frac{1+ka^2-a^2(1+k)}{(1+ka^2)^2} \times \ldots \left[V_i^2 g_{sc} - a V_i V_j \left(g_{sc} \cos\theta_{ij} + b_{sc} \sin\theta_{ij} \right) \right], \quad (31)$$

$$\frac{\partial Q_{ij}}{\partial k} = \frac{1+ka^2-a^2(1+k)}{(1+ka^2)^2} \times \ldots \left[-V_i^2 b_{sc} - a V_i V_j \left(g_{sc} \sin\theta_{ij} - b_{sc} \cos\theta_{ij} \right) \right]. \quad (32)$$

On the other hand, if the measuring location, i.e. bus i, is connected to the untapped winding, (7) should be used instead of (6) to obtain the conductances and susceptances used in (29) and (30). Thus,

$$g_{si} + g_{ij} = \frac{a^2(1+k)}{1+ka^2} g_{sc}, \quad b_{si} + b_{ij} = \frac{a^2(1+k)}{1+ka^2} b_{sc}. \quad (33)$$

The substitution of (28) and (33) in (29) and (30) leads to

$$P_{ij} = \frac{a(1+k)}{1+ka^2} \left[a V_i^2 g_{sc} - V_i V_j \left(g_{sc} \cos\theta_{ij} + b_{sc} \sin\theta_{ij} \right) \right], \quad (34)$$

$$Q_{ij} = \frac{a(1+k)}{1+ka^2} \left[-a V_i^2 b_{sc} - V_i V_j \left(g_{sc} \sin\theta_{ij} - b_{sc} \cos\theta_{ij} \right) \right]. \quad (35)$$

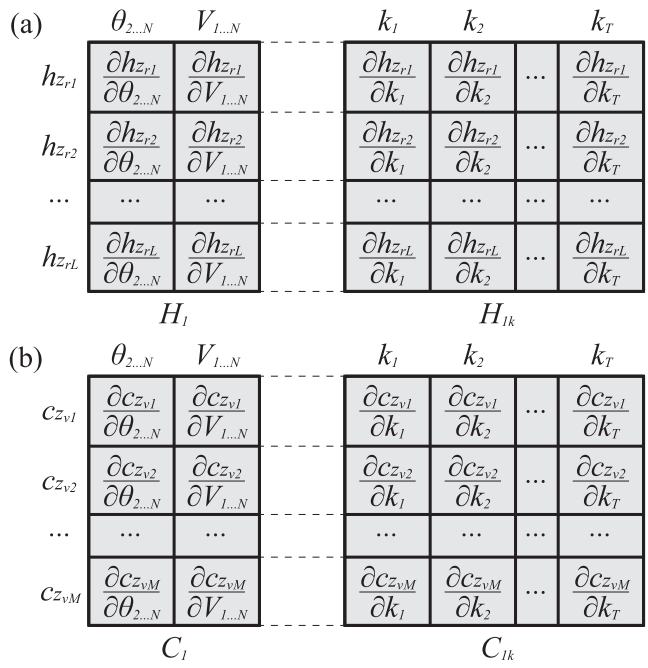

Fig. 3. Formation of the augmented Jacobian matrices for a single snapshot. (a) H matrix, and (b) C matrix.

And the derivatives of P_{ij} and Q_{ij} in terms of k in this second case can be expressed as

$$\frac{\partial P_{ij}}{\partial k} = \frac{a(1+ka^2)-a^3(1+k)}{(1+ka^2)^2} \times \ldots \left[a V_i^2 g_{sc} - V_i V_j \left(g_{sc} \cos\theta_{ij} + b_{sc} \sin\theta_{ij} \right) \right], \quad (36)$$

$$\frac{\partial Q_{ij}}{\partial k} = \frac{a(1+ka^2)-a^3(1+k)}{(1+ka^2)^2} \times \ldots \left[-a V_i^2 b_{sc} - V_i V_j \left(g_{sc} \sin\theta_{ij} - b_{sc} \cos\theta_{ij} \right) \right]. \quad (37)$$

B. Formation of Jacobian Matrices for the SE Process

In the formulation of the augmented matrix approach for SE [6], [15], the derivatives of the h_z–functions of a set of L regular measurements, z_r, reside in the H matrix, while the derivatives of the c_z–functions of a set of M virtual measurements, z_v, reside in the C matrix shown in (8). Both matrices are augmented in this proposal with a new set of state variables, k, corresponding to the transformer impedance ratios of the T tapped-transformers embedded in the grid under study.

If the estimation of k is carried out considering just a single snapshot of measurements, the extension of the Jacobian matrices is rather straightforward. In this case, a new column has to be added, both to the H and C matrices, to account for each of the T elements of k. Thus, the use of the new derivatives described in Section IV-A together with the classical set [6], allows to form the augmented H and C matrices as depicted in Fig. 3. Notice that in this figure and w.l.o.g, the phase angle at bus 1, θ_1, has been taken as reference, and thus, excluded from the set of

state variables. This is a similar approach to other augmentation techniques such as those previously presented in [8]–[13].

According to Fig. 3, two parts can be distinguished in the new H and C matrices: H_1 and C_1, that account for the derivatives of regular and virtual measurements with respect to the conventional state variables, and H_{1k} and C_{1k}, that hold the derivatives of regular and virtual measurements in terms of the transformer impedance ratios, k. The final H and C matrices are formed by horizontal concatenation of H_1, H_{1k} and C_1, C_{1k} respectively.

The difficulties of estimating the p.u. impedance ratios of tap-changing transformers from a single snapshot of measurements have been previously discussed in Section I. As it was pointed out, an adaptation of a multi-snapshot of measurements is proposed in this work to overcome those obstacles. This is a suitable approach for the estimation of the parameters under study, which can be considered time-invariant during long periods. Indeed, parameter estimation, conducted as an offline task, can sacrifice computation time in favor of the accuracy of the estimation.

In SE theory, measurement redundancy is defined as the ratio between the number of measurements and the number of state variables. Hence, as L is the number of regular measurements and M is the number of virtual measurements, the base case redundancy of the problem, ε_0, i.e., the one in which p.u. impedance ratios are not included as state variables, can be calculated as

$$\varepsilon_0 = \frac{L+M}{2N-1}. \tag{38}$$

In a single snapshot or multi-snapshot implementation of the augmented problem, in which Q snapshots and T time-invariant transformer impedance ratios are included as additional state variables, the redundancy level is deteriorated according to

$$\varepsilon_Q = \frac{Q(L+M)}{Q(2N-1)+T} = \frac{L+M}{2N-1+\frac{T}{Q}}. \tag{39}$$

From (39), it can be concluded that, increasing the number of snapshots in the estimation process, allows to move the redundancy level of the augmented problem as close as desired to the redundancy of the base case. Thus, provided that a sufficient number of snapshots are included into the problem, the application of the augmented approach cannot be blamed for deteriorating the redundancy level.

The formation of the augmented matrices, H and C, for the case of the multi-snapshot problem is depicted in Fig. 4. Each snapshot q involves a specific set of conventional state variables, $[V\theta]_q$, together with a specific set of h–functions, $[h_{zr}]_q$, and c–functions, $[c_{zv}]_q$, associated with regular and virtual measurements, respectively. Notice that the conventional state variables change at each snapshot but the augmented ones, k, remain always the same. Thus, the parts of the Jacobian matrices linked to conventional state variables are augmented diagonally by means of H_q and C_q, while the parts associated with the transformer impedance ratios are augmented vertically by means of H_{qk} and C_{qk}.

It is worth noting that, in order to apply (8) in the multisnapshot context, the covariance matrix, R, should be formed by diagonal augmentation of the respective covariance matrices of each snapshot. Likewise, Δz and Δx vectors are respectively formed by vertical concatenation of measurement residuals and state variable deviations from each snapshot.

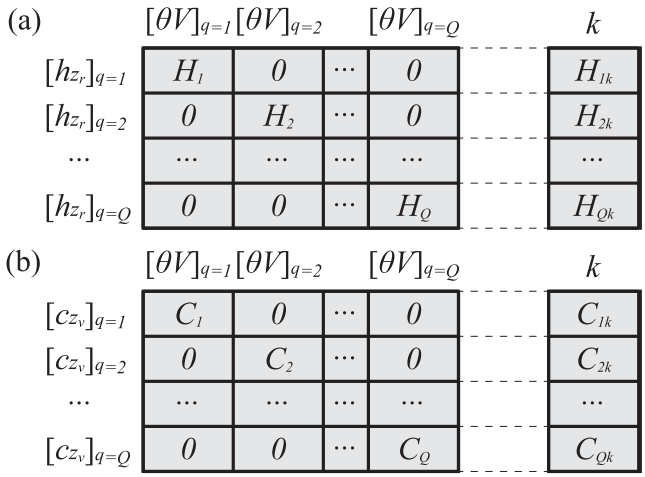

Fig. 4. Formation of the augmented Jacobian matrices in a multi-snapshot problem. (a) H matrix, and (b) C matrix.

Equation (8) can now be iteratively solved to provide estimates of the full set of state variables. Among them, the final values of k constitute the estimated parameters of the p.u. impedance ratios of the tap-changing transformers.

C. Treatment of Bad Data

The treatment of bad data is a crucial concern for any state estimator. However, as it is pointed out in Section I, the parameter estimator proposed in this work is designed to work offline. Thus, it uses historical data comprised of measurement snapshots in which any possible bad data has been already detected, identified and removed by the online state estimator used in the operation of the grid. Of course, removal of bad data may reduce the redundancy of the measurement set. However, as it is shown in the case studies presented in Section V, the proposed algorithm converges to the solution even in low redundancy scenarios. In summary, as the bad data is pre-treated by the online state estimator, the proposed offline parameter estimator does not need further filtering of the input measurements.

Nevertheless, it is interesting to point out that model inaccuracies, such as those that may appear during the initialization process (i.e. when $k = 1$ is adopted as an educated guess of the transformer impedance ratios), can lead the online state estimator to an undesired removal of measurements (erroneously flagged as bad data). The influence of this aspect on the proper estimation of the parameters is studied in Section V-E.

D. Initialization and Pseudomeasurement Strategy

The initialization of the iterative process presented in (8) is conducted considering a flat profile, i.e. all the bus voltage magnitudes are set to 1 p.u. and all the bus voltage phase angles are set to 0 deg. For the case of transformer impedance ratios, k, they are set to 1, which is a sensible educated guess according to [4].

Nonetheless, once the algorithm has been run for the first time in a particular grid, the initialization of the transformer impedance ratios can be changed to adopt the estimated parameters provided as an output by the last execution.

As it is analysed in Subsection IV-B, adding new elements to the state vector reduces measurement redundancy. To counteract this fact, a general practice was common in parameter estimation methods: the inclusion of the last available estimates of the suspicious parameters as pseudomeasurements in the problem. This practice can be applied to the case of the estimation of transformer impedance ratios; however, this strategy has been argued as controversial [6], [14]. Certainly, if the system is not observable without the pseudomeasurements, then the parameters become critical and their estimates become equal to the initialization values. On the other hand, if the pseudomeasurements are not critical, but redundant, the arbitrary weights assigned to them can lead to largely biased results. For this reason, transformer impedance ratios have not been included as pseudomeasurements in the present implementation.

It is important to note that, if pseudomeasurements of the estimated parameters are not used, as in the case of the present proposal, initiating the iterative process from a flat start leads to the singularity of the Jacobian matrix at the first iteration. Certainly, all the derivatives with respect to the parameters become zero at this operating point. This problem can be easily counteracted by including the parameters in the state vector only after the first iteration [6]. This is the strategy followed by the authors in the present contribution.

V. Case Studies

A well-tested industrial power system, previously used in [17], has been adopted in these case studies to validate and analyze the proposal. The topology of the network, which includes four tap-changing transformers, together with the voltage levels are depicted in Fig. 5. The specific data of the lines, transformers and loads are summarized in Table I.

In order to generate data for the multi-snapshot scenario, the tap position of the transformers and the value of the loads are randomly assigned at each instant. All the transformers provide a voltage regulating range of $\pm 7\%$, with a regulating step, ΔU, of 1%. Thus, each p.u. turns ratio is calculated at every snapshot according to

$$a = \frac{1}{1 + \Delta U \times I}, \tag{40}$$

with I being a random integer which follows a uniform discrete distribution in the range -7 to $+7$. It is worth mentioning that, according to (2)–(7), at central taps, i.e. $a = 1$, the impedance ratio, k, has no effect on the impedance values of the π-equivalent transformer model. Thus, any snapshot with one or more transformers operating at the central tap positions does not aid in the estimation of the impedance ratio of those particular machines. However, provided that there is not a transformer in the grid permanently connected at the central tap position (i.e. during the T snapshots considered in the problem), the measurement sets include information on every transformer impedance ratio, and thus, all those parameters become observable. The diversity of each snapshot is further guaranteed by assigning random values to each active and reactive power injection. Thus, a random value from a continuous uniform distribution within the range of -50% to $+50\%$ is added to the mean value of each of the loads shown in Table I. In this way, the case studies presented in this section incorporate the possible influence of the variation of

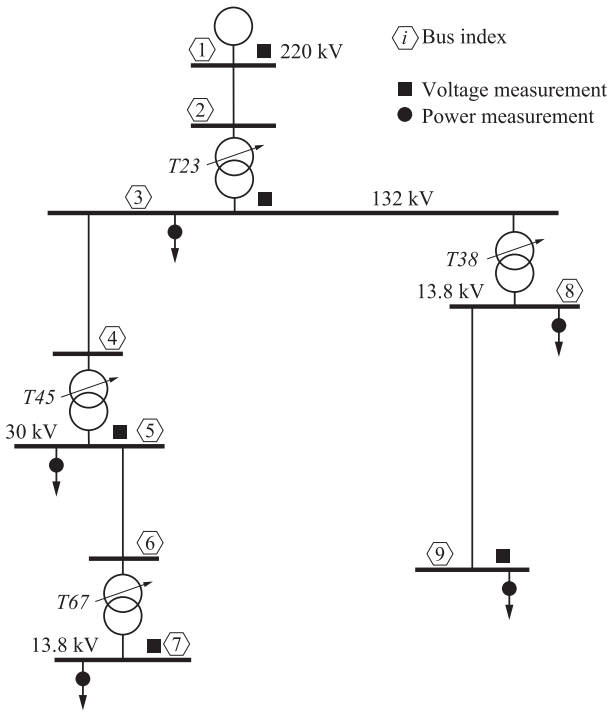

Fig. 5. 9-bus test grid. The specific set of measurements used in the case study shown in Section V-D are highlighted in this figure.

TABLE I
Parameters of the 9-Bus Test Grid

Line Data

From bus	To bus	Length [km]	Impedance [Ω/km]
1	2	4.7	$0.025 + 0.240i$
3	4	1.5	$0.161 + 0.151i$
5	6	0.3	$0.568 + 0.133i$
8	9	1.8	$0.161 + 0.112i$

Transformer Data

No.	a-range[1] [p.u.]	Rating[2] [MVA]	R_{sc} [%]	X_{sc} [%]	k [p.u.]
T23	0.934 : 1.075	2×270	0.90	12.97	0.75
T45	0.934 : 1.075	3×37.5	0.90	8.95	1.25
T67	0.934 : 1.075	10	0.95	4.76	0.70
T38	0.934 : 1.075	3×50	0.92	7.95	1.35

Load Data - Mean values[3]

Bus	P [MW]	Q [Mvar]	Bus	P [MW]	Q [Mvar]
3	84.0	26.0	8	52.0	39.0
5	34.0	12.0	9	1.7	1.5
7	7.5	5.0	–	–	–

[1] Taps are randomly selected within this range.
[2] Preceded by the number of transformers connected in parallel.
[3] Load data are randomly generated around the mean values.

TABLE II
COMPARISON OF ACTUAL AND ESTIMATED IMPEDANCE RATIOS - FULL REDUNDANCY - 20 SNAPSHOTS

Transformer p.u. Impedance Ratios			
No.	k^{AC} [p.u.]	k^{SE} [p.u.]	$\|e\|$ [%]
T23	0.7500	0.7396	1.04
T45	1.2500	1.2471	0.29
T67	0.7000	0.6994	0.06
T38	1.3500	1.3306	1.94

the transformer load level in the performance of the parameter estimation algorithm.

With the aim of emulating the measurement acquisition process, the topological information and assigned values for taps and loads were used to conduct a power flow of the grid for each snapshot. The system states, which were verified with OpenDSS [18], were used to calculate the full set of ideal measurements: bus voltages magnitudes, active and reactive power injections and active and reactive line power flows. Eventually, Gaussian noise was added to these measurements in order to obtain a set of corrupted regular measurements which, together with virtual measurements (from zero injection buses), were included in the SE process. According to [6], sensible values for the standard deviation of the measurements can be selected as $\sigma = 0.1 \cdot \gamma \cdot FS$ for voltage measurements and as $\sigma = \gamma \cdot FS$ for power measurements, where γ stands for the accuracy class of the measurement device and FS stands for the full scale value in accordance with the largest magnitude expected at the respective measurement point. In the present proposal, devices of accuracy class 0.1 according to [19] were considered and, for the sake of simplicity, the value of the corresponding ideal measurement was adopted as the full scale value.

A. Validation of the Proposal

For an initial validation of the proposal, a full redundancy scenario is considered. This includes measurements for bus voltage magnitudes, sending and receiving branch power flows, and power injections at each bus (except for bus 1 that is taken as the slack). According to (38), a redundancy of 3.35 corresponds to this base case. However, considering (39), the inclusion of k parameters in a single-snapshot implementation of the augmented SE problem reduces the redundancy level to 2.71. To recover most of the redundancy of the base case, 20 snapshots are considered in this initial study, which, according to (39), increases its level to 3.31. In this full redundancy scenario, the algorithm converges in 7 iterations using a threshold of $1e-8$ for the maximum absolute value of the state variable deviations, Δx. The conventional state variables, not shown here for space constraints, are found to be very close to the actual values, previously obtained from the power flow analysis. Finally, the estimated values of the transformer p.u. impedance ratios, k^{SE}, are presented in Table II, together with their actual values, k^{AC}, and absolute errors, $|e|$. A maximum absolute error (MAE) of 1.94% and an average absolute error (AAE) of 0.83% allow to demonstrate the validity of the proposal.

TABLE III
COMPARISON OF ESTIMATION ERRORS IN STATE VARIABLES - A) USING AN EDUCATED GUESS, $k_t = 1$, B) USING ESTIMATES OF k_t

	σ^2_{av}	$MAE(V), [\%]$	$MAE(\theta), [deg.]$
Case A	1.2776 e-4	0.0438	0.0449
Case B	0.0106 e-4	0.0078	0.0049

B. Improvement in SE Results

In [4], [5], through several case studies, the advantages of using the new transformer model with an educated guess of $k = 1$, was established. However, as the present proposal allows for the offline estimation of accurate values of transformer p.u. impedance ratios, it is interesting to assess the expected improvement in the accuracy of SE results, as those provided by an online state estimator, as a consequence of this refinement. With this aim, a single snapshot standard WLS augmented matrix state estimator was used to calculate the state variables of the grid in Fig. 5 for the 20 measurement snapshots considered in the previous case study (i.e. the one shown in subSection V-A). This test was carried out with two different setups of the transformer impedance ratios: Case A) uses the educated guess proposed in [4], [5], i.e. all the parameters are assumed as equal to 1; conversely, in Case B) the estimated parameters shown in the 3rd column of Table II were used along the SE process.

As it is highlighted in [4], [5], the errors derived from the use of an inaccurate value of k become more significant at extreme tap positions and are highly dependent on the power factor of the power flow. As the case study reported in subSection V-A uses both load values and tap positions randomly generated, a diverse influence of the errors caused by k is assured. Two figures of merit have been used to assess the comparison: (1) the MAE of bus voltage magnitudes and phase angles with respect to the true state, calculated considering the full set of buses and snapshots, and (2), the average value of the sum of variances over Q snapshots, defined as

$$\sigma^2_{av} = \frac{1}{Q}\sum_{q=1}^{Q}\left[\frac{1}{S}\sum_{s=1}^{S}\left(\hat{x}_{sq} - x_{sq}\right)^2\right], \tag{41}$$

with $\hat{x}_{sq}$ and x_{sq} being the estimated and true state of the s-th state variable of the system at snapshot q, which has been used with this aim in similar studies [20]. The true state of the system was previously obtained for each snapshot by using a power flow algorithm with the true values of k, i.e, those shown in the 2nd column of Table II. The results in Table III show the values of the aforementioned figures of merit.

From Table III, it becomes evident that the errors in the estimated states are significantly reduced with the use of accurate estimates of transformer impedance ratios. This result ensures the practical usefulness of the proposal.

C. Influence of the Number of Snapshots

As it is stated in (39), using a large number of snapshots should return the redundancy of the SE problem close to the one from the base case. However, it is still interesting to analyze if

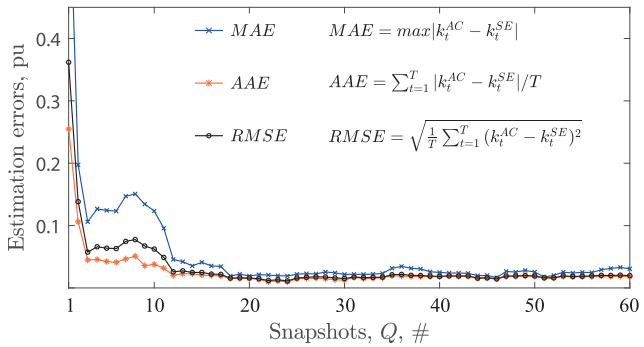

Fig. 6. Estimation errors of transformer impedance ratios vs. number of snapshots - full redundancy.

the quality of the estimates of the transformer impedance ratios keeps improving with the number of snapshots or if, from a certain point, adding more snapshots is not really worthy. This case study is designed to test this specific feature, and for that, the same base case of subSection V-A is used. However, now, the test is repeated with an increasing number of snapshots, Q, ranging from 1 to 60. The quality of these multi-snapshot estimates is assessed by using different figures of merit. Thus, Fig. 6 represents the value of the MAE, AAE and root mean square error (RMSE). The definitions of these figures of merit, in the context of this test, are included in the legend of the figure. Note that k_t^{AC} and k_t^{SE} are the actual and estimated values of p.u. impedance ratios, t, and T being the particular and the total number of transformer impedance ratios to be estimated.

From Fig. 6, it can be concluded that using a very low number of snapshots is not feasible, as Q in ranges from 1 to 11 may lead to gross errors in the estimation of the parameters. On the other hand, the graph shows that these errors decline very fast as new information is included into the problem by increasing the number of snapshots. In this case study, the MAE is always lower than 5% when 12 or more snapshots are included into the problem, and lower than 3.5% if Q is raised to 17. Regarding the RMSE, it is always lower than 5% if at least 11 snapshots are used and lower than 3.5% if more than 12 snapshots are included. Similarly, 9 and 11 snapshots are enough to assure an AAE under 5% and 3.5%, respectively.

It is also interesting to note that, from a certain number of Q, the benefit of adding new snapshots is only marginally significant. Thus, none of the p.u. impedance ratio estimation shows an error higher than 5% (compared with the actual values) when the number of snapshots included in the problem is at least 20. This comparison is presented in Table IV. In any case, a compromise between accuracy and computational burden should be assumed by the user.

D. Influence of the Redundancy Level

An interesting concern related to the utilisation of the proposed methodology, is to analyze the influence of the redundancy level on its capability to provide accurate estimates of the transformer impedance ratios. With this aim, the base case used in Section V-A is downgraded now by removing some of

TABLE IV
COMPARISON OF ACTUAL AND ESTIMATED VALUES - FULL REDUNDANCY - DIFFERENT SNAPSHOTS

Transformer p.u. Impedance Ratios					
		$Q = 20$		$Q = 60$	
No.	k^{AC} [p.u.]	k^{SE} [p.u.]	$\|e\|$ [%]	k^{SE} [p.u.]	$\|e\|$ [%]
T23	0.7500	0.7429	0.71	0.7354	1.46
T45	1.2500	1.2309	1.91	1.2194	3.06
T67	0.7000	0.6812	1.88	0.6889	1.11
T38	1.3500	1.3342	1.57	1.3333	1.67

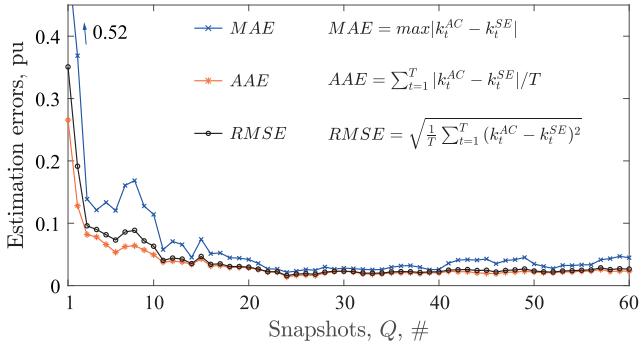

Fig. 7. Estimation errors of transformer impedance ratios vs. number of snapshots - minimum redundancy.

the measurements, down to the point in which the system is just observable with a single snapshot. In this minimum redundancy case study, the 17 state variables and 4 parameters to be estimated in the single snapshot scenario, are obtained from a set of 21 measurements, thus leading, according to (39), to a redundancy level of 1 for a single-snapshot implementation, i.e. $\varepsilon_1 = 1$. Specifically, all the power flow measurements, less common at certain parts of the grid, have been completely removed. On the other hand, 5 of the 9 bus voltage magnitudes as well as the full set of power injection measurements are retained. For the benefit of the reader, the specific set of measurements considered in the problem is depicted in Fig. 5.

The same multi-snapshot analysis previously conducted in Section V-C for the full redundancy case, has been carried out here for the new minimum redundancy scenario. Fig. 7 shows the values of the different figures of merit, i.e. MAE, AAE and RMSE for the different number of snapshots included into the problem, ranging from 1 to 60. Thus, according to (39), the maximum redundancy level considered along the test is limited to $\varepsilon_{60} = 1.23$.

As it can be seen in Fig. 7, a similar pattern to the one derived from the full redundancy scenario is obtained, though slightly higher errors arise in this case. However, it is important to highlight that the convergence ratio of the problem is not deteriorated and not more than 8 iterations are needed to solve the SE for any value of Q. This is an important observation for those parts of the grid where full redundancy is typically far from the reality of standard infrastructures. Specifically, the MAE needs at least 18 snapshots to drop under 5%. For the case of the RMSE, 11 snapshots are needed to go under this error threshold. Finally,

TABLE V
COMPARISON OF ACTUAL AND ESTIMATED VALUES - MINIMUM REDUNDANCY - DIFFERENT SNAPSHOTS

Transformer p.u. Impedance Ratios					
		$Q = 30$		$Q = 60$	
No.	k^{AC} [p.u.]	k^{SE} [p.u.]	$\|e\|$ [%]	k^{SE} [p.u.]	$\|e\|$ [%]
T23	0.7500	0.7735	2.35	0.7626	1.26
T45	1.2500	1.2220	2.80	1.2052	4.48
T67	0.7000	0.6779	2.21	0.6841	1.59
T38	1.3500	1.3324	1.76	1.3301	1.99

just 10 snapshots are enough to reduce the AAE under 5%. Estimations from specific snapshots are presented in Table V for the minimum redundancy case. This allows to conclude that, in order to achieve similar accuracy levels, the user should be aware of including a higher number of snapshots when redundancy is compromised. Indeed, this observation is aligned with the nature of the problem, as fewer information about the system is being provided if this compensation is not conducted.

E. Influence of Bad Data

As it was stated in Section IV-C, the proposed parameter estimation algorithm is designed to work offline, and thus, a conventional online state estimator is responsible for the detection, identification and removal of bad data. However, using inaccurate values of the transformer impedance ratios (as during the initialization process in which an educated guess is used, $k = 1$), can lead the online state estimator to erroneously flag and remove measurements as bad data. The present case study analyses if the removal of these measurements from the data set could have a significant influence on the estimation of transformer impedance ratios by the offline algorithm.

To replicate the performance of an online state estimator, a single snapshot standard WLS augmented matrix algorithm was applied to the 60 snapshots considered in the full redundancy case study analysed in Section V-C. A value of $k = 1$ was assigned to the impedance ratio of each of the four tapped transformers in Fig. 5. The normalized residual test, with a threshold level of 4, was used to detect, identify and remove bad data. The estimation process and bad data test are sequentially repeated until the complete filtering of the input data. As a result, bad data was identified in 28 of the 60 snapshots. Up to a maximum of 4 measurements had to be removed from a single snapshot to reach a set of fully filtered data.

The parameter estimation algorithm proposed in this work was applied to the filtered set of measurements for an increasing number of snapshots (from 1 to 60). Fig. 8 compares the value of the average absolute error of the estimated parameters with those obtained in Section V-C. As can be observed in Fig. 8, the removal of measurements can lead to a slight increase in parameter estimation errors when a low number of snapshots are used as input data. However, this effect is practically obliterated by the addition of more snapshots.

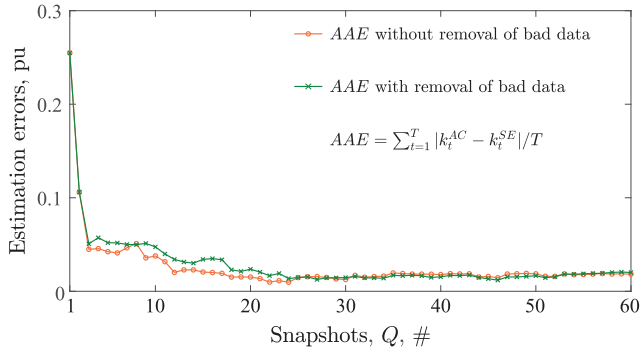

Fig. 8. Estimation errors of transformer impedance ratios vs. number of snapshots - influence of bad data.

It is important to highlight that this situation is only expected during the first execution of the algorithm in a particular grid. Once a realistic approximation to the values of k is available for the online estimator, erroneous bad data detections due to transformer model inaccuracies are not likely to occur. Thus, using a larger number of snapshots during the initialization can be considered a sensible recommendation.

Finally, in a context of lower redundancy, the same pattern shown in Section V-D is expected. Notice that if the removal of bad data causes the loss of observability, the corresponding snapshot would just not be provided by the online estimator, and thus, it will not have any influence on the parameter estimation algorithm.

VI. CONCLUSION

An offline state-vector-augmented parameter estimation method, capable of providing accurate estimates of transformer impedance ratios, is proposed, validated, and analyzed in this work. Moreover, the derivatives of the different measurement functions in terms of the new parameter, which are essential for this or any other linearized state estimator, are provided as a contribution. This study, calls attention to the hindrances found in the estimation of these parameters, such as the significantly lower sensitivity of the measurement functions with respect to p.u. impedance ratios and the reduction of redundancy that their inclusion causes in the state estimation problem. To overcome these difficulties, the authors propose a method based on the use of a multi-snapshots scenario. A set of case studies are presented in order to validate and demonstrate the usefulness of the proposal, including an analysis of the effect of the number of snapshots and the redundancy level on the accuracy of the estimation. They allow to conclude that, a lower number of snapshots, in the range 1 to 10, are not enough to derive accurate results regardless of the redundancy level. However, the inclusion of a higher number of snapshots always allows to reach acceptable estimates. Though a low measurement redundancy level requires a higher number of snapshots to reach the same accuracy, this work demonstrates that even those systems close to the limit of observability can be handled successfully by the proposed algorithm.

REFERENCES

[1] J. D. Glover, M. S. Sarma, and T. Overbye, *Power System Analysis and Design.*, 5th ed., Boston, MA, USA: Cengage Learning, 2012.

[2] Powerworld User's Guide, 2011. [Online]. Available: http://www.powerworld.com.

[3] L. V. Barboza, H. Zurn, and R. Salgado, "Load tap change transformers: A modeling reminder," *IEEE Power Eng. Rev.*, vol. 21, no. 2, pp. 51–52, Feb. 2001.

[4] J. M. Cano, M. R. R. Mojumdar, and G. A. Orcajo, "Reconciling tap-changing transformer models," *IEEE Trans. Power Del.*, vol. 34, no. 6, pp. 2266–2268, Dec. 2019.

[5] J. M. Cano, M. R. R. Mojumdar, and G. A. Orcajo, "On the consistency of tap-changing transformer models in power system studies," in *Proc. IEEE Power Energy Soc. Gen. Meeting*., 2020, pp. 1–5.

[6] A. Abur and A. G. Exposito, *Power System State Estimation: Theory and Implementation*. Boca Raton, FL, USA: CRC Press, 2004.

[7] A. Monticelli, *State Estimation in Electric Power Systems: A Generalized Approach*. Berlin, German: Springer Science & Business Media, 2012.

[8] O. Alsac, N. Vempati, B. Stott, and A. Monticelli, "Generalized state estimation," *IEEE Trans. Power Syst.*, vol. 13, no. 3, pp. 1069–1075, Aug. 1998.

[9] M. Castillo, J. London Jr, and N. Bretas, "Identification and estimation of power system branch parameter error," in *Proc. IEEE Power Energy Soc. Gen. Meeting*, 2009, pp. 1–8.

[10] P. A. Teixeira, S. R. Brammer, W. L. Rutz, W. Merritt, and J. Salmonsen, "State estimation of voltage and phase-shift transformer tap settings," *IEEE Trans. Power Syst.*, vol. 7, no. 3, pp. 1386–1393, Aug. 1992.

[11] Y. Lin and A. Abur, "Enhancing network parameter error detection and correction via multiple measurement scans," *IEEE Trans. Power Syst.*, vol. 32, no. 3, pp. 2417–2425, May 2017.

[12] Y. Lin and A. Abur, "Robust state estimation against measurement and network parameter errors," *IEEE Trans. Power Syst.*, vol. 33, no. 5, pp. 4751–4759, Sep. 2018.

[13] G. N. Korres, P. J. Katsikas, and G. C. Contaxis, "Transformer tap setting observability in state estimation," *IEEE Trans. Power Syst.*, vol. 19, no. 2, pp. 699–706, May 2004.

[14] P. Zarco and A. G. Exposito, "Power system parameter estimation: A survey," *IEEE Trans. Power Syst.*, vol. 15, no. 1, pp. 216–222, Feb. 2000.

[15] F. Aschmoneit, N. Peterson, and E. Adrian, "State estimation with equality constraints," in *Proc. 10th PICA Conf.*, 1977, pp. 427–430.

[16] A. Gjelsvik, S. Aam, and L. Holten, "Hachtel's augmented matrix method-a rapid method improving numerical stability in power system static state estimation," *IEEE Trans. Power App. Syst.*, vol. PAS-104, no. 11, pp. 2987–2993, Nov. 1985.

[17] M. R. R. Mojumdar, J. M. Cano, S. Jaman, and G. A. Orcajo, "Smoothing parameter optimization routine for high-quality a priori estimates in forecasting-aided state estimation," in *Proc. IEEE Power Energy Soc. Gen. Meeting*, 2018, pp. 1–5.

[18] R. C. Dugan and D. Montenegro, "Open distribution system simulator (OpenDSS): Reference guide," *Elect. Power Res. Inst.*, Inc., Knoxville, TN, Jun. 2019. [Online]. Available: https://sourceforge.net/p/electricdss/wiki/Home/

[19] *Electricity Meters, 0.1, 0.2 and 0.5 Accuracy Classes*. ANSI C12. 20.2015, American National Standards Institute, Washington, D.C., Standard, 2015.

[20] S. Chakrabarti, E. Kyriakides, G. Ledwich, and A. Ghosh, "Inclusion of PMU current phasor measurements in a power system state estimator," *IET Gener., Transmiss. Distrib.*, vol. 4, no. 10, pp. 1104–1115, 2010.

Md Rejwanur R. Mojumdar (Graduate Student Member, IEEE) received the Joint M.Sc. degree in 2014 from the Erasmus Mundus Master Course in Sustainable Transportation and Electrical Power Systems (EMMC STEPS). He is currently working toward the Ph.D. degree from the University of Oviedo, Spain. He started as a SCADA Engineer for AREVA T&D. Then he was in several research positions with the University of Oviedo, Spain, University of Stavanger, Norway, and INESC TEC, Portugal. In 2020, he joined the Electrical Control System Department, ABB AS, Norway. His research interests include the state estimation, modeling and algorithms for power management systems, distributed generation and smart grids.

José M. Cano (Senior Member, IEEE) received the M.Sc. and Ph.D. degrees in electrical engineering from the University of Oviedo, Spain, in 1996 and 2000, respectively. In 1996, he joined the Department of Electrical Engineering, University of Oviedo, Spain, where he is currently a Full Professor. During 2012 and 2014, he was a Visiting Associate Professor with the Department of Electrical and Computing Engineering, University of British Columbia, Canada. His main research interests include power quality solutions for industry, power converters, power system state estimation, distributed generation and smart grids.

Gonzalo A. Orcajo (Member, IEEE) was born in Gijón, Spain, in 1965. He received the M.Sc. and Ph.D. degrees in electrical engineering from the University of Oviedo, Spain, in 1990 and 1998, respectively. In 1992, he joined the Department of Electrical Engineering, University of Oviedo, where he is currently an Associate Professor. His main research interests include power quality in industrial power systems. In recent years, he has focused on the detection and location of faults in distribution systems and on reactive power compensation systems.

Step-Voltage Regulator Model Test System

Md Rejwanur Rashid Mojumdar, Pablo Arboleya, *Senior Member, IEEE*
and Cristina González-Morán, *Member, IEEE*

***Abstract*—In this paper, a 4-node test feeder will be proposed as the Step-Voltage Regulator (SVR) model test system. The formulation for modelling a SVR bank consisting on three single phase Type A regulators in raise position will be stated in an extended way. However, the procedure to extend the formulation to any other connection will be also explained, and the results consider all possible connections and types. In the literature, there exist standard systems for testing, comparing and validate power transformers models, like for instance the IEEE 4-node test feeder, but the authors did not found any standardised system for testing and validate SVRs models. Thats why the authors decided to modify the IEEE 4-node test system, embedding into it the SVR models implemented with the well known exact model equations.**

***Index Terms*—4-node test feeder, SVR modelling, conventional power flow results, voltage regulation.**

I. Introduction

MODELING of SVRs possess particular importance in power flow studies of unbalanced distribution networks. The IEEE test feeders of reference [1] were developed, mainly, to provide a set of common data to be used in testing and validation of distribution analysis software. There the 4-node test feeder was developed primarily for the purpose of testing transformer models [2]. There is no such SVR model test system available in literature. Hence, in this paper, the IEEE 4-node test feeder [1] will be modified for SVR model test system.

Kersting's voltage regulator modelings [3], [4] are the major works in matrix-equation based SVR modeling. Those works covered the distribution system SVR modeling in abc reference frame, SVR control mechanism by calculating the compensator R and X settings and other applications of SVRs in distribution systems. Though he did not present all of the configuration but he laid proper baseline for each of them. For this paper, similar matrix equation based models were developed and validated for twenty possible SVR configurations in grounded-wye, closed-delta and three possible open-delta connection with Type A and Type B regulators at both raise and lower position. These models were incorporated in the complex vector based model of unbalanced distribution system in $\alpha\beta 0$ stationary reference frame [5] to solve for conventional power flow results.

Finally, the benchmark conventional power flow result will be presented for all these SVR configurations, serving an unbalanced load, for both at raise and lowering at a fixed tap position of 8 with Type B configurations and at different tap positions with Type A configurations, in the proposed SVR model test system.

The authors are with the Department of Electrical Engineering, University of Oviedo, Gijón, Spain (e-mail: m.r.r.mojumdar@gmail.com; arboleyapablo@uniovi.es; gonzalezmorcristina@uniovi.es).

This work was partially supported by the Spanish Ministry of Science and Innovation under Grant ENE2013-44245-R (MICROHOLO Development of a Holistic and Systematical Approach to AC Microgrids Design and Management).

II. The Regulator Model

Basics of SVRs modeling, equations for single-phase Type A or Type B regulators and possible SVR configurations have been described in [4]. Summarizing in the Table I, the relationships between the source voltage and current to the load voltage and current, for both the Type A and Type B regulators whether in raise or lower:

TABLE I
Generalized Equations for Single-Phase Regulators [4]

Type	Voltage Eq	Current Eq	a_R for Raise	a_R for Lower
A	$V_S = \frac{1}{a_R} V_L$	$I_S = a_R I_L$	$a_R = 1 + \frac{N_2}{N_1}$	$a_R = 1 - \frac{N_2}{N_1}$
B	$V_S = a_R V_L$	$I_S = \frac{1}{a_R} I_L$	$a_R = 1 - \frac{N_2}{N_1}$	$a_R = 1 + \frac{N_2}{N_1}$

No matter how the regulators are connected, the relationships between the series and shunt winding voltages and currents for each single-phase SVR must be satisfied. Here, N_1 and N_2 are the primary and secondary turn number of the single-phase regulators and the value of effective regulator ratio is denoted as a_R.

For an overview of configurations, a closed-delta connected Type A regulator in raise, wye connected Type B regulator in lowering and open-delta connected (case. a) Type B regulator in raise has been presented in Fig. 1, Fig. 2 and Fig. 3 respectively. However, for the basic modeling idea, the model will be presented below, only for closed-delta connected SVR with Type A regulators in raise.

As shown in Fig. 1, three single-phase Type A regulators in raise can be connected in a closed delta, to be used in three-wire delta feeders.

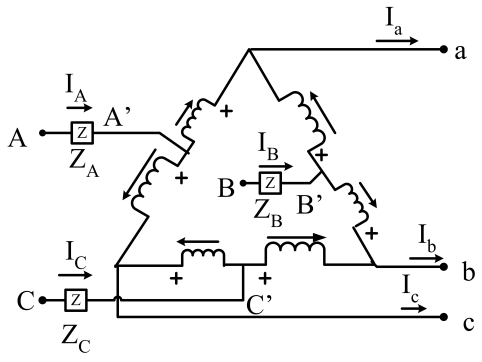

Fig. 1. Closed delta-connected type A regulators in raise

978-1-4673-8040-9/15/$31.00 ©2015 IEEE

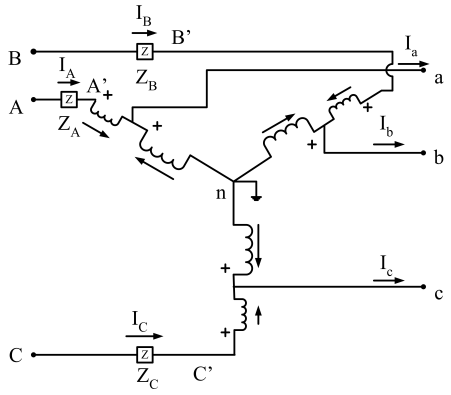

Fig. 2. Wye connected Type B regulators in lowering

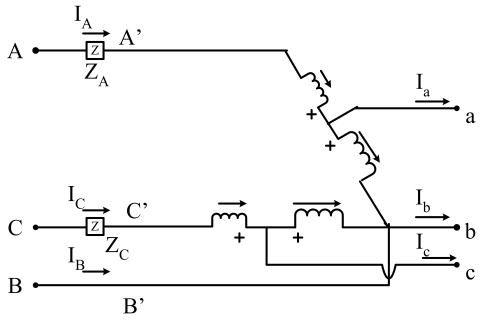

Fig. 3. Open-delta connected (case. a) Type B regulators in raise

A. Voltage Equations

KVL can be applied around a closed loop to obtain equations for the line-to-line voltages. For example, for the line-to-line voltages between phases A and B on the source side refer to the Fig. 1:

$$V_{A'B'} = V_{A'a} + V_{aB'} \tag{1}$$

But, winding voltages can be related in terms of turns ratios:

$$\begin{aligned} V_{A'a} &= \frac{\mathrm{N_2}}{\mathrm{N_1}} V_{cA'} = \frac{\mathrm{N_2}.\mathrm{N_1}}{\mathrm{N_1}.(\mathrm{N_1}+\mathrm{N_2})} V_{ca} \\ &= \frac{\frac{\mathrm{N_2}}{\mathrm{N_1}}}{1+\frac{\mathrm{N_2}}{\mathrm{N_1}}} V_{ca} = \frac{\mathrm{a_{Rca}}-1}{\mathrm{a_{Rca}}} V_{ca} \end{aligned} \tag{2}$$

$$V_{aB'} = \frac{\mathrm{N_1}}{\mathrm{N_1}+\mathrm{N_2}} V_{ab} = \frac{1}{1+\frac{\mathrm{N_2}}{\mathrm{N_1}}} V_{ab} = \frac{1}{\mathrm{a_{Rab}}} V_{ab} \tag{3}$$

Substituting Equations (2) and (3) in (1) and simplify:

$$V_{A'B'} = \frac{1}{\mathrm{a_{Rab}}} V_{ab} + \frac{\mathrm{a_{Rca}}-1}{\mathrm{a_{Rca}}} V_{ca} \tag{4}$$

To determine the relationships between the other line-to-line voltages, the same procedure can be followed and the three-phase voltage equation relating source side and load side without consideration of drop in winding impedances for this regulator configuration will be:

$$\begin{bmatrix} V_{A'B'} \\ V_{B'C'} \\ V_{C'A'} \end{bmatrix} = \begin{bmatrix} \frac{1}{\mathrm{a_{Rab}}} & 0 & \frac{\mathrm{a_{Rca}}-1}{\mathrm{a_{Rca}}} \\ \frac{\mathrm{a_{Rab}}-1}{\mathrm{a_{Rab}}} & \frac{1}{\mathrm{a_{Rbc}}} & 0 \\ 0 & \frac{\mathrm{a_{Rbc}}-1}{\mathrm{a_{Rbc}}} & \frac{1}{\mathrm{a_{Rca}}} \end{bmatrix} \begin{bmatrix} V_{ab} \\ V_{bc} \\ V_{ca} \end{bmatrix} \tag{5}$$

However, the regulator winding impedances can be considered as equal in each phase so that, in a matrix form, they can be denoted as:

$$\mathbf{Z}_{reg} = \begin{pmatrix} Z_{\mathrm{A}} & 0 & 0 \\ 0 & Z_{\mathrm{B}} & 0 \\ 0 & 0 & Z_{\mathrm{C}} \end{pmatrix} = Z \begin{pmatrix} 1 & 0 & 0 \\ 0 & 1 & 0 \\ 0 & 0 & 1 \end{pmatrix} \tag{6}$$

Now, using Equation (6), the voltage drops in the regulator impedances can be expressed as:

$$\begin{bmatrix} V_{AA'} \\ V_{BB'} \\ V_{CC'} \end{bmatrix} = \mathbf{Z}_{reg} \begin{bmatrix} I_A \\ I_B \\ I_C \end{bmatrix} \tag{7}$$

And, let's introduce the $\mathbf{T}_{DY}$ matrix [5] which is a matrix to obtain phase-phase quantities from phase-neutral quantities. But it is a singular matrix. This implies that phase-to-neutral quantities can not be obtained from phase-to-phase voltages. This $\mathbf{T}_{DY}$ matrix as shown in Equation (8) will be used repeatedly for other configurations also.

$$\mathbf{T}_{DY} = \begin{pmatrix} 1 & -1 & 0 \\ 0 & 1 & -1 \\ -1 & 0 & 1 \end{pmatrix} \tag{8}$$

Now, in the next equation, per phase voltage drops in the regulator impedances are related to the phase-to-phase voltages in the primary side of the regulator [5]:

$$\begin{bmatrix} V_{AB} - V_{A'B'} \\ V_{BC} - V_{B'C'} \\ V_{CA} - V_{C'A'} \end{bmatrix} = \begin{bmatrix} V_{AA'} - V_{BB'} \\ V_{BB'} - V_{CC'} \\ V_{CC'} - V_{AA'} \end{bmatrix} = \mathbf{T}_{DY} \begin{bmatrix} V_{AA'} \\ V_{BB'} \\ V_{CC'} \end{bmatrix} \tag{9}$$

Combining (5), (7) and (9) the relationship between primary voltages, secondary voltages and primary line currents can be written as:

$$\begin{bmatrix} V_{AB} \\ V_{BC} \\ V_{CA} \end{bmatrix} = \mathbf{T}_{DY}\mathbf{Z}_{reg} \begin{bmatrix} I_A \\ I_B \\ I_C \end{bmatrix} + \begin{bmatrix} \frac{1}{\mathrm{a_{Rab}}} & 0 & \frac{\mathrm{a_{Rca}}-1}{\mathrm{a_{Rca}}} \\ \frac{\mathrm{a_{Rab}}-1}{\mathrm{a_{Rab}}} & \frac{1}{\mathrm{a_{Rbc}}} & 0 \\ 0 & \frac{\mathrm{a_{Rbc}}-1}{\mathrm{a_{Rbc}}} & \frac{1}{\mathrm{a_{Rca}}} \end{bmatrix} \begin{bmatrix} V_{ab} \\ V_{bc} \\ V_{ca} \end{bmatrix} \tag{10}$$

B. Current Equations

Applying KCL at the load side terminal a:

$$I_a = I_{A'a} + I_{B'a} \tag{11}$$

But as:

$$I_A = I_{A'c} + I_{A'a} = \frac{\mathrm{N_2}}{\mathrm{N_1}} I_{A'a} + I_{A'a} = (1 + \frac{\mathrm{N_2}}{\mathrm{N_1}}) I_{A'a} \tag{12}$$

So that:

$$I_{A'a} = \frac{1}{1+\frac{\mathrm{N_2}}{\mathrm{N_1}}} I_A = \frac{1}{\mathrm{a_{Rca}}} I_A \tag{13}$$

Again as:

$$I_B = I_{B'a} + I_{B'b} = \frac{\mathrm{N_1}}{\mathrm{N_2}} I_{B'a} + I_{B'a} = (1 + \frac{\mathrm{N_1}}{\mathrm{N_2}}) I_{B'a} \tag{14}$$

Again so:

$$I_{B'a} = \frac{1}{(1+\frac{N_1}{N_2})} I_B = \frac{\frac{N_2}{N_1}}{1+\frac{N_2}{N_1}} I_B = \frac{a_{Rab}-1}{a_{Rab}} I_B \quad (15)$$

Substituting Equations (13) and (15) into Equation (11):

$$I_a = \frac{1}{a_{Rca}} I_A + \frac{a_{Rab}-1}{a_{Rab}} I_B \quad (16)$$

Following same procedure at the other two load side terminals, for this configuration, three-phase equation between source and load line currents can be obtained as:

$$\begin{bmatrix} I_a \\ I_b \\ I_c \end{bmatrix} = \begin{bmatrix} \frac{1}{a_{Rca}} & \frac{a_{Rab}-1}{a_{Rab}} & 0 \\ 0 & \frac{1}{a_{Rab}} & \frac{a_{Rbc}-1}{a_{Rbc}} \\ \frac{a_{Rca}-1}{a_{Rca}} & 0 & \frac{1}{a_{Rbc}} \end{bmatrix} \begin{bmatrix} I_A \\ I_B \\ I_C \end{bmatrix} \quad (17)$$

C. Generalized Equations

We can denote, $\mathbf{A_{R\text{-}KVL}}_{-04}$ and $\mathbf{A_{R\text{-}KCL}}_{-04}$ matrices for closed delta connection with Type A regulators both in raise position and lower position as:

$$\mathbf{A_{R\text{-}KVL}}_{-04} = \begin{bmatrix} \frac{1}{a_{Rab}} & 0 & \frac{a_{Rca}-1}{a_{Rca}} \\ \frac{a_{Rab}-1}{a_{Rab}} & \frac{1}{a_{Rbc}} & 0 \\ 0 & \frac{a_{Rbc}-1}{a_{Rbc}} & \frac{1}{a_{Rca}} \end{bmatrix} \quad (18)$$

$$\mathbf{A_{R\text{-}KCL}}_{-04} = \begin{bmatrix} \frac{1}{a_{Rca}} & \frac{a_{Rab}-1}{a_{Rab}} & 0 \\ 0 & \frac{1}{a_{Rab}} & \frac{a_{Rbc}-1}{a_{Rbc}} \\ \frac{a_{Rca}-1}{a_{Rca}} & 0 & \frac{1}{a_{Rbc}} \end{bmatrix} \quad (19)$$

In the similar structure, all other SVR configurations were modeled. Therefore, denoting $\mathbf{A_{R\text{-}KVL}}$ matrices for voltage equations and $\mathbf{A_{R\text{-}KCL}}$ matrices for current equations of each connections and expressing three-phase voltage and branch current in short form, we can express Equations like (10) and (17) in very compact form.

Finally, by observing all the models, there was only one structure of the general current equation for all the configurations which is:

$$\left[\boldsymbol{I}_{Br}\right]^S_{abc} = \mathbf{A_{R\text{-}KCL}} \left[\boldsymbol{I}_{Br}\right]^P_{abc} \quad (20)$$

But there are two structures of the general voltage equation. For all the wye configurations:

$$\left[\boldsymbol{V}_{ph-n}\right]^P_{abc} = \mathbf{Z}_{reg} \left[\boldsymbol{I}_{Br}\right]^P_{abc} + \mathbf{A_{R\text{-}KVL}} \left[\boldsymbol{V}_{ph-n}\right]^S_{abc} \quad (21)$$

For all closed and open delta configurations:

$$\left[\boldsymbol{V}_{ph-ph}\right]^P_{abc} = \mathbf{T}_{DY}\mathbf{Z}_{reg} \left[\boldsymbol{I}_{Br}\right]^P_{abc} + \mathbf{A_{R\text{-}KVL}} \left[\boldsymbol{V}_{ph-ph}\right]^S_{abc} \quad (22)$$

D. Incorporation and Simulation

Generalized voltage and current equations developed in the regulator models were incorporated as linear equations in the complex vector based model of unbalanced distribution system in $\alpha\beta 0$ stationary reference frame [5]. Then, other non-linear equations were also included in the the power flow problem. Finally, each power flow problem with different SVR configurations, was simulated using 'FSOLVE' function of MATLAB® to solve all linear or non-linear equations to provide the benchmark conventional power flow results.

III. The Test System

The system to be used in testing SVR models is proposed and shown in Fig. 4.

A. Line Configuration

We propose, the line segment on the source side and the line segment on the load side of the regulator bank will have the configuration 601 of proposed IEEE 13-node test feeder at [1]. Like other line configurations in that 13-node test feeder (Configurations 601 - 607) with single or multiple laterals, configuration 601 is provided in the form derived after following modified Carson's equation [4] and corresponding Kron reduction [4]. Finally, (3×3) phase frame matrice of configuration 601 will be used. And the phase impedance of configuration 601, $\mathbf{Z}_{abc}$ in Ω /mile is:

$$\mathbf{Z}_{abc} = \begin{bmatrix} 0.4572 + j1.0791 & 0.1556 + j0.5027 & 0.1531 + j0.3860 \\ 0.1556 + j0.5027 & 0.4663 + j1.0492 & 0.1577 + j0.4247 \\ 0.1531 + j0.3860 & 0.1577 + j0.4247 & 0.4611 + j1.0661 \end{bmatrix} \quad (23)$$

B. Regulator Impedance

And the regulator winding impedance, $\mathbf{Z}_{reg}$ in Ω, used for the results is:

$$\mathbf{Z}_{reg} = \begin{bmatrix} 0.00768 + j0.2304 & 0 + j0 & 0 + j0 \\ 0 + j0 & 0.00768 + j0.2304 & 0 + 0 \\ 0 + j0 & 0 + j0 & 0.00768 + j0.2304 \end{bmatrix} \quad (24)$$

It's important to note that, for the regulator with three possible open delta connections, corresponding phasing impedance were taken out from the $\mathbf{Z}_{reg}$ mentioned here. Specifically, Z_{B} for case a, Z_{C} for case b and Z_{A} for case c will be zero (0) in the $\mathbf{Z}_{reg}$ of three cases of open delta configurations.

C. Unbalanced Loads and Generations

For the benchmark power flow results presented in the following section, the unbalanced load profile used at node 4 of Fig. 4 was:

TABLE VI
Unbalanced Load Data for Test Results

Phase-1			Phase-2			Phase-3		
kW	kVar	p.f	kW	kVar	p.f	kW	kVar	p.f
50	16.43	0.95	26	12.59	0.9	37	15.76	0.92

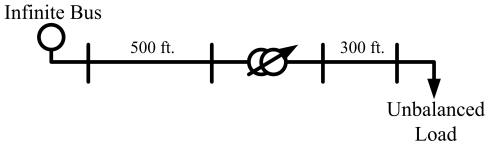

Fig. 4. 4-node test feeder with regulator.

TABLE II
TYPE B IN RAISE REGULATORS (TAPS AT 8)

Connection	Gnd-Y	Cld-Delta	Op-Delta-a	Op-Delta-b	Op-Delta-c
Taps	[8 8 8]	[8 8 8]	[8 8 −]	[− 8 8]	[8 − 8]
Voltage Node-2					
V_1	$391.6\angle -1.2\,^\circ$	$391.9\angle -1.2\,^\circ$	$389.9\angle -0.3\,^\circ$	$398.6\angle -0.3\,^\circ$	$384.5\angle -3.2\,^\circ$
V_2	$399.5\angle -120.3\,^\circ$	$399\angle -120.3\,^\circ$	$391.3\angle -121.6\,^\circ$	$393.7\angle -119.7\,^\circ$	$401.3\angle -120.4\,^\circ$
V_3	$392.7\angle 119.5\,^\circ$	$392.8\angle 119.5\,^\circ$	$401.5\angle 118.9\,^\circ$	$387\angle 117.4\,^\circ$	$391\angle 120.1\,^\circ$
Voltage Node-3					
V_1	$398.9\angle -5.6\,^\circ$	$408.8\angle -2.8\,^\circ$	$396\angle -4.9\,^\circ$	$577.7\angle -23.6\,^\circ$	$404.8\angle -3.2\,^\circ$
V_2	$411.8\angle -122.4\,^\circ$	$420.6\angle -119.9\,^\circ$	$411.9\angle -121.6\,^\circ$	$404.1\angle -122.1\,^\circ$	$229.5\angle -129.1\,^\circ$
V_3	$401.6\angle 116.3\,^\circ$	$412.1\angle 118.8\,^\circ$	$363.9\angle 148.3\,^\circ$	$407.4\angle 117.4\,^\circ$	$398.1\angle 116.5\,^\circ$
Voltage Node-4					
V_1	$394.6\angle -6.4\,^\circ$	$404.6\angle -3.5\,^\circ$	$391.8\angle -5.5\,^\circ$	$574.7\angle -23.9\,^\circ$	$400.6\angle -3.7\,^\circ$
V_2	$411.6\angle -122.6\,^\circ$	$420.3\angle -120.1\,^\circ$	$410.3\angle -121.8\,^\circ$	$402.2\angle -122.4\,^\circ$	$226.1\angle -129.9\,^\circ$
V_3	$397.6\angle 116\,^\circ$	$408.2\angle 118.5\,^\circ$	$360.5\angle 147.8\,^\circ$	$404.5\angle 117\,^\circ$	$395.2\angle 116.1\,^\circ$
Current I_{1-2}					
I_a	$140.4\angle -24.6\,^\circ$	$139.4\angle -23.8\,^\circ$	$141.4\angle -23.7\,^\circ$	$96.4\angle -42.1\,^\circ$	$298.9\angle -12.5\,^\circ$
I_b	$73.9\angle -148.4\,^\circ$	$76.5\angle -150.5\,^\circ$	$163.8\angle -139.4\,^\circ$	$75.6\angle -148.2\,^\circ$	$134.5\angle -155.7\,^\circ$
I_c	$106.5\angle 92.9\,^\circ$	$105.4\angle 93.5\,^\circ$	$117.4\angle 124.7\,^\circ$	$236.8\angle 103.6\,^\circ$	$107.1\angle 93\,^\circ$
Current I_{3-4}					
I_a	$133.4\angle -24.6\,^\circ$	$130.1\angle -21.7\,^\circ$	$134.3\angle -23.7\,^\circ$	$91.6\angle -42.1\,^\circ$	$131.4\angle -21.9\,^\circ$
I_b	$70.2\angle -148.4\,^\circ$	$68.7\angle -145.9\,^\circ$	$70.4\angle -147.6\,^\circ$	$71.8\angle -148.2\,^\circ$	$127.8\angle -155.7\,^\circ$
I_c	$101.2\angle 92.9\,^\circ$	$98.5\angle 95.5\,^\circ$	$111.5\angle 124.7\,^\circ$	$99.4\angle 94\,^\circ$	$101.8\angle 93\,^\circ$

TABLE III
TYPE B IN LOWER REGULATORS (TAPS AT 8)

Connection	Gnd-Y	Cld-Delta	Op-Delta-a	Op-Delta-b	Op-Delta-c
Taps	[8 8 8]	[8 8 8]	[8 8 −]	[− 8 8]	[8 − 8]
Voltage Node-2					
V_1	$391.6\angle -1.2\,^\circ$	$391.3\angle -1.2\,^\circ$	$389.8\angle -0.3\,^\circ$	$398.6\angle -0.3\,^\circ$	$384.5\angle -3.2\,^\circ$
V_2	$399.5\angle -120.3\,^\circ$	$400\angle -120.3\,^\circ$	$3913\angle -121.6\,^\circ$	$393.7\angle -119.7\,^\circ$	$401.3\angle -120.4\,^\circ$
V_3	$392.6\angle 119.5\,^\circ$	$392.4\angle 119.6\,^\circ$	$401.4\angle 118.8\,^\circ$	$387\angle 117.4\,^\circ$	$391\angle 120.1\,^\circ$
Voltage Node-3					
V_1	$360.7\angle -5.7\,^\circ$	$351.4\angle -8.2\,^\circ$	$358.2\angle -5\,^\circ$	$522.7\angle -23.7\,^\circ$	$366.2\angle -3.2\,^\circ$
V_2	$372.6\angle -122.4\,^\circ$	$364.1\angle -124.7\,^\circ$	$372.7\angle -121.6\,^\circ$	$365.6\angle -122.1\,^\circ$	$207.9\angle -129.1\,^\circ$
V_3	$363.3\angle 116.3\,^\circ$	$352.6\angle 114\,^\circ$	$328.7\angle 148.3\,^\circ$	$368.6\angle 117.4\,^\circ$	$360.1\angle 116.5\,^\circ$
Voltage Node-4					
V_1	$356\angle -6.6\,^\circ$	$346.5\angle -9.2\,^\circ$	$353.5\angle -5.7\,^\circ$	$519.4\angle -24\,^\circ$	$361.5\angle -3.8\,^\circ$
V_2	$372.4\angle -122.6\,^\circ$	$363.9\angle -124.9\,^\circ$	$370.9\angle -121.8\,^\circ$	$363.5\angle -122.5\,^\circ$	$204.1\angle -130\,^\circ$
V_3	$358.8\angle 115.9\,^\circ$	$348\angle 113.6\,^\circ$	$325\angle 147.7\,^\circ$	$365.3\angle 116.9\,^\circ$	$356.9\angle 116\,^\circ$
Current I_{1-2}					
I_a	$140.8\angle -24.8\,^\circ$	$142.2\angle -25.6\,^\circ$	$141.8\angle -23.8\,^\circ$	$96.5\angle -42.2\,^\circ$	$299.7\angle -12.6\,^\circ$
I_b	$73.9\angle -148.5\,^\circ$	$71.9\angle -146.3\,^\circ$	$164\angle -139.5\,^\circ$	$75.7\angle -148.3\,^\circ$	$134.8\angle -155.8\,^\circ$
I_c	$106.7\angle 92.9\,^\circ$	$108.2\angle 92\,^\circ$	$117.9\angle 124.6\,^\circ$	$237.2\angle 103.5\,^\circ$	$107.3\angle 92.9\,^\circ$
Current I_{3-4}					
I_a	$147.9\angle -24.8\,^\circ$	$151.9\angle -27.4\,^\circ$	$148.9\angle -23.8\,^\circ$	$101.3\angle -42.2\,^\circ$	$145.6\angle -22\,^\circ$
I_b	$77.6\angle -148.5\,^\circ$	$79.4\angle -150.7\,^\circ$	$77.9\angle -147.7\,^\circ$	$79.5\angle -148.3\,^\circ$	$141.5\angle -155.8\,^\circ$
I_c	$112.1\angle 92.9\,^\circ$	$115.6\angle 90.5\,^\circ$	$123.8\angle 124.6\,^\circ$	$110.1\angle 93.9\,^\circ$	$112.7\angle 92.9\,^\circ$

IV. VALIDATION OF THE PORPOSED FORMULATION

At [4], Kersting developed regulator models for a number of configurations at abc reference frame. In this paper the author proposed and alternative formulation based in $\alpha\beta 0$ reference frame. The two formulations represent exact equivalent models, so the authors used the original formulation to validate the proposed one. Once the results using the $\alpha\beta 0$ based formulation were obtained, they were transformed to abc reference and compared with those obtained directly from the original formulation. In all cases, the solutions were exactly the same as it was expected.

V. BENCHMARK POWER FLOW RESULTS FOR SVRS

In tables II and III, the obtained results for type B regulators in raise and lower positions are shown. In both cases, the tap position is set to 8 and the considered configurations were Grounded-Wye, Closed-Delta and Open-Delta considering the three different possibilities - connection with regulators between phases AB and CB, between BC and AC and finally between CA and BA which are denoted as case a, case b and case c connection respectively. In tables IV and V, the results are represented for all type A regulator connections, however, in different tap positions at different single-phase regulators.

It's worth mentioning that, for three wire delta configurations, the voltages in results provided here are phase-phase

TABLE IV
CASE C TEST RESULTS: TYPE A IN RAISE REGULATORS (TAPS AT DIFFERENT POSITIONS)

Connection	Gnd-Y	Cld-Delta	Op-Delta-a	Op-Delta-b	Op-Delta-c
Optimum Taps	[9 4 8]	[6 2 7]	[10 4 −]	[− 7 6]	[7 − 9]
Voltage Node-2					
V_1	$391.6\angle -1.2\,^\circ$	$391.5\angle -1.1\,^\circ$	$390\angle -0.3\,^\circ$	$398.6\angle -0.3\,^\circ$	$384.3\angle -3.2\,^\circ$
V_2	$399.5\angle -120.3\,^\circ$	$399.1\angle -120.3\,^\circ$	$390.4\angle -121.6\,^\circ$	$393.7\angle -119.7\,^\circ$	$401.3\angle -120.4\,^\circ$
V_3	$392.7\angle 119.5\,^\circ$	$393.2\angle 119.5\,^\circ$	$401.5\angle 118.9\,^\circ$	$386.9\angle 117.4\,^\circ$	$391\angle 120.1\,^\circ$
Voltage Node-3					
V_1	$400.3\angle -5.6\,^\circ$	$401.3\angle -7.7\,^\circ$	$399.8\angle -4.9\,^\circ$	$570.1\angle -23.9\,^\circ$	$401.1\angle -3.2\,^\circ$
V_2	$401\angle -122.4\,^\circ$	$401\angle -124.5\,^\circ$	$400.1\angle -121.6\,^\circ$	$400.7\angle -122.1\,^\circ$	$228.3\angle -129.7\,^\circ$
V_3	$400.6\angle 116.3\,^\circ$	$401.4\angle 115.5\,^\circ$	$367.9\angle 146.9\,^\circ$	$401.4\angle 117.4\,^\circ$	$399.5\angle 116.6\,^\circ$
Voltage Node-4					
V_1	$396\angle -6.4\,^\circ$	$397\angle -8.4\,^\circ$	$395.7\angle -5.5\,^\circ$	$567\angle -24.2\,^\circ$	$396.9\angle -3.7\,^\circ$
V_2	$400.7\angle -122.6\,^\circ$	$400.6\angle -124.6\,^\circ$	$398.4\angle -121.8\,^\circ$	$398.8\angle -122.4\,^\circ$	$224.8\angle -130.4\,^\circ$
V_3	$396.6\angle 116\,^\circ$	$397.5\angle 115.2\,^\circ$	$364.6\angle 146.4\,^\circ$	$398.4\angle 117\,^\circ$	$396.6\angle 116.1\,^\circ$
Current I_{1-2}					
I_a	$140.4\angle -24.6\,^\circ$	$139.9\angle -25.6\,^\circ$	$141.3\angle -23.6\,^\circ$	$96.3\angle -42.4\,^\circ$	$300.3\angle -12.9\,^\circ$
I_b	$73.9\angle -148.4\,^\circ$	$75.4\angle -149.5\,^\circ$	$170.3\angle -142.3\,^\circ$	$75.6\angle -148.2\,^\circ$	$134.1\angle -156.2\,^\circ$
I_c	$106.5\angle 92.9\,^\circ$	$105.3\angle 95\,^\circ$	$113.1\angle 123.3\,^\circ$	$237.3\angle 103.4\,^\circ$	$107.1\angle 93.1\,^\circ$
Current I_{3-4}					
I_a	$132.9\angle -24.6\,^\circ$	$132.6\angle -26.6\,^\circ$	$133\angle -23.6\,^\circ$	$92.8\angle -42.4\,^\circ$	$132.6\angle -21.9\,^\circ$
I_b	$72.1\angle -148.4\,^\circ$	$72.1\angle -150.5\,^\circ$	$72.5\angle -147.6\,^\circ$	$72.4\angle -148.2\,^\circ$	$128.5\angle -156.2\,^\circ$
I_c	$101.4\angle 92.9\,^\circ$	$101.2\angle 92.1\,^\circ$	$110.3\angle 123.3\,^\circ$	$100.9\angle 94\,^\circ$	$101.4\angle 93.1\,^\circ$

TABLE V
CASE C TEST RESULTS: TYPE A IN LOWER REGULATORS (TAPS AT DIFFERENT POSITIONS)

Connection	Gnd-Y	Cld-Delta	Op-Delta-a	Op-Delta-b	Op-Delta-c
Optimum Taps	[1 6 2]	[3 7 1]	[1 7 −]	[− 1 2]	[1 − 5]
Voltage Node-2					
V_1	$391.6\angle -1.2\,^\circ$	$391.5\angle -1.2\,^\circ$	$390\angle -0.3\,^\circ$	$398.6\angle -0.3\,^\circ$	$384.1\angle -3.2\,^\circ$
V_2	$399.5\angle -120.3\,^\circ$	$399.2\angle -120.3\,^\circ$	$390.3\angle -121.6\,^\circ$	$393.7\angle -119.7\,^\circ$	$401.3\angle -120.4\,^\circ$
V_3	$392.7\angle 119.5\,^\circ$	$393.1\angle 119.5\,^\circ$	$401.5\angle 118.9\,^\circ$	$386.9\angle 117.4\,^\circ$	$391\angle 120.1\,^\circ$
Voltage Node-3					
V_1	$376.5\angle -5.6\,^\circ$	$369.6\angle -5.4\,^\circ$	$373.8\angle -4.9\,^\circ$	$542.7\angle -24\,^\circ$	$374.5\angle -3.2\,^\circ$
V_2	$376.6\angle -122.4\,^\circ$	$369.5\angle -121.5\,^\circ$	$373.2\angle -121.6\,^\circ$	$381.5\angle -122.1\,^\circ$	$213.8\angle -130\,^\circ$
V_3	$376.7\angle 116.3\,^\circ$	$370.8\angle 118.4\,^\circ$	$343.8\angle 146.8\,^\circ$	$382.1\angle 117.4\,^\circ$	$375.8\angle 116.6\,^\circ$
Voltage Node-4					
V_1	$371.9\angle -6.5\,^\circ$	$364.9\angle -6.3\,^\circ$	$369.4\angle -5.5\,^\circ$	$539.4\angle -24.3\,^\circ$	$370\angle -3.8\,^\circ$
V_2	$376.2\angle -122.6\,^\circ$	$369.1\angle -121.7\,^\circ$	$371.4\angle -121.8\,^\circ$	$379.5\angle -122.4\,^\circ$	$210.1\angle -130.8\,^\circ$
V_3	$372.5\angle 116\,^\circ$	$366.6\angle 118\,^\circ$	$340.2\angle 146.3\,^\circ$	$378.9\angle 117\,^\circ$	$372.7\angle 116.1\,^\circ$
Current I_{1-2}					
I_a	$140.6\angle -24.7\,^\circ$	$142.5\angle -24.9\,^\circ$	$141.6\angle -23.7\,^\circ$	$96.3\angle -42.5\,^\circ$	$301.6\angle -13.3\,^\circ$
I_b	$73.9\angle -148.5\,^\circ$	$74.7\angle -150.8\,^\circ$	$170.9\angle -142.6\,^\circ$	$75.6\angle -148.3\,^\circ$	$134\angle -156.7\,^\circ$
I_c	$106.6\angle 92.9\,^\circ$	$104.5\angle 94.6\,^\circ$	$113\angle 123.2\,^\circ$	$237.6\angle 103.3\,^\circ$	$107.2\angle 93\,^\circ$
Current I_{3-4}					
I_a	$141.5\angle -24.7\,^\circ$	$144.2\angle -24.5\,^\circ$	$142.5\angle -23.7\,^\circ$	$97.6\angle -42.5\,^\circ$	$142.2\angle -22\,^\circ$
I_b	$76.8\angle -148.5\,^\circ$	$78.3\angle -147.6\,^\circ$	$77.8\angle -147.7\,^\circ$	$76.1\angle -148.3\,^\circ$	$137.5\angle -156.7\,^\circ$
I_c	$108\angle 92.9\,^\circ$	$109.7\angle 95\,^\circ$	$118.2\angle 123.2\,^\circ$	$106.1\angle 93.9\,^\circ$	$107.9\angle 93\,^\circ$

and for four wire wye configurations, they are phase-neutral.

VI. CONCLUSIONS

The IEEE 4-node test feeder has been modified and adapted to test Step-Voltage Regulators (SVR). As an example, the extended formulation was presented for closed-delta connected SVR with Type A regulators in raise. Due to the lack of space the formulation was not extended for other types of SVR. However, the guidelines for obtaining other types of SVR with different connections were also presented. In the benchmark section the results for 20 different SVR types with different connections were presented. In further works, the proposed formulation will be used for analyse large low voltage distribution networks.

REFERENCES

[1] *Distribution Test Feeders: http://ewh.ieee.org/soc/pes/dsacom/testfeeders/*, IEEE PES Distribution System Analysis Subcommittee's. Distribution Test Feeder Working Group Std.

[2] W. H. Kersting, "Transformer model test system," in *Transmission and Distribution Conference and Exposition, 2003 IEEE PES*, vol. 3. IEEE, 2003, pp. 1022–1026.

[3] W. Kersting, "The modeling and application of step voltage regulators," in *Power Systems Conference and Exposition, 2009. PSCE'09. IEEE/PES*. IEEE, 2009, pp. 1–8.

[4] W. H. Kersting, *Distribution system modeling and analysis*. CRC press, 2012.

[5] P. Arboleya, C. Gonzalez-Moran, and M. Coto, "Unbalanced power flow in distribution systems with embedded transformers using the complex theory in $\alpha\beta 0$ stationary reference frame," *Power Systems, IEEE Transactions on*, vol. 29, no. 3, pp. 1012–1022, May 2014.

Electrical Power and Energy Systems 94 (2018) 245–255

Contents lists available at ScienceDirect

Electrical Power and Energy Systems

journal homepage: www.elsevier.com/locate/ijepes

4-Node Test Feeder with Step Voltage Regulators ☆

Cristina González-Morán *, Pablo Arboleya, Rejwan R. Mojumdar, Bassam Mohamed

Department of Electrical Engineering, University of Oviedo, Spain

ARTICLE INFO

Article history:
Received 26 January 2017
Received in revised form 14 June 2017
Accepted 23 June 2017
Available online 27 July 2017

Keywords:
Distribution System Analysis
Forward-backward sweep
Power transformers
Step Voltage Regulators
Unbalanced operation

ABSTRACT

This work has two main contributions; First, the development of a general, exact and standardized Step Voltage Regulator model considering all possible configurations and second, the proposal of a 4-Node Test System for testing and evaluation of three-phase Step Voltage Regulator connections. Although the 4-Node Test Feeder for testing three phase transformer configurations is already available in the literature, there is not such model for the inclusion, testing and validation of Step Voltage Regulators in a test feeder. With the work presented in this paper, a new test system will be available to evaluate and benchmark programs or algorithms that attempt to include different configurations of Step Voltage Regulators. The formulation is stated for all three phase Step Voltage Regulators; i.e. wye, close-delta and open-delta connections, both type A and B regulators, in raise or lower positions. Then, all these models are included in a 4-Node Test Feeder to obtain several power flow solutions. All obtained results will be available for power flow software developers on-line.

1. Introduction

Step Voltage Regulators (SVRs) have been employed in power feeders for many decades [1–4]. Its modeling posses particular importance in power flow studies of unbalanced distribution networks [5–7] and is gaining even more importance in distribution feeders with the proliferation of Distributed Generation (DG) [8]; several voltage control possibilities can be achieved by coordinating the small generators and storage units installed near customers and the well-known switched capacitors and step voltage regulators [9]. As an example, the authors in [10] proposed a coordinated control of energy storage systems with SVRs to mitigate the voltage rise caused for high penetration levels of photovoltaic systems. Similar applications can be found in [11] or [12]; In both works the combination of SVRs, Static VAR Compensators (SVC) and Shunt Capacitors (SC) are applied to achieve voltage control in distribution feeders including DG. In [13] the control schedules of SVRs are updated according to wind power predictions to compensate voltage variations derived form high penetration of wind power plants. Many other works related to coordination of SVRs in distributed systems with DG can be found in the literature [14–17]. In [14] a voltage estimation is used to control over-voltages in residential networks with varying PV penetrations. In [15] the authors coordinate the location of reactive power injections from the PV inverters with transformer tap positions in a distributed system as a way to constrain voltage variations. In [16] an unbalanced power flow is used to obtain the influence of SVRs and DGs penetrations in power losses and voltage profiles. In [17] several voltage control techniques; On Load Tap Changers (OLTC), SVR, SC, Shunt Reactor (ShR), and SVC are optimally controlled in coordination with DG.

In [18] a robust, low-cost and high-efficiency voltage regulator is designed for rural networks with serial voltage compensation. In [19] the authors propose distributed voltage control for multiple voltage regulation devices; on-load tap changers, step voltage regulators and switched capacitors in the presence of PV. They tested the scheme in a medium voltage feeder in California. In [20] detailed models for open-delta connected SVR are presented. The authors developed a bus admittance model suitable for unbalanced power flow studies.

Regarding the optimization of tap positions, in [21] an algorithm to set the positions of regulating transformers is proposed. The algorithm is valid for unbalanced and distributed systems. In [22], the authors propose a linear power flow formulation to optimally configure a distribution system using, among other control variables, the tap positions in voltage regulators. In [23], also the tap positions of transformers are included as optimization variables.

☆ This work has been supported by the Research, Technological Development and Innovation Program Oriented to the Society Challenges of the Spanish Ministry or Economy and Competitiveness under Grant ENE 2013-44245-R.

* Corresponding author.
E-mail address: gonzalezmorcristina@uniovi.es (C. González-Morán).
URLs: http://cristina.dieecs.com/contact (C. González-Morán), http://arboleya.dieecs.com (P. Arboleya).

http://dx.doi.org/10.1016/j.ijepes.2017.06.027
0142-0615/

Directly related to SVR modeling, we can find the work in [24], in which there is a brief description of a SVR model to be included in an unbalanced power flow formulation based on the current injection method. In [25] the authors are capable of designing dynamic SVRs, but they considered a single phase model. From their point of view, this model can be used into a 3 phase system taking into account that each phase works separately, so they do not considered closed delta or open delta configurations. In [26,27] Kersting addressed the modeling of some SVR configurations to study some of their applications. Those works cover the distribution system modeling in *abc* reference frame, the SVR control mechanism by estimating *R* and *X* line settings and other applications of SVRs in distribution systems.

Looking at this literature review we can conclude that SVR modeling and testing are of great importance for distribution systems and power flow studies, and are expected to be even more present with the proliferation of DG. However, we have found that, although there are many extensive works dealing with SVR inclusion in power flow studies, there is not any work presenting general models and results for all possible configurations. This work might be also used as a benchmark for other researchers.

Reviewing the IEEE test feeders [28] of the IEEE PES Distribution System Analysis Subcommittee's Distribution Test Feeder Working Group, we will find a set of common data for testing and validation of Distribution System Analysis software. More specifically, the 4-Node Test Feeder offers a set of comparison results to deal with transformers of various configurations [29].

In this paper, the IEEE 4-Node Test System in [28] will be modified; The transformer is removed to introduce SVRs instead. We propose the general model for SVR and the 4-Node Test Feeder with SVR, both of them will be available for designers and power flow developers as a test system with detailed SVR modeling and results.

The paper is structured as follows: First, a general matrix formulation will be stated for all possible configurations: 2 grounded-wye connections (type A and B regulators), 2 close-delta connections (type A and B) and 6 open-delta connections depending on the selection of phases (3 cases for type A and 3 other cases for type B). The regulators can be at raise or at lower positions. All these SVR configurations defined a 4-Node Test Feeder that has been formulated in $\alpha\beta 0$ frame, following the procedure of [30], but adapted for SVRs. Then, the power flow formulation is presented for balanced and unbalanced loading at different tap positions. Finally, the problem is solved with the Backward Forward Sweep (BFS) algorithm of [31] to obtain the results for all possible configurations. Due to the high extension of results that were obtained, only some examples are included in this paper. The rest of results will be available on line (see Supplementary material).

2. SVR modeling

2.1. Single phase Step Voltage Regulator

A model for an ideal single phase regulator can be derived from [27]. If the series impedance is to be also considered, then, that ideal model needs to be modified: In Fig. 1 the single phase configurations are displayed. *P* stands for primary (or source side) and *S* stands for secondary (load side). For the sake of simplicity, as it will be justified later, the series impedance is concentrated at the secondary side for type A configurations and at the primary side for type B configurations. The relationships between voltages and currents for the ideal SVR are summarized in Table 1, where N_1 and N_2 are the number of turns of the shunt and series windings respectively. a_R is the effective turns ratio and is defined in a different way depending on the type of regulator, as it is shown in the table. From Fig. 1 it can be deducted that P = P′ for type A and S = S′ for type B regulators.

The relationship between primary and secondary voltages for type A, single phase regulators can then be written as follows:

$$V_{P'} = V_{S'}\frac{1}{a_R} \tag{1}$$

$$V_{P'} = V_P \tag{2}$$

$$V_{S'} = V_S + ZI_S \tag{3}$$

replacing (2) and (3) into (1) and taking V_P apart, it is obtained:

$$V_P = \frac{1}{a_R}V_S + \frac{1}{a_R}ZI_S \tag{4}$$

For type A regulators, the primary and secondary currents can be related by:

$$I_P = a_R I_S \tag{5}$$

The corresponding equations for type B, single phase regulators, with impedance on the primary side are stated as:

$$V_{P'} = V_{S'}a_R \tag{6}$$

$$V_{S'} = V_S \tag{7}$$

$$V_P = ZI_P + V_{P'} \tag{8}$$

replacing (6) and (7) into (8) it is deducted that:

$$V_P = a_R V_S + ZI_P \tag{9}$$

And finally, primary and secondary currents for type B regulators can be related in:

$$I_P = \frac{1}{a_R}I_S \tag{10}$$

Single phase Eqs. (4), (5) for type A regulators and (9), (10) for type B regulators are the baseline for the definition of the three phase configurations.

2.2. Three phase connections

Three phase configurations to be considered are wye, close delta and open delta. In following subsections, upper cases letters will be used for primary (or source) side and lower case letters will represent secondary (or load) side. In the present work, type A regulators have been chosen for three phase connections. However, the same procedure can be extended to type B regulators. For the power flow calculations, the mathematical model in [30] and a BFS algorithm are going to be used. The formulation is valid for any transformer connection, and the algorithm in $\alpha\beta 0$ frame solves the problems of some transformer connections including three wire configurations (Δ and ungrounded wye) in *abc* frame; especially $Y_g\Delta$ connection. The problems are solved by means of the zero components of voltages and currents that in $\alpha\beta 0$ frame are always available [30].

There are three general equations that represent all three phase connections:

$$[\mathbf{V}]^{P}_{\alpha\beta 0} = \mathbf{N}_{\mathbf{II}_{\alpha\beta 0}}[\mathbf{V}]^{S}_{\alpha\beta 0} + Z\mathbf{N}_{\mathbf{I}_{\alpha\beta 0}}[\mathbf{I}]^{PS}_{\alpha\beta 0} \tag{11}$$

$$[0] = -[\mathbf{I}]^{P}_{\alpha\beta 0} + \mathbf{N}_{\mathbf{IV}_{\alpha\beta 0}}[\mathbf{I}]^{PS}_{\alpha\beta 0} \tag{12}$$

$$[0] = [\mathbf{I}]^{S}_{\alpha\beta 0} + \mathbf{N}_{\mathbf{III}_{\alpha\beta 0}}[\mathbf{I}]^{PS}_{\alpha\beta 0} \tag{13}$$

The sub-index $\alpha\beta 0$ are used in the expressions because all the elements in brackets are three phase $\alpha\beta 0$ components (voltages or currents). The super-indexes P and S stand for primary and secondary respectively. The super-index PS stands for primary or secondary, depending on the transformer connection. Eqs. (11)–(13)

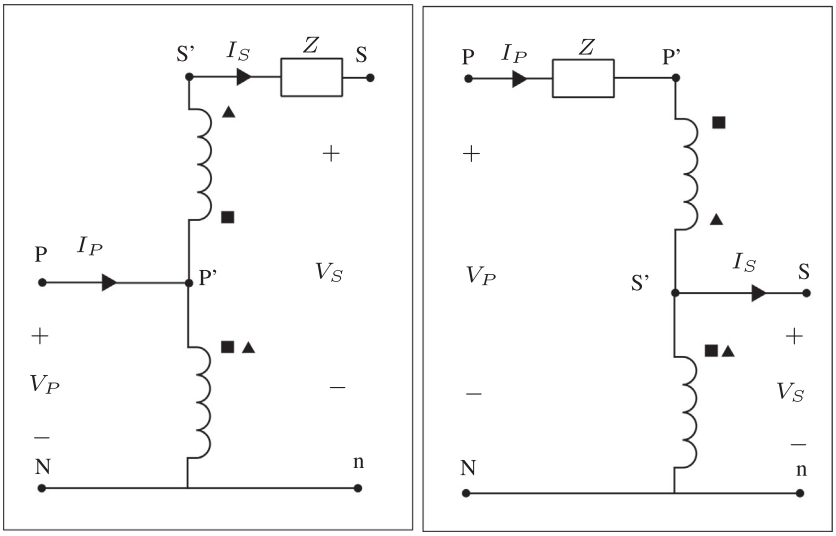

(a) Single Phase Type A (b) Single Phase Type B

Fig. 1. SVR: Single Phase connections. ▲ Raise position. ■ Lower position.

Table 1
Equations for ideal single phase SVRs.

Type	Operator ⊕		a_R	$\frac{V_{P'}}{V_{S'}}$	$\frac{I_P}{I_S}$
	Lower	Raise			
A	–	+	$1 \oplus \frac{N_2}{N_1}$	$\frac{1}{a_R}$	a_R
B	+	–		a_R	$\frac{1}{a_R}$

comprise an exact model for three phase transformers, so they can be directly included in the power flow solver. The matrices $\mathbf{N}_{\mathrm{I}_{\alpha\beta0}}, \mathbf{N}_{\mathrm{II}_{\alpha\beta0}}, \mathbf{N}_{\mathrm{III}_{\alpha\beta0}}$ and $\mathbf{N}_{\mathrm{IV}_{\alpha\beta0}}$ are different for each transformer connection. Any transformer connection is defined by these four matrices and the phase impedance Z. These equations can be also used to model SVRs as it will be demonstrated.

The meaning of superscript PS will change with the type of regulator. If (11) is compared to (4) and (9), it seems as in the SVR case, it will be easy to consider that PS stands for secondary in type A regulators and for primary in type B regulators. This fact will be proven for each transformer connection. Z is the transformer impedance, that is suppose to be the same for all the phases.

In the present work, the matrices $\mathbf{N}_{\mathrm{I}_{\alpha\beta0}}$, $\mathbf{N}_{\mathrm{II}_{\alpha\beta0}}$, $\mathbf{N}_{\mathrm{III}_{\alpha\beta0}}$ and $\mathbf{N}_{\mathrm{IV}_{\alpha\beta0}}$ will be defined to include any type of SVR configuration in the power flow solution. The equations are firstly described in *abc* frame, so those matrices are obtained in *abc* frame and transformed into $\alpha\beta0$ frame using the transformation matrix $\mathbf{A}$ in (14).

$$\mathbf{A} = \sqrt{\frac{2}{3}} \begin{pmatrix} 1 & 0 & \frac{1}{\sqrt{2}} \\ -\frac{1}{2} & \frac{\sqrt{3}}{2} & \frac{1}{\sqrt{2}} \\ -\frac{1}{2} & -\frac{\sqrt{3}}{2} & \frac{1}{\sqrt{2}} \end{pmatrix} \tag{14}$$

2.2.1. Wye-connected regulators

Three phase wye-connected regulators are depicted in Fig. 2a (type A) and Fig. 2b (type B). The winding polarities are shown for both raise and lower positions. The equations that relate primary and secondary phase to neutral voltages are similar to those for the single phase (4), but extended to the three phase wye connection:

$$\begin{bmatrix} V_A \\ V_B \\ V_C \end{bmatrix} = \begin{pmatrix} \frac{1}{a_{R_a}} & 0 & 0 \\ 0 & \frac{1}{a_{R_b}} & 0 \\ 0 & 0 & \frac{1}{a_{R_c}} \end{pmatrix} \begin{bmatrix} V_a \\ V_b \\ V_c \end{bmatrix} + \cdots + \cdots Z \begin{pmatrix} \frac{1}{a_{R_a}} & 0 & 0 \\ 0 & \frac{1}{a_{R_b}} & 0 \\ 0 & 0 & \frac{1}{a_{R_c}} \end{pmatrix} \begin{bmatrix} I_a \\ I_b \\ I_c \end{bmatrix} \tag{15}$$

This equation can be expressed in matrix form:

$$[\mathbf{V}]^{\mathrm{P}}_{abc} = \mathbf{N}_{\mathrm{II}_{abc}} [\mathbf{V}]^{\mathrm{S}}_{abc} + Z \mathbf{N}_{\mathrm{I}_{abc}} [\mathbf{I}]^{\mathrm{S}}_{abc} \tag{16}$$

where

$$\mathbf{N}_{\mathrm{I}_{abc}} = \mathbf{N}_{\mathrm{II}_{abc}} = \begin{pmatrix} \frac{1}{a_{R_a}} & 0 & 0 \\ 0 & \frac{1}{a_{R_b}} & 0 \\ 0 & 0 & \frac{1}{a_{R_c}} \end{pmatrix} \tag{17}$$

Translating Eq. (16) into $\alpha\beta0$ frame, the resulting equation is:

$$\mathbf{A}[\mathbf{V}]^{\mathrm{P}}_{\alpha\beta0} = \mathbf{N}_{\mathrm{II}_{abc}} \mathbf{A} [\mathbf{V}]^{\mathrm{S}}_{\alpha\beta0} + Z \mathbf{N}_{\mathrm{I}_{abc}} \mathbf{A} [\mathbf{I}]^{\mathrm{S}}_{\alpha\beta0} \tag{18}$$

and taking $[\mathbf{V}]^{\mathrm{P}}_{\alpha\beta0}$ apart, the following equation applies:

$$[\mathbf{V}]^{\mathrm{P}}_{\alpha\beta0} = \mathbf{N}_{\mathrm{II}_{\alpha\beta0}} [\mathbf{V}]^{\mathrm{S}}_{\alpha\beta0} + Z \mathbf{N}_{\mathrm{I}_{\alpha\beta0}} [\mathbf{I}]^{\mathrm{S}}_{\alpha\beta0} \tag{19}$$

where two of the four generalized matrices are defined:

$$\mathbf{N}_{\mathrm{I}_{\alpha\beta0}} = \mathbf{A}^{-1} \mathbf{N}_{\mathrm{I}_{abc}} \mathbf{A} \tag{20}$$

$$\mathbf{N}_{\mathrm{II}_{\alpha\beta0}} = \mathbf{A}^{-1} \mathbf{N}_{\mathrm{II}_{abc}} \mathbf{A} \tag{21}$$

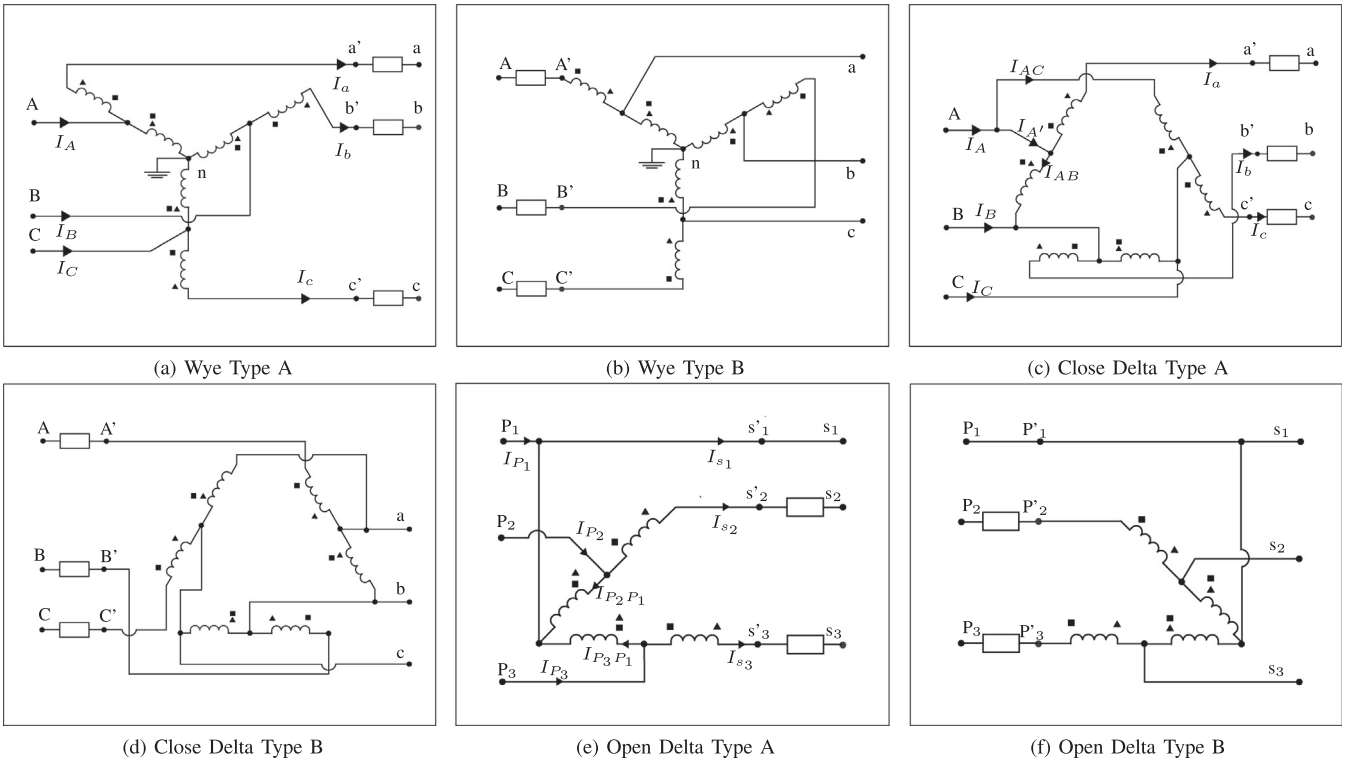

(a) Wye Type A (b) Wye Type B (c) Close Delta Type A

(d) Close Delta Type B (e) Open Delta Type A (f) Open Delta Type B

Fig. 2. SVR: Three Phase connections. ▲ Raise position. ■ Lower position.

Eq. (19) is already of the same form as (11), proving that $[\mathbf{I}]^{PS}_{\alpha\beta 0}$ are secondary currents for wye type A configurations. For the case of type B regulators primary currents would be needed instead.

To derive the relationships between primary and secondary currents, from (5) the resulting three phase equation is:

$$\begin{bmatrix} I_A \\ I_B \\ I_C \end{bmatrix} = \begin{pmatrix} a_{R_a} & 0 & 0 \\ 0 & a_{R_b} & 0 \\ 0 & 0 & a_{R_c} \end{pmatrix} \begin{bmatrix} I_a \\ I_b \\ I_c \end{bmatrix} \tag{22}$$

Rewriting this equation in matrix form:

$$[\mathbf{I}]^{P}_{abc} = \mathbf{N}_{\mathrm{IV}_{abc}} [\mathbf{I}]^{S}_{abc} \tag{23}$$

where

$$\mathbf{N}_{\mathrm{IV}_{abc}} = \begin{pmatrix} a_{R_a} & 0 & 0 \\ 0 & a_{R_b} & 0 \\ 0 & 0 & a_{R_c} \end{pmatrix} \tag{24}$$

Translating this equation into $\alpha\beta 0$ frame and taking all terms to the right, Eq. (25) applies:

$$[0] = -[\mathbf{I}]^{P}_{\alpha\beta 0} + \mathbf{N}_{\mathrm{IV}_{\alpha\beta 0}} [\mathbf{I}]^{S}_{\alpha\beta 0} \tag{25}$$

Eq. (25) can be now identified with (12), being $[\mathbf{I}]^{PS}_{\alpha\beta 0}$ equal to $[\mathbf{I}]^{S}_{\alpha\beta 0}$ in this case. From (25) another generalized matrix in $\alpha\beta 0$ frame can be derived as:

$$\mathbf{N}_{\mathrm{IV}_{\alpha\beta 0}} = \mathbf{A}^{-1} \mathbf{N}_{\mathrm{IV}_{abc}} \mathbf{A} \tag{26}$$

To obtain the last generalized matrix $\mathbf{N}_{\mathrm{III}_{\alpha\beta 0}}$, an equation similar to (13) has to be written. First, it can be assured that Eq. (27) applies:

$$[0] = [\mathbf{I}]^{S}_{abc} - [\mathbf{I}]^{S}_{abc} \tag{27}$$

Then, introducing matrix $\mathbf{N}_{\mathrm{III}_{abc}}$ in (28)

$$\mathbf{N}_{\mathrm{III}_{abc}} = -\begin{pmatrix} 1 & 0 & 0 \\ 0 & 1 & 0 \\ 0 & 0 & 1 \end{pmatrix} \tag{28}$$

Eq. (27) becomes:

$$[0] = [\mathbf{I}]^{S}_{abc} + \mathbf{N}_{\mathrm{III}_{abc}} [\mathbf{I}]^{S}_{abc} \tag{29}$$

Translating into $\alpha\beta 0$ frame the resulting expression is:

$$[0] = [\mathbf{I}]^{S}_{\alpha\beta 0} + \mathbf{N}_{\mathrm{III}_{\alpha\beta 0}} [\mathbf{I}]^{S}_{\alpha\beta 0} \tag{30}$$

where

$$\mathbf{N}_{\mathrm{III}_{\alpha\beta 0}} = \mathbf{A}^{-1} \mathbf{N}_{\mathrm{III}_{abc}} \mathbf{A} \tag{31}$$

Considering in this case that $[\mathbf{I}]^{PS}_{\alpha\beta 0}$ are secondary currents, (30) is of the same form as (13), so the model is feasible to be introduced into the power flow formulation of [30].

The four Eqs. (20), (21), (26) and (31) demonstrate that for a generic matrix in *abc* frame, $\mathbf{N}_{abc}$, the corresponding matrix in $\alpha\beta 0$ frame, $\mathbf{N}_{\alpha\beta 0}$, can be computed as:

$$\mathbf{N}_{\alpha\beta 0} = \mathbf{A}^{-1} \mathbf{N}_{abc} \mathbf{A} \tag{32}$$

The four matrices $\mathbf{N}_{\mathrm{I}_{abc}}$, $\mathbf{N}_{\mathrm{II}_{abc}}$, $\mathbf{N}_{\mathrm{III}_{abc}}$ and $\mathbf{N}_{\mathrm{IV}_{abc}}$ are presented in Table 4 for this connection and also for subsequent connections. $I_{d(3\times 3)}$ stands for the identity matrix with dimensions (3×3). Because all matrices are defined in terms of effective turns ratio instead of number of turns, they are valid for both raise and lower positions.

2.2.2. Close delta-connected regulators

Three single phase regulators can be connected in close-delta configurations as shown in Fig. 2c (type A) and 2d (type B). Both lower and raise positions give different polarities in the windings, as it is also depicted. For close-delta connections line to line voltages have to be considered. The relationship between primary

and secondary phase-to-phase voltages in type A close-delta case, is given by (refer to 2c):

$$V_{AB} + V_{Bb'} + V_{b'a'} + V_{a'A} = 0 \tag{33}$$

So secondary voltage $V_{a'b'}$ can be written as:

$$V_{a'b'} = V_{AB} + V_{Bb'} + V_{a'A} \tag{34}$$

The voltages V_{AB} and $V_{a'A}$ are related by the effective turns ratio for the regulator connected between phases A and B [27]. The same assumption can be made for voltages V_{BC} and $V_{b'B}$. If the shunt winding has a number of turns N_1, the series winding has a number of turns N_2 and the raise position is taken in consideration then:

$$\frac{V_{AB}}{V_{a'A}} = \frac{N_1}{N_2} \tag{35}$$

$$\frac{V_{BC}}{V_{b'B}} = \frac{N_1}{N_2} \tag{36}$$

If $V_{Bb'}$ and $V_{a'A}$ are replaced into (34) by their relations to V_{AB} and V_{BC} using (35) and (36) it is deducted that:

$$V_{a'b'} = V_{AB}\left(1 + \frac{N_2}{N_1}\right) + V_{BC}\left(-\frac{N_2}{N_1}\right) \tag{37}$$

If the positions of the reversing switches of all regulators are in raise, this equation can be rewritten in terms of the effective turns ratios (see Table 1); i.e. $a_{R_{ab}}$ (for the regulator between phases A and B) and $a_{R_{bc}}$ (for the regulator between phases B and C):

$$V_{a'b'} = a_{R_{ab}} V_{AB} + (1 - a_{R_{bc}}) V_{BC} \tag{38}$$

If the same procedure is followed for obtaining the voltages $V_{b'c'}$ and $V_{c'a'}$, the resulting three phase equation is:

$$\begin{bmatrix} V_{a'b'} \\ V_{b'c'} \\ V_{c'a'} \end{bmatrix} = \begin{pmatrix} a_{R_{ab}} & 1 - a_{R_{bc}} & 0 \\ 0 & a_{R_{bc}} & 1 - a_{R_{ca}} \\ 1 - a_{R_{ab}} & 0 & a_{R_{ca}} \end{pmatrix} \begin{bmatrix} V_{AB} \\ V_{BC} \\ V_{CA} \end{bmatrix} \tag{39}$$

With a similar reasoning for lower positions in the regulators, the same expression would be derived, so regardless of whether the regulators are raising or lowering the voltages, the same Eq. (39) applies. If the matrix of Eq. (39) is renamed as $\mathbf{A}_{R_V}$ (it is a non-singular matrix and has inverse) the primary voltages are obtained as:

$$[\mathbf{V}]^{S'}_{abc} = \mathbf{A}_{R_V} [\mathbf{V}]^{P}_{abc} \tag{40}$$

As it was explained in the previous subsection, being the regulators of type A, the impedances must be considered into the secondary side. Then, the matrix equation that includes the drop across those impedances is given by:

$$\begin{bmatrix} V_{a'a} \\ V_{b'b} \\ V_{c'c} \end{bmatrix} = Z \begin{bmatrix} I_a \\ I_b \\ I_c \end{bmatrix} \tag{41}$$

The phase to phase voltages in the secondary side are then computed as:

$$\begin{bmatrix} V_{a'b'} \\ V_{b'c'} \\ V_{c'a'} \end{bmatrix} = \begin{bmatrix} V_{ab} \\ V_{bc} \\ V_{ca} \end{bmatrix} + \begin{pmatrix} 1 & -1 & 0 \\ 0 & 1 & -1 \\ -1 & 0 & 1 \end{pmatrix} \begin{bmatrix} V_{a'a} \\ V_{b'b} \\ V_{c'c} \end{bmatrix} \tag{42}$$

The matrices of Eq. (42) will be labeled as $\mathbf{T}_{DY}$. It is a singular matrix. Substituting Eq. (41) into (42) and writing it into matrix form:

$$[\mathbf{V}]^{S'}_{abc} = [\mathbf{V}]^{S}_{abc} + Z\mathbf{T}_{DY} [\mathbf{I}]^{S}_{abc} \tag{43}$$

Merging Eqs. (40) and (43) and taking primary voltages apart, the resulting equation is:

$$[\mathbf{V}]^{P}_{abc} = \mathbf{A}^{-1}_{R_V} [\mathbf{V}]^{S}_{abc} + \mathbf{A}^{-1}_{R_V} Z\mathbf{T}_{DY} [\mathbf{I}]^{S}_{abc} \tag{44}$$

Eq. (44) might be written in the same form of (11). A comparison between both equations reveals:

$$\mathbf{N}_{\mathbf{I}_{abc}} = \mathbf{A}^{-1}_{R_V} \mathbf{T}_{DY} \tag{45}$$

$$\mathbf{N}_{\mathbf{II}_{abc}} = \mathbf{A}^{-1}_{R_V} \tag{46}$$

To derive the relationships between primary and secondary currents, if current references are taken as they are shown in Fig. 2c, it can be assured that:

$$I_A = I_{A'} + I_{AC} \tag{47}$$

$$I_{A'} = I_a + I_{AB} \tag{48}$$

Again, the relationship between currents through shunt and series windings can be computed in terms of the turns ratio:

$$\frac{I_{AC}}{I_c} = -\frac{N_2}{N_1} \tag{49}$$

$$\frac{I_{AB}}{I_a} = \frac{N_2}{N_1} \tag{50}$$

Merging Eqs. (47)–(50) into one equation it can be said that:

$$I_A = I_a\left(1 + \frac{N_2}{N_1}\right) + I_c\left(-\frac{N_2}{N_1}\right) \tag{51}$$

Because the regulators are in raise position, Eq. (51) can be written as (see Table 1):

$$I_A = a_{R_{ab}} I_a + (1 - a_{R_{ca}}) I_c \tag{52}$$

In a similar manner, the primary currents I_B and I_C can be also expressed in terms of secondary currents and effective turns ratios. The generalized matrix equation that relates primary and secondary currents is finally given by:

$$\begin{bmatrix} I_A \\ I_B \\ I_C \end{bmatrix} = \begin{pmatrix} a_{R_{ab}} & 0 & 1 - a_{R_{ca}} \\ 1 - a_{R_{ab}} & a_{R_{bc}} & 0 \\ 0 & 1 - a_{R_{bc}} & 0 \end{pmatrix} \begin{bmatrix} I_a \\ I_b \\ I_c \end{bmatrix} \tag{53}$$

Labeling the matrix of (53) as A_{R_I}, the Eq. (53) becomes:

$$[\mathbf{I}]^{P}_{abc} = \mathbf{A}_{R_I} [\mathbf{I}]^{S}_{abc} \tag{54}$$

Eq. (54) is written in the same form as (12) so matrix $\mathbf{N}_{\mathrm{IV}_{abc}}$ is already known:

$$\mathbf{N}_{\mathrm{IV}_{abc}} = \mathbf{A}_{R_I} \tag{55}$$

In this case, Eq. (29) also applies, so matrix $\mathbf{N}_{\mathrm{III}_{abc}}$ is the same as in (28).

The four matrices $\mathbf{N}_{\mathrm{I}_{abc}}$, $\mathbf{N}_{\mathrm{II}_{abc}}$, $\mathbf{N}_{\mathrm{III}_{abc}}$ and $\mathbf{N}_{\mathrm{IV}_{abc}}$ are included in Table 4 for both close delta connections (type A and B). All these matrices are defined again in terms of turns ratios, so they are the same for both raise and lower positions.

2.2.3. Open-Delta connections

Two single phase regulators can be connected giving rise to a three phase configuration. This is an open-Delta connection. Because there are two regulators to be connected between three phases, there are three different connections (or cases). In this work, the notation case a, case b and case c is going to be used. All configurations are depicted in Fig. 2e for type A regulators and in Fig. 2f for type B regulators. As in previous connections, the impedances are considered in the primary side for type B and in the secondary side for type A regulators.

In Fig. 2e and f, characters P_1, P_2, P_3, P'_1, P'_2 and P'_3 are used in the primary side and s_1, s_2, s_3, s'_1, s'_2 and s'_3 denote secondary side. The schemes are general for all open delta configurations; the meaning of each character in both figures depends on the

Table 2
Terminals notation for Open Delta connections.

Regulators	Case a ab & ca		Case b bc & ab		Case c ca & bc	
Type	A	B	A	B	A	B
P_1 P_2 P_3	A B C	A B C	B C A	B C A	C A B	C A B
P'_1 P'_2 P'_3	–	A′ B′ C′	–	B′ C′ A′	–	C′ A′ B′
s_1 s_2 s_3	a b c	a b c	b c a	b′ c′ a′	c a b	c′ a′ b′
s'_1 s'_2 s'_3	a′ b′ c′	–	b′ c′ a′	–	c′ a′ b′	–

considered case, as it is detailed in Table 2. For instance, in case *b* the two regulators are connected between phases *bc* and *ab*. As before, upper case letters are employed for the terminals at primary side and lower case letters are used for secondary side. The meaning of each character P_1, P_2 and P_3 are B, C and A respectively for both types of regulators; P'_1, P'_2 and P'_3 mean B', C' and A' for type B regulators and has no meaning for type A because those points do not exist in open delta connected type A regulators (see Fig. 2e).

In this section, the open-delta connection, case *a* with type A regulators has been chosen as the case to explain the open-delta general model. The regulators are supposed to be in raise position. The matrices needed for the power flow problem are going to be deducted for this specific case, but with the general notation of Fig. 2e and f and Table 2. The same reasoning may be applied to any other open-delta configuration.

First, it has to be noted for the studied configuration that phase A in the primary and phase a in the secondary are directly connected, so it can be written $A = a'$. From Fig. 2e the voltages through the first regulator are related by:

$$V_{a'b'} = V_{Ab'} = V_{AB} + V_{Bb'} \tag{56}$$

Being N_1 the turns number for the shunt winding and N_2 the turns number for the series winding (in the regulator connected to phases *ab*), the voltages V_{AB} and $V_{Bb'}$ can be related:

$$\frac{V_{Bb'}}{V_{AB}} = \frac{N_2}{N_1} \tag{57}$$

Merging (56) and (57) into one equation it is obtained:

$$V_{a'b'} = V_{AB} + V_{AB}\frac{N_2}{N_1} = V_{AB}\left(1 + \frac{N_2}{N_1}\right) \tag{58}$$

Being the type A regulators in raise position and according to Table 1, the equation becomes:

$$V_{a'b'} = a_{R_{ab}} V_{AB} \tag{59}$$

For voltage $V_{c'a'}$ the same procedure can be followed to obtain these expressions:

$$V_{c'a'} = V_{c'C} + V_{CA} \tag{60}$$

$$\frac{V_{c'C}}{V_{CA}} = \frac{N_2}{N_1} \tag{61}$$

$$V_{c'a'} = V_{CA}\frac{N_2}{N_1} + V_{CA} \tag{62}$$

$$V_{c'a'} = V_{CA}\left(1 + \frac{N_2}{N_1}\right) \tag{63}$$

$$V_{c'a'} = a_{R_{ca}} V_{CA} \tag{64}$$

In matrix form, primary voltages as a function of secondary voltages are now obtained from the combination of (59) and (64) and taking into account that for three phase-three wire configurations the primary voltages have to satisfy $V_{AB} + V_{BC} + V_{CA} = 0$.

$$\begin{bmatrix} V_{AB} \\ V_{BC} \\ V_{CA} \end{bmatrix} = \begin{pmatrix} \frac{1}{a_{R_{ab}}} & 0 & 0 \\ -\frac{1}{a_{R_{ab}}} & 0 & -\frac{1}{a_{R_{ca}}} \\ 0 & 0 & \frac{1}{a_{R_{ca}}} \end{pmatrix} \begin{bmatrix} V_{a'b'} \\ V_{b'c'} \\ V_{c'a'} \end{bmatrix} \tag{65}$$

The number of turns have been replaced by the effective turns ratios of the regulators, as it was done before.

If the same reasoning is carried out for lower positions, the matrix of (65) is also obtained. If this matrix is called $\mathbf{A}_{R_{v2}}$, the equation can be written in compact form as:

$$[\mathbf{V}]^{\mathrm{P}}_{abc} = \mathbf{A}_{R_{v2}}[\mathbf{V}]^{S'}_{abc} \tag{66}$$

For the studied connection, the drops across the secondary side impedances are given as:

$$\begin{bmatrix} V_{a'a} \\ V_{b'a} \\ V_{c'c} \end{bmatrix} = Z\begin{pmatrix} 0 & 0 & 0 \\ 0 & 1 & 0 \\ 0 & 0 & 1 \end{pmatrix} \begin{bmatrix} I_a \\ I_b \\ I_c \end{bmatrix} \tag{67}$$

There is no voltage drop due to current I_a because of the regulators connection (from Fig. 2e it easily deducted that $A = a = a'$).

Eq. (42) must be also satisfied in this case, so the secondary voltages can be deducted merging Eqs. (42) and (67):

$$\begin{bmatrix} V_{a'b'} \\ V_{b'c'} \\ V_{c'a'} \end{bmatrix} = \begin{bmatrix} V_{ab} \\ V_{bc} \\ V_{ca} \end{bmatrix} + Z\mathbf{T}_{\mathrm{DY}}\begin{pmatrix} 0 & 0 & 0 \\ 0 & 1 & 0 \\ 0 & 0 & 1 \end{pmatrix} \begin{bmatrix} I_a \\ I_b \\ I_c \end{bmatrix} \tag{68}$$

Substituting (68) into (65), and writing the new equation in compact form, it is obtained:

$$[\mathbf{V}]^{\mathrm{P}}_{abc} = \mathbf{A}_{R_{v2}}[\mathbf{V}]^{\mathrm{S}}_{abc} + Z\mathbf{A}_{R_{v2}}\mathbf{T}_{\mathrm{DY}a}[\mathbf{I}]^{\mathrm{S}}_{abc} \tag{69}$$

where

$$\mathbf{T}_{\mathrm{DY}a} = \begin{pmatrix} 0 & -1 & 0 \\ 0 & 1 & -1 \\ 0 & 0 & 1 \end{pmatrix} \tag{70}$$

Matrix $\mathbf{T}_{\mathrm{DY}a}$ in (70) is the same matrix as $\mathbf{T}_{\mathrm{DY}}$ in (43) in which the first column was replaced by zeros. For open-delta configurations case *b* and case *c*, the matrices $\mathbf{T}_{\mathrm{DY}b}$ and $\mathbf{T}_{\mathrm{DY}c}$ would be obtained. In the former, the second column in $\mathbf{T}_{\mathrm{DY}}$ has been replaced by zeros and in the latter the third column in $\mathbf{T}_{\mathrm{DY}}$ is changed by zeros.

To derive the relationship between primary and secondary currents in Fig. 2e, the depicted current references as well as the corresponding phases related in Table 2 are needed. From the figure it can be said:

$$I_B = I_b + I_{BA} \tag{71}$$

$$I_C = I_c + I_{CA} \tag{72}$$

If for both regulators the numbers of turns are N_1 and N_2 for the shunt and series wingdings respectively and the raise position is considered, then it can be assured that:

$$\frac{I_{BA}}{I_b} = \frac{N_2}{N_1} \tag{73}$$

$$\frac{I_{CA}}{I_c} = \frac{N_2}{N_1} \tag{74}$$

Merging the last four equations, and writing them in terms of turns relations, it is obtained that:

$$I_B = I_b\left(1 + \frac{N_2}{N_1}\right) = a_{R_{ab}} I_b \tag{75}$$

$$I_C = I_c\left(1 + \frac{N_2}{N_1}\right) = a_{R_{ca}} I_c \tag{76}$$

Merging (75) and (76) and taking into account that for a three phase three wire connection the equation $I_A + I_B + I_C = 0$ must be satisfied, a matrix equation is obtained:

$$\begin{bmatrix} I_A \\ I_B \\ I_C \end{bmatrix} = \begin{pmatrix} 0 & -a_{R_{ab}} & -a_{R_{ca}} \\ 0 & a_{R_{ab}} & 0 \\ 0 & 0 & a_{R_{ca}} \end{pmatrix} \begin{bmatrix} I_a \\ I_b \\ I_c \end{bmatrix} \tag{77}$$

Being the matrix in Eq. (77) named as $\mathbf{A}_{R_{I2}}$, this equation if of the same form as (12):

$$[\mathbf{I}]^{\mathrm{P}}_{abc} = \mathbf{A}_{R_{I2}} [\mathbf{I}]^{\mathrm{S}}_{abc} \tag{78}$$

Then, matrix $\mathbf{N}_{\mathrm{IV}_{abc}}$ can be obtained:

$$\mathbf{N}_{\mathrm{IV}_{abc}} = \mathbf{A}_{R_{I2}} \tag{79}$$

In this case, Eq. (29) also applies, so matrix $\mathbf{N}_{\mathrm{III}_{abc}}$ is the same matrix as in (28).

Matrices $\mathbf{N}_{\mathrm{I}_{abc}}$, $\mathbf{N}_{\mathrm{II}_{abc}}$, $\mathbf{N}_{\mathrm{III}_{abc}}$ and $\mathbf{N}_{\mathrm{IV}_{abc}}$ are included in Table 4 for all open delta configurations (cases *a*, *b* and *c*, type A and B regulators). They are defined in terms of effective turns ratios, so they are the same for both raise and lower positions. To obtain the corresponding $\alpha\beta 0$ frame matrices, the same transformation that was used for previous connections may be applicable (32).

With the generalized matrices detailed in Table 4, the SVR models are prepared for the power flow solver. All the configurations in the table were simulated in the 4-Node Test Feeder, as it will be explained later.

2.3. Comparison to previous works

There are several related works in the literature that present similar SVR models, however, none of them includes all possible configurations. In Table 3 a comparison to the models described in previous works is summarized. It can be seen how the type B regulators are usually considered due to the fact they are mainly installed in the distribution systems. With our work we aim to include not only the most common configurations, but all of them; We describe and propose a general model that will allow the inclusion any SVR configuration in a power flow analysis. Besides, a 4-Node Test Feeder with SVR is provided.

Table 3
Comparison to previous modeling works.

Refs.	Connection	Type	Frame
[9]	**OΔ**	not specified	abc
[11]	**YY**	B	abc
[16]	**YY**	B	abc
[20]	**OΔ**, case b	B	abc
[26]	**YY**	B	abc
[27]	**YY**, **ΔΔ**, **OΔ**, case b	B	abc
Present work	All	A and B	abc/$\alpha\beta 0$

3. 4-Node Test Feeder including SVRs

To introduce SVRs in the 4-Node Test Feeder [28], the transformer was replaced by a SVR. The power flow problem to be solved is the one in which the transformer matrices $\mathbf{N}_{\mathrm{I}}$, $\mathbf{N}_{\mathrm{II}}$, $\mathbf{N}_{\mathrm{III}}$ and $\mathbf{N}_{\mathrm{IV}}$ are taken from Table 4 for each specific SVR configuration. The matrices in this table are defined in *abc* frame, so they need to be translated into $\alpha\beta 0$ frame by means of Eq. (32).

Several configurations were solved for defining a benchmark of results. The effective turns ratios for the different regulators were taken considering that most of the SVRs have a reversing switch enabling ±10% regulator range in 32 steps (16 in raise and 16 in lower positions). That means a change of 0.625 per unit per step. With these numbers, the effective turns ratio in terms of number of turns might be replaced by expression [27, Chapter 7]:

$$a_R = 1 \oplus 0.00625\ \mathrm{Tap} \tag{80}$$

where Tap has a value between 0 and 16, depending on the tap position and the operator $\oplus$ has to be taken from Table 1. The model has been defined in such a way that for wye and close-delta configurations three single phase regulators are connected together. That means the taps of each regulator can change separately. This implies different values for the effective turns ratio per phase. Nevertheless, three phase regulators (in which the taps in all windings change the same) might be also modeled by choosing the same values of a_R in the three phases. For open delta connections only single phase regulators are used, so the values for the different turns ratio a_R can be equal or not.

The resulting 4-Node Test Feeder including a SVR is depicted in Fig. 3. The SVR is always connected between nodes 2 and 3, node 1 works as an infinite or slack bus and the load is connected at node 4. Line configurations and load types were chosen from the conventional test feeder [28]. In this case, because the transformer has been replaced by a SVR the rated voltage is the same in primary and secondary sides of the regulator. This value has been chosen as 12.47 kV that is one of the rated voltages at load side in the original test feeder.

The used algorithm is an unbalanced BFS solver [27] in which linear equations were defined in matrix form including all system KVL and KCL equations:

$$\mathbf{M}\mathbf{z}^T = 0 \tag{81}$$

The vector $\mathbf{z}$ contains all complex, three phase system voltages and currents as follows:

$$\mathbf{z} = \left[\mathbf{I}_{12}\ \mathbf{I}_{23}\ \mathbf{I}_{34}\ \mathbf{I}_{\mathbf{Load}_4}\ \mathbf{I}_{\mathbf{G}_1}\ \mathbf{V}_1\ \mathbf{V}_2\ \mathbf{V}_3\ \mathbf{V}_4\right]_{\alpha\beta 0} \tag{82}$$

where $\mathbf{I}_{12}$ and $\mathbf{I}_{34}$ are the line currents depicted in Fig. 3, $\mathbf{I}_{G_1}$ are the currents from the infinite bus (the only generator), $\mathbf{I}_{Load_4}$ are the load currents and $\mathbf{I}_{23}$ are the SVR primary or secondary currents depending on its configuration. The structure of $\mathbf{M}$ is shown in (83).

$$\mathbf{M} = \left(\begin{array}{c|c|c|c} \mathbf{Z}_{\alpha\beta 0} & 0 & 0 & -\Gamma \\ \hline \Gamma^T & \mathbf{I}_d & -\mathbf{I}_d & 0 \end{array}\right) \tag{83}$$

where the matrices Γ and Γ^T are the modified node incidence matrices in which the SVR matrices $\mathbf{N}_{\mathrm{I}}$, $\mathbf{N}_{\mathrm{II}}$, $\mathbf{N}_{\mathrm{III}}$ and $\mathbf{N}_{\mathrm{IV}}$ are included at the corresponding positions where a SVR is connected. This is the same procedure that the one for transformers described in [30].

The load will add the following non-linear equations:

$$\mathbf{P}_{abc} = \mathrm{real}\left(\mathbf{AV}_{\alpha\beta 0} \circ \mathrm{conj}\left[\mathbf{AI}_{L_{\alpha\beta 0}}\right]\right) \tag{84}$$

$$\mathbf{Q}_{abc} = \mathrm{imag}\left(\mathbf{AV}_{\alpha\beta 0} \circ \mathrm{conj}\left[\mathbf{AI}_{L_{\alpha\beta 0}}\right]\right) \tag{85}$$

where the operator $\circ$ is the Hadamard (element-wise) product.

Table 4
Matrices for all SVR configurations.

	$\mathbf{N}_{\mathrm{I}_{abc}}$	$\mathbf{N}_{\mathrm{II}_{abc}}$	$\mathbf{N}_{\mathrm{III}_{abc}}$	$\mathbf{N}_{\mathrm{IV}_{abc}}$
YY type A	$\begin{pmatrix} \frac{1}{a_{R_a}} & 0 & 0 \\ 0 & \frac{1}{a_{R_b}} & 0 \\ 0 & 0 & \frac{1}{a_{R_c}} \end{pmatrix}$	$\begin{pmatrix} \frac{1}{a_{R_a}} & 0 & 0 \\ 0 & \frac{1}{a_{R_b}} & 0 \\ 0 & 0 & \frac{1}{a_{R_c}} \end{pmatrix}$	$-\mathbf{I}_{d\,(3\times3)}$	$\begin{pmatrix} a_{R_a} & 0 & 0 \\ 0 & a_{R_b} & 0 \\ 0 & 0 & a_{R_c} \end{pmatrix}$
YY type B	$\mathbf{I}_{d\,(3\times3)}$	$\begin{pmatrix} a_{R_a} & 0 & 0 \\ 0 & a_{R_b} & 0 \\ 0 & 0 & a_{R_c} \end{pmatrix}$	$-\begin{pmatrix} a_{R_a} & 0 & 0 \\ 0 & a_{R_b} & 0 \\ 0 & 0 & a_{R_c} \end{pmatrix}$	$\mathbf{I}_{d\,(3\times3)}$
ΔΔ type A	$\begin{pmatrix} a_{R_{ab}} & 1-a_{R_{bc}} & 0 \\ 0 & a_{R_{bc}} & 1-a_{R_{ca}} \\ 1-a_{R_{ab}} & 0 & a_{R_{ca}} \end{pmatrix}^{-1}.\mathbf{T}_{\mathbf{DY}}$	$\begin{pmatrix} a_{R_{ab}} & 1-a_{R_{bc}} & 0 \\ 0 & a_{R_{bc}} & 1-a_{R_{ca}} \\ 1-a_{R_{ab}} & 0 & a_{R_{ca}} \end{pmatrix}^{-1}$	$-\mathbf{I}_{d\,(3\times3)}$	$\begin{pmatrix} a_{R_{ab}} & 0 & 1-a_{R_{ca}} \\ 1-a_{R_{ab}} & a_{R_{bc}} & 0 \\ 0 & 1-a_{R_{bc}} & a_{R_{ca}} \end{pmatrix}$
ΔΔ type B	$\mathbf{T}_{\mathbf{DY}}$	$\begin{pmatrix} a_{R_{ab}} & 1-a_{R_{bc}} & 0 \\ 0 & a_{R_{bc}} & 1-a_{R_{ca}} \\ 1-a_{R_{ab}} & 0 & a_{R_{ca}} \end{pmatrix}$	$-\begin{pmatrix} a_{R_{ab}} & 0 & 1-a_{R_{ca}} \\ 1-a_{R_{ab}} & a_{R_{bc}} & 0 \\ 0 & 1-a_{R_{bc}} & a_{R_{ca}} \end{pmatrix}$	$\mathbf{I}_{d\,(3\times3)}$
OΔ type A case a	$\begin{pmatrix} \frac{1}{a_{R_{ab}}} & 0 & 0 \\ -\frac{1}{a_{R_{ab}}} & 0 & -\frac{1}{a_{R_{ca}}} \\ 0 & 0 & \frac{1}{a_{R_{ca}}} \end{pmatrix}.\mathbf{T}_{\mathbf{DY}a}$	$\begin{pmatrix} \frac{1}{a_{R_{ab}}} & 0 & 0 \\ -\frac{1}{a_{R_{ab}}} & 0 & -\frac{1}{a_{R_{ca}}} \\ 0 & 0 & \frac{1}{a_{R_{ca}}} \end{pmatrix}$	$-\mathbf{I}_{d\,(3\times3)}$	$\begin{pmatrix} 0 & -a_{R_{ab}} & -a_{R_{ca}} \\ 0 & a_{R_{ab}} & 0 \\ 0 & 0 & a_{R_{ca}} \end{pmatrix}$
OΔ type A case b	$\begin{pmatrix} \frac{1}{a_{R_{ab}}} & 0 & 0 \\ 0 & \frac{1}{a_{R_{bc}}} & 0 \\ -\frac{1}{a_{R_{ab}}} & -\frac{1}{a_{R_{bc}}} & 0 \end{pmatrix}.\mathbf{T}_{\mathbf{DY}b}$	$\begin{pmatrix} \frac{1}{a_{R_{ab}}} & 0 & 0 \\ 0 & \frac{1}{a_{R_{bc}}} & 0 \\ -\frac{1}{a_{R_{ab}}} & -\frac{1}{a_{R_{bc}}} & 0 \end{pmatrix}$	$-\mathbf{I}_{d\,(3\times3)}$	$\begin{pmatrix} a_{R_{ab}} & 0 & 0 \\ -a_{R_{ab}} & 0 & -a_{R_{bc}} \\ 0 & 0 & a_{R_{bc}} \end{pmatrix}$
OΔ type A case c	$\begin{pmatrix} 0 & -\frac{1}{a_{R_{bc}}} & -\frac{1}{a_{R_{ca}}} \\ 0 & \frac{1}{a_{R_{bc}}} & 0 \\ 0 & 0 & \frac{1}{a_{R_{ca}}} \end{pmatrix}.\mathbf{T}_{\mathbf{DY}c}$	$\begin{pmatrix} 0 & -\frac{1}{a_{R_{bc}}} & -\frac{1}{a_{R_{ca}}} \\ 0 & \frac{1}{a_{R_{bc}}} & 0 \\ 0 & 0 & \frac{1}{a_{R_{ca}}} \end{pmatrix}$	$-\mathbf{I}_{d\,(3\times3)}$	$\begin{pmatrix} a_{R_{bc}} & 0 & 0 \\ 0 & a_{R_{cb}} & 0 \\ -a_{R_{bc}} & -a_{R_{ca}} & 0 \end{pmatrix}$
OΔ type B case a	$\mathbf{T}_{\mathbf{DY}a}$	$\begin{pmatrix} a_{R_{ab}} & 0 & 0 \\ -a_{R_{ab}} & 0 & -a_{R_{ca}} \\ 0 & 0 & a_{R_{ca}} \end{pmatrix}$	$-\begin{pmatrix} 0 & -\frac{1}{a_{R_{ab}}} & -\frac{1}{a_{R_{ca}}} \\ 0 & \frac{1}{a_{R_{ab}}} & 0 \\ 0 & 0 & \frac{1}{a_{R_{ca}}} \end{pmatrix}$	$\mathbf{I}_{d\,(3\times3)}$
OΔ type B case b	$\mathbf{T}_{\mathbf{DY}b}$	$\begin{pmatrix} a_{R_{ab}} & 0 & 0 \\ 0 & a_{R_{bc}} & 0 \\ -a_{R_{ab}} & -a_{R_{bc}} & 0 \end{pmatrix}$	$-\begin{pmatrix} \frac{1}{a_{R_{ab}}} & 0 & 0 \\ -\frac{1}{a_{R_{ab}}} & 0 & -\frac{1}{a_{R_{bc}}} \\ 0 & 0 & \frac{1}{a_{R_{bc}}} \end{pmatrix}$	$\mathbf{I}_{d\,(3\times3)}$
OΔ type B case c	$\mathbf{T}_{\mathbf{DY}c}$	$\begin{pmatrix} 0 & -a_{R_{bc}} & -a_{R_{ca}} \\ 0 & a_{R_{bc}} & 0 \\ 0 & 0 & a_{R_{ca}} \end{pmatrix}$	$-\begin{pmatrix} \frac{1}{a_{R_{ca}}} & 0 & 0 \\ 0 & \frac{1}{a_{R_{bc}}} & 0 \\ -\frac{1}{a_{R_{ca}}} & -\frac{1}{a_{R_{bc}}} & 0 \end{pmatrix}$	$\mathbf{I}_{d\,(3\times3)}$

Where **Δ** stands for Delta **Y** for wye and **OΔ** for Open Delta.

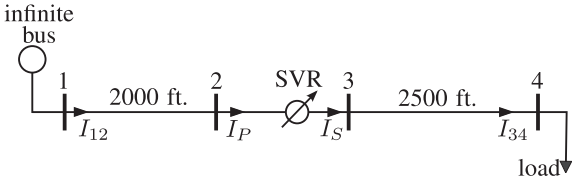

Fig. 3. 4 Node Test Feeder system.

To test the different configurations for the regulators in lower and raise positions, both types of loads; capacitive and inductive were considered. In all studied cases the algorithm has shown good convergence.

Due to the extension of this paper and the lack of space that would be necessary to properly describe and present all cases, this manuscript presents some examples. Additional results will be available on-line (see Supplementary material).

4. Basic data

The data for describing loads, lines and SVR were chosen similar to those described in the 4-Node Test Feeder with transformers [28] but with some modifications needed to replace the transformer by a SVR.

4.1. Step Voltage Regulators

The SVR configurations used in this work were taken from [27, chapter 7]. Depending on the way that the single-phase regulators are connected, the resulting configurations are different. In wye and close delta there are 3 regulators, but in case of open delta there are only 2 regulators. In open delta, 3 different connections (cases a, b and c) are defined: In case a, the regulators are connected to phases ab and ca, in case b to phases ab and ca and finally, in case c to phases ab and ca. There is only a four-wire configuration: wye-grounded connection; Close delta and open delta are three-wire. That means the lines connected to a wye-grounded SVR have to be four-wire and in the other four cases they have to be three-wire configured.

The 3-phase SVR has rated values as follows: Power of 6000 kVA; voltage 12.47 kV; R = 1% and X = 6%.

4.2. Loads

A 3-phase load is connected to node 4. Depending on the SVR connection and the line configuration between nodes 3 and 4,

Table 5
Loads.

		Balanced	Unbalanced
Phase 1	P (kW)	1800	1275
	Power factor	0.9 lag/lead	0.85 lag/lead
Phase 2	P (kW)	1800	1800
	Power factor	0.9 lag/lead	0.9 lag/lead
Phase 3	P (kW)	1800	2375
	Power factor	0.9 lag/lead	0.95 lag/lead

the load is wye-grounded or delta type. Loads are given in terms of constant active and reactive power (PQ). Different loading scenarios were considered trying to achieve different positions in taps (raise and lower positions). The loads are defined in Table 5. For each balanced or unbalanced loading scenario two possibilities are considered: lag and lead power factor. In the table, there is no reference to phases a, b and c as the nomenclature phase 1, 2 and 3 is employed instead. This is because the spot loads are not always connected to a given phase: For 3-wire nodes loads are connected line-to-line and for 4-wire nodes the loads are connected between a phase and the neutral conductor.

4.3. Lines

The lines were chosen to be exactly the same configurations and lengths as in the 4-Node Test Feeder.

The line model is the exact segment model described in [27, chapter 6]. The matrices derived from Carson's equations and Kron's reduction are always of dimensions 3×3 and are available in the web site [28] for both three-wire and four-wire configurations.

5. Study cases

The cases have been selected in such a way that each SVR configuration (type A and type B regulators) has been tested under several conditions: Balanced and unbalanced, inductive (lag power factor) and capacitive (lead power factor) loading and two different cases: Before and after optimization. The optimization has to do with tap positions; Each regulator has 32 taps; The neutral position is in the middle, there are 16 taps for raise positions and other 16 taps for lower positions. Before and after optimization refer to the comparison between two different scenarios: The first one with the SVR in the neutral position, and the second scenario with regulation to achieve the minimum value in voltage magnitude for the whole grid, without violating the voltage constraint.

The load can be inductive or capacitive, so the taps will need to be sometimes in raise and other times in lower positions. The different combinations between connections, regulator types and loading scenarios, as well as the cases before/after optimization have given rise to 80 different cases.

For wye and close delta connections there are 3 taps per regulator, that can be changed independently, but in case of open delta there are only 2 tap changers per regulator, that means one less grade of freedom for optimization.

For the voltage constraint, 0.95 per unit was selected as the minimum voltage. That means 11847 V phase-to-phase or 6840 V phase-to-neutral. There was no need of fixing a maximum value, because the optimization aims to find the minimum voltage profile that satisfies the constraint, so the maximum value is never reached.

Because the system is radial, the furthest node from the slack is node 4. As a result, it happened for all inductive loading scenarios that the minimum voltage magnitudes are obtained at that node, so if the minimum voltage constraint is satisfied at this node it will be satisfied at all nodes. Then, it is expected that the optimization algorithm searches for a power flow solution that meets the minimum voltage profile per phase (0.95 pu) at node 4 in inductive cases. For capacitive loading cases the voltage profile changes because node 4 does not always present the minimum voltage per phase in the network.

6. Results

The results to the 80 cases are available on line (16 tables in total; see Supplementary material). They have been organized in tables. Two examples of them are included in here: Tables 6 and 7. They include three phase voltages in nodes 2, 3 and 4 and three phase currents in lines 1 (from node 1 to 2) and line 2 (from node 3 to 4). The currents are line currents in phases a, b and c while the voltages are line-to-line voltages for 3-wire nodes and line-to-neutral voltages for 4-wire nodes. Each single current or voltage is represented by its magnitude in Amps or Volts and its phase in degrees. The columns correspond to the different connections: Y_gY_g, $\Delta\Delta$ and $O\Delta$ stand for wye grounded, close delta and open delta respectively. All the results in a table correspond to the same loading scenario (in this case balanced and inductive loading case) and the same optimization stage (before and after optimization in these two tables).

Table 6
Type A regulators. Inductive balanced loading. Before Optimization.

	Taps	Y_gY_g [0 0 0]	$\Delta\Delta$ [0 0 0]	$O\Delta$ case a [0 − 0]	$O\Delta$ case b [0 0 −]	$O\Delta$ case c [− 0 0]
Node 2	V_1	7125∠ − 0.3°	12360∠29.7°	12364∠29.7°	12365∠29.7°	12362∠29.7°
	V_2	7145∠ − 120.4°	12370∠ − 120.4°	12375∠ − 90.4°	12376∠ − 90.4°	12373∠ − 90.4°
	V_3	7136∠119.6°	12346∠149.6°	12351∠149.6°	12353∠149.6°	12349∠149.6°
Node 3	V_1	6842∠ − 3.4°	11870∠26.7°	12364∠29.7°	11951∠28.8°	11891∠26.7°
	V_2	6863∠ − 123.4°	11882∠ − 93.4°	12125∠ − 93.0°	12194∠ − 89.8°	11950∠ − 91.2°
	V_3	6854∠116.6°	11857∠146.6°	11749∠149.4°	12330∠148.6°	12296∠147.5°
Node 4	V_1	6752∠ − 3.8°	11737∠26.3°	12231∠29.3°	11821∠28.4°	11762∠26.3°
	V_2	6798∠ − 123.9°	11764∠ − 94.0°	12012∠ − 93.5°	12077∠ − 90.3°	11832∠ − 91.8°
	V_3	6778∠116.0°	11709∠146.0°	11601∠148.9°	12187∠148.0°	12150∠147.0°
Line 12	I_a	296.2∠ − 29.7°	295.2∠ − 29.7°	290.3∠ − 27.6°	288.1∠ − 27.1°	290.9∠ − 28.7°
	I_b	294.2∠ − 149.7°	295.2∠ − 149.7°	289.8∠ − 147.7°	288.0∠ − 147.1°	290.7∠ − 148.7°
	I_c	295.1∠90.2°	295.2∠90.3°	290.0∠92.4°	288.0∠92.9°	290.8∠91.4°
Line 34	I_a	296.2∠ − 29.7°	295.2∠ − 29.7°	290.3∠ − 27.6°	288.1∠ − 27.1°	290.9∠ − 28.7°
	I_b	294.2∠ − 149.7°	295.2∠ − 149.7°	289.8∠ − 147.7°	288.0∠ − 147.1°	290.7∠ − 148.7°
	I_c	295.1∠90.2°	295.2∠90.3°	290.0∠92.4°	288.0∠92.9°	290.8∠91.4°

Where V_1, V_2 and V_3 are phase to neutral voltages in wye connections and phase to ground voltages in the others.

Table 7
Type A regulators. Inductive balanced loading. After Optimization

		Y_gY_g	ΔΔ	OΔ case a	OΔ case b	OΔ case c
	Taps	[2 1 2]	[2 1 2]	[-5 – 4]	[1 –3 –]	[– 1 2]
Node 2	V_1	7125∠ – 0.3°	12360∠29.7°	12365∠29.7°	12363∠29.7°	12362∠29.7°
	V_2	7145∠ – 120.3°	12371∠ – 90.4°	12377∠ – 90.4°	12377∠ – 90.4°	12373∠ – 90.4°
	V_3	7136∠119.6°	12346∠149.6°	12347∠149.6°	12354∠149.6°	12349∠149.6°
Node 3	V_1	6936∠ – 3.3°	12075∠27.1°	11979∠29.7°	12025∠28.8°	12015∠26.4°
	V_2	6910∠ – 123.3°	12046∠ – 92.7°	12070∠ – 90.2°	11965∠ – 89.8°	12031∠ – 91.2°
	V_3	6947∠116.7°	12098∠147.3°	12040∠149.4°	12253∠149.8°	12450∠147.6°
Node 4	V_1	6847∠ – 3.7°	11944∠26.7°	11847∠29.3°	11895∠28.4°	11887∠26.0°
	V_2	6845∠ – 123.8°	11930∠ – 93.2°	11953∠ – 90.7°	11848∠ – 90.3°	11914∠ – 91.7°
	V_3	6873∠116.1°	11952∠146.8°	11894∠148.9°	12107∠149.2°	12305∠147.0°
Line 12	I_a	295.8∠ – 29.6°	295.5∠ – 29.7°	290.6∠ – 29.5°	291.7∠ – 26.7°	289.8∠ – 28.8°
	I_b	294.0∠ – 149.7°	293.7∠ – 149.7°	282.1∠ – 146.7°	288.1∠ – 148.0°	291.3∠ – 148.7°
	I_c	294.6∠90.3°	294.6∠90.6°	298.4∠93.3°	284.5∠93.3°	290.6∠91.0°
Line 34	I_a	292.1∠ – 29.6°	290.1∠ – 29.1°	291.1∠ – 29.7°	289.9∠ – 26.7°	288.0∠ – 28.8°
	I_b	292.2∠ – 149.7°	290.1∠ – 149.1°	291.2∠ – 146.7°	289.9∠ – 146.7°	287.7∠ – 148.7°
	I_c	291.0∠90.3°	290.1∠90.9°	291.1∠93.3°	289.9∠93.3°	288.0∠91.3°

Where V_1, V_2 and V_3 are phase to neutral voltages in wye connections and phase to ground voltages in the others.

For each connection, a vector named *Taps* is included in the tables, at second row. It represents the tap positions for the different regulators. As it can be seen, this vector includes 3 values for wye and close delta connections (1 regulator per phase) and 2 values for open delta configurations (2 regulators for three phases). For open delta cases there is always an empty position in *Taps*, that corresponds to the phase in which there is no regulator. As an example, consider case a: The 2 regulators are connected between phases a/b and c/a (first and third positions), so the corresponding vector *Taps* is of the form [0 – 0]. Between phases b/c (second position) there is no regulator, so the corresponding position at vector *Taps* is empty. The same reasoning applies to open delta cases b and c. A zero in *Taps* means neutral position. A positive value corresponds to a raise position, varying form 1 to 16, and a negative value is obtained for lower positions, varying from −1 to −16.

Looking at the tables, several analysis can be done. First, comparing the voltage profiles for this specific case before and after optimization: Before optimizing, in Y_gY_g case the voltage level at node 4 is violating the voltage constraint in the 3 phases (less than 6840 V), but after optimization the constraint is not violated in any phase. The minimum voltage is obtained at node 4, phase b 6845 V (0.951 pu). A similar reasoning can be applied to connections ΔΔ and open Δ; it can be observed that in all cases the voltage constraint is fulfilled (11847 V for three wire connections).

Then, in balanced loading cases, with wye and close delta connections, the tap positions are quiet similar among different phases but not exactly the same because of the unbalanced nature of lines. In contrast, open delta connections give rise to great differences among taps because the SVR itself is not symmetric (two regulators for three phases), so even for a balanced loading scenario one regulator can be at raise position while the other can be at lower position.

Finally, for unbalanced loading cases it can be seen that the SVR, not only improves the voltage in magnitude but also leads to a more balanced scenario.

7. Conclusion

This work provides for the theoretical background, the model description and the diagrams needed for the inclusion of Step Voltage Regulators into a general, there phase and unbalanced power flow problem. The general model for three phase Step Voltage Regulators has been included in a 4 Node Test Feeder and solved by means of an unbalanced Backward-Forward Sweep solver. The obtained results are presented as a benchmark. The main contribution of this work is, besides the guidelines for the SVR model development, the proposal of a new 4-Node Test System for testing and evaluation of three-phase SVRs connections. The authors would like to encourage software developers to test their software using the model and data presented in this work. All results are available on-line (see Supplementary material).

Appendix A. Supplementary material

Supplementary data associated with this article can be found, in the online version, at http://dx.doi.org/10.1016/j.ijepes.2017.06.027.

References

[1] Hobson JE, Lewis WA. Regulating transformers in power-system analysis. Electr Eng 1939;58(11):874–86.
[2] Hill LH. Step type feeder voltage regulators. Electr Eng 1935;54(2):154–8.
[3] Saidy M, Hughes F. A predictive integrated voltage regulator and power system stabilizer. Int J Electric Power Energy Syst 1995;17(2):101–11. cited By 8.
[4] Dzafic I, Jabr RA, Halilovic E, Pal BC. A sensitivity approach to model local voltage controllers in distribution networks. IEEE Trans Power Syst 2014;29(3):1419–28.
[5] Pereira C, Castro C. Optimal placement of voltage regulators in distribution systems. In: PowerTech, 2009 IEEE Bucharest. p. 1–5. June.
[6] Watson JD, Watson NR, Das B. Effectiveness of power electronic voltage regulators in the distribution network. IET Gener Transm Distrib 2016;10(15):3816–23.
[7] Brito MEC, Limongi LR, Cavalcanti MC, Neves FAS, Azevedo GMS. A step-dynamic voltage regulator based on cascaded reduced-power series transformers. Electric Power Syst Res 2014;108:245–53. cited By:3.
[8] Senjyu T, Miyazato Y, Yona A, Urasaki N, Funabashi T. Optimal distribution voltage control and coordination with distributed generation. IEEE Trans Power Deliv 2008;23(2):1236–42.
[9] Hossain MI, Yan R, Saha TK. Investigation of the interaction between step voltage regulators and large-scale photovoltaic systems regarding voltage regulation and unbalance. IET Renew Power Gener 2016;10(3):299–309.
[10] Liu X, Aichhorn A, Liu L, Li H. Coordinated control of distributed energy storage system with tap changer transformers for voltage rise mitigation under high photovoltaic penetration. IEEE Trans Smart Grid 2012;3(2):897–906. June.
[11] Youssef KH. A new method for online sensitivity-based distributed voltage control and short circuit analysis of unbalanced distribution feeders. IEEE Trans Smart Grid 2015;6(3):1253–60.
[12] Rahbarimagham H, Sanjari MJ, Tavakoli A, Gharehpetian GB, Jafari R. Emission reduction in a micro grid including pv considering voltage profile improvement. In: 2013 Smart Grid Conference (SGC), Dec. p. 219–24.
[13] Tang Z, Hill D, Liu T, Ma H. Hierarchical voltage control of weak subtransmission networks with high penetration of wind power. IEEE Trans Power Syst 2017;PP(99). 1–1.

[14] Murphy KM, Nair NKC. Voltage control in distribution networks with penetration of solar pv: estimated voltages as a control input. In: 2016 IEEE Power and Energy Society General Meeting (PESGM), July. p. 1–5.
[15] Ceylan O, Dimitrovski A, Starke M, Tomsovic K. Optimal reactive power allocation for photovoltaic inverters to limit transformer tap changes. In: 2016 IEEE Power and Energy Society General Meeting (PESGM), July. p. 1–5.
[16] Farag H, El-Saadany E, El Shatshat R, Zidan A. A generalized power flow analysis for distribution systems with high penetration of distributed generation. Electric Power Syst Res 2011;81(7):1499–506. cited By 35.
[17] Oshiro M, Tanaka K, Uehara A, Senjyu T, Miyazato Y, Yona A, et al. Optimal voltage control in distribution systems with coordination of distribution installations. Int J Electric Power Energy Syst 2010;32(10):1125–34. cited By 26.
[18] Frias P, Platero CA, Soler D, Blazquez F. High-efficiency voltage regulator for rural networks. IEEE Trans Power Deliv 2010;25(3):1666–72.
[19] Chamana M, Chowdhury BH, Jahanbakhsh F. Distributed control of voltage regulating devices in the presence of high pv penetration to mitigate ramp-rate issues. IEEE Trans Smart Grid 2017;PP(99). 1–1.
[20] Yan R, Li Y, Saha T, Wang L, Hossain M. Modelling and analysis of open-delta step voltage regulators for unbalanced distribution network with photovoltaic power generation. IEEE Trans n Smart Grid 2017;PP(99). 1–1.
[21] Robbins BA, Zhu H, Domínguez-García AD. Optimal tap setting of voltage regulation transformers in unbalanced distribution systems. IEEE Trans Power Syst 2016;31(1):256–67.
[22] Ahmadi H, Martí JR. Distribution system optimization based on a linear power-flow formulation. IEEE Trans Power Deliv 2015;30(1):25–33.
[23] Araujo LR, Penido DRR, Carneiro S, Pereira JLR. A three-phase optimal power-flow algorithm to mitigate voltage unbalance. IEEE Trans Power Deliv 2013;28(4):2394–402.
[24] Ghatak U, Mukherjee V. An improved load flow technique based on load current injection for modern distribution system. Int J Electric Power Energy Syst 2017;84:168–81.
[25] Liu JW, Choi SS, Chen S. Design of step dynamic voltage regulator for power quality enhancement. IEEE Trans Power Deliv 2003;18(4):1403–9.
[26] Kersting WH. The modeling and application of step voltage regulators. In: 2009 IEEE/PES power systems conference and exposition, March. p. 1–8.
[27] Kersting WH. Distribution system modeling and analysis. Abingdon: CRC Press; 2001.
[28] Distribution Test Feeders, IEEE PES Distribution System Analysis Subcommittee's. Distribution Test Feeder Working Group. Available: <http://ewh.ieee.org/soc/pes/dsacom/testfeeders/>.
[29] Kersting WH. Transformer model test system. In: Transmission and distribution conference and exposition, 2003 IEEE PES 3. IEEE; 2003. p. 1022–6.
[30] Arboleya P, González-Morán C, Coto M. Unbalanced power flow in distribution systems with embedded transformers using the complex theory in $\alpha\beta 0$ stationary reference frame. IEEE Trans Power Syst 2014;PP(99):1–11.
[31] González-Morán C, Arboleya P, Mohamed B. Matrix backward forward sweep for unbalanced power flow in $\alpha\beta 0$ frame. Electric Power Syst Res 2017;148:273–81.

Electrical Power and Energy Systems 91 (2017) 71–79

Contents lists available at ScienceDirect

Electrical Power and Energy Systems

journal homepage: www.elsevier.com/locate/ijepes

Phase shifting transformer model for direct approach power flow studies

José M. Cano *, Md. Rejwanur R. Mojumdar, Joaquín G. Norniella, Gonzalo A. Orcajo

Department of Electrical Engineering, University of Oviedo, Spain

ARTICLE INFO

Article history:
Received 11 January 2017
Received in revised form 2 March 2017
Accepted 12 March 2017
Available online 22 March 2017

Keywords:
Direct approach method
Phase shifting transformer
Power flow
Weakly-meshed network

ABSTRACT

This proposal is intended to extend the field of application of an extremely efficient power flow algorithm used in radial and weakly meshed grids, the so-called Direct Approach (DA) method. In this work the method is broadened with the possibility of handling shunt admittances, transformers with taps, and phase shifting transformers. While the integration of the two former elements in the DA solver is quite straightforward, the use of phase shifting transformers is far from obvious due to their inherent non-symmetrical admittance matrix. Thus, a model for phase shifting transformers is proposed in this contribution, which allows the use of the DA method in grids that include such devices. A set of case studies is conducted in the contexts of a balanced industrial grid and a standard testbed to demonstrate the validity of the proposal.

1. Introduction

Power flow solvers are an essential tool in the operation and planning of power systems. They allow the assessment of voltage profiles, power flows and losses in the grid, and thus, they are crucial to detect unacceptable voltage deviations and identify overloaded components. Furthermore, power flow algorithms are used to conduct reliability studies and foresee the impact of future demand [1,2].

The most traditional power flow methods such as Newton-Raphson and Gauss-Seidel, used widely in transmission systems, do not offer the best performance and robustness when applied to the distribution level [3]. This is due to the especial nature of the distribution network, characterized by a radial or weakly meshed topology and a high R/X ratio. Several approaches have been proposed in order to deal with these particular features, such as the implicit Z-bus Gauss method [4] and backward-forward sweep methods [5,6]. In the latter group, a very efficient formulation called the direct approach (DA) was proposed in [7]. The DA method avoids the time-consuming tasks of LU factorization and forward and backward substitution of the Jacobian or admittance matrices, which are a commonplace in traditional formulations. The characteristics of DA method make it ideal for real-time applications in the smart grid context. In [8], the DA solver is used in the core of an optimal power flow (OPF) algorithm to provide references to a distribution FACTS in an industrial grid. High update rates are needed in this type of applications and the DA solver accommodates perfectly to this requirement.

The three-phase approach used in [7] takes series self-impedances and mutual couplings into consideration; however, shunt admittances are neglected. Even if that assumption can be enough to run a power flow analysis at the lowest voltage levels of the distribution grid, characterized by short-length lines and untapped transformers, ignoring shunt admittances strongly limits the application of the method to higher voltage levels. The extension of the method to accommodate medium-length lines and transformers with tap changers in a balanced environment is presented in this paper. Though no previous references to this use have been found, its application is fairly straightforward.

In a pure radial grid, a post-processing of the voltage phase angles after the application of the power flow solver is enough to account for the transformer phase shift. However, if a weakly meshed grid is to be considered, this method is no longer valid. Thus, a model of the phase shifting transformer, both to consider specific devices used to control the active power flow in the loop and to include the phase shift of common power transformers, is mandatory. Modeling of phase shifting transformers in power flow studies is a non-trivial problem, as they cannot be represented by a pi-equivalent component due to their inherent asymmetric admittance matrix [1]. A set of different phase shifting transformer models is available for application in various fields of study, to both steady state [9–13] and transient simulation [14]. In [15], a survey on phase shifting transformer models for steady state analysis is presented; however, none of them are expressed in a suitable form to be embedded in the DA solver. In this work, a new model is proposed to overcome this limitation.

* Corresponding author.
E-mail address: jmcano@uniovi.es (J.M. Cano).

http://dx.doi.org/10.1016/j.ijepes.2017.03.007
0142-0615/

The DA method, as described in [7], is presented in Section 2 for the benefit of the reader. Section 3 presents a straightforward method to include shunt admittances in the DA solver. Thus, those components capable of being represented by pi-equivalent models, such as medium-length lines and transformers with tap changers, can be easily included in the problem. In Section 4, the new phase shifting transformer model is presented together with minor modifications to be performed in the DA algorithm. Three case studies are presented in Section 5 in order to illustrate the implementation procedure and demonstrate the validity of the proposal. Finally, Section 6 summarizes the most important results of this study.

2. Direct approach power flow

The method to be proposed in this contribution is based on the DA formulation of the power flow problem [7]. This is a technique, especially designed for radial networks, inspired by well-known backward-forward sweep methods such as Ladder Iterative Technique [6]. DA provides a very compact vectorized formulation with excellent computational and convergence characteristics.

In the application of DA to balanced grids, lines and transformers are modeled as series impedances, z_{ik}, as it is shown in Fig. 1. The equivalent bus current injection vector, $\boldsymbol{I_g}$, is calculated from the power injection at each bus, i, given the estimation of the bus voltage vector $\boldsymbol{V}$ at iteration (n) as

$$I_{gi}^{(n)} = \frac{P_i - jQ_i}{conj(V_i^{(n)})}. \tag{1}$$

Assuming a radial grid, the branch current vector can be calculated as

$$\boldsymbol{B}^{(n)} = \mathbf{BIBC} \cdot \boldsymbol{I_g}^{(n)}, \tag{2}$$

where **BIBC** is the so-called bus-injection to branch-current matrix. The entry $BIBC_{bi}$ equals 1 if the current injection of node i contributes to the branch current B_b, and equals 0 otherwise. Finally, a better approximation to the voltage profile can be obtained from

$$\boldsymbol{\Delta V}^{(n+1)} = \mathbf{BCBV} \cdot \boldsymbol{B}^{(n)}, \tag{3}$$

where **BCBV** is the branch-current to bus-voltage matrix. The entry $BCBV_{ib}$ equals the series impedance of branch b if that branch is in the path from node i to the slack bus, and equals 0 otherwise. $\boldsymbol{\Delta V}$ is a vector with the voltage of the slack bus referred to the different bus voltages. An improved approximation to the state variables is subsequently obtained by

$$\boldsymbol{V}^{(n+1)} = \boldsymbol{V_s} - \boldsymbol{\Delta V}^{(n+1)}, \tag{4}$$

where $\boldsymbol{V_s}$ is a column vector with the slack bus voltage at each entry.

Starting from a flat voltage profile, the solution of the distribution power flow is reached by solving (1)–(4) iteratively up to a specified convergence threshold.

In order to include the treatment of meshes in the network, Teng [7] proposes minor modifications to be conducted in the definition of **BIBC** and **BCBV** and in the solution technique. A brief summary of these changes can be described as:

- Specific branches are selected to break the meshed grid into a radial network. Then, new entries are included in the current injection vector to account for the currents at the selected branches, i.e. $[\boldsymbol{I_g B}_{\text{new}}]^T$.
- The **BIBC** matrix is built as in the base case, by considering the currents of the branches used to break the network as additional current injections. However, entries with the value -1 appear now to account for the contribution of the receiving node of the branches used to break the network due to the inverted current reference. Notice that the double-sided contribution of the sending and receiving nodes of a branch used to break the network, B_c, to the current of those branches upstream from the first common parent node, B_b, is null, as they have the same value but opposite references.
  Additionally, new rows are added to the **BIBC** matrix with a single non-null entry in order to identify the currents of the branches used to break the network. Taking all this into account the modified **BIBC** matrix can be obtained as

$$\begin{bmatrix} \boldsymbol{B} \\ \boldsymbol{B}_{\text{new}} \end{bmatrix}^{(n)} = \mathbf{BIBC} \cdot \begin{bmatrix} \boldsymbol{I_g} \\ \boldsymbol{B}_{\text{new}} \end{bmatrix}^{(n)}. \tag{5}$$

- The **BCBV** matrix is built as in the base case, but a new row is added for each loop in the grid to account for KVL. The impedances included in the entries of the new rows of the matrix are signed positive or negative according to the reference of the current at the different branches. Then, (3) is reformulated as

$$\begin{bmatrix} \boldsymbol{\Delta V} \\ 0 \end{bmatrix}^{(n+1)} = \mathbf{BCBV} \cdot \begin{bmatrix} \boldsymbol{B} \\ \boldsymbol{B}_{\text{new}} \end{bmatrix}^{(n)}. \tag{6}$$

- By using (5) and (6) and rewriting the resulting matrix, it follows that

$$\begin{bmatrix} \boldsymbol{\Delta V} \\ 0 \end{bmatrix}^{(n+1)} = \mathbf{BCBV} \cdot \mathbf{BIBC} \cdot \begin{bmatrix} \boldsymbol{I} \\ \boldsymbol{B}_{\text{new}} \end{bmatrix}^{(n)} = \begin{bmatrix} \boldsymbol{A} & \boldsymbol{P} \\ \boldsymbol{M} & \boldsymbol{N} \end{bmatrix} \begin{bmatrix} \boldsymbol{I} \\ \boldsymbol{B}_{\text{new}} \end{bmatrix}^{(n)}.$$

The application of Kron reduction to (7) leads to

$$\boldsymbol{\Delta V}^{(n+1)} = (\boldsymbol{A} - \boldsymbol{M}^T \boldsymbol{N}^{-1} \boldsymbol{M}) \boldsymbol{I_g}^{(n)}. \tag{7}$$

The iterative use of (1), (7) and (4), in this order, allows the application of the DA method to weakly meshed grids.

3. Including pi-equivalent models

The DA method in [7] models the lines and transformers in balanced systems by simple series impedances. While this is acceptable for short-length lines and untapped transformers, minor

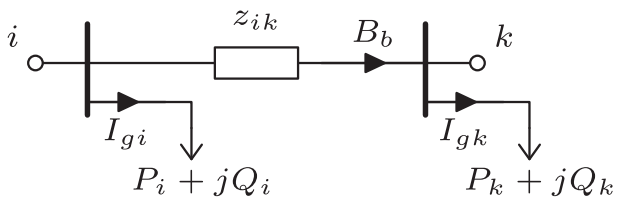

Fig. 1. Scheme used in the DA method.

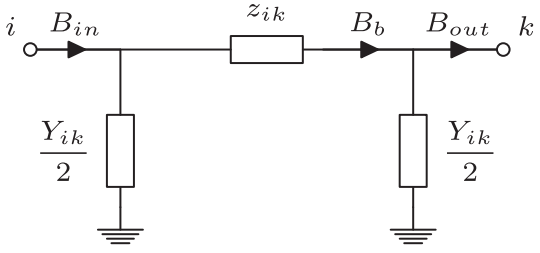

Fig. 2. Pi-equivalent line model.

modifications must be included in the method in order to deal with other common device models.

By considering a pi-equivalent model as the one shown in Fig. 2, medium-length lines with series impedance z_{ik} and total lumped shunt admittance Y_{ik} can be included in the DA method. In this case, an intermediate variable arises, B_b, which is to be included in the branch current matrix $\boldsymbol{B}$. The current injection vector, $\boldsymbol{I_g}$, is now replaced in (2) by an augmented vector $\boldsymbol{I}$ that includes the currents drawn by the shunt admittances as

$$\boldsymbol{I}^{(n)} = \boldsymbol{I}_{\boldsymbol{g}}^{(n)} + \mathbf{Y_B} \circ \boldsymbol{V}^{(n)}, \tag{8}$$

where $\circ$ is the Hadamard product and $\mathbf{Y_B}$ is the bus admittance vector. The sending and receiving end currents, B_{in} and B_{out}, do not appear explicitly in the formulation, but can be subsequently obtained from the state variables by

$$B_{in} = B_b + \frac{Y_{ik}}{2} V_i, \tag{9}$$

$$B_{out} = B_b - \frac{Y_{ik}}{2} V_k. \tag{10}$$

Once the structure in Fig. 3 is adopted, no further modifications are required in the DA method if z_{ik} is used within the **BCBV** matrix.

Even more important than medium-length lines in radial grids is the inclusion of tap changing transformers in the DA solver. The latter devices are massively used along the power system and are of particular importance in the regulation of voltages in radial grids, to which the DA method is specifically devoted. Considering a tap changing transformer as in Fig. 4, where Y_{sc} stands for its short circuit admittance and a represents the regulation between the primary and secondary voltages, the following equations apply

$$V_i = aV_p = a\left(\frac{B_{out}}{Y_{sc}} + V_k\right), \tag{11}$$

$$B_{out} = aB_{in}. \tag{12}$$

As it is well established in [16], from (11) and (12) the tap changing transformer can be represented through a pi-equivalent model as in Fig. 5, which accounts for the nodal equations of the machine

$$B_{in} = \frac{1}{a^2} Y_{sc} V_i - \frac{1}{a} Y_{sc} V_k, \tag{13}$$

$$-B_{out} = -\frac{1}{a} Y_{sc} V_i + Y_{sc} V_k. \tag{14}$$

Using the same methodology described for pi-equivalent lines, the inclusion of tap changing transformers in the DA method is thus achieved. Notice that, in this case, the input and output currents of the transformer can be derived from the state variables as

$$B_{in} = B_b + \frac{1-a}{a^2} Y_{sc} V_i, \tag{15}$$

$$B_{out} = B_b - \frac{a-1}{a} Y_{sc} V_k. \tag{16}$$

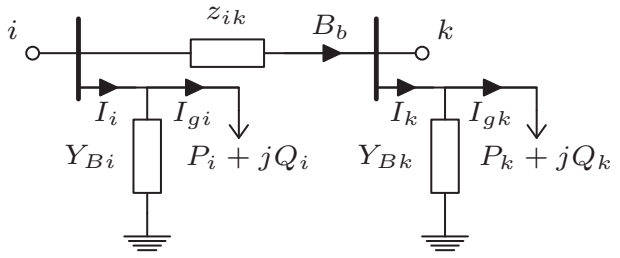

Fig. 3. Modified scheme for the DA method.

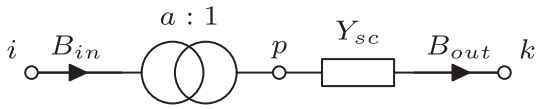

Fig. 4. Equivalent circuit for the tap changing transformer.

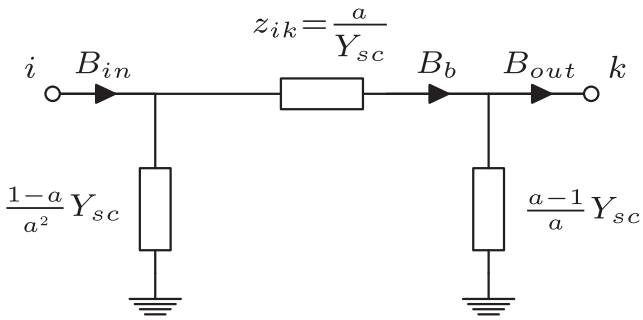

Fig. 5. Pi-equivalent model of the tap changing transformer.

4. Phase shifting transformer model

Phase shifting transformers cannot be represented through a pi-equivalent model due to the asymmetry of its admittance matrix. As a consequence, the methodology described in Section 3 is not valid for the integration of these devices within the DA method. However, an alternative equivalent model, which is suitable to be used with the DA method provided that slight modifications are included, is described in this section.

4.1. Pseudo pi-equivalent model

The equivalent circuit shown in Fig. 4 is still valid to represent a phase shifting transformer, provided that a is now a complex number, i.e. $a = |a|e^{j\theta}$, $|a|$ being the regulation between the primary and secondary voltage magnitudes and θ being the phase shift. The fundamental equations of such a machine can be written as

$$V_i = aV_p = a\left(\frac{B_{out}}{Y_{sc}} + V_k\right), \tag{17}$$

$$B_{out} = a^* B_{in}, \tag{18}$$

where a^* is the complex conjugate of a.

The nodal equations of a phase shifting transformer can be derived from (17) and (18) as

$$B_{in} = \frac{1}{a\,a^*} Y_{sc} V_i - \frac{1}{a^*} Y_{sc} V_k, \tag{19}$$

$$-B_{out} = -\frac{1}{a} Y_{sc} V_i + Y_{sc} V_k. \tag{20}$$

where the asymmetry of the admittance matrix becomes clear.

In order to comply with the principles of the DA method, a suitable equivalent of the phase shifting transformer should maintain the structure of (3). From (17) and (18), it can be derived that

$$V_i - V_k = \frac{a}{Y_{sc}}\left(B_{out} + \frac{a-1}{a} Y_{sc} V_k\right) = \frac{a}{Y_{sc}} B_b, \tag{21}$$

where B_b, defined as

$$B_b = B_{out} + \frac{a-1}{a} Y_{sc} V_k, \tag{22}$$

is an intermediate variable used to calculate the voltage between nodes i and k. Finally, using (17), (18) and (21), the input current to the transformer can be formulated as

$$B_{in} = e^{j2\theta}B_b + \frac{1-a}{|a|^2}Y_{sc}V_i. \quad (23)$$

The equivalent circuit shown in Fig. 6 meets the set of Eqs. (21)–(23) and constitutes the transformer phase shifting model proposed in this contribution. Though it is obviously not a pure pi-equivalent circuit, it is especially suited to be embedded in the DA power flow method, as is demonstrated in the following.

4.2. Integration of the model in the DA method

Slight modifications in the application of the DA method have to be conducted in order to integrate the pseudo pi-equivalent circuit of the phase shifting transformer into the DA power flow calculation method. The first two considerations are in fact extensions from the conclusions drawn in Section 3 for the inclusion of pi-equivalent models:

- The series impedance z_{ik} shown in Fig. 6 is used to represent the impedance between nodes i and k within the BCBV matrix.
- In the calculation of the current injection augmented vector $\boldsymbol{I}$ according to (8), $\mathbf{Y_B}$ has to include new shunt admittance terms at the sending bus, i, and receiving bus, k, according to Fig. 6.

The third consideration requires the modification of the **BIBC** matrix. As is depicted in Fig. 7(a), let i', k' and b' be the sending node, receiving node and branch index of a phase shifting transformer. In the same way, let b be the index of a branch located upstream from that transformer. According to (23) and Fig. 6, the effect of all the augmented current injections of the nodes downstream from i' on the branch current, B_b, can be evaluated as $e^{j2\theta}B_{b'}$. This fact can be easily considered by modifying the entries $BIBC_{bi}$ of the matrix. If node i is now downstream from the receiving node of branch b, the following term,

$$BIBC_{bi} = \prod_t e^{j2\theta_t} = e^{j2\sum_t \theta_t}, \quad (24)$$

applies instead of 1, with t being the different phase shifting transformers between the receiving node of branch b and node i, and θ_t being their corresponding phase angle shifts. Fig. 7 illustrates the process for the cases of one phase shifting transformer, example (a), and two series connected phase shifting transformers, example (b).

4.3. Dealing with weakly meshed grids

Additional changes, apart from those described in Section 2, must be conducted to include the proposed phase shifting transformer model in the DA method in the context of weakly meshed topologies. Those modifications can be summarized in the following aspects:

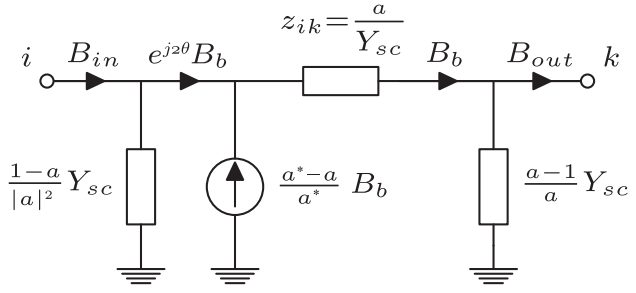

Fig. 6. Pseudo pi-equivalent model of the tap changing transformer.

- The double-sided contribution of the current of a branch used to break the network, B_c, to a branch current upstream from the first common parent node, B_b, is no longer canceled in this case, as it is shown in Fig. 8. Notice that even if B_c arises with different current references in each path, both sides can be affected by different phase angle jumps. As a consequence, a minor modification of the **BIBC** matrix is required. For those branches, b, upstream from the first common parent node, the contribution of a branch used to break the network, c, whose current branch is at position i in the augmented injection vector $[\boldsymbol{I_g B}_{\text{new}}]^T$, is evaluated by the term

$$BIBC_{bi} = \prod_{t_s} e^{j2\theta_{ts}} - \prod_{t_r} e^{j2\theta_{tr}} = e^{j2\sum_{t_s}\theta_{ts}} - e^{j2\sum_{t_r}\theta_{tr}}. \quad (25)$$

  In (25) t_s stands for the different phase shifting transformers found in the path between the receiving node of branch b and the receiving node of branch c that includes the sending node of branch c. In the same way, t_r stands for the different phase shifting transformers found in the path between the receiving node of branch b and the receiving node of branch c that does not include the sending node of branch c. Finally, θ_{ts} and θ_{tr} account for their corresponding phase angle shifts. The example shown in Fig. 8 illustrates this situation using a simple network. Notice that, in this example, one phase shifting transformer exists between node n and the receiving node k' of branch c along the path that includes the sending node of branch c. However, no phase shifting transformers exist along the alternative path connecting the same pair of nodes, which obviously leads to -1 in the second addend of (25).
- From the application of (5) and (6) to this case, it follows that

$$\begin{bmatrix}\boldsymbol{\Delta V}\\ 0\end{bmatrix}^{(n+1)} = \mathbf{BCBV}\cdot\mathbf{BIBC}\cdot\begin{bmatrix}\boldsymbol{I}\\ \boldsymbol{B}_{\text{new}}\end{bmatrix}^{(n)} = \begin{bmatrix}\boldsymbol{A} & \boldsymbol{P}\\ \boldsymbol{M} & \boldsymbol{N}\end{bmatrix}\begin{bmatrix}\boldsymbol{I}\\ \boldsymbol{B}_{\text{new}}\end{bmatrix}^{(n)}.$$

  Notice that the symmetry found in (7) does not appear in (26). In any case, the application of Kron reduction leads to

$$\boldsymbol{\Delta V}^{(n+1)} = (\boldsymbol{A} - \boldsymbol{P}\boldsymbol{N}^{-1}\boldsymbol{M})\boldsymbol{I}^{(n)}. \quad (26)$$

The iterative use of (1), (8), (26) and (4), in this order, allows the application of the DA method to weakly meshed grids including phase shifting transformers.

5. Case studies

To demonstrate the validity of the proposed methodology, three case studies are carried out in this section. In the first one, the DA method is applied to a radial network in which the phase shifts associated to the embedded power transformers are considered. In the second case study, the same radial grid is turned into a weakly meshed grid by using a phase shifting transformer. While the first two case studies take advantage of the low number of nodes of an industrial grid to give insight into the matrices building process, the third case study is used to demonstrate the good convergence characteristics of the method in a standard medium-size testbed.

5.1. Case 1: Radial network

A simplified version of the customer owned grid of a steelworks in the north of Spain, already tested in previous works [8], is considered in this case study. The grid is shown in Fig. 9 and the parameters and configuration of the embedded transformers are listed in Table 1. Table 2 shows the lengths and per km impedances

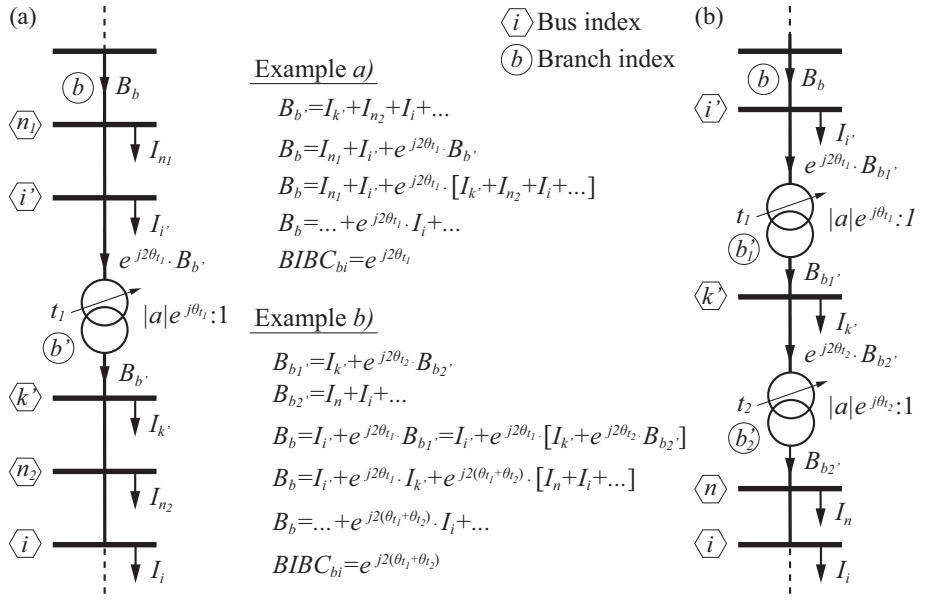

Fig. 7. Building process of the **BIBC** matrix for grids with embedded phase shifting transformers. (a) Example with one phase shifting transformer, and (b) example with two phase shifting transformers.

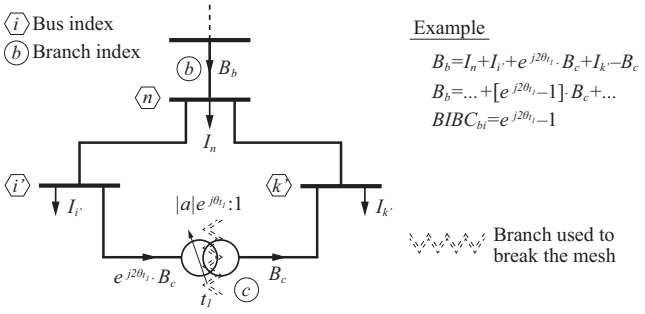

Fig. 8. Example of the building process of the **BIBC** matrix for weakly meshed grids with embedded phase-shifting transformers.

of the lines, together with the series impedances, z_{ik}, of each branch for lines and transformers, according to Figs. 2 and 6 respectively.

In [8], a proposal aimed to improve the efficiency of the grid and provide dynamic voltage support to the facility was presented. This objective is conducted through the application of a distribution FACTS usually known as Loop Power Flow Controller (LPFC). The real-time optimization of the device is based on a heuristic algorithm out of the scope of this paper. However, the proper operation of that heuristic algorithm relies upon the availability of a fast power flow algorithm, compatible with such a real-time application. Even if other algorithms were considered, the DA method shows very good performance in this environment, characterized by a small number of nodes and radial nature. The controller uses the DA power flow algorithm to analyze the effect of different power injections at the power converter terminals (i.e. the real power, P, flowing from terminal A to B in Fig. 9, and the decoupled reactive power injections at both terminals, Q_A and Q_B). The addition of these values to the rest of the power injections at buses 7 and 9 turns the power flow problem into a pure radial case, despite of the mesh created by the distribution FACTS. Table 3 shows the specific power injection values considered in this case study. Note that the negative value of the reactive power injection in bus 9 is due to the reactive power supply of the LPFC at terminal B for the current operation point. The voltage at the slack bus is taken as 1.0 pu and as the origin of phase angles.

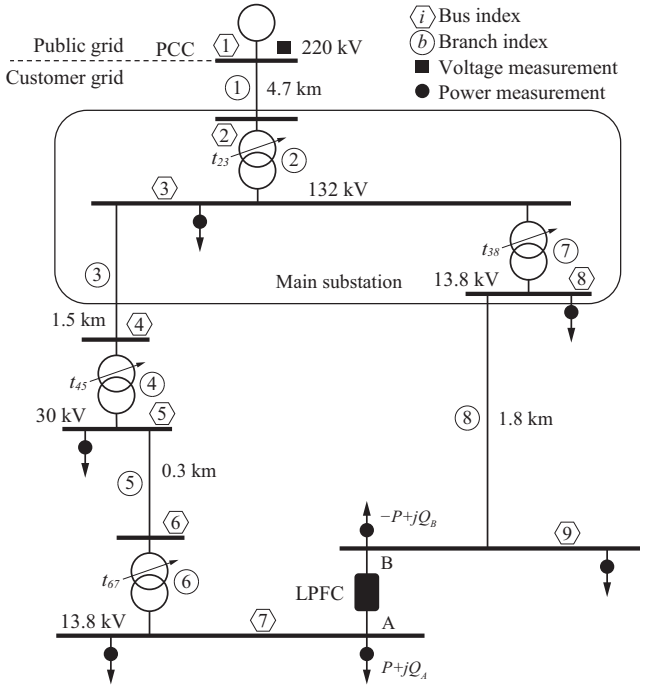

Fig. 9. Industrial installation with a distribution-FACTS-based mesh.

The use of the phase shifting model proposed in this contribution for the tapped transformers in such a radial network is not really mandatory, as it would be in Case 2. This is due to the fact that, in a radial network, the phase shift of the transformers can be initially disregarded and later taken into account on a subsequent post-processing of the results that would correct the phase angle jump in each voltage area. Nevertheless, the use of the proposed phase shifting transformer model is applied in this case study in order to avoid any post-processing of the results.

The **BIBC** and **BCBV** matrices are calculated according to the considerations disclosed in sub-Section 4.2. Their structure is shown in (27) and (28) for the sake of clarity.

$$\begin{bmatrix} 1 & e^{j2\theta_{23}} & e^{j2\theta_{23}} & e^{j2(\theta_{23}+\theta_{45})} & e^{j2(\theta_{23}+\theta_{45})} & e^{j2(\theta_{23}+\theta_{45}+\theta_{67})} & e^{j2(\theta_{23}+\theta_{38})} & e^{j2(\theta_{23}+\theta_{38})} \\ 0 & 1 & 1 & e^{j2\theta_{45}} & e^{j2\theta_{45}} & e^{j2(\theta_{45}+\theta_{67})} & e^{j2\theta_{38}} & e^{j2\theta_{38}} \\ 0 & 0 & 1 & e^{j2\theta_{45}} & e^{j2\theta_{45}} & e^{j2(\theta_{45}+\theta_{67})} & 0 & 0 \\ 0 & 0 & 0 & 1 & 1 & e^{j2\theta_{67}} & 0 & 0 \\ 0 & 0 & 0 & 0 & 1 & e^{j2\theta_{67}} & 0 & 0 \\ 0 & 0 & 0 & 0 & 0 & 1 & 0 & 0 \\ 0 & 0 & 0 & 0 & 0 & 0 & 1 & 1 \\ 0 & 0 & 0 & 0 & 0 & 0 & 0 & 1 \end{bmatrix} \quad (27)$$

$$\begin{bmatrix} z_{12} & 0 & 0 & 0 & 0 & 0 & 0 & 0 \\ z_{12} & z_{23} & 0 & 0 & 0 & 0 & 0 & 0 \\ z_{12} & z_{23} & z_{34} & 0 & 0 & 0 & 0 & 0 \\ z_{12} & z_{23} & z_{34} & z_{45} & 0 & 0 & 0 & 0 \\ z_{12} & z_{23} & z_{34} & z_{45} & z_{56} & 0 & 0 & 0 \\ z_{12} & z_{23} & z_{34} & z_{45} & z_{56} & z_{67} & 0 & 0 \\ z_{12} & z_{23} & 0 & 0 & 0 & 0 & z_{38} & 0 \\ z_{12} & z_{23} & 0 & 0 & 0 & 0 & z_{38} & z_{89} \end{bmatrix} \quad (28)$$

A flat voltage profile is considered for the initial iteration step. The set (1)–(4) is applied iteratively together with (8) to account for the augmented current injection vector, until a threshold of $1e-6$ is reached in the maximum absolute deviation of two consecutive entries in $\boldsymbol{V}$. The voltages at the different buses, as state variables of the grid, are presented in Table 4. The system has also been implemented in the PowerWorld™ Simulator software to crosscheck and demonstrate the validity of the results. Even if this tool uses a Newton-Raphson approach to solve the system, the results are identical up to the threshold level, hence their representation is avoided in this paper.

Table 1
Transformer parameters.

Transf. #	S_n [MVA]	R_{sc} [%]	X_{sc} [%]	a [pu]	θ [deg.]
t_{23}	2×270	0.90	12.90	1.0125	−30
t_{45}	3×37.5	0.90	9.00	0.9875	0
t_{67}	10	0.95	4.80	0.9250	30
t_{38}	3×50	0.92	8.50	0.9750	30

Table 2
Branch parameters.

Branch #	Length [km]	z_{line} [Ω/km]	z_{ik} [pu]
1	4.7	$0.025 + j0.240$	$2.428e-5 + j2.331e-4$
2	–	–	$1.356e-3 + j2.010e-3$
3	1.5	$0.161 + j0.151$	$1.386e-4 + j1.300e-4$
4	–	–	$7.900e-4 + j7.900e-3$
5	0.3	$0.568 + j0.133$	$1.893e-3 + j4.433e-4$
6	–	–	$-1.459e-2 + j4.285e-2$
7	–	–	$-2.245e-3 + j5.084e-3$
8	1.8	$0.161 + j0.112$	$1.522e-2 + j1.059e-2$

Table 3
Power injections.

Bus #	Real power, P_i [MW]	Reactive power, Q_i [Mvar]
2	0.0	0.0
3	84.0	26.0
4	0.0	0.0
5	34.0	12.0
6	0.0	0.0
7	4.9	12.6
8	52.0	39.0
9	2.7	−3.4

Table 4
Case 1 – Results: state variables.

Bus #	$\lvert V_i \rvert$ [pu]	θ_i [deg.]	Bus #	$\lvert V_i \rvert$ [pu]	θ_i [deg.]
2	0.9972	−0.226	6	0.9419	25.588
3	0.9579	27.278	7	0.9496	−5.097
4	0.9570	27.270	8	0.9574	−4.478
5	0.9436	25.436	9	0.9569	−4.980

5.2. Case 2: Weakly meshed grid

In this case study, the industrial network considered in the previous subsection is used to verify the correct performance of the DA method with embedded phase shifting transformers in the context of a weakly meshed grid. With this aim, a similar role as the one played by the LPFC in Case 1 is played by a tapped phase shifting transformer. This device regulates the power flow between nodes 7 and 9. The new setup is depicted in Fig. 10. The parameters and selected tap of the phase shifting transformer used to mesh the grid is shown in Tables 5 and 6 displays the series impedance, z_{79}, of the new branch according to the model shown in Fig. 6.

Only the proposal presented in this paper allows the application of the efficient DA method to this type of system. Notice that in this case a post-processing of the phase-angle jumps of the transformers is not possible, due to the coupling between both sides of the grid downstream from the first common parent node. The new branch, $c = 9$, is selected to break the mesh, though any other branch within the loop (i.e. 3 to 8) could be used with this aim. According to Section 2 and Sub-Section 4.3, once the selection is made, this branch is treated as an additional source of current injection at nodes 7 and 9. However, the use of Kron reduction allows a straightforward consideration of the mesh, i.e. no additional iterative processes are involved. For clarity purposes, the same power injections considered in Case 1 are adopted here and once again the voltage at the slack bus is taken as 1.0 pu and as the origin of phase angles.

The **BIBC** and **BCBV** matrices are calculated according to the specific considerations described in sub-Section 4.3. Their structure is shown in (29) and (30). The entries $BIBC_{19}$ and $BIBC_{29}$ account for the double contribution of B_9 to the branch currents B_1 and B_2, respectively. Notice, as an example, that for $BIBC_{19}$ the phase shifts to be considered fit $t_r = [t_{23}, t_{45}, t_{67}, t_{79}]^T$ and $t_s = [t_{23}, t_{38}]^T$. It should be highlighted that both $BIBC_{19}$ and $BIBC_{29}$ would be zero in a meshed network not including phase shifting transformers, as the contribution of both sides would be canceled upstream from the first common parent node in such a case.

$$\begin{bmatrix} 1 & e^{j2\theta_{23}} & e^{j2\theta_{23}} & e^{j2(\theta_{23}+\theta_{45})} & e^{j2(\theta_{23}+\theta_{45})} & e^{j2(\theta_{23}+\theta_{45}+\theta_{67})} & e^{j2(\theta_{23}+\theta_{38})} & e^{j2(\theta_{23}+\theta_{38})} & e^{j2(\theta_{23}+\theta_{45}+\theta_{67}+\theta_{79})} - e^{j2(\theta_{23}+\theta_{38})} \\ 0 & 1 & 1 & e^{j2\theta_{45}} & e^{j2\theta_{45}} & e^{j2(\theta_{45}+\theta_{67})} & e^{j2\theta_{38}} & e^{j2\theta_{38}} & e^{j2(\theta_{45}+\theta_{67}+\theta_{79})} - e^{j2\theta_{38}} \\ 0 & 0 & 1 & e^{j2\theta_{45}} & e^{j2\theta_{45}} & e^{j2(\theta_{45}+\theta_{67})} & 0 & 0 & e^{j2(\theta_{45}+\theta_{67}+\theta_{79})} \\ 0 & 0 & 0 & 1 & 1 & e^{j2\theta_{67}} & 0 & 0 & e^{j2(\theta_{67}+\theta_{79})} \\ 0 & 0 & 0 & 0 & 1 & e^{j2\theta_{67}} & 0 & 0 & e^{j2(\theta_{67}+\theta_{79})} \\ 0 & 0 & 0 & 0 & 0 & 1 & 0 & 0 & e^{j2\theta_{79}} \\ 0 & 0 & 0 & 0 & 0 & 0 & 1 & 1 & -1 \\ 0 & 0 & 0 & 0 & 0 & 0 & 0 & 1 & -1 \\ 0 & 0 & 0 & 0 & 0 & 0 & 0 & 0 & 1 \end{bmatrix} \quad (29)$$

$$\begin{bmatrix} z_{12} & 0 & 0 & 0 & 0 & 0 & 0 & 0 & 0 \\ z_{12} & z_{23} & 0 & 0 & 0 & 0 & 0 & 0 & 0 \\ z_{12} & z_{23} & z_{34} & 0 & 0 & 0 & 0 & 0 & 0 \\ z_{12} & z_{23} & z_{34} & z_{45} & 0 & 0 & 0 & 0 & 0 \\ z_{12} & z_{23} & z_{34} & z_{45} & z_{56} & 0 & 0 & 0 & 0 \\ z_{12} & z_{23} & z_{34} & z_{45} & z_{56} & z_{67} & 0 & 0 & 0 \\ z_{12} & z_{23} & 0 & 0 & 0 & 0 & z_{38} & 0 & 0 \\ z_{12} & z_{23} & 0 & 0 & 0 & 0 & z_{38} & z_{89} & 0 \\ 0 & 0 & z_{34} & z_{45} & z_{56} & z_{67} & -z_{38} & -z_{89} & z_{79} \end{bmatrix} \quad (30)$$

As in the previous case study, a flat voltage profile is considered for the initial iteration step. The set (1), (8), (26) and (4) is applied iteratively in this order until convergence. With this aim, a threshold of $1e-6$ in the maximum absolute deviation of two consecutive values in $\boldsymbol{V}$ is considered. The solution of the power flow problem, in the form of the bus voltages taken as state variables of the system, is presented in Table 7. The new setup was also implemented in the PowerWorld™ Simulator software package to demonstrate the validity of the results. As in the previous case study, those results are not showed here, due to a perfect match with the proposed methodology.

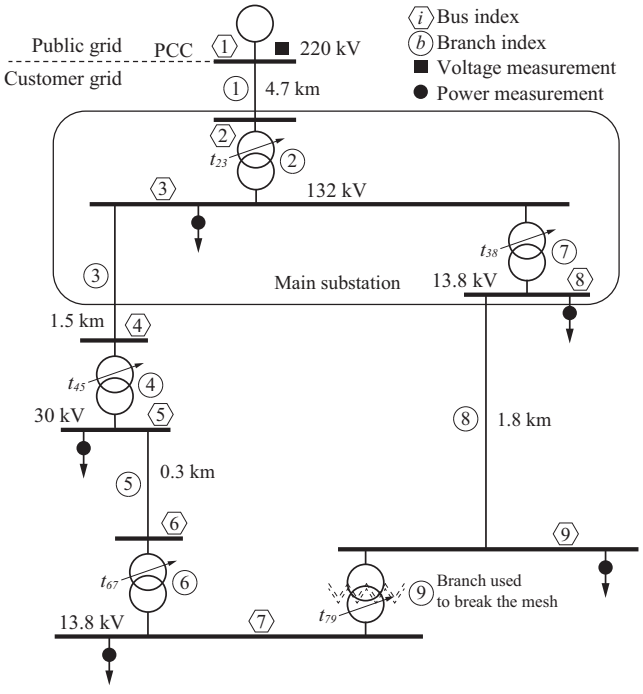

Fig. 10. Industrial installation meshed through a phase shifting transformer.

Table 5
Phase shifting transformer parameters.

Transf. #	S_n [MVA]	R_{sc} [%]	X_{sc} [%]	a [pu]	θ [deg.]
t_{79}	10	0.95	4.80	1.0000	5

Table 6
New branch parameters.

Branch #	Length [km]	z_{line} [Ω/km]	z_{ik} [pu]
9	–	–	$5.280e-3+j4.865e-2$

Table 7
Case 2 – Results: state variables.

Bus #	$\lvert V_i \rvert$ [pu]	θ_i [deg.]	Bus #	$\lvert V_i \rvert$ [pu]	θ_i [deg.]
2	0.9972	−0.223	6	0.9423	25.955
3	0.9578	27.275	7	0.9485	−2.824
4	0.9569	27.273	8	0.9574	−4.714
5	0.9428	25.766	9	0.9478	−5.775

5.3. Case 3: Standard test grid

The IEEE 33-bus test distribution system [17] is used in this case study to assess the impact of the inclusion of the proposed phase shifting transformer model on the convergence characteristics of the DA method. This standard testbed describes a radial grid with 33 buses and 5 tie lines. A modified version of this testbed is presented in this contribution in order to test the proposed model. The modified version, shown in Fig. 11, uses two of the existing tie lines to mesh the network through phase shifting transformers. With this aim, two additional buses, 34 and 35, are added to the standard system. The power injections and line parameters of the IEEE 33-bus test distribution system can be found in [17]. The parameters of the phase shifting transformers, which are the only data of the modified topology not presented in the original testbed, are shown in Table 8.

While the original version is solved using the traditional DA formulation [7], only the proposal included in this paper allows the DA method to solve the modified testbed. The results for both cases are shown in Tables 9 and 10. The validity of these results was checked by using PowerWorld™ Simulator software. System losses are reduced from 211.00 kW to 183.14 kW thanks to the control of the power flows offered by the use of phase shifting transformers. Furthermore, the minimum bus voltage in the grid increases from 0.9038 pu to 0.9203 pu, which illustrates the voltage support capability of the modified topology. A threshold of $1e-6$ in the maximum absolute deviation of two consecutive values in $\boldsymbol{V}$ was considered and, starting from a flat voltage profile,

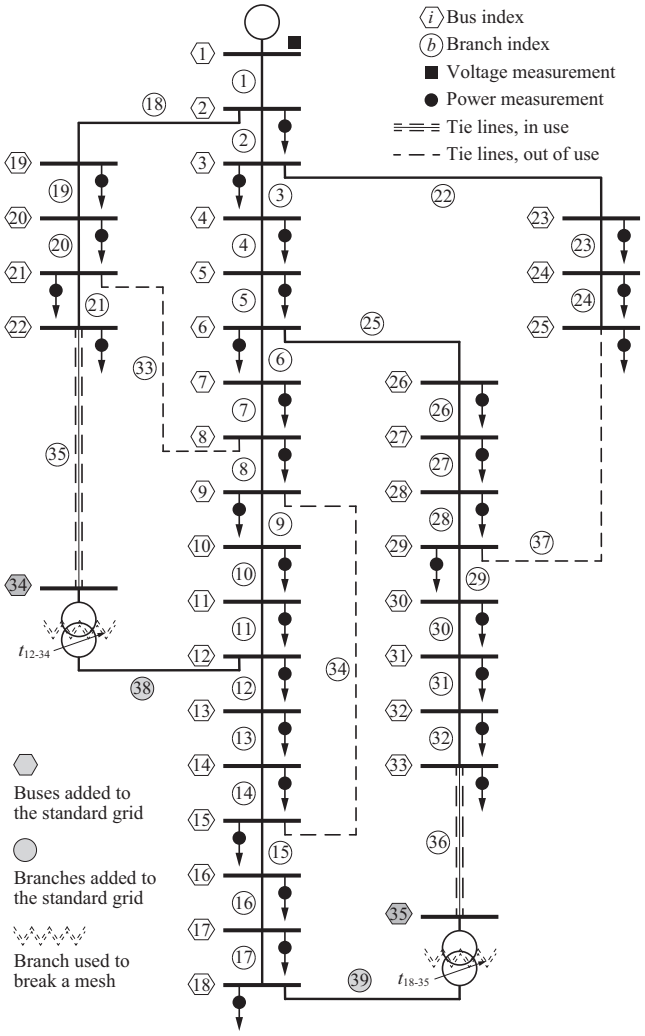

Fig. 11. Modified IEEE 33-bus test distribution system.

Table 8
Phase shifting transformer parameters.

Transf. #	S_n [kVA]	R_{sc} [%]	X_{sc} [%]	a [pu]	θ [deg.]
t_{12-34}	250	0.95	4.80	1.0000	5
t_{18-35}	400	0.95	4.80	1.0000	−3

Table 9
Case 3 – IEEE 33-bus system: state variables.

Bus #	$\lvert V_i \rvert$ [pu]	θ_i [deg.]	Bus #	$\lvert V_i \rvert$ [pu]	θ_i [deg.]
2	0.9970	0.015	19	0.9965	0.004
3	0.9829	0.097	20	0.9929	−0.063
4	0.9754	0.163	21	0.9922	−0.083
5	0.9680	0.230	22	0.9916	−0.103
6	0.9495	0.136	23	0.9793	0.066
7	0.9460	−0.096	24	0.9726	−0.023
8	0.9323	−0.249	25	0.9693	−0.067
9	0.9260	−0.324	26	0.9475	0.175
10	0.9201	−0.388	27	0.9450	0.232
11	0.9192	−0.380	28	0.9335	0.315
12	0.9177	−0.368	29	0.9253	0.393
13	0.9115	−0.462	30	0.9218	0.498
14	0.9092	−0.542	31	0.9176	0.413
15	0.9078	−0.580	32	0.9167	0.390
16	0.9064	−0.604	33	0.9164	0.383
17	0.9044	−0.683	34	–	–
18	0.9038	−0.693	35	–	–

Table 10
Case 3 – Modified IEEE 33-bus system: state variables.

Bus #	$\lvert V_i \rvert$ [pu]	θ_i [deg.]	Bus #	$\lvert V_i \rvert$ [pu]	θ_i [deg.]
2	0.9970	0.016	19	0.9959	−0.010
3	0.9845	0.116	20	0.9873	−0.204
4	0.9781	0.196	21	0.9851	−0.275
5	0.9719	0.277	22	0.9819	−0.401
6	0.9562	0.263	23	0.9809	0.085
7	0.9537	0.088	24	0.9742	−0.003
8	0.9445	−0.043	25	0.9709	−0.047
9	0.9409	−0.104	26	0.9544	0.313
10	0.9377	−0.155	27	0.9520	0.384
11	0.9372	−0.154	28	0.9412	0.545
12	0.9365	−0.154	29	0.9334	0.683
13	0.9296	−0.347	30	0.9302	0.815
14	0.9272	−0.480	31	0.9266	0.814
15	0.9255	−0.563	32	0.9258	0.821
16	0.9237	−0.637	33	0.9255	0.853
17	0.9213	−0.847	34	0.9750	−0.605
18	0.9203	−0.909	35	0.9257	0.896

Table 11
Convergence characteristics: set of 10,000 simulations.

Topology	Av. iter. #	Max. iter. #	Av. sim. time [ms]
Base case	6.0244	7	1.4019
Modified version	5.9528	7	3.5503

only 6 iterations were needed to reach convergence in both topologies. This fact proves that the excellent convergence characteristics of the DA method persist with the inclusion of the proposed phase shifting transformer model.

In order to generalize this result, a set of 10,000 cases was solved with the aim of putting additional stress on the convergence test. With this purpose, the power injections of the 33-bus testbed were randomly varied using independent normal distribution functions for each real power and reactive power. The mean of these distribution functions was set to their corresponding values in the original testbed, P_i and Q_i, and the standard deviation to 40% of these values, i.e. $N(P_i, (0.4P_i)^2)$ and $N(Q_i, (0.4Q_i)^2)$. The set was solved by applying the traditional DA formulation to the original testbed topology, and by applying the formulation proposed in this paper to the modified topology. Table 11 shows the key results of this demanding test. The average and maximum number of iterations were not increased by the use of the phase shifting transformer model even when the meshed configuration used in the modified version results in a more complex topology. In fact, the average number of iterations is slightly reduced, as the voltage support capability of the phase shifting transformers leads to solutions closer to the flat voltage profile used as an initial iteration point. The time required for these calculations was estimated by averaging the results over the full set of simulation runs, which were carried out in an Intel Core i5 - 2467M - CPU 1.60 GHz. This time increases from 1.4 ms to 3.6 ms, which is due to the higher number of buses used in the modified topology, 35 vs. 33, and particularly, to the additional matrix manipulations involved in the treatment of meshed grids, according to Subsection 4.3. This test clearly demonstrates that the convergence characteristics of the DA method are not negatively affected by the inclusion of the phase shifting model proposed in this contribution.

6. Concluding remarks

This paper proposes an extension of the well-known DA power flow method applied to balanced networks in order to allow its use

with common grid components not previously considered in the existing formulation. The inclusion of pi-equivalent line models and transformer tap changers is quite straightforward, and only a formal formulation of the considerations needed to use these components is stated in this work. However, the inclusion of phase shifting transformer models in the DA method is far from obvious, due to the inherent asymmetry of their admittance matrix. Only a custom model of these devices can allow the application of the DA method in weakly meshed networks, where the phase angle of transformers cannot be corrected by post-processing. Thus, this proposal introduces a new phase shifting transformer model, together with a set of slight modifications to be included in the standard DA power flow formulation. Two case studies in the context of the application of fast power flow algorithms to industrial networks are presented. Those cases allow to demonstrate the validity of the proposal both with radial and weakly-meshed topologies. A third case study is carried out in a medium-size test system in order to prove that the excellent convergence characteristics of the DA method are not deteriorated by the inclusion of the new phase shifting transformer model. In each case, the results are compared with those obtained from a popular software package that uses a different approach, leading to a perfect match.

Acknowledgment

This work was supported by the Spanish Ministry of Economy and Competitiveness through the National Plan for Scientific and Technical Research and Innovation under grant ENE2014-52272-R.

References

[1] Gómez-Expósito A, Conejo AJ, Cañizares C. Electric energy systems: analysis and operation. 1st ed. Boca Raton, FL: CRC Press LLC; 2009.
[2] Martinez JA, Mahseredjian J. Load flow calculations in distribution systems with distributed resources: a review. In: 2011 IEEE power and energy society general meeting. p. 1–8. http://dx.doi.org/10.1109/PES.2011.6039172.
[3] Das D, Kothari DP, Kalam A. Simple and efficient method for load flow solution of radial distribution networks. Int J Electr Power Energy Syst 1995;17(5):335–46. http://dx.doi.org/10.1016/0142-0615(95)00050-0.
[4] Chen TH, Chen MS, Hwang KJ, Kotas P, Chebli EA. Distribution system power flow analysis-a rigid approach. IEEE Trans Power Deliv 1991;6(3):1146–52. http://dx.doi.org/10.1109/61.85860.
[5] Shirmohammadi D, Hong HW, Semlyen A, Luo GX. A compensation-based power flow method for weakly meshed distribution and transmission networks. IEEE Trans Power Syst 1988;3(2):753–62. http://dx.doi.org/10.1109/59.192932.
[6] Kersting WH. Distribution system modeling and analysis. 1st ed. Boca Raton, FL: CRC Press LLC; 2002.
[7] Teng J-H. A direct approach for distribution system load flow solutions. IEEE Trans Power Deliv 2003;18(3):882–7. http://dx.doi.org/10.1109/TPWRD.2003.813818.
[8] Cano JM, Norniella JG, Rojas CH, Orcajo GA, Jatskevich J. Application of loop power flow controllers for power demand optimization at industrial customer sites. In: 2015 IEEE power energy society general meeting. p. 1–5. http://dx.doi.org/10.1109/PESGM.2015.7285766.
[9] Bandler J, El-Kady M, Grewal H. An application of complex branch modeling to nonreciprocal power transmission elements. IEEE Trans Circ Syst 1985;32(12):1292–5. http://dx.doi.org/10.1109/TCS.1985.1085671.
[10] Jimenez JC, Nwankpa CO. Circuit model of a phase-shifting transformer for analog power flow emulation. In: 2011 IEEE international symposium of circuits and systems (ISCAS). p. 1864–7. http://dx.doi.org/10.1109/ISCAS.2011.5937950.
[11] Youssef RD. Phase-shifting transformers in load flow and short-circuit analysis: modelling and control. IEE Proc C – Gener Transm Distrib 1993;140(4):331–6. http://dx.doi.org/10.1049/ip-c.1993.0049.
[12] Acha E, Ambriz-Perez H, Fuerte-Esquivel CR. Advanced transformer control modeling in an optimal power flow using Newton's method. IEEE Trans Power Syst 2000;15(1):290–8. http://dx.doi.org/10.1109/59.852135.
[13] Nabavi Niaki SA. A novel steady-state model and principles of operation of phase-shifting transformer comparable with FACTS new devices. Proceedings of international conference on power system technology, vol. 3. p. 1450–7. http://dx.doi.org/10.1109/ICPST.2002.1067770.
[14] Tziouvaras DA, Jimenez R. 138 kV phase shifting transformer protection: EMTP modeling and model power system testing. 2004 Eighth IEE international conference on developments in power system protection, vol. 1. p. 343–7. http://dx.doi.org/10.1049/cp:20040133.
[15] Okon T, Wilkosz K. Phase shifter models for steady state analysis. In: 2016 17th International scientific conference on electric power engineering (EPE). p. 1–6. http://dx.doi.org/10.1109/EPE.2016.7521831.
[16] Barboza LV, Zürn HH, Salgado R. Load tap change transformers: a modeling reminder. IEEE Power Eng Rev 2001;21(2):51–2. http://dx.doi.org/10.1109/MPER.2001.4311274.
[17] Baran ME, Wu FF. Network reconfiguration in distribution systems for loss reduction and load balancing. IEEE Trans Power Deliv 1989;4(2):1401–7. http://dx.doi.org/10.1109/61.25627.

Wide Voltage-Regulation Range Tap-changing Transformer Model for Power System Studies

Jose M. Cano
Dept. Electrical Engineering
University of Oviedo
Gijón, Spain
jmcano@uniovi.es

Md Rejwanur R. Mojumdar
Electrical Control Systems Dept.
ABB AS
Stavanger, Norway
rejwanur-rashid.mojumdar@no.abb.com

Gonzalo A. Orcajo
Dept. Electrical Engineering
University of Oviedo
Gijón, Spain
gonzalo@uniovi.es

***Abstract*—Tap-changing transformer models used in power system studies tend to neglect the change in the short-circuit impedance of the device at the different tap positions. However, the variation of the short-circuit impedance can be significant in transformers with a wide voltage-regulation range. Fortunately, in those cases in which the voltage variation of $\pm 5\%$ is exceeded, the manufacturer is obliged to test and provide data for the short-circuit impedance at terminal taps. The present contribution provides an update of a recently proposed model of the tap-changing transformer so that it can take advantage of the additional information available in the aforementioned cases. The increased accuracy of the resulting model has the potential to improve the quality of the results from power system studies with embedded tap-changing transformers.**

***Index Terms*—power transformers, tap changers, transformer models, power system studies**

I. Introduction

Tap-changing transformers are a key element in achieving voltage regulation at the different parts of the power system. Indeed, either in the form of off-load or on-load tap changers, their presence is ubiquitous both in the transmission and distribution system. Thus, a proper modeling of the tap-changing transformer is essential to conduct accurate power system studies, either in the operating or planning environment. Power flow analysis, economic dispatch or state estimation are just a sample of the tools which require this type of model in order to provide reliable results.

Recently, a consensus model of the tap-changing transformer, [1], was proposed by the authors to reconcile the significant difference arising from the use of traditional versions, widely spread in literature, [2], and software packages [3], [4]. The consensus model introduces a new parameter, which stands for the ratio between the impedances at both sides of the device. An educated guess of this parameter is enough to provide better results than the traditional models, which are based on extreme assumptions. However, the authors have recently proposed the use of parameter estimation techniques based on historical data in order to obtain accurate values of the aforementioned parameters, since they are not typically specified by the manufacturer [5]. Only in this way can the consensus model be fully exploited in its capabilities to provide enhanced results.

Neither the consensus tap-changing transformer model nor the traditional versions include the effect of the change of tap in the variation of short-circuit impedance that takes place in the tapped winding due to the modification of the series resistance and leakage inductance. In fact, this effect is completely neglected in transformers with a low voltage regulation range, to the extent that international standards do not require manufacturers to provide data on the short-circuit impedance of these devices out of the principal tap. However, according to [6], those tap-changing transformers with a wide voltage-regulation range, defined here as those exceeding a voltage variation of $\pm 5\%$ from the principal tap, must additionally provide the short-circuit impedance at the terminal taps. Indeed, this wide voltage variation range may imply a significant variation on the short-circuit impedance of the transformer at the different taps, which should be considered in the model to avoid a deterioration of its accuracy.

The present proposal contributes with an improved version of the consensus tap-changing transformer model which allows to include information on the short-circuit impedance of the transformer at different taps. Though the new model can be universally adopted to improve the accuracy of the results if detailed information of the device is available, it is of especial relevance for tap-changing transformers with a wide voltage regulation range, in which the accuracy can be seriously compromised when using other approaches. Thus, for the benefit of the reader, section II presents the consensus tap-changing transformer model. Section III introduces the update of the consensus model which allows for the inclusion of a varying short-circuit impedance at different taps. Two case studies are depicted in section IV to illustrate the benefits of the proposal and highlight the expected improvement in accuracy when compared with conventional implementations. Finally, the most important conclusions of this contribution are drawn in the last section.

II. Consensus Tap-changing Transformer Model

A new model of the tap-changing transformer was proposed in [1] with the aim of putting an end to the discrepancies

This work was supported by the Spanish Government Innovation Development and Research Office (MEC) under research Grant DPI2017-89186-R.

978-1-6654-4875-8/21/$31.00 ©IEEE

occurring when using two different traditional versions of the model of this device widely spread in literature and different software packages. The aforementioned contribution demonstrates that those differences are caused by an extreme assumption adopted by traditional models, which allocate all the short-circuit impedance of the device to either the off-nominal or nominal side of the transformer. The consensus model introduces a new parameter, k, which stands for the ratio between the short-circuit impedance at the nominal side, z_n, and the one at the off-nominal side, z_o. According to Fig. 1, in a transformer with an off-nominal turns ratio $a_t : 1$, where a_t is related with the tap, t, expressed as the voltage regulation (in percentage) through,

$$a_t = \frac{1}{1 + t/100}, \tag{1}$$

the short-circuit admittance of the device, as seen from the off-nominal side, can be formulated as

$$y_{sc}^{off} = \frac{1}{z_o + a_t^2 z_n} = \frac{1+k}{1 + a_t^2 k} y_{sc}, \tag{2}$$

where y_{sc} stands for the p.u. short-circuit admittance. This is a value obtained through the short-circuit test, and always provided by the manufacturer as nameplate data in the form of the short-circuit impedance, z_{sc} at the principal tap.

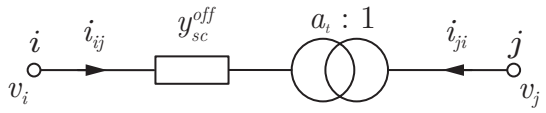

Fig. 1. Consensus model of the tap-changing transformer with the short-circuit admittance represented at the off-nominal side.

The application of Kirchhoff Laws, together with the well-known relationships that apply to ideal transformers, allows to express the terms of the bus admittance matrix of the nodal equations of the device as

$$Y_{ii} = \frac{1+k}{1 + a_t^2 k} y_{sc}, \tag{3}$$

$$Y_{ij} = Y_{ji} = -\frac{a_t\,(1+k)}{1 + a_t^2 k} y_{sc}, \tag{4}$$

$$Y_{jj} = \frac{a_t^2\,(1+k)}{1 + a_t^2 k} y_{sc}. \tag{5}$$

Due to the symmetrical nature of the bus admittance matrix of the tap-changing transformer, it is possible to obtain a π-equivalent model of the device, as the one shown in Fig. 2. Straightforward calculations let us express the value of both the series and shunt branches of this equivalent as

$$y_{ij} = -Y_{ij} = \frac{a_t\,(1+k)}{1 + a_t^2 k} y_{sc}, \tag{6}$$

$$y_{si} = Y_{ii} + Y_{ij} = \frac{(1 - a_t)\,(1+k)}{1 + a_t^2 k} y_{sc}, \tag{7}$$

$$y_{sj} = Y_{jj} + Y_{ij} = \frac{a_t\,(a_t - 1)\,(1+k)}{1 + a_t^2 k} y_{sc}, \tag{8}$$

where y_{si} stands for the shunt branch at the off-nominal turns side and y_{sj} stands for the shunt branch at the nominal turns side.

As it is demonstrated in [1], [7], traditional models correspond to extreme values of k, such as 0 and ∞, which equal to allocating all the short-circuit impedance to the off-nominal or nominal windings, respectively. In the absence of further information, selecting $k = 1$, i.e. assuming a balanced contribution of both sides to the short-circuit impedance, minimizes the maximum expected error. In any case, [5] provides the tools for an accurate identification of this parameter in the context of a real grid.

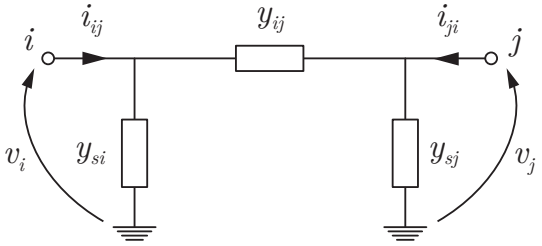

Fig. 2. π-equivalent model of the tap-changing transformer.

III. Including the Effect of Short-Circuit Impedance Variations

As it was stated in section I, neither the consensus model nor the traditional ones include the effect of the inherent short-circuit impedance variation that takes place when a tap change occurs. There are good reasons to support this approach in tap-changing transformers with a reduced voltage regulation range: (a) the influence of this variation may be not very significant in this case due to the small part of the winding affected, and (b), this data is not typically available, as manufacturers do not need to specify this variation provided that the voltage regulation range remains within $\pm 5\%$, [6]. On the contrary, a significant effect could be expected in transformers with a wider voltage regulation range, and [6] guarantees the availability of further data in this case. According to this standard, the short-circuit impedance at extreme tap positions should be "referred to the rated tapping voltage (at that tapping) and the rated power of the transformer".

Let z_{sc_0} and z_{sc_t} be the short-circuit impedance of the transformer at the principal tap, 0, and at a different tap, t. Let k_0 be the transformer impedance ratio at the principal tap, whether obtained from a deep knowledge of the constructive characteristics of the machine, as an educated guess (typically $k = 1$) or through the application of a parameter estimation technique based on historical data. As the contribution to the short-circuit impedance of the nominal turns side is not affected by the tap position, it can be stated that

$$z_{sc_0} = z_{o_0} + z_n, \tag{9}$$

$$z_{sc_t} = z_{o_t} + z_n, \tag{10}$$

where z_{o_0} and z_{o_t} stand for the short-circuit impedance provided by the tapped winding at taps 0 and t, respectively. Considering (9) and the definition of $k_{_0}$, it is possible to calculate z_{o_0} from the given values, i.e.

$$z_{o_0} = z_{sc_0} - z_n = z_{sc_0} - k_{_0} z_{o_0} \rightarrow z_{o_0} = \frac{z_{sc_0}}{1 + k_{_0}}. \tag{11}$$

Thus, applying (10) and (11), the value of the short-circuit impedance ratio for tap t can be determined as

$$k_{_t} = \frac{z_n}{z_{o_t}} = \frac{1}{\frac{z_{sc_t}}{k_{_0} z_{o_0}} - 1} \rightarrow k_{_t} = \frac{1}{\frac{(1+k_{_0}) z_{sc_t}}{k_{_0} z_{sc_0}} - 1}. \tag{12}$$

Equation (12) can be expressed in terms of the corresponding short-circuit admittances at both taps, y_{sc_0} and y_{sc_t}, which is typically preferred in power system studies. Thus,

$$k_{_t} = \frac{1}{\frac{(1+k_{_0}) y_{sc_0}}{k_{_0} y_{sc_t}} - 1}. \tag{13}$$

According to this development, the model of the consensus tap changing transformer can now be reformulated. Thus, in the same sense as it was conveyed by (2), the short-circuit impedance of the transformer as seen from the off-nominal side for each particular tap t can now be expressed as

$$y_{sc_t}^{off} = \frac{1}{z_{o_t} + a_{_t}^2 z_n} = \frac{1 + k_{_t}}{1 + a_{_t}^2 k_{_t}} y_{sc_t}. \tag{14}$$

As a result, the terms of the bus admittance matrix of the nodal equations of the transformer turn to be not only dependant on the tap position through $a_{_t}$, but also through the impact of the short-circuit impedance variation. Thus, (3)–(5) can now be expressed as

$$Y_{ii_t} = \frac{1 + k_{_t}}{1 + a_{_t}^2 k_{_t}} y_{sc_t}, \tag{15}$$

$$Y_{ij_t} = Y_{ji_t} = -\frac{a_{_t} (1 + k_{_t})}{1 + a_{_t}^2 k_{_t}} y_{sc_t}, \tag{16}$$

$$Y_{jj_t} = \frac{a_{_t}^2 (1 + k_{_t})}{1 + a_{_t}^2 k_{_t}} y_{sc_t}. \tag{17}$$

Accordingly, the π-equivalent model of the device is now a function of the short-circuit impedance of the transformer at each particular tap position, as shown in Fig. 3, and the values of the admittances in this model can be expressed as

$$y_{ij_t} = -Y_{ij_t} = \frac{a_{_t} (1 + k_{_t})}{1 + a_{_t}^2 k_{_t}} y_{sc_t}, \tag{18}$$

$$y_{si_t} = Y_{ii_t} + Y_{ij_t} = \frac{(1 - a_{_t}) (1 + k_{_t})}{1 + a_{_t}^2 k_{_t}} y_{sc_t}, \tag{19}$$

$$y_{sj_t} = Y_{jj_t} + Y_{ij_t} = \frac{a_{_t} (a_{_t} - 1) (1 + k_{_t})}{1 + a_{_t}^2 k_{_t}} y_{sc_t}. \tag{20}$$

Notice that the different components of the π-equivalent model are not only affected by the short-circuit impedance measured at each particular tap, y_{sc_t}, but also by the variation of the impedance ratio of the contribution of each winding through, $k_{_t}$, caused by the change of tap.

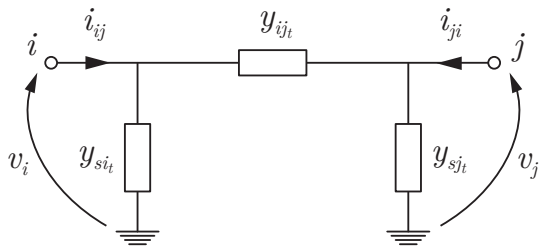

Fig. 3. π-equivalent model of the tap-changing transformer considering the effect of the short-circuit impedance variation caused by the tapped winding.

Although the practising engineering will typically be provided with only the short-circuit impedance at three taps (the principal and terminal ones), using a simple interpolation, which accounts for the rated voltage of each tap position, allows to determine a custom model for each tap based on sensible assumptions. Thus, considering y_{sc_0}, y_{sc_T} the short-circuit impedances at the principal and an extreme tap referred to the same bases, and T the voltage regulation percentage of the extreme tap, the short-circuit impedance of any intermediate tap, y_{sc_t} with a voltage regulation percentage of t should be calculated as

$$y_{sc_t} = y_{sc_0} + \frac{t}{T} \left(y_{sc_T} - y_{sc_0} \right). \tag{21}$$

IV. Case Studies

A. Case Study I

In order to highlight the importance of adopting the model proposed in this contribution for wide voltage-regulation range tap-changing transformers, a standard device, similar to the one previously analyzed in [1] is considered in this case study. Thus, the performance of an 80 MVA, 50 Hz, 230/132 kV $\pm 10\%$ transformer is studied in the following. The manufacturer provides data of the short-circuit impedance of the device at the principal tap, z_{sc_0}, which amounts for $0.01 + 0.12j$ p.u. The tap changer, which is located at the high voltage side of the transformer, has 21 positions, with a voltage regulation step of 1%. As the voltage regulation range exceeds $\pm 5\%$, and in order to comply with regulations, [6], the manufacturer provides the value of the short-circuit impedance of the device at terminal taps, $z_{sc_{10}}$ and $z_{sc_{-10}}$, which amounts for $0.0092 + 0.1104j$ p.u. and $0.0109 + 0.1308j$ p.u., respectively. Notice that, according to [6], "if the impedance (at non-principal taps) is expressed in percentage (or p.u. values), it shall be referred to the rated tapping voltage". For the sake of simplicity, short-circuit impedances at terminal taps have been already referred here to the rated voltage of the transformer at the principal tap.

According to (21), the use of interpolation allows for the calculation of a sensible estimate of the short-circuit admittance of the machine at the different tap positions. Notice that $T{=}10$ and $y_{sc_{10}}$ are used for taps, t, in the positive voltage regulation

range and $T{=}-10$ and $y_{sc_{-10}}$ are considered for those in the negative range. In [1], [7], the authors demonstrated that, in the absence of detailed transformer construction data (which is the most common case), assigning a value of one to the transformer impedance ratio of the machine at the principal tap, $k_0{=}1$, is a prudent decision which minimizes the maximum expected error. This criterion is adopted in the following. Thus, all the information needed to calculate a custom value of the transformer impedance ratio at each tap position, k_t, by applying (13) is now available. Finally, (18)–(20), lead to the model of the tap-changing transformer shown in Fig. 3, which is the subject of this contribution.

Fig. 4 compares the results obtained from the consensus model described in section II with those derived from the new model proposed in section III, which includes the effect of impedance variations on the tapped winding. Thus, the voltage at the nominal side of the transformer at each tap is shown in both cases. At each operating point, the transformer is fed at rated voltage and current at the off-nominal side. Furthermore, three extreme power factors are considered, by varying the angle of the off-nominal side current with respect to the off-nominal side voltage, θ: unity (0°), pure capacitive (90°) and pure inductive ($-90°$).

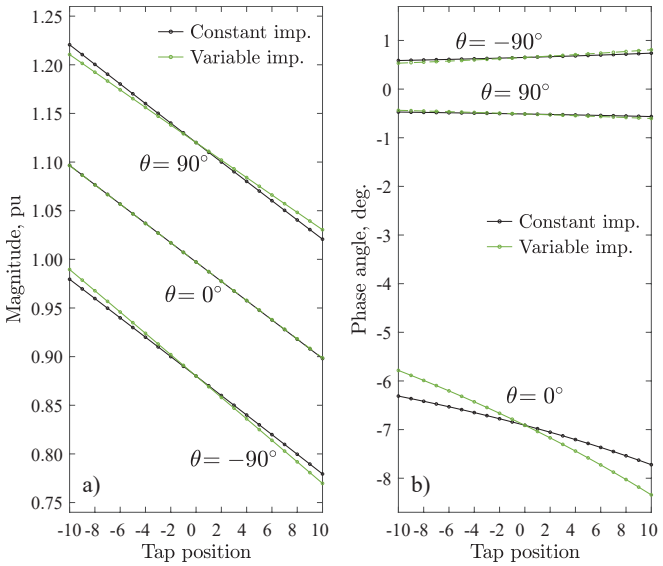

Fig. 4. Nominal turns side voltage of the transformer at the different tap positions for the constant impedance model and the proposed variable impedance model: a) voltage magnitude, and b) voltage phase angle. The transformer is operated at rated voltage and current from the off-nominal side with different power factors: unity ($\theta = 0$), pure capacitive ($\theta = 90$) and pure inductive ($\theta = -90$).

As expected, the effect of the impedance variation of the tapped winding is magnified at terminal taps. According to Fig. 4.a), the maximum difference among both models in terms of voltage magnitude appears with pure capacitive or pure inductive power factors, reaching values of 1.01% at $t{=}-10$ and 0.97% at $t{=}10$ in both cases. Conversely, the effect of impedance variation on voltage magnitude at high power factors is practically negligible. From Fig. 4.b), it is clear that the nominal turns side voltage phase angle is hardly affected at any tap, provided that the transformer is operated at poor power factors. Indeed, the maximum difference between both models appears now at unity power factor, when discrepancies of 0.53 deg. and 0.62 deg. are confirmed at $t{=}-10$ and $t{=}10$, respectively.

Thus, this case study confirms that neglecting the effect of the impedance variation on the tapped winding can lead to significant errors in the results obtained from the transformer model, which may appear as voltage magnitude or phase angle errors depending on the operating point of the device. Specifically, according to Fig. 4.a), the voltage regulation range of the transformer can be overestimated at the lower taps and underestimated at the higher ones if this impedance variation is not considered.

B. Case Study II

A standard test grid has been used in this case study in order to highlight the improvements in the quality of the results that can be derived from the use of the tap-changing transformer model proposed in this contribution. Thus, the IEEE 57-bus system [8], which represents an approximation of the American Electric Power system in the U.S. Midwest as it was in the early 1960s, was selected for this case study due to the large amount of tap-changing transformers embedded in it. The IEEE 57-bus system, shown in Fig. 5, comprises 57 buses, 7 generators, 42 loads and 17 transformers. It is important to note that 15 of these transformers are set out of the principal tap at the operating point defined by the test case. This fact makes the system especially suitable to test the proposed model and compare it with other alternatives which do not consider the impedance variation.

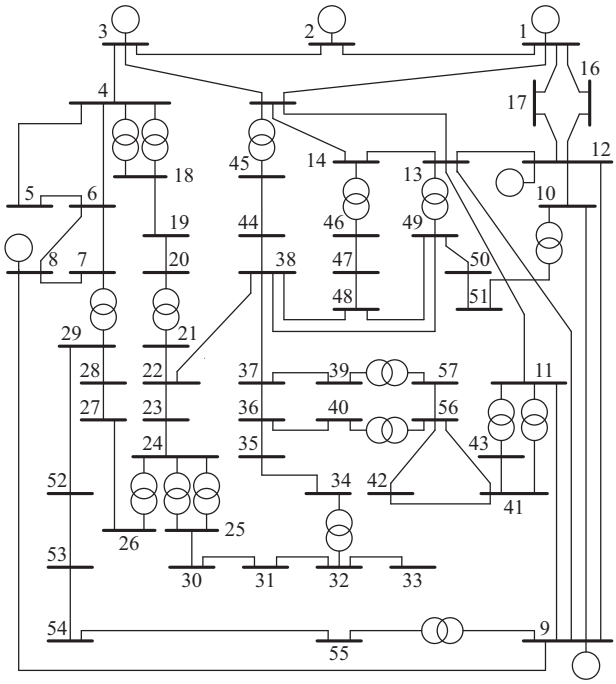

Fig. 5. IEEE 57-bus system.

Table I shows the parameters and set-up of the transformers in the IEEE 57-bus system as described in the test data files. This information suffices to run a power flow analysis of the grid in the case of traditional tap-changing transformer models. Thus, the bus voltages for a set of specific buses using the models which assume that all the short-circuit impedance is provided exclusively by the off-nominal turns side ($k_t = 0$) or by the nominal turns side ($k = \infty$) are shown in Table II. In the same way, this table shows the results derived from the use of the consensus model previously proposed by the authors [1]. Due to the lack of detailed information on the tap-changing transformers, an equal sharing of the short-circuit impedance between the off-nominal and nominal side is assumed, i.e. $k_t = 1$. Notice that in this case, the influence of the impedance variation on k_t is not taken into account.

TABLE I
TRANSFORMER DATA IN THE IEEE 57-BUS SYSTEM

From bus	**To bus**	$\boldsymbol{R}$, p.u	$\boldsymbol{X}$, p.u	**Tap,** $\boldsymbol{a_t}$
4	18	0	0.5550	0.970
4	18	0	0.4300	0.978
21	20	0	0.7767	1.043
24	25	0	1.1820	1.000
24	25	0	1.2300	1.000
24	26	0	0.0473	1.043
7	29	0	0.0648	0.967
34	32	0	0.9530	0.975
11	41	0	0.7490	0.955
11	45	0	0.1042	0.955
14	46	0	0.0735	0.900
10	51	0	0.0712	0.930
13	49	0	0.1910	0.895
11	43	0	0.1530	0.958
40	56	0	1.1950	0.958
39	57	0	1.3550	0.980
9	55	0	0.1205	0.940

TABLE II
BUS VOLTAGES SHOWING THE MAXIMUM DISCREPACIES

Voltage magnitude					
Bus	$k_t = 0$	$k_t = \infty$	$k_t = 1$	k_t variable	MAE (%)
49	1.029	1.036	1.032	1.030	0.196
56	0.963	0.968	0.966	0.964	0.152
57	0.959	0.965	0.962	0.961	0.147
50	1.017	1.023	1.020	1.019	0.143
Voltage phase angle					
Bus	$k_t = 0$	$k_t = \infty$	$k_t = 1$	k_t variable	MAE (deg.)
57	-16.972	-16.584	-16.780	-16.939	0.159
56	-16.430	-16.065	-16.249	-16.407	0.158
42	-15.875	-15.533	-15.705	-15.852	0.147
33	-19.081	-18.552	-18.819	-18.964	0.145

According to Table I, the most extreme positions of the tap-changing transformers correspond to the one between buses 13 and 49, with a positive voltage regulation, t, of 11.73%, and those between buses 21 and 20 and 24 and 26, with a negative voltage regulation, t, of -4.12%. To complete the information provided by the test case according to [6], a maximum voltage regulation range, T, of $\pm 15\%$ was selected for all the transformers. Furthermore, the p.u. impedances of the transformers shown in Table I were used to determine the admittances at the central tap, y_{sc_0}, while these admittances were increased or decreased in a 15% to estimate the values at extreme tap positions, $y_{sc_{+15}}$ and y_{sc-15}. As in the previous case, an equal contribution of both windings to the short-circuit impedance is assumed, but now this corresponds exclusively to the central tap position, i.e. $k_0 = 1$. With those assumptions the power flow analysis was repeated for the tap-changing transformer model proposed in the present contribution, and the results are shown in Table II. The maximum absolute error, MAE, showing the discrepancies between the consensus model, $k_t = 1$, and the one considering the variable nature of the short-circuit impedance, is provided in the last column of this table. In fact, those buses showing the greatest differences, both in voltage magnitude or phase angle, were selected to highlight the benefits of the proposal. Note that even though the transformers in the study were not configured in extreme tap positions, the results can be significantly improved by considering the influence of the impedance variation on the tapped winding.

V. CONCLUSION

The variation of the short-circuit impedance of a tap-changing transformer at different tap positions can have a significant impact on the accuracy of the models used to represent this crucial equipment in power system studies. This is especially important in the case of tap-changers with a wide voltage regulation range. The present proposal introduce the modifications needed to adapt the recently proposed consensus model of the tap-changing transformer in order to include this important effect. The new version of the model relies on the additional information provided by manufacturers on the short-circuit impedance of the machine at terminal tap positions, which is required by international standards. The impact of the new model in the accurate identification of the impedance ratio of the transformer at the principal tap by using parameter estimation techniques, which was previously tackled by the authors for the standard consensus model, is left here for further investigation.

REFERENCES

[1] J. M. Cano, M. R. R. Mojumdar, and G. A. Orcajo, "Reconciling tap-changing transformer models," *IEEE Transactions on Power Delivery*, vol. 34, no. 6, pp. 2266–2268, 2019.

[2] L. V. Barboza, H. H. Zürn, and R. Salgado, "Load tap change transformers: A modeling reminder," *IEEE Power Engineering Review*, vol. 21, no. 2, pp. 51–52, Feb. 2001.

[3] *PowerWorld User's Guide*, PowerWorld Corporation, 2011, [Online]. Available: http://www.powerworld.com.

[4] C. Grande-Moran, "Phase-shifting transformer modeling in PSS®E," *Siemens Power Technology*, vol. 1, no. 111, pp. 1–7, Mar. 2012.

[5] M. R. R. Mojumdar, J. M. Cano, and G. Alonso Orcajo, "Estimation of impedance ratio parameters for consistent modeling of tap-changing transformers," *IEEE Transactions on Power Systems*, pp. 1–1, 2021.

[6] *Power transformers - Part 1: General, IEC 60076-1:2011*, IEC Std., 2011.

[7] J. M. Cano, M. R. R. Mojumdar, and G. A. Orcajo, "On the consistency of tap-changing transformer models in power system studies," in *2020 IEEE Power Energy Society General Meeting (PESGM)*, 2020, pp. 1–5.

[8] A. R. Al-Roomi, "Power Flow Test Systems Repository," Halifax, Nova Scotia, Canada, 2015. [Online]. Available: https://al-roomi.org/power-flow